WITHAFERIN A TARGETS HSP90 IN PANCREATIC CANCER CELLS

by

Yanke Yu

A dissertation submitted in partial fulfillment
of the requirements for the degree of
Doctor of Philosophy
(Pharmaceutical Sciences)
in The University of Michigan
2011

Doctoral Committee:

Associate Professor Duxin Sun, Chair
Associate Professor Gus R. Rosania
Professor David E. Smith
Professor Shaomeng Wang

DEDICATION

Dedicated to my parents, Mr. Mengrong Yu and Mrs. Liping Sun

To my wife, Mrs. Xiaofei Zhang and my daughter, Linda Yu

Acknowledgements

First and foremost I would like to extend my sincerest gratitude to my advisor, Dr. Duxin Sun for his valuable advices, scientific inputs, financial support, and continuous encouragement throughout my thesis. Dr. Sun's broad knowledge in multiple disciplines, insightful thinking, optimistic attitude toward research, great management skills, and leadership benefited me in my graduate study and would also benefit me in my future career and personal life.

I am also thankful to my dissertation committee, Dr. Shaomeng Wang, Dr. David E. Smith, and Dr. Gus R. Rosania for their time and insightful comments on my thesis and for their help on improving my presentation skills.

Sincere thanks to the following people: Dr. A.A. Leslie Gunatilaka of the University of Arizona for the collaboration on withaferin A projects; Dr. Dan Bolon of the University of Massachusetts for providing purified yeast Hsp90, human full length Hsp90, N-terminus Hsp90 and C-terminus Hsp90; Dr. Luke Whitesell of Whitehead Institute for Biomedical Research for his insightful comments; Dr. Suzanna Zick for the collaboration on ginger pharmacokinetic study; Mr. Benjamin Wright for the help of colon tissue homogenization; Ms. Donna McEachern for the help of animal works; and Dr. Jianfang Chen for the help of BCL2 inhibitor synthesis. Special thanks to Dr. Lanyan (Lucy) Fang for her generous help in biodistribution study of HuCC49deltaCH2-beta-galactosidase.

I would also like to thank all my former lab members and current lab members. I enjoyed such a colorful and joyful research and personal life with them. I would also like to thank all my fellow graduate students for their friendship, discussions, and technical help during my research.

Finally, I would like to thank my wife Xiaofei for her support, patience, encouragement and tolerance of my occasional bad tempers during stressful research works. I would also like to thank my little angel, Linda. Her smiling face makes my life much more meaningful.

TABLE OF CONTENTS

LIST OF TABLES

LIST OF FIGURES

LIST OF APPENDICES

CHAPTER I

INTRODUCTION

Pancreatic cancer status

Pancreatic cancer is among the most aggressive and challenging cancers to treat. In US, the number of estimated pancreatic cancer incidence is 43,140, and the number of estimated deaths from pancreatic cancer is 36,800 (1). Compared to the other cancer types such as Lung & bronchus cancer (estimated incidence 222,520 and death 157,300), Prostate cancer (estimated incidence 217,730 and death 32,050), Breast cancer (estimated incidence 209,060 and death 40,230), Colon cancer (estimated incidence 102,900 and death 51,370), Skin cancer (estimated incidence 74,010 and death 11,790), and Non-Hodgkin lymphoma (estimated incidence 65,540 and death 20,210), although pancreatic cancer has relatively low incidence, pancreatic cancer has the highest death rate as of 85.3% and is the fourth leading cause of cancer death in the United States with five-year survival of less than 5% (1-3).

Pancreatic cancer was suggested to be resulted from progressive accumulation of gene mutations and molecular abnormalities (4, 5). Activation of

the oncogene *KRAS2*, inactivation of the tumor-suppressor genes *CDKN2A/INK4A*, *TP53*, and *DPC4/SMAD4/MADH4*, mutation of the caretaker gene *BRCA2*, over-expression of growth factors and their receptors EGFR, TGF-beta, VEGF and AKT, reactivation of developmental signaling Notch and Hedgehog signaling are all indicated in pancreatic cancer development (6-11).

The treatment regimens for pancreatic cancer have no substantial improvement over the past few decades (12). Due to the anatomic location of the pancreas and insidious nature of the disease, the diagnosis of pancreatic cancer is extremely challenging and patients are often diagnosed in the late stage of pancreatic cancer with advanced or metastatic tumors (3, 13). For the early stage pancreatic cancer patients, surgery is the only curative therapy. However, only 15-20% of pancreatic cancer patients are amenable to curative resection while 80% of patients generally have nonresectable advanced or metastatic late stage tumors (14). Furthermore, even in patients with resectable disease, 86% of patients had local pancreatic cancer recurrence which resulted in the overall 5-year survival less than 15% (3, 14).

For unresectable advanced or metastatic pancreatic cancer patients, the treatment options include chemotherapy, radiotherapy, and adjuvant therapy. However, late stage pancreatic cancer is highly resistant to conventional chemotherapy and radiotherapy (15-17). Less than 20% reproducible response rates were observed for various chemotherapeutic agents including antimetabolites, alkylating agents, antibiotics, and anthracyclines tested as single agent or in combination therapy in clinical trials (11, 18, 19). Whereas,

radiotherapy is also challenging due to the fact that the location of pancreas in close proximity of adjacent radiosensitive organs (11). Currently, 5-Fluorouracil (5FU, an inhibitor of thymidylate synthetase which is essential for synthesis of DNA nucleotides) and gemcitabine (nucleoside analogue which replaces cytidine during DNA replication) are commonly used in the treatment of pancreatic cancer with gemcitabine as the standard therapeutic agent for pancreatic cancer. Gemcitabine was demonstrated to improve pancreatic tumor related symptoms such as pain, functional impairment, and weight loss, and increase the median survival durations 5.65 months (4.1 months for 5-FU) and 1 year survival rate of 18% (2% for 5-FU) (20). A few gemcitabine based combination therapy were also examined. For instance, a phase III clinical trial conducted by Louvet *et al.* demonstrated that combination of gemcitabine with oxaliplatin (platinum analogue) was superior to gemcitabine alone with improved response rate (26.8% *vs* 17.3%, respectively), progression-free survival (5.8 *vs* 3.7 months, respectively), clinical benefit (38.2% *vs* 26.9%, respectively), and median overall survival (7.1 *vs* 9.0 months, respectively) (21). Another phase III randomized study showed that combination of gemcitabine and capecitabine (5FU precursor, which is converted to 5FU in the liver and tumors) significantly improved objective response rate compared to gemcitabine alone (19.1% *vs* 12.4%, respectively) (22). Targeted therapy against oncogenic protein overexpressed in pancreatic tumor was also proposed for treatment of pancreatic cancer. Erlotinib (epidermal growth factor receptor (EGFR) inhibitor) was assessed in combination with gemcitabine in a double-blind phase III trial, and the combination was shown

to have higher 1 year survival rate of 24% compared to 17% for the gemcitabine alone (19, 23). By specifically targeting the EGFR expressing advanced pancreatic cancer patients, cetuximab (monoclonal antibody targeting EGFR) in combination with gemcitabine showed much higher 1 year survival rate of 37% compared to gemcitabine monotherapy as of 18% in a phase II clinical trial (24).

Despite the development of surgical techniques, chemotherapeutic agents and therapeutic regimens, pancreatic cancer is still far away from the curable disease as dictated by the miserable 5 year survival rate less than 5%. Therefore, novel chemotherapeutic agents would still be highly desired.

Withaferin A and *Withania somnifera*

The importance of the natural products as the source of pharmaceutical agents has been recognized from ancient times (25-27). Plants (paclitaxel, irinotecan, and etoposide), microorganisms (dactimomycin, doxorubicin, and bleomycin) and marine organisms (citarabine) are all sources of natural products applied in human medicine (27). About 40% of the newly approved drugs in the past years are either natural products or their derivatives and analogues (26, 28); specific to anticancer agents, 73% of the newly approved agents during1940s to 2006 are other than synthetic and 47% are either natural products or their derivatives and analogues (29).

Withania somnifera

Withania somnifera (*W. somnifera*, commonly known as Ashwagandha) is an Indian medicinal plant and has a reputation of Indian ginseng owing to its

magical benefits on human health. It is a green shrub and belongs to Solanaceae family which includes about 90 species such as *Physalis*, *Nicandra*, *Dunalia*, *Datura*, *Jaborosa*, and *Acnistus* (30). *W. somnifera* could be found in the drier parts of India, Baluchistan, Pakistan, Afghanistan, Sri Lanka, Congo, South Africa, Egypt, Morocco, and Jordan (31, 32). For over 3,000 years, Indian people have cultivated and employed its whole plant extract or separate constituents in ayurvedic and indigenous medicine (33). It was shown to have anti-inflammatory, antitumor, antistress, antioxidant, immunomodulatory, hemopoetic, and rejuvenating properties as well as benefiting the endocrine, cardiopulmonary, and central nervous systems (34). A variety of formulations of *W. somnifera* including decoctions, infusions, ointments, powder, and syrup were developed and applied to treat various physiological disorders including burns, wounds, infections, gastrointestinal diseases, infertility, and cutaneous abscesses (35).

A variety of biologically active constituents including alkaloids, steroidal lactones (also known as withanolides), saponins containing an additional acyl group, sitoindosides (withanolides with glucose molecule at carbon 27), flavonoids, and tannins were identified, extracted, and isolated from *W. somnifera* by phytochemical examination (34, 36, 37). Up to date, over 130 withanolides are known and more than 40 withanolides, 12 alkaloids, and several sitoindosides were isolated from different parts (leaves, roots and cherries) of *W. somnifera* and their structures were elucidated (32, 38, 39). Withanolides as the major constituents were shown to mainly localize in leaves and account for 0.001 to 0.5% dry weight of the plants depending on the different species (40-42).

Withanolides are a class of C28 – steroidal lactones with an ergostane skeleton in which C-22 and C-26 are oxidized to form a six - membered δ-lactone ring (43, 44). Figure 1.1 shows the structural skeleton of withanolides (22-hydroxyergostan-26-oic acid-26,22-lactone). Naturally occurred modifications of the carbocyclic skeleton and the side chain of the withanolides have resulted in various novel structural variants which can be classified as withaphysalins, physalins, ixocarpalactones, perulactones, and acnistins (45, 46). The withanolides are generally polyoxygenated and produced via steroids oxidation. The diversity of the structures of the withanolides and their structural variants might lead to their various pharmacological activities, as the withanolides are demonstrated to have antitumor, antibacterial, anti-inflammatory, antidepressant, antioxidant, antiulcer, cytotoxic, quinone reductase induction, antileishmanial, antitrypanosomal, immunosuppressive, cognition-enhancing and memory-improving effects, as well as hypotensive, bradycardic and respiratory-stimulant action (33, 46, 47).

Withaferin A

Withaferin A was the first withanolide to be isolated from *W. somnifera* (45, 48). Figure 1.2 shows the chemical structure of withaferin A. Withaferin A can be described as 4β,27-dihydroxy-1-oxo-5β,6β-epoxywitha-2-24-dienolide. Similar to other withanolides, withaferin A is mainly present in leaves and absent in roots, stems, seeds and persistent calyx of fruits of *W. somnifera* and accounts for 1.6% of the dry weight (33, 49).

Pharmacological activities of withaferin A

As a prototype of the withanolides, withaferin A has been extensively studied for its pharmacological activities. Anti-inflammatory (35, 50, 51), anti-tumor (52, 53), anti-angiogenesis (54), radio-sensitizing activity(55-57), chemopreventive (58, 59), and immunosuppressive (60) properties of withaferin A were demonstrated.

Anti-inflammatory activity

Sabina *et al.* examined the anti-inflammatory effect of withaferin A on a experimental mice model for gouty arthritis monosodium with urate crystal-induced inflammation (50). After monosodium urate crystal induction, mice paw volume, the levels of lysosomal enzymes, lipid peroxidation, and inflammatory mediator tumor necrosis factor-α (TNF-α) were found to be increased significantly; whereas, withaferin A treatment (30 mg/kg, *i.p.*) could reverse monosodium urate crystal induced inflammation, which was comparable to the effect of a standard non-steroidal anti-inflammatory drug indomethacin.

A cellular model of cystic fibrosis inflammation was established by Maitra *et al.* to assess the anti-inflammatory activity of withaferin A (51). The KKLEB immortalized cystic fibrosis epithelial cell line bearing cystic fibrosis transmembrane conductance regulator (CFTR) gene mutations was incubated with filtrates of *Pseudomonas aeruginosa* (PAF) microbes isolated from a cystic fibrosis patient to mimic the inflammation induction in vivo. NFκB-responsive luciferase reporter construct was established to estimate the anti-inflammatory activity of withaferin A as NFκB regulates various pro-inflammatory genes. It was shown that 3 μM withaferin A pretreatment decreased PAF induced luciferase

activity by 70% and decreased PAF induced pro-inflammatory gene IL-8 secretion by 50%.

Anti-tumor and radio-sensitizing activities

The anti-tumor activity of withaferin A was first reported in 1967 by Shohat *et al* (61). Their studies showed that withaferin A induced mitotic arrest in the metaphase of mouse Ehrlich ascites carcinoma cells and induced vacuolization of the cytoplasma *in vitro*, and caused Ehrlich ascites growth reduction and disappearance of the tumor in 80% of the mice with Ehrlich ascites implantation (62, 63). Sharada *et al.* confirmed the anti-tumor effect of withaferin A against mouse Ehrlich ascites carcinoma cells indicated by the inhibition of the tumor growth and increased mice survival of the Ehrlich ascites implanted mice (53). In addition, radiosensitizing effect of withaferin A was first demonstrated and an optimum dose of 30 mg/kg withaferin A in combination with 7.5 Gy gamma radiation for Ehrlich ascites implanted mice was demonstrated (52, 53).

Thereafter, the anti-tumor and radio-sensitizing activities of withaferin A was examined in various cancer cell lines. Devi *et al.* showed that withaferin A induced dose-dependent cell killing of Chinese hamster V79 cells with IC50 of 16 μM, and pretreatment of 2.1 μM withaferin A before irradiation significantly enhanced cell killing effect with a sensitizer enhancement ratio (SER) of 1.5 for 37% survival and 1.4 for 10% survival (64). In addition, Devi *et al.* evaluated the radio-sensitizing effect of withaferin A on B16F1 mouse melanoma cells and found that injection of 30-50 mg/kg withaferin A followed by 30 Gy local gamma irradiation significantly enhanced the growth inhibition and administration of

withaferin A 1 h before irradiation was identified to be the best regimen (55). The withaferin A treatment, and irradiation were further employed to combine with hyperthermia to test the tumor inhibitory activity against B16F1 mouse melanoma and mouse fibrosarcoma grown in C57Bl and Swiss albino mice (56). It was shown that withaferin A, 30 mg/kg injected intraperitoneally 1 h before each irradiation, with fractionated radiotherapy (5 fractions of 10 Gy for 5 consecutive days) synergistically increased complete response (complete regression with no regrowth at the primary site during 120 days of observation) of both tumors (61.11% for B16F1 melanoma and 76.00% for fbrosarcoma, respectively); whereas subsequent hyperthermia further enhanced the effect (68.42% for B16F1 melanoma and 90.00% for fbrosarcoma, respectively) (56). Kalthur *et al.* confirmed that withaferin A, hyperthermia and irradiation acted synergistically against B16F1 melanoma and withaferin A served as a better radio-sensitizer than hyperthermia (65).

Srinivasan *et al.* tested anti-tumor effect of withaferin A against human prostate cancer cell lines (66). Interestingly, withaferin A exhibited androgen receptor (AR) dependent cell killing against prostate cancer cell lines. It was shown that withaferin A had potent anti-proliferative activity against AR negative PC-3 and DU145 prostate cancer cells with IC50s of 3.5 and 4.0 μM, respectively; whereas, withaferin A (up to 8 μM) had no significant effect on AR-transfected PC-3/AR cells, AR mutant expressing LNCaP or CWR22Rv-2 prostate cancer cells, and normal/immortalized prostate epithelial PzHPV-7 cells. In addition, neither anti-androgen (flutamide) nor withaferin A caused apoptosis in the

CWR22Rv-2 cancer cells, however, combined anti-androgen and withaferin A treatment induced significant apoptosis in CWR22Rv-2 cancer cells. The anti-tumor effect of withaferin A on prostate tumor growth was further confirmed in PC-3 xenografts in nude mice (66).

Stan *et al.* demonstrated that withaferin A inhibited proliferation of breast cancer cells with IC50s of 1.5 μM for MCF-7 (estrogen-responsive and p53 wild type) cancer cells and 2.0 μM for MDA-MB-231 (estrogen-independent and p53 mutant) cancer cells indicating that withaferin A suppressed survival of human breast cancer cells was not dependent on estrogen responsiveness or p53 status (67).

Malik *et al.* demonstrated that withaferin A exhibited anti-proliferative activity against human promyelocytic leukemia cells HL-60 with IC50 of 2 μM (68). Oh et al. also showed that withaferin A inhibited human leukemia U937 cells growth with IC50 of 1.0 μM (69). Mandal *et al.* also found that withaferin A inhibited the growth of leukemic cells of lymphoid origin human T-(MOLT-4, Jurkat) and B-(REH)-ALL cell lines, and myeloid origin K-562 leukemic cells with IC50s less than 0.5 μM, but not the normal lymphocytes peripheral blood mononuclear cells (PBMC) (70).

Koduru *et al.* showed that withaferin A inhibited cell survival in three human colon cancer cell lines SW-480, SW-620, and HCT-116 with IC50s of 3.56, 5.0, and 5.33 μM, respectively; whereas, withaferin A showed no significant effect against normal colon epithelial FHC cells (71).

The anti-proliferative activity of withaferin A was also demonstrated against human head and neck squamous cell carcinoma UM-SCC-2, MDA1986, JMAR, and JHU011 cell lines with IC50s of 0.5, 0.8, 2.0, and 2.2 μM, respectively (72).

Anti-angiogenesis activity

Mohan *et al.* first demonstrated the anti-angiogenesis activity of withaferin A (54). Withaferin A was shown to inhibit human umbilical vein endothelial cell (HUVEC) sprouting in three-dimensional collagen-I matrix, inhibit HUVEC cell proliferation with IC50 of 12 nM, and exert potent anti-angiogenic activity in FGF-2 Matrigel™ plug angiogenesis mice model at doses as low as 7 μg/kg/day which were 500-fold lower than the reported doses to exert anti-tumor activity *in vivo* (54). Withaferin A significantly inhibited neovascularization in injury-induced corneal neovascularization mouse model by about 70% (73).

Chemopreventive activity

Manoharan *et al.* demonstrated chemopreventive role of withaferin A (59). It was shown that 7,12-dimethylbenz[a]anthracene (DMBA) induced oral carcinogenesis in Syrian golden hamsters, whereas oral administration of 20 mg/kg withaferin A could completely prevent the tumor induction by DMBA (58, 59).

Molecular targets of withaferin A

As the various pharmacological effects including immunosuppression, anti-inflammatory, anti-angiogenesis, chemoprevention, anti-tumor, and radio-

sensitizing activity of withaferin A were demonstrated, numerous studies were carried out to explore the underlying mechanisms and molecular targets of withaferin A for its biological activities.

The mechanism of radio-sensitizing activity of withaferin A was proposed to be the inhibition of DNA repair by withaferin A (57). To test this theory, Uma Devi *et al.* constructed two DNA repair deficient single gene mutants Rad54$^{-/-}$, Ku$^{-/-}$ and one double gene mutant Ku$^{-/-}$ Rad54$^{-/-}$ DT40 chicken B-lymphocyte cell lines. Ku70 plays an important role in non-homologous end-joining (NHEJ) mediated DNA double strand breaks repair after irradiation; whereas Rad54 is important in homologous recombination (HR) mediated DNA double strand breaks repair. Pretreatment with 5 μM withaferin A followed by X-rays on the wild-type DT40 chicken B-lymphocyte and the three mutant constructs, significantly proliferation inhibition of wild-type DT40, Ku$^{-/-}$, and Ku$^{-/-}$ Rad54$^{-/-}$ cells, but not Rad54$^{-/-}$ cells were observed, indicating that withaferin A contributes to the radio-sensitizing effect mainly through the inhibition of the homologous repair (57).

Mandal *et al.* showed that withaferin A induced leukemic cells apoptosis was through activation of p38 mitogen-activated protein kinase signaling cascade (70). Withaferin A activated p38MAPK, which triggered the downstream apoptosis cascade including activation and phosphorylation the transcription factors activating transcription factor 2 (ATF2) and heat shock protein 27 (Hsp27), externalization of phosphatidylserine, increase of Bax/Bcl-2 ratio, loss of mitochondrial transmembrane potential, cytochrome *c* release, and caspase 9

and 3 activation; whereas knockdown of p38MAPK by siRNA can greatly protect leukemic MOLT-4 cells against withaferin A induced apoptosis with reduction of apoptosis by 3.72 fold.

Sen *et al.* demonstrated that withaferin A inhibited protein kinase C (PKC) activity in leishmanial cells and inhibited growth of *L. donovani* AG83 promastigotes (74). Incubation of leishmanial cell extract with different concentrations of withaferin A exhibited dose-dependent inhibition of the phosphorylation of PKC substrate peptide HCV (1487-1500) indicating the inhibition of PKC by withaferin A. Withaferin A also showed inhibition of the phosphorylation of the HCV peptide by the purified rat brain PKC (74).

As stated earlier, NFκB inhibition by withaferin A contributes to its anti-inflammatory activity (51). In addition, Mohan *et al.* found that the inhibition of NFκB by withaferin A at doses correlated with the inhibition of human umbilical vein endothelial cell (HUVEC) sprouting in three-dimensional collagen-I matrix indicating that NFκB inhibition of withaferin A might also contribute to its anti-angiogenesis activity (54). Withaferin A inhibited TNF-α induced NFκB activation in endothelial cells with IC50 0.5 μM, and inhibited the degradation of the (lipopolysaccharide) LPS-activated phosphorylated form of IκBα (54). Kaileh *et al.* further elucidated that withaferin A inhibited TNF-α induced activation of IκB kinase β (IKKβ) via a thioalkylation-sensitive redox mechanism (35). IKKβ Ser-181 hyperphosphorylation induced by withaferin A led to the inhibition of IKKβ-

dependent IκBa degradation, which inactivated NFκB translocation, NFκB/DNA binding, and gene transcription (35).

Srinivasan *et al.* demonstrated that withaferin A inhibited prostate cancer cell growth through the induction of prostate apoptosis response-4 (Par-4) protein expression (66). Withaferin A induced apoptosis was inhibited by inhibition of Par-4 either with siRNA knockdown or with dominant-negative Par-4 in prostate PC-3 cancer cells. Withaferin A was further show to fail to inhibit NFκB activity when Par-4 was knockdown (66).

Yang *et al.* demonstrated that withaferin A inhibited the chymotrypsin-like activity of proteasome (75). The computational modeling showed that C1 and C24 of withaferin A can interact with the proteasomal β5 subunit, which was confirmed by the inhibition of the chymotrypsin-like activity of purified rabbit 20S proteasome with IC50 4.5 μM, and inhibition of the cellular 26S proteasomal chymotrypsin-like activity with IC50 20 μM. The inhibition of the proteasome was further evidenced by the accumulation of ubiquitinated proteins and three proteasome target proteins (Bax, p27, and IκBα) (75).

Falsey *et al.* demonstrated that withaferin A directly bound to adapter protein annexin II and stimulated annexin II mediated F-actin aggregation and bundling (76). Incubation of fibroblast with withaferin A revealed that the actin cytoskeleton was disrupted with formation of F-actin aggregation. Over-expression of annexin II in HepG2 cells (with little or no endogenous annexin II) showed much higher sensitivity of the cells to withaferin treatment in terms of

cytoskeletal perturbation, rapid shape change and rounding up, which indicated the central role of annexin II in withaferin A induced F-actin aggregation. In addition, withaferin A binding to annexin II mediated F-actin aggregation contributed to the inhibition of the migration and invasion of cancer cells (76). Interestingly, Bargagna-Mohan *et al.* showed that withaferin A induced F-acting aggregation and cellular cytoskeletal disruption could also be mediated by the intermediate filament protein vimentin (73). Their data suggested that withaferin A directly bound to the cystein residue in the highly conserved α-helical coiled coil 2B domain of vimetin and induced vimentin filaments to aggregate and colocalize with F-actin aggregates. Withaferin A inhibited neovascularization in a mouse model of injury induced corneal neovascularization, whereas, it only showed marginal effect against neovascularization in vimentin-null mice indicating the anti-angiogenesis activity of withaferin A was mediated by vimentin (73). Bargagna-Mohan *et al.* further argued that the inhibition of the ubiquitin-proteasome pathway by withaferin A was also mediated by vimentin as evidenced by the enhanced polyubiquitinated protein level in vimentin-transfected MCF-7 cells compared to the wild type MCF-7 or the vector control transfected MCF-7 cells (73).

Stan *et al.* showed that withaferin A induced apoptosis in human breast cancer cells was regulated by the transcription factor Foxo3a and its transcriptional target Bim (67). FOXO3a depletion in MCF-7 cells by FOXO3a-targeted siRNA decreased withaferin A induced Bim-s isoform protein level and partially protected withaferin A induced apoptosis. In addition, Bim-targeted

siRNA transfection could also protect breast cancer cells from withaferin A induced apoptosis.

Oh *et al.* demonstrated that JNK pathway and Akt signaling played important roles in withaferin A induced apoptosis in U937 leukemic cells (69). Withaferin A treatment increased the level of phosphorylated JNK level, whereas co-treatment withaferin A with JNK inhibitor SP600125 dramatically decreased the sub-G1 phase cells (apoptotic cells) compared with withaferin A treatment alone. In addition, PI3K inhibitor LY294002 (inhibits Akt phosphorylation) could increase withaferin A induced accumulation of sub-G1 phase cells. Furthermore, ectopic expression of constitutive active Akt in U937 cells reduced withaferin A induced accumulation of sub-G1 phase cells.

Malik *et al.* demonstrated that withaferin A acted as pro-oxidant: induced oxidative stress in human leukemia Hl-60 cells which resulted in mitochondrial membrane potential ($\Delta\psi_{mt}$) loss, cytochrome c release, translocation of Bax to mitochondria, and apoptosis inducing factor to cell nuclei as well as activation of caspases -9, -3 and PARP cleavage (68). Whereas, antioxidant *N*-acetyl cysteine (NAC) could rescue withaferin A induced oxidative stress and protect cells from withaferin A induced cytotoxicity (68). Lee *et al.* also showed that withaferin A induced reactive oxygen species (ROS) generation, up-regulation of C/EBP homologous protein (CHOP) and death receptor 5 (DR5) which can be reversed by the co-treatment of antioxidants NAC or catalase, and sensitize tumor necrosis factor-related apoptosis-inducing ligand (TRAIL) induced apoptosis in human renal cancer Caki cells (77).

The pro-survival Notch-1 signaling was also suggested to be inhibited by withaferin A (71). Withaferin A treatment decreased Notch-1 and its downstream target Hes-1 and Hey-1 expression in colon cancer cells. Withaferin A also down-regulated Akt, mammalian target of rapamycin (mTOR) signaling components (p70-S6K and 4E-BP1) and activated c-Jun-NH2-kinase mediated apoptosis in colon cancer cells, whereas Akt and mTOR signaling were regulated by Notch-1.

Lee *et al.* showed that signal transducer and activator of transcription 3 (STAT3) might be another molecular target of withaferin A (78). Their data showed that withaferin A decreased both the constitutive and the interleukin-6 (IL-6) induced phosphorylated STAT3 protein level and its upstream regulator Janus-activated kinase 2 (JAK2) protein level in breast cancer MDA-MB-231 cells. In addition, although IL-6 stimulated activation of STAT3 did not affect withaferin A induced cancer cell apoptosis, it increased cell invasion modestly which was inhibited by withaferin A.

Structural activity relationship of withaferin A and its pharmacological activity

As various pharmacological activities including anti-tumor, radio-sensitizing, anti-angiogenesis, and anti-inflammatory were demonstrated and the underlying biochemical mechanisms and potential molecular targets were also elucidated, it would be valuable to assess the key structural components in withaferin A which contribute to its biological activities.

Withaferin A is highly reactive towards proteins as the ketone containing unsaturated A-ring (double bond at position C2-3), the epoxide within B ring, and

the unsaturated lactone ring were all demonstrated to be involved in Michael addition thioalkylation reactions (79-82). Fuska *et al.* found that the unsatuarated A ring was crucial for the cytotoxicity of withaferin A, as the withaferin A derivatives with dissociated double bond possessed little cytotoxicity (79). Whereas, the C27 hydroxyl group and the α,β-unsaturated δ-lactone ring (double bond at C24-25) were not required for the cytotoxicity of withaferin A (79). Kuroyanagi *et al.* demonstrated that the 4β-hydroxy-5β, 6β-epoxy-2-en-1-one moiety was crucial for withaferin A's ability to induce cell differentiation, whereas α,β-unsaturated δ-lactone ring was not (83). Damu *et al.* also demonstrated the importance of the 5β, 6β-epoxide group for withanalides' cytotoxicity (46).

Yang *et al.* showed that the conjugated ketone carbon in the A ring was required for the proteasome inhibition (75). The computational electron density analysis and in silico docking study showed that the conjugated ketone carbon in the A ring could accept nucleophilic attack by the OH group of N-Thr of the proteasomal β5 subunit and inhibit the chymotrypsin-like activity. By reducing the conjugated ketone carbon in the A ring, the new reduced withaferin A analogue showed significant reduction in inhibition of proteasome (30% to 90% inhibition at concentration 10 μM) (75).

In addition, Mohan *et al.* demonstrated that the C2-C3 unsaturated position of the A-ring and C5-C6 epoxide group could contribute to the binding of withaferin to vimentin as suggested by the molecular modeling studies; whereas, withaferin A derivatives 3β-methoxy-dihydrowithaferin A (without C2-C3 double

bond) or 3β-thiophenoxy-dihydrowithaferin A (without C2-C3 double bond) failed to inhibit vimentin (73).

Heat shock protein 90 (Hsp90)

Heat shock protein 90 (Hsp90) is a molecular chaperone found from bacteria to human. In eukaryotic cells, it is highly abundant and accounts for 1-2% of total cytosolic protein. As a molecular chaperone, more than 200 proteins (known as clients) rely on Hsp90 and its associated cochaperone proteins for their conversion into active conformation (84). Many of those Hsp90 client proteins, including HER-2, EGFR, Akt, Raf-1, Cdk4, mutated p53, etc. are constitutively active and involved in transformation and tumorigenesis (85). More than 20 cochaperones were identified, including activator of Hsp90 ATPase 1 (AHA1), prostaglandin E synthase 3 (PTGES3 or p23), STIP1 (p60Hop), cell division cycle 37 homologue (Cdc37), FKBP51, FKBP52, and etc.. (84). Those cochaperones regulate Hsp90's ATPase activity and the rate of Hsp90 cycle as well as help load the client proteins to Hsp90 (84, 86).

Hsp90 primarily exists as homodimer in the cytoplasm. Hsp90 monomer can be divided into three major domains: N-terminal domain, middle domain, and C-terminal domain. N-terminal domain contains an adenine-nucleotide binding pocket and functions as ATPase. The hydrolysis of ATP to ADP is crucial for the chaperoning activity of Hsp90 (87). N-terminal domain also participates in cochaperone binding such as Cdc37, which helps deliver the kinases client proteins to Hsp90 (88, 89). Middle domain plays a role in regulation of ATPase activity by binding to the γ-phosphate of ATP which are bound in the N-terminal

ATP binding pocket and by binding to the cochaperone Aha1 which stimulates Hsp90's ATPase activity (90, 91). Middle domain is also involved in client protein binding (87). C-terminal domain is responsible for dimerization and cochaperone binding such as immunophilins, Hop and protein phosphatase 5 (PP5) (87). In addition, a second ATP binding pocket was implicated in C-terminal domain (92-94).

Hsp90 chaperoning activity is regulated by dimerization, ATP/ADP binding and turnover, as well as binding of the various cochaperones (95). Hessling *et al.* applied fluorescence resonance energy transfer (FRRET) to understand the kinetics of conformational changes of Hsp90 in response to nucleotides (96). A Hsp90 cycle model was proposed: first, an open apo-state of Hsp90 homodimer via C-terminus dimerization is assumed and ATP binds to the N-terminal ATP binding pocket in each monomer in a fast reaction, subsequently, an I_1 conformation is slowly formed in which a short segment in N-terminal domain (known as ATP lid) is released from the contacting N-terminal segment and flaps over the binding pocket; then, the N-terminal domains are dimerized in addition to the dimerized C-terminal domains through the contacting of the N-terminal segment (originally contacting to ATP lid) to the corresponding segment in the other monomer (I_2 conformation); the contact between N-terminal domain to middle domain further twists Hsp90 conformation to a closed state, in which ATP is hydrolyzed to ADP and P_i, finally, ADP is released and Hsp90 returns to the open state (96). Besides ATP/ADP binding and turnover, cochaperone binding could also alter the rate of Hsp90 cycle. Sti1 and Cdc37 could block the Hsp90

conformation change in the early stages, and prevent N-terminal dimerization (97, 98). Whereas, Aha1 could accelerate the Hsp90 cycle leading to I_2 conformation transition even without ATP binding (96). In addition, p23/Sba1 could stabilize Hsp90 at the N-terminally dimerized conformation at the late stage of Hsp90 chaperone cycle, and thus, decrease the ATP turnover rate of Hsp90 (99, 100).

Newly synthesized, conformationally labile client proteins bind to Hsp90 to form an intermediate complex with other cochaperones (such as Cdc37, Hop, Hsp70, Hsp40, and Hip). Depending on the type of the client proteins, the involved cochaperones could be difference. For instance, Cdc37 is specifically responsible for the loading of the kinase client protein. Dynamic association of the client proteins in this intermediate complex prevents the client proteins from aggregation, assists in intracellular trafficking and membrane translocation, and maintains the client proteins at metastable state from which the client proteins can be further activated by specific stimuli (87, 101). For client proteins subjected to be activated, multiple rounds of ATP hydrolysis are required to facilitate Hsp90 chaperoning cycling and drive Hsp90 catalyze the maturation of the client proteins (87, 102).

Since the introduction of benzoquinone ansamycin geldanamycin as the first in line Hsp90 inhibitor in 1994 by Whitesell *et al.*, various types of Hsp90 inhibitors with structural diversities have been designed and synthesized, including geldanamycin (GA, and its derivatives 17-AAG, IPI-504, 17-DMAG), radicicol and its derivatives, purine and its derivatives, pyrazoles and isoxazoles, sulfanyl analogues, resorcinol-bearing compounds, and 2-aminopyrimidine-

bearing derivatives (87, 103-107). The above inhibitors all target to the N-terminal ATP binding pocket, which prevents ATP binding, locks the client proteins in the intermediate complex state, interrupts the Hsp90 chaperone cycle, and finally leads to the release of the immature client protein from the complex which are further subjected to proteasome mediated degradation. Besides blocking the N-terminal ATP binding pocket, C-terminal ATP binding pocket might also be a viable target for inhibition of Hsp90 as well. Novobiocin and its derivatives were synthesized and demonstrated to bind to Hsp90 C-terminal ATP binding pocket and induce cancer cell death (92, 108-110). In addition, cisplatin was also shown to bind to Hsp90 C-terminal ATP binding pocket, although it's still arguable whether inhibition of Hsp90 by cisplatin contributes to its potent anticancer activities as much higher concentration of cisplatin is required to inhibit Hsp90 than the pharmacologically active concentration (93, 111). In addition to ATP binding blockage of Hsp90, researchers have also identified other Hsp90 inhibition mechanisms. For example, the histone deacetylase inhibitors (hydroxamic acid analogue, LAQ 824 and LBH589) were shown to induce the hyperacetylation of Hsp90, resulting in inhibition of ATP binding and attenuation of chaperone activity (112). One of the advantages for Hsp90 inhibitors as anticancer agents is that inhibition of Hsp90 could lead to simultaneous degradation of its client proteins many of which are oncogenic proteins. Since those oncogenic proteins could be involved in various pathways which are all crucial for tumor development, it reduces the possibility of tumor drug resistance development for single therapeutic pathway (95). In addition,

Hsp90 inhibitors show high selectivity. Oncogenes in cancer cells are more dependent on Hsp90 chaperoning activity. In addition, Hsp90 was demonstrated to be highly expressed in various cancerous tissues compared to the non-cancerous tissue (102, 113-115). Furthermore, Hsp90 in tumor exists in multi-chaperone complexes with high ATPase activity, whereas hsp90 in normal tissues is present in a latent, uncomplexed state (102, 116). Therefore, it's not surprising that the binding affinity of Hsp90 inhibitor 17-AAG to Hsp90 in cancer cells is 100-fold higher than that to Hsp90 in normal cells (102). Consequently, the antiproliferative activity of Hsp90 in tumor cells is much higher than that in normal cells (95).

To date, 13 Hsp90 inhibitors have entered clinical trials in different phases for different indications (95, 104, 117-122). For instance, 17-AAG is in phase III clinical trial against multiple myeloma, whereas IPI-504 is also in phase III clinical trial against gastrointestinal stromal tumor (GIST) (95).

Heat shock response and heat shock protein 70 (Hsp70)

Heat shock response is mediated by the transcriptional regulator heat shock factor 1 (Hsf1). Hsf1 transiently binds to Hsp90 in cytosol and its transcriptional activity is sequestered by Hsp90 (123). Under stress such as heat, oxidative stress and massive mutant protein presence or inhibition of Hsp90 by Hsp90 inhibitors, Hsf1 is released from Hsp90 complex, hyperphosphorylated, homotrimerized and translocated into nucleus to bind to the heat shock elements (HSE) in the promoter of *hsp70* gene and activate its transcription (123-125).

Heat shock response induced by Hsp90 inhibitors was demonstrated to contribute to the development of drug resistance to Hsp90 inhibitors (126-130).

Researchers have conducted many studies to explore the possibility of targeting heat shock response to sensitize cancer cells to Hsp90 inhibitors. For example, KNK437 and Quercetin, which inhibited the DNA binding and transcriptional activation of Hsf1, were found to sensitize multidrug resistant cancer cells against hyperthermal therapy and chemotherapeutic drugs including 17-AAG (125, 131-133). However, KNK437 and Quercetin exhibit low inhibitory efficiency of Hsf1 (at 200 μM level and require multiple dosing). In addition, knockdown Hsp70 expression by siHsp70 was also shown to enhance the anticancer activity of classical Hsp90 inhibitors such as GA, 17-AAG and EC78 (129, 130).

Hsp70 is an ATP-dependent molecular chaperone assisting nascent polypeptides folding, assembly and translocation (134). In normal cells, the expression of Hsp70 is at basal level; under heat shock response, Hsp70 is upregulated and assists in the recovery from stress and promoting cell survival (135). Hsp70 also acts as Hsp90 cochaperone (136). Studies have shown that Hsp70 exhibits antiapoptotic effects, which is related to heat shock response. Hsp70 inhibits the mitochondrial pathway of apoptosis by associating with apoptotic protease activating factor 1 (Apaf-1), blocking the assembly of functional apoptosomes (137), and suppressing the activity of caspase-3 (126, 138). In addition, Hsp70 also inhibits caspase-independent death effecter apoptosis inducing factor (AIF) by directly binding to AIF, which prevents its

translocation into nucleus and induces chromatin condensation and DNA fragmentation (126, 139, 140). Hsp70 is constitutively expressed in most cancer cells and human cancer tissues from various origins (132, 141, 142). The high Hsp70 expression in various human cancers has been demonstrated to associate with metastasis, poor prognosis and resistance to radiation therapy or chemotherapy (127, 143-148).

Specific aims

Although Hsp90 inhibitors targeting the ATP binding pocket of Hsp90 have entered clinical trial, it is still premature to conclude it would work as there's no such inhibitor approved by FDA and entered market yet. We propose another mechanism for inhibition of Hsp90 --- targeting the reactive cysteine residues of Hsp90 based on the following evidences: Hsp90 is sensitive to cellular redox conditions and tend to form disulfide bond under oxidative stress (149, 150); in addition, susceptible cysteine residues in C-terminal Hsp90 were revealed and *S*-nitrosylation of the cysteine residues of Hsp90 inhibited Hsp90 ATPase activity (151, 152); the reactive cysteine residues were also demonstrated to be required for the interaction between Hsp90 and molybdate, a metal oxyanion shown to stabilize the Hsp90-protein complexes (153, 154).

Therefore, we hypothesized that specific targeting Hsp90 C-terminus reactive cysteine would lead to decreased Hsp90 chaperoning activity, destabilize Hsp90-protein complexes, and result in client protein degradation and cancer cell death.

The specific aims of this study are:

1. To investigate the anticancer efficacy of withaferin A in pancreatic cancer cells and its mechanism of Hsp90 inhibition.
2. To investigate the synergistic effect of withaferin A and myricetin in pancreatic cancer cells.
3. To investigate the functional groups in withanolides which are crucial for their Hsp90 inhibitory and anticancer effects.

References

1. Jemal A, Siegel R, Xu J, Ward E. Cancer statistics, 2010. CA Cancer J Clin 2010; 60: 277-300.
2. Li D, Xie K, Wolff R, Abbruzzese JL. Pancreatic cancer. Lancet 2004; 363: 1049-57.
3. Dunphy EP. Pancreatic cancer: a review and update. Clin J Oncol Nurs 2008; 12: 735-41.
4. Vogelstein B, Kinzler KW. Cancer genes and the pathways they control. Nat Med 2004; 10: 789-99.
5. Hidalgo M. Pancreatic cancer. N Engl J Med 2010; 362: 1605-17.
6. Di Costanzo F, Carlini P, Doni L, et al. Gemcitabine with or without continuous infusion 5-FU in advanced pancreatic cancer: a randomised phase II trial of the Italian oncology group for clinical research (GOIRC). British Journal of Cancer 2005; 93: 185-9.
7. Kindler HL, Dugan WM, Hochster H, et al. Phase II study of pemetrexed plus gemcitabine in advanced pancreatic cancer. American Journal of Cancer (Auckland, New Zealand) 2005; 4: 185-91.
8. Xiong HQ. Molecular targeting therapy for pancreatic cancer. Cancer Chemother Pharmacol 2004; 54 Suppl 1: S69-77.
9. Buchler P, Reber HA, Buchler M, et al. Hypoxia-inducible factor 1 regulates vascular endothelial growth factor expression in human pancreatic cancer. Pancreas 2003; 26: 56-64.
10. Feldmann G, Beaty R, Hruban RH, Maitra A. Molecular genetics of pancreatic intraepithelial neoplasia. J Hepatobiliary Pancreat Surg 2007; 14: 224-32.
11. Ghaneh P, Costello E, Neoptolemos JP. Biology and management of pancreatic cancer. Postgrad Med J 2008; 84: 478-97.
12. Michaud DS. Epidemiology of pancreatic cancer. Minerva Chir 2004; 59: 99-111.
13. Sun V. Update on pancreatic cancer treatment. Nurse Pract 2010; 35: 16-22; quiz -3.
14. Schnall SF, Macdonald JS. Chemotherapy of adenocarcinoma of the pancreas. Semin Oncol 1996; 23: 220-8.
15. Shore S, Raraty MG, Ghaneh P, Neoptolemos JP. Review article: chemotherapy for pancreatic cancer. Aliment Pharmacol Ther 2003; 18: 1049-69.
16. Neoptolemos JP, Cunningham D, Friess H, et al. Adjuvant therapy in pancreatic cancer: historical and current perspectives. Ann Oncol 2003; 14: 675-92.
17. Sultana A, Tudur Smith C, Cunningham D, et al. Systematic review, including meta-analyses, on the management of locally advanced pancreatic cancer using radiation/combined modality therapy. Br J Cancer 2007; 96: 1183-90.
18. Ghaneh P, Smith R, Tudor-Smith C, Raraty M, Neoptolemos JP. Neoadjuvant and adjuvant strategies for pancreatic cancer. Eur J Surg Oncol 2008; 34: 297-305.

19. Li J, Wientjes MG, Au JL. Pancreatic cancer: pathobiology, treatment options, and drug delivery. Aaps J 2010; 12: 223-32.
20. Burris HA, III, Moore MJ, Andersen J, et al. Improvements in survival and clinical benefit with gemcitabine as first-line therapy for patients with advanced pancreas cancer: a randomized trial. Journal of Clinical Oncology 1997; 15: 2403-13.
21. Louvet C, Labianca R, Hammel P, et al. Gemcitabine in combination with oxaliplatin compared with gemcitabine alone in locally advanced or metastatic pancreatic cancer: results of a GERCOR and GISCAD phase III trial. J Clin Oncol 2005; 23: 3509-16.
22. Cunningham D, Chau I, Stocken DD, et al. Phase III randomized comparison of gemcitabine versus gemcitabine plus capecitabine in patients with advanced pancreatic cancer. J Clin Oncol 2009; 27: 5513-8.
23. Moore MJ, Goldstein D, Hamm J, et al. Erlotinib plus gemcitabine compared with gemcitabine alone in patients with advanced pancreatic cancer: a phase III trial of the National Cancer Institute of Canada Clinical Trials Group. J Clin Oncol 2007; 25: 1960-6.
24. Xiong HQ, Rosenberg A, LoBuglio A, et al. Cetuximab, a monoclonal antibody targeting the epidermal growth factor receptor, in combination with gemcitabine for advanced pancreatic cancer: a multicenter phase II Trial. J Clin Oncol 2004; 22: 2610-6.
25. Farnsworth NR, Akerele O, Bingel AS, Soejarto DD, Guo Z. Medicinal plants in therapy. Bull World Health Organ 1985; 63: 965-81.
26. Cragg GM, Newman DJ, Snader KM. Natural products in drug discovery and development. J Nat Prod 1997; 60: 52-60.
27. da Rocha AB, Lopes RM, Schwartsmann G. Natural products in anticancer therapy. Curr Opin Pharmacol 2001; 1: 364-9.
28. Tietze LF, Bell HP, Chandrasekhar S. Natural product hybrids as new leads for drug discovery. Angew Chem Int Ed Engl 2003; 42: 3996-4028.
29. Newman DJ, Cragg GM. Natural products as sources of new drugs over the last 25 years. J Nat Prod 2007; 70: 461-77.
30. Kuroyanagi M, Arakawa T, Hirayama Y, Hayashi T. Antibacterial and antiandrogen flavonoids from Sophora flavescens. J Nat Prod 1999; 62: 1595-9.
31. Dafni A, Yaniv Z. Solanaceae as medicinal plants in Israel. J Ethnopharmacol 1994; 44: 11-8.
32. Kulkarni SK, Dhir A. Withania somnifera: an Indian ginseng. Prog Neuropsychopharmacol Biol Psychiatry 2008; 32: 1093-105.
33. Mirjalili MH, Moyano E, Bonfill M, Cusido RM, Palazon J. Steroidal lactones from Withania somnifera, an ancient plant for novel medicine. Molecules 2009; 14: 2373-93.
34. Mishra LC, Singh BB, Dagenais S. Scientific basis for the therapeutic use of Withania somnifera (ashwagandha): a review. Altern Med Rev 2000; 5: 334-46.
35. Kaileh M, Vanden Berghe W, Heyerick A, et al. Withaferin a strongly elicits IkappaB kinase beta hyperphosphorylation concomitant with potent inhibition of its kinase activity. J Biol Chem 2007; 282: 4253-64.

36. Kuo PC, Kuo TH, Damu AG, et al. Physanolide A, a novel skeleton steroid, and other cytotoxic principles from Physalis angulata. Org Lett 2006; 8: 2953-6.
37. Bandyopadhyay M, Jha S, Tepfer D. Changes in morphological phenotypes and withanolide composition of Ri-transformed roots of Withania somnifera. Plant Cell Rep 2007; 26: 599-609.
38. Tursunava RN, Maslennikova VA, NK A. Withanolides in the vegetable kingdom Chem Nat Comp 1977; 13: 131-8.
39. Matsuda H, Murakami T, Kishi A, Yoshikawa M. Structures of withanosides I, II, III, IV, V, VI, and VII, new withanolide glycosides, from the roots of Indian Withania somnifera DUNAL. and inhibitory activity for tachyphylaxis to clonidine in isolated guinea-pig ileum. Bioorg Med Chem 2001; 9: 1499-507.
40. Kapoor LD. Handbook of Ayurvedic Medicinal Plants. 2001; CRC Press: London, UK: 337-38.
41. Atal CKG, O.P.; Ranghunathan, K.; Dhar, K.L. Central Council for Research in Indian Medicine and Homeopathy. 1975; New Delhi, India.
42. Anonymous. Monograph. Withania somnifera. Altern Med Rev 2004; 9: 211-4.
43. Elsakka M, Grigorescu E, Stanescu U, Dorneanu V. New data referring to chemistry of Withania somnifera species. Rev Med Chir Soc Med Nat Iasi 1990; 94: 385-7.
44. Grandhi A, Mujumdar AM, Patwardhan B. A comparative pharmacological investigation of Ashwagandha and Ginseng. J Ethnopharmacol 1994; 44: 131-5.
45. Glotter E. Withanolides and related ergostane-type steroids. Nat Prod Rep 1991; 8: 415-40.
46. Damu AG, Kuo PC, Su CR, et al. Isolation, structures, and structure - cytotoxic activity relationships of withanolides and physalins from Physalis angulata. J Nat Prod 2007; 70: 1146-52.
47. Lee SW, Pan MH, Chen CM, Chen ZT. Withangulatin I, a new cytotoxic withanolide from Physalis angulata. Chem Pharm Bull (Tokyo) 2008; 56: 234-6.
48. Kupchan SM, Doskotch RW, Bollinger P, McPhail AT, Sim GA, Renauld JA. The isolation and structural elucidation of a novel steroidal tumor inhibitor from Acnistus arborescens. J Am Chem Soc 1965; 87: 5805-6.
49. Gupta APV, R.K.; Misra, H.O.; Gupta, M.M. Quantitative determination of withaferin A in different plant parts of *Withania somnifera* by TLC densitometry. J Med Arom Plant Sci 1996; 18: 788-90.
50. Sabina EP, Chandal S, Rasool MK. Inhibition of monosodium urate crystal-induced inflammation by withaferin A. J Pharm Pharm Sci 2008; 11: 46-55.
51. Maitra R, Porter MA, Huang S, Gilmour BP. Inhibition of NFkappaB by the natural product Withaferin A in cellular models of Cystic Fibrosis inflammation. J Inflamm (Lond) 2009; 6: 15.
52. Devi PU, Sharada AC, Solomon FE. In vivo growth inhibitory and radiosensitizing effects of withaferin A on mouse Ehrlich ascites carcinoma. Cancer Lett 1995; 95: 189-93.

53. Sharada AC, Solomon FE, Devi PU, Udupa N, Srinivasan KK. Antitumor and radiosensitizing effects of withaferin A on mouse Ehrlich ascites carcinoma in vivo. Acta Oncol 1996; 35: 95-100.
54. Mohan R, Hammers HJ, Bargagna-Mohan P, et al. Withaferin A is a potent inhibitor of angiogenesis. Angiogenesis 2004; 7: 115-22.
55. Devi PU, Kamath R, Rao BS. Radiosensitization of a mouse melanoma by withaferin A: in vivo studies. Indian J Exp Biol 2000; 38: 432-7.
56. Uma Devi P, Kamath R. Radiosensitizing effect of withaferin A combined with hyperthermia on mouse fibrosarcoma and melanoma. J Radiat Res (Tokyo) 2003; 44: 1-6.
57. Uma Devi P, Utsumiz H, Takata M, Takeda S. Enhancement of radiation induced cell death in chicken B lymphocytes by withaferin A. Indian J Exp Biol 2008; 46: 437-42.
58. Manoharan S, Panjamurthy K, Balakrishnan S, Vasudevan K, Vellaichamy L. Circadian time-dependent chemopreventive potential of withaferin-A in 7,12-dimethylbenz[a]anthracene-induced oral carcinogenesis. Pharmacol Rep 2009; 61: 719-26.
59. Manoharan S, Panjamurthy K, Menon VP, Balakrishnan S, Alias LM. Protective effect of Withaferin-A on tumour formation in 7,12-dimethylbenz[a]anthracene induced oral carcinogenesis in hamsters. Indian J Exp Biol 2009; 47: 16-23.
60. Shohat B, Kirson I, Lavie D. Immunosuppressive activity of two plant steroidal lactones withaferin A and withanolide E. Biomedicine 1978; 28: 18-24.
61. Shohat B, Gitter S, Abraham A, Lavie D. Antitumor activity of withaferin A (NSC-101088). Cancer chemotherapy reports 1967; 51: 271-6.
62. Shohat B, Gitter S, Lavie D. Effect of withaferin A on Ehrlich ascites tumor cells--cytological observations. Int J Cancer 1970; 5: 244-52.
63. Shohat B, Joshua H. Effect of withaferin A on ehrlich ascites tumor cells. II. Target tumor cell destruction in vivo by immune activation. Int J Cancer 1971; 8: 487-96.
64. Devi PU, Akagi K, Ostapenko V, Tanaka Y, Sugahara T. Withaferin A: a new radiosensitizer from the Indian medicinal plant Withania somnifera. Int J Radiat Biol 1996; 69: 193-7.
65. Kalthur G, Pathirissery UD. Enhancement of the response of B16F1 melanoma to fractionated radiotherapy and prolongation of survival by withaferin A and/or hyperthermia. Integr Cancer Ther 2010; 9: 370-7.
66. Srinivasan S, Ranga RS, Burikhanov R, Han SS, Chendil D. Par-4-dependent apoptosis by the dietary compound withaferin A in prostate cancer cells. Cancer Res 2007; 67: 246-53.
67. Stan SD, Hahm ER, Warin R, Singh SV. Withaferin A causes FOXO3a-and Bim-dependent apoptosis and inhibits growth of human breast cancer cells in vivo. Cancer Res 2008; 68: 7661-9.
68. Malik F, Kumar A, Bhushan S, et al. Reactive oxygen species generation and mitochondrial dysfunction in the apoptotic cell death of human myeloid leukemia HL-60 cells by a dietary compound withaferin A with concomitant protection by N-acetyl cysteine. Apoptosis 2007; 12: 2115-33.

69. Oh JH, Lee TJ, Kim SH, et al. Induction of apoptosis by withaferin A in human leukemia U937 cells through down-regulation of Akt phosphorylation. Apoptosis 2008; 13: 1494-504.
70. Mandal C, Dutta A, Mallick A, Chandra S, Misra L, Sangwan RS. Withaferin A induces apoptosis by activating p38 mitogen-activated protein kinase signaling cascade in leukemic cells of lymphoid and myeloid origin through mitochondrial death cascade. Apoptosis 2008; 13: 1450-64.
71. Koduru S, Kumar R, Srinivasan S, Evers MB, Damodaran C. Notch-1 inhibition by Withaferin-A: a therapeutic target against colon carcinogenesis. Mol Cancer Ther 2010; 9: 202-10.
72. Samadi AK, Tong X, Mukerji R, Zhang H, Timmermann BN, Cohen MS. Withaferin A, a cytotoxic steroid from Vassobia breviflora, induces apoptosis in human head and neck squamous cell carcinoma. J Nat Prod 2010; 73: 1476-81.
73. Bargagna-Mohan P, Hamza A, Kim YE, et al. The tumor inhibitor and antiangiogenic agent withaferin A targets the intermediate filament protein vimentin. Chem Biol 2007; 14: 623-34.
74. Sen N, Banerjee B, Das BB, et al. Apoptosis is induced in leishmanial cells by a novel protein kinase inhibitor withaferin A and is facilitated by apoptotic topoisomerase I-DNA complex. Cell Death Differ 2007; 14: 358-67.
75. Yang H, Shi G, Dou QP. The tumor proteasome is a primary target for the natural anticancer compound Withaferin A isolated from "Indian winter cherry". Mol Pharmacol 2007; 71: 426-37.
76. Falsey RR, Marron MT, Gunaherath GM, et al. Actin microfilament aggregation induced by withaferin A is mediated by annexin II. Nat Chem Biol 2006; 2: 33-8.
77. Lee TJ, Um HJ, Min do S, Park JW, Choi KS, Kwon TK. Withaferin A sensitizes TRAIL-induced apoptosis through reactive oxygen species-mediated up-regulation of death receptor 5 and down-regulation of c-FLIP. Free Radic Biol Med 2009; 46: 1639-49.
78. Lee J, Hahm ER, Singh SV. Withaferin A inhibits activation of signal transducer and activator of transcription 3 in human breast cancer cells. Carcinogenesis 2010; 31: 1991-8.
79. Fuska J, Fuskova A, Rosazza JP, Nicholas AW. Novel cytotoxic and antitumor agents. IV. Withaferin A: relation of its structure to the in vitro cytotoxic effects on P388 cells. Neoplasma 1984; 31: 31-6.
80. Liang MC, Bardhan S, Pace EA, et al. Inhibition of transcription factor NF-kappaB signaling proteins IKKbeta and p65 through specific cysteine residues by epoxyquinone A monomer: correlation with its anti-cancer cell growth activity. Biochem Pharmacol 2006; 71: 634-45.
81. Oh JH, Lee TJ, Park JW, Kwon TK. Withaferin A inhibits iNOS expression and nitric oxide production by Akt inactivation and down-regulating LPS-induced activity of NF-kappaB in RAW 264.7 cells. Eur J Pharmacol 2008; 599: 11-7.
82. Yokota Y, Bargagna-Mohan P, Ravindranath PP, Kim KB, Mohan R. Development of withaferin A analogs as probes of angiogenesis. Bioorg Med Chem Lett 2006; 16: 2603-7.

83. Kuroyanagi M, Shibata K, K U. Cell differentiation inducing steroids from *Withania somnifera* L. (Dun.). Chem Pharm Bull 1999; 47: 1646-9.
84. Trepel J, Mollapour M, Giaccone G, Neckers L. Targeting the dynamic HSP90 complex in cancer. Nat Rev Cancer; 10: 537-49.
85. Rowlands MG, Newbatt YM, Prodromou C, Pearl LH, Workman P, Aherne W. High-throughput screening assay for inhibitors of heat-shock protein 90 ATPase activity. Anal Biochem 2004; 327: 176-83.
86. Taipale M, Jarosz DF, Lindquist S. HSP90 at the hub of protein homeostasis: emerging mechanistic insights. Nat Rev Mol Cell Biol; 11: 515-28.
87. Whitesell L, Lindquist SL. HSP90 and the chaperoning of cancer. Nat Rev Cancer 2005; 5: 761-72.
88. Roe SM, Ali, M.M.U., Meyer, P., Vaughan, C.K., Panaretou, B., Piper, P.W., Prodromou, C. and Pearl, L.H. The mechanism of Hsp90 regulation by the protein kinase-specific cochaperone p50(cdc37). Cell 2004; 116: 87-98.
89. Pearl LH. Hsp90 and Cdc37 -- a chaperone cancer conspiracy. Curr Opin Genet Dev 2005; 15: 55-61.
90. Meyer P, Prodromou C, Hu B, et al. Structural and functional analysis of the middle segment of hsp90: implications for ATP hydrolysis and client protein and cochaperone interactions. Mol Cell 2003; 11: 647-58.
91. Meyer P, Prodromou C, Liao C, et al. Structural basis for recruitment of the ATPase activator Aha1 to the Hsp90 chaperone machinery. Embo J 2004; 23: 511-9.
92. Marcu MG, Chardli A, Bouhouche I, Catelli M, Neckers LM. The heat shock protein 90 antagonist novobiocin interacts with a previously unrecognized ATP-binding domain in the carboxyl terminus of the chaperone. J Biol Chem 2000; 275: 37181-6.
93. Soti C, Racz A, Csermely P. A Nucleotide-dependent molecular switch controls ATP binding at the C-terminal domain of Hsp90. N-terminal nucleotide binding unmasks a C-terminal binding pocket. J Biol Chem 2002; 277: 7066-75.
94. Garnier C, Lafitte D, Tsvetkov PO, et al. Binding of ATP to heat shock protein 90: evidence for an ATP-binding site in the C-terminal domain. J Biol Chem 2002; 277: 12208-14.
95. Biamonte MA, Van de Water R, Arndt JW, Scannevin RH, Perret D, Lee WC. Heat shock protein 90: inhibitors in clinical trials. J Med Chem 2010; 53: 3-17.
96. Hessling M, Richter K, Buchner J. Dissection of the ATP-induced conformational cycle of the molecular chaperone Hsp90. Nat Struct Mol Biol 2009; 16: 287-93.
97. Richter K, Muschler P, Hainzl O, Reinstein J, Buchner J. Sti1 is a non-competitive inhibitor of the Hsp90 ATPase. Binding prevents the N-terminal dimerization reaction during the atpase cycle. J Biol Chem 2003; 278: 10328-33.
98. Roe SM, Ali MM, Meyer P, et al. The Mechanism of Hsp90 regulation by the protein kinase-specific cochaperone p50(cdc37). Cell 2004; 116: 87-98.
99. Richter K, Walter, S. & Buchner, J. The Co-chaperone Sba1 connects the ATPase reaction of Hsp90 to the progression of the chaperone cycle. J Mol Biol 2004; 342: 1403-13.

100. Wandinger SK, Richter K, Buchner J. The Hsp90 chaperone machinery. J Biol Chem 2008; 283: 18473-7.
101. Bagatell R, Whitesell L. Altered Hsp90 function in cancer: a unique therapeutic opportunity. Mol Cancer Ther 2004; 3: 1021-30.
102. Kamal A, Thao L, Sensintaffar J, et al. A high-affinity conformation of Hsp90 confers tumour selectivity on Hsp90 inhibitors. Nature 2003; 425: 407-10.
103. Janin YL. Heat shock protein 90 inhibitors. A text book example of medicinal chemistry? J Med Chem 2005; 48: 7503-12.
104. Chiosis G. Targeting chaperones in transformed systems--a focus on Hsp90 and cancer. Expert Opin Ther Targets 2006; 10: 37-50.
105. Neckers L. Development of small molecule Hsp90 inhibitors: utilizing both forward and reverse chemical genomics for drug identification. Curr Med Chem 2003; 10: 733-9.
106. Powers MV, Workman P. Inhibitors of the heat shock response: biology and pharmacology. FEBS Lett 2007; 581: 3758-69.
107. Taldone T, Sun W, Chiosis G. Discovery and development of heat shock protein 90 inhibitors. Bioorg Med Chem 2009; 17: 2225-35.
108. Donnelly AC, Mays JR, Burlison JA, et al. The design, synthesis, and evaluation of coumarin ring derivatives of the novobiocin scaffold that exhibit antiproliferative activity. J Org Chem 2008; 73: 8901-20.
109. Burlison JA, Avila C, Vielhauer G, Lubbers DJ, Holzbeierlein J, Blagg BS. Development of novobiocin analogues that manifest anti-proliferative activity against several cancer cell lines. J Org Chem 2008; 73: 2130-7.
110. Zhao H, Donnelly AC, Kusuma BR, et al. Engineering an Antibiotic to Fight Cancer: Optimization of the Novobiocin Scaffold to Produce Anti-proliferative Agents. J Med Chem; 54: 3839-53.
111. Itoh H, Ogura M, Komatsuda A, Wakui H, Miura AB, Tashima Y. A novel chaperone-activity-reducing mechanism of the 90-kDa molecular chaperone HSP90. Biochem J 1999; 343 Pt 3: 697-703.
112. Nimmanapalli R, Fuino L, Bali P, et al. Histone deacetylase inhibitor LAQ824 both lowers expression and promotes proteasomal degradation of Bcr-Abl and induces apoptosis of imatinib mesylate-sensitive or -refractory chronic myelogenous leukemia-blast crisis cells. Cancer Res 2003; 63: 5126-35.
113. Yufu Y, Nishimura J, Nawata H. High constitutive expression of heat shock protein 90 alpha in human acute leukemia cells. Leuk Res 1992; 16: 597-605.
114. Ogata M, Naito Z, Tanaka S, Moriyama Y, Asano G. Overexpression and localization of heat shock proteins mRNA in pancreatic carcinoma. Journal of Nippon Medical School 2000; 67: 177-85.
115. Plescia J, Salz W, Xia F, et al. Rational design of shepherdin, a novel anticancer agent. Cancer Cell 2005; 7: 457-68.
116. Dickey CA, Kamal A, Lundgren K, et al. The high-affinity HSP90-CHIP complex recognizes and selectively degrades phosphorylated tau client proteins. J Clin Invest 2007; 117: 648-58.
117. Adams J, Elliott PJ. New agents in cancer clinical trials. Oncogene 2000; 19: 6687-92.

118. Egorin MJ, Zuhowski EG, Rosen DM, Sentz DL, Covey JM, Eiseman JL. Plasma pharmacokinetics and tissue distribution of 17-(allylamino)-17-demethoxygeldanamycin (NSC 330507) in CD2F1 mice1. Cancer Chemother Pharmacol 2001; 47: 291-302.
119. Ramanathan RK, Trump DL, Eiseman JL, et al. Phase I pharmacokinetic-pharmacodynamic study of 17-(allylamino)-17-demethoxygeldanamycin (17AAG, NSC 330507), a novel inhibitor of heat shock protein 90, in patients with refractory advanced cancers. Clin Cancer Res 2005; 11: 3385-91.
120. Amin K, Ip C, Jimenez L, Tyson C, Behrsing H. In vitro detection of differential and cell-specific hepatobiliary toxicity induced by geldanamycin and 17-allylaminogeldanamycin using dog liver slices. Toxicol Sci 2005; 87: 442-50.
121. Schnur RC, Corman ML, Gallaschun RJ, et al. Inhibition of the oncogene product p185erbB-2 in vitro and in vivo by geldanamycin and dihydrogeldanamycin derivatives. J Med Chem 1995; 38: 3806-12.
122. Kim YS, Alarcon SV, Lee S, et al. Update on Hsp90 inhibitors in clinical trial. Curr Top Med Chem 2009; 9: 1479-92.
123. Zou J, Guo Y, Guettouche T, Smith DF, Voellmy R. Repression of heat shock transcription factor HSF1 activation by HSP90 (HSP90 complex) that forms a stress-sensitive complex with HSF1. Cell 1998; 94: 471-80.
124. Nakai A, Tanabe M, Kawazoe Y, Inazawa J, Morimoto RI, Nagata K. HSF4, a new member of the human heat shock factor family which lacks properties of a transcriptional activator. Mol Cell Biol 1997; 17: 469-81.
125. Guo F, Rocha K, Bali P, et al. Abrogation of heat shock protein 70 induction as a strategy to increase antileukemia activity of heat shock protein 90 inhibitor 17-allylamino-demethoxy geldanamycin. Cancer Res 2005; 65: 10536-44.
126. Guo F, Sigua C, Bali P, et al. Mechanistic role of heat shock protein 70 in Bcr-Abl-mediated resistance to apoptosis in human acute leukemia cells. Blood 2005; 105: 1246-55.
127. Schmitt E, Maingret L, Puig PE, et al. Heat shock protein 70 neutralization exerts potent antitumor effects in animal models of colon cancer and melanoma. Cancer Res 2006; 66: 4191-7.
128. Zaarur N, Gabai VL, Porco JA, Jr., Calderwood S, Sherman MY. Targeting heat shock response to sensitize cancer cells to proteasome and Hsp90 inhibitors. Cancer Res 2006; 66: 1783-91.
129. Powers MV, Clarke PA, Workman P. Dual targeting of HSC70 and HSP72 inhibits HSP90 function and induces tumor-specific apoptosis. Cancer Cell 2008; 14: 250-62.
130. McCollum AK, TenEyck CJ, Stensgard B, et al. P-Glycoprotein-mediated resistance to Hsp90-directed therapy is eclipsed by the heat shock response. Cancer Res 2008; 68: 7419-27.
131. Mello CC, Conte D, Jr. Revealing the world of RNA interference. Nature 2004; 431: 338-42.
132. Creagh EM, Sheehan D, Cotter TG. Heat shock proteins--modulators of apoptosis in tumour cells. Leukemia 2000; 14: 1161-73.

133. Koishi M, Yokota S, Mae T, et al. The effects of KNK437, a novel inhibitor of heat shock protein synthesis, on the acquisition of thermotolerance in a murine transplantable tumor in vivo. Clin Cancer Res 2001; 7: 215-9.
134. Beckmann RP, Mizzen LE, Welch WJ. Interaction of Hsp 70 with newly synthesized proteins: implications for protein folding and assembly. Science 1990; 248: 850-4.
135. Jolly C, Morimoto RI. Role of the heat shock response and molecular chaperones in oncogenesis and cell death. J Natl Cancer Inst 2000; 92: 1564-72.
136. Arlander SJ, Felts SJ, Wagner JM, Stensgard B, Toft DO, Karnitz LM. Chaperoning checkpoint kinase 1 (Chk1), an Hsp90 client, with purified chaperones. J Biol Chem 2006; 281: 2989-98.
137. Beere HM, Wolf BB, Cain K, et al. Heat-shock protein 70 inhibits apoptosis by preventing recruitment of procaspase-9 to the Apaf-1 apoptosome. Nat Cell Biol 2000; 2: 469-75.
138. Jaattela M, Wissing D, Kokholm K, Kallunki T, Egeblad M. Hsp70 exerts its anti-apoptotic function downstream of caspase-3-like proteases. EMBO J 1998; 17: 6124-34.
139. Ravagnan L, Gurbuxani S, Susin SA, et al. Heat-shock protein 70 antagonizes apoptosis-inducing factor. Nat Cell Biol 2001; 3: 839-43.
140. Gurbuxani S, Schmitt E, Cande C, et al. Heat shock protein 70 binding inhibits the nuclear import of apoptosis-inducing factor. Oncogene 2003; 22: 6669-78.
141. Garrido C, Brunet M, Didelot C, Zermati Y, Schmitt E, Kroemer G. Heat shock proteins 27 and 70: anti-apoptotic proteins with tumorigenic properties. Cell Cycle 2006; 5: 2592-601.
142. Parcellier A, Gurbuxani S, Schmitt E, Solary E, Garrido C. Heat shock proteins, cellular chaperones that modulate mitochondrial cell death pathways. Biochem Biophys Res Commun 2003; 304: 505-12.
143. Brondani Da Rocha A, Regner A, Grivicich I, et al. Radioresistance is associated to increased Hsp70 content in human glioblastoma cell lines. Int J Oncol 2004; 25: 777-85.
144. Vargas-Roig LM, Gago FE, Tello O, Aznar JC, Ciocca DR. Heat shock protein expression and drug resistance in breast cancer patients treated with induction chemotherapy. Int J Cancer 1998; 79: 468-75.
145. Nanbu K, Konishi I, Mandai M, et al. Prognostic significance of heat shock proteins HSP70 and HSP90 in endometrial carcinomas. Cancer Detect Prev 1998; 22: 549-55.
146. Sliutz G, Karlseder J, Tempfer C, Orel L, Holzer G, Simon MM. Drug resistance against gemcitabine and topotecan mediated by constitutive hsp70 overexpression in vitro: implication of quercetin as sensitiser in chemotherapy. Br J Cancer 1996; 74: 172-7.
147. Samali A, Cotter TG. Heat shock proteins increase resistance to apoptosis. Exp Cell Res 1996; 223: 163-70.
148. Creagh EM, Cotter TG. Selective protection by hsp 70 against cytotoxic drug-, but not Fas-induced T-cell apoptosis. Immunology 1999; 97: 36-44.

149. Cumming RC, Andon NL, Haynes PA, Park M, Fischer WH, Schubert D. Protein disulfide bond formation in the cytoplasm during oxidative stress. J Biol Chem 2004; 279: 21749-58.
150. Chen WY, Chang FR, Huang ZY, Chen JH, Wu YC, Wu CC. Tubocapsenolide A, a novel withanolide, inhibits proliferation and induces apoptosis in MDA-MB-231 cells by thiol oxidation of heat shock proteins. J Biol Chem 2008; 283: 17184-93.
151. Martinez-Ruiz A, Villanueva L, Gonzalez de Orduna C, et al. S-nitrosylation of Hsp90 promotes the inhibition of its ATPase and endothelial nitric oxide synthase regulatory activities. Proc Natl Acad Sci U S A 2005; 102: 8525-30.
152. Nardai G, Sass B, Eber J, Orosz G, Csermely P. Reactive cysteines of the 90-kDa heat shock protein, Hsp90. Arch Biochem Biophys 2000; 384: 59-67.
153. Hutchison KA, Stancato LF, Jove R, Pratt WB. The protein-protein complex between pp60v-src and hsp90 is stabilized by molybdate, vanadate, tungstate, and an endogenous cytosolic metal. J Biol Chem 1992; 267: 13952-7.
154. Hutchison KA, Brott BK, De Leon JH, Perdew GH, Jove R, Pratt WB. Reconstitution of the multiprotein complex of pp60src, hsp90, and p50 in a cell-free system. J Biol Chem 1992; 267: 2902-8.

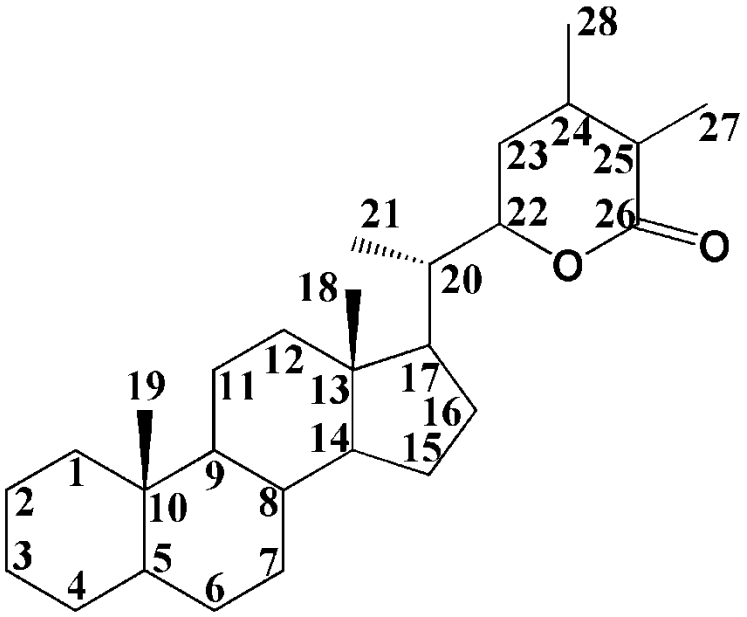

Figure 1.1 Withanolide structural skeleton

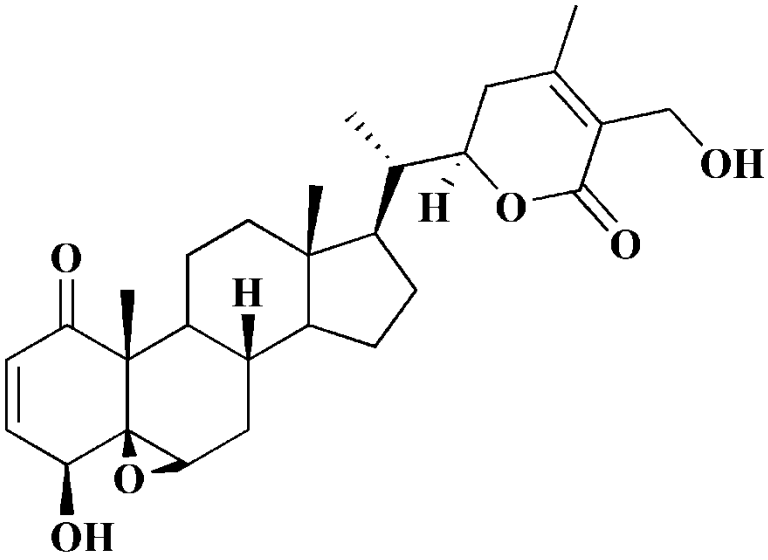

Figure 1.2 Withaferin A chemical structure

CHAPTER II

WITHAFERIN A TARGETS HEAT SHOCK PROTEIN 90 IN PANCREATIC CANCER CELLS

Abstract

The purpose of this study is to investigate the efficacy and the mechanism of Hsp90 inhibition of withaferin A (WA), a steroidal lactone occurring in *Withania somnifera*, in pancreatic cancer *in vitro* and *in vivo*. Withaferin A exhibited potent antiproliferative activity against pancreatic cancer cells *in vitro* (with IC_{50}s of 1.24, 2.93 and 2.78 μM) in pancreatic cancer cell lines Panc-1, MiaPaca2 and BxPc3, respectively. Annexin V staining showed that WA induced significant apoptosis in Panc-1 cells in a dose dependent manner. Western blotting demonstrated that WA inhibited Hsp90 chaperone activity to induce degradation of Hsp90 client proteins (Akt, Cdk4 and glucocorticoid receptor), which was reversed by the proteasomal inhibitor, MG132. WA-Biotin pull-down assay of Hsp90 using Panc-1 cancer cell lysates and purified Hsp90 showed that WA-biotin binds to C-terminus of Hsp90, which was competitively blocked by unlabeled WA. Co-immunoprecipitation exhibited that WA (10 μM) disrupted Hsp90-Cdc37

complexes from 1-24 hour post treatment, while it neither blocked ATP binding to Hsp90, nor changed Hsp90-P23 association. WA (3, 6 mg/kg) inhibited tumor growth in pancreatic cancer Panc-1 xenografts by 30% and 58%, respectively. These data demonstrate that withaferin A binds Hsp90, inhibits Hsp90 chaperone activity through an ATP independent mechanism, results in Hsp90 client protein degradation, and exhibits *in vivo* anticancer activity against pancreatic cancer.

Key words: Withaferin A; Pancreatic cancer; Hsp90; Reactive cysteine; Client protein; Cdc37;

Introduction

Pancreatic cancer is the fourth leading cause of cancer deaths in the United States (1, 2) with one- and five-year survival of 23% and 4% (1). The mortality rates associated with pancreatic cancer are almost equal to its incidence rates. The underlying mechanism of pancreatic tumor formation is rather complex. A number of biochemical and genetic abnormalities have been reported, which include mutations or overexpression of oncogenes (such as *KRAS, ERBB2, and AKT)* and tumor-suppressor genes (such as *P53*, *BRCA2*) (3-6). In addition, over-expression of growth factors and their receptors, such as TGF-beta, VEGF, and EGFR (6), have also been linked to pancreatic cancer.

The treatment regimens for pancreatic cancer have no substantial improvement over the past few decades (7). Currently, surgery is the main

therapeutic option since chemotherapy and radiation only achieve minimal effects due to rapid progression, late diagnosis, and drug resistance of pancreatic cancer (1). Unfortunately, only 15-20% of pancreatic cancer patients are amenable to curative resection while 80% of patients generally have nonresectable advanced or metastatic tumors (8). Furthermore, even in patients with resectable disease, the overall 5-year survival is 15%. Currently, gemcitabine is the standard therapeutic drug for treatment of pancreatic cancer. However, it only improves the disease symptoms with no significant survival benefits. Thus, novel agents for prevention and treatment of pancreatic cancers are highly desired.

Natural products appear to be promising sources of drugs for cancer treatment (9). Withaferin A (WA), a major active constituent purified from the Indian medicinal plant *Withania somnifera*, was shown to have antitumor, antiangiogenesis and radiosensitizing activity (10, 11). The anticancer activity of Withaferin A has been demonstrated in prostate cancer cells (12, 13), breast cancer cells (14), leukemia cells (15), and melanoma cells (16). It was shown that WA inhibits nuclear factor-κB (NF-κB) activation (11), induces apoptosis in prostate cancer cells through Par-4 induction (12), inhibits IκB kinase activation via a thioalkylation-sensitive redox mechanism (17), inhibits the chymotrypsin-like activity of proteasome (13), and targets the intermediate filament protein vimentin by covalently modifying the cysteine residue (18). In addition, WA also targets annexin II to induce Actin microfilament aggregation (19).

In our preliminary study, we found that withaferin A exhibited Hsp90 inhibition characteristics in pancreatic cancer cells by decreasing the levels of Hsp90 client proteins. Thus we intend to investigate the efficacy of WA and Hsp90 inhibition mechanisms in this study. Hsp90 is a molecular chaperone which mediates the folding, assembly, and maturation of many client proteins, including HER-2, EGFR, Akt, Raf-1, Cdk4, mutated p53, which are directly involved in the malignancy (20). Hsp90 has three distinct domains. The N-terminal domain has the ATP binding site, the middle domain may interact with clients, and the C-terminal domain is responsible for dimerization of Hsp90. An additional ATP binding site is also found to be present in the C-terminus. The ATP binding sites act as a conformational switch to regulate Hsp90 chaperone activity (21). In cancer cells, the newly synthesized oncogenic client proteins bind to Hsp90 to form an intermediate complex with other co-chaperones (such as Cdc37, Hop, Hsp70, Hsp40, and Hip). Upon ATP binding to Hsp90, client proteins and Hsp90 form a mature complex. This mature superchaperone complex catalyzes the conformational maturation of client proteins (22). These oncogenic client proteins stimulate cancer cell proliferation and survival. Several Hsp90 inhibitors, which block the ATP binding sites of Hsp90, have been developed and tested in preclinical and clinical models for their anticancer activity (23-26). Geldanamycin (GA, and its derivatives 17-AAG, IPI-504, 17-DMAG), radicicol and derivatives, purines and derivatives, pyrazoles and isoxazoles, sulfanyl analogues, resorcinol-bearing compounds, and 2-aminopyrimidine-bearing derivatives block the N-terminal ATP binding pocket, whereas novobiocin

(and its derivatives) and cisplatin block the C-terminal ATP binding pocket (23, 27-31). To date, many of these Hsp90 inhibitors have entered preclinical or phase I/II clinical studies (24, 25, 32, 33).

In this study, we investigate the efficacy and mechanism of withaferin A (WA) for Hsp90 inhibition and its use against pancreatic cancer. Our data suggest that withaferin A exhibits potent cytotoxicity against pancreatic cancer cells both *in vitro* and *in vivo* xenograft models. The anticancer activity of WA is partially due to its direct binding to Hsp90 C-terminus, and inhibiting Hsp90 chaperone activity, inducing Hsp90 client protein degradation through an ATP independent mechanism.

Materials and methods

Cell culture and reagents.

Human pancreatic cancer cell lines Panc-1, BxPC3 and MiaPaCa-2 were cultured in 10% FBS RPMI-1640 or 10% FBS DMEM at 37ºC and 5% CO_2. Withaferin A was purchased from Calbiochem, Inc. (San Diego, CA). The following antibodies were used for western blot: Akt (Cell Signaling, Beverly, MA), Hsp70 and Hop (StressGen, Victoria, BC, Canada), Cdk4, Cdc37 and Hsp90 (Santa Cruz, Santa Cruz, CA), Actin and p23 (Abcam, Cambridge, MA). Monoclonal Hsp90 antibody H9010 for immunoprecipitation was purchased from Alexis Biochemicals (San Diego, CA), and purified Hsp90β protein for ATP binding assay was a kind gift of Dr. David Toft (Mayo Clinic, Rochester, MN).

MTS assay.

Pancreatic cancer cells were seeded in 96-well plates at a density of 5000 cells per well. 24 hours later the cells were treated with increasing concentrations of WA as indicated. MTS assay was performed to assess cell viability after 48 h incubation. The IC_{50} value for cytotoxicity was estimated by WinNonlin software (Pharsight, Mountain View, CA).

Apoptosis study.

The Annexin V-EGFP Apoptosis Detection Kit was purchased from BioVision Research Products (Mountain View, CA) and used as recommended by manufacturer. Human pancreatic Panc-1 cells were treated with 1, 5, and 10 μM WA for 12 h, and stained with Annexin V-EGFP to analyze the phosphoserine inversion. Early apoptotic cells were observed with a fluorescence microscopy.

Withaferin A-Biotin pull down assay.

Withaferin A-Biotin (WA-biotin) was prepared and used in the pull down assay as described previously (19). Briefly, 500 μg of Panc-1 pancreatic cancer cell whole cell extracts or 5 μg of purified human Hsp90 beta, N-terminus Hsp90 beta, C-terminus Hsp90 beta and yeast Hsp90 were incubated with immobilized WA-Biotin for 2 h at 4 °C in TNEK buffer (5 mM Tris, pH 7.4; NP-40 1%; EDTA 2 mM; KCl 200 mM) supplemented with protease inhibitors. To perform competition assay, the samples were preincubated with 100 μM WA for 1 hr before add with WA-Biotin. The beads were then washed with TNEK buffer for 3 times, and were boiled in loading buffer for 4 min to isolate the bound proteins. Western blot was

carried out to analyze the levels of Hsp90 proteins.

ATP-sepharose binding assay.

The assay was performed as previously described (34, 35). Total of 5 µg of human hsp90β protein with DMSO, WA or 17-AAG were incubated on ice in 200 µl incubation buffer consisting of 10 mM Tris-HCl, 50 mM KCl, 5 mM $MgCl_2$, 2 mM DTT, 20 mM Na_2MoO_4, 0.01% Nonidet P-40, pH 7.5. After 30 min, 25 µl of pre-equilibrated γ-phosphate-linked ATP-Sepharose (Jena Bioscience GmbH, Jena, Germany) was added to tubes, which were then incubated at 37 °C for another 30 min with frequent mixing to resuspend the resin. Following incubation, the sepharose was washed, pelleted and analyzed by SDS-PAGE.

Coimmunoprecipitation and Western Blotting assay.

The general procedure for coimmunoprecipitation was described as follows. 500 µg of whole cell extracts was incubated with 5 µl H9010 anti-Hsp90 antibody or anti-P23 antibody for 1 h at 4^{o}C, rotating. 30 µl protein G agarose (Pierce, Rockford, IL) was added to each sample, and incubated for another 2 h at 4^{o}C. The beads were washed 3 times with PBS plus protease inhibitors. The beads were boiled in loading buffer for 4 min to isolate the bound proteins. Western blot was carried out to analyze the levels of coimmunoprecipitated proteins. Western blot was performed as previously described (35, 36). Non-reducing SDS-PAGE was used to analyze the disulfide-bonded protein as described previously (37). Isolation of triton-soluble and triton-insoluble proteins was performed as described by Chen et al (37).

Real-time PCR assay.

RT-PCR is carried out as described previously (36). Briefly, Panc-1 cancer cells are treated with 5 μM WA for 12 hrs. TRIzol reagents (Invitrogen, Carlsbad, CA) are used to extract total cellular RNAs as described in protocol provided by manufacturer. Superscript III first strand synthesis kit from Invitrogen is used to reverse transcribe the cDNA. Then the real-time PCR is carried out in ABI PRISM 7900T real-time PCR system (PerkinElmer, Branchburg, NJ) with SYBR Green PCR Master Mix (Applied Biosystems, Foster City, CA). The primers used in RT-PCR are as follows: Akt, forward, 5'-TCT ATG GCG CTG AGA TTG TG-3', reverse, 5'-CTT AAT GTG CCC GTC CTT GT-3'; Cdk4, forward, 5'-GAA ACT CTG AAG CCG ACC AG-3', reverse, 5'-GCC CTC TCA GTG TCC AGA AG-3'; glucocorticoid receptor (GR), forward, 5'-GAG AGG GGA GAT GTG ATG GA-3', reverse, 5'-GTT TTC ACT TGG GGC AGT GT-3'. Internal standard β-actin, forward, 5'-GCT CGT CGT CGA CAA CGG CTC-3'; reverse, 5'-CAA ACA TGC TCT GGG TCA TCT TCT C-3'. mRNA levels are calculated as fold change of control. After completion of the RT-PCR, Ct values (cycle numbers in which signal intensity equal to the threshold value) will be obtained from the software. For each samples, ΔCt is calculated as $\Delta Ct = Ct_{Akt/Cdk4/GR} - Ct_{actin}$. Then ΔΔCt is calculated as $\Delta\Delta Ct = \Delta Ct_{treatment} - \Delta Ct_{control}$. The fold change of the Akt/Cdk4/GR mRNA levels relative to control group are calculated as $2^{-\Delta\Delta Ct}$.

Pancreatic tumor xenograft.

The pancreatic tumor xenograft mouse model was used to test anticancer activity of WA similar to previous reports (35, 36). Briefly, 4 to 6-week old nu/nu

athymic female mice were obtained from Charles River Laboratories (Charles River, Wilmington, MA). Pancreatic cancer Panc-1 cells (5-10×10^6) were mixed with reconstituted basement membrane (Collaborative Research, Bedford, MA) and inoculated s.c. to the right and left flanks of the mice. When the tumors became palpable (~100 mm^3), mice were randomly divided into different groups for treatment (n= 6/group). WA was dissolved in the vehicle (10% DMSO, 40% Cremophor/ethanol (3:1), and 50% PBS) (13), and administered at 6 mg/kg or 3 mg/kg by i.p. injection for two continuous days. Then the dosing schedule was changed to two injections per week for 4 weeks. Tumor sizes and body weights were measured twice a week. After 30 days' drug treatment, and tumor sizes and body weights were monitored until 70 days.

RESULTS

Withaferin A inhibits proliferation in pancreatic cancer cells.

The antiproliferative effect of WA (Figure 2.1A) against human pancreatic cancer cell lines was examined by MTS assay. A 48-h exposure to different concentrations of WA induced a dose-dependent inhibition in cell proliferation. WA exhibited high cytotoxicity against Panc-1 cells with an IC50 of 1.24 μM (Figure 2.1B), whereas, WA showed relatively lower cytotoxicity against MiaPaca2 and BxPc3, with IC50s of 2.93 μM and 2.78 μM (Figure 2.1C and 2.1D). Overall, WA showed potent antiproliferative effect against these three human pancreatic cancer cell lines.

Withaferin A induces apoptosis in pancreatic cancer cells.

To illustrate that WA induces apoptosis in pancreatic cancer cells, annexin-V staining was conducted in Panc-1 cells with WA treatment. As shown in Figure 2.2, the Annexin-V positive staining cells accounted for 18.5±1.68, 46.8±5.22 and 68.1±7.14 of the overall cell population in Panc-1 cells treated with 1, 5, and 10 μM WA for 12 h, respectively. In contrast, only marginal apoptotic cells were observed in control Panc-1 cells.

Withaferin A induces Hsp90 client protein degradation.

WA exhibited potent cytotoxicity against pancreatic cancer cells and induced apoptosis in Panc-1 cells. To investigate the underlying mechanism, we screened a panel of protein level changes in Panc-1 cells in response to WA treatment. Hsp90 client proteins (Akt, Cdk4 and Glucocorticoid receptor (GR)) were observed to be decreased. These proteins exhibited time- and dose-dependent degradation in response to WA treatment (Figure 2.3A and 2.3B). After exposure to 10 μM WA for 6 h, Akt and Cdk4 protein levels started to decrease by 1.88- and 1.95- fold. After 24 h treatment, the protein levels were undetectable. GR protein levels decreased even faster and became undetectable as early as 2 h after exposure to 10 μM WA (Figure 2.3C). Previous studies have shown that these proteins are clients of Hsp90, and inhibiting Hsp90 chaperone activity would lead to the degradation of these proteins (35, 38). These data suggest that inhibition of Hsp90 chaperone activity might contribute to the anticancer activity of WA.

To further confirm inhibition of Hsp90 by WA, we examined two additional

protein expression level changes, Hsp70 and Cdk2. The induction of Hsp70 is another molecular signature in response to Hsp90 inhibition (39). As shown in Figure 2.3D, 10 μM WA increased the protein level of Hsp70 by 13.47-fold after 6 h while without affecting the Hsp90 protein level. To demonstrate WA specifically inhibits Hsp90, a non-Hsp90 client protein Cdk2 was examined. Indeed, Cdk2 levels were not significantly altered after WA treatment (Figure 2.3E). These data demonstrate that WA inhibited Hsp90 chaperone activity.

Withaferin A directly binds to Hsp90.

Previous study reported that Hsp90 is sensitive to cellular redox conditions and tend to form disulfide bond under oxidative stress (37, 40). In addition, susceptible cysteine residues in C-terminal Hsp90 were revealed including Cys-521, Cys-589/590 and Cys597 (41, 42). WA was demonstrated to be highly reactive with cysteine residues in proteins (43, 44), such as annexin II (19) and vimentin (18) to form covalent bonds. Therefore, we tested whether WA will bind to Hsp90 using WA-biotin pull down assay. The results show that WA-biotin successfully pulled down Hsp90 both from the cell lysate and purified full length human hsp90 (Figure 2.4A). To further illustrate the binding domains of Hsp90 with WA-biotin, we performed the pull down assay against Hsp90 fragments N-terminus Hsp90 (without cysteine residue), C-terminus Hsp90 (with cysteine residue), and full length yeast Hsp90 (without cysteine residues). As shown in Figure 2.4A, WA-biotin can only pull down C-terminus Hsp90 (with cysteine residues), but not N-terminus Hsp90 nor yeast Hsp90. Hence, WA-Biotin binding to Hsp90 is dependent on cysteine residues on Hsp90. In addition, the WA-biotin

binding to Hsp90 was in a competitive manner since 100 μM unlabeled WA preincubation for 1 hr would significantly decrease the WA-biotin binding to Hsp90 both in cell lysate and purified full length Hsp90 as well as C-terminus Hsp90 (Figure 2.4B).

Next we examined the aggregation of Hsp90 after WA treatment. Non-reducing gel electrophoresis was performed to detect the formation of Hsp90 aggregation, which would exhibit a slower migration pattern and appeared as higher molecular weight bands. As shown in Figure 2.4C, WA induced Hsp90 aggregation in a dose-dependent manner.

Withaferin A induces Hsp90 client protein degradation through proteasome.

Since classical Hsp90 inhibitor induced Hsp90 client protein degradation was proteasome mediated, we further investigated whether WA induced Hsp90 client protein degradation was also proteasome-dependent. Two proteasome inhibitors Bortezomib and MG132 were used to reverse the protein degradation. As shown in Figure 2.5A, preincubation with 10 μM Bortezomib and MG132 could rescue the degradation of Hsp90 client proteins. All of the three Hsp90 client proteins (Akt, Cdk4, and GR) under investigation were found to accumulate in the triton-insoluble fraction after combination treatment of WA and proteasomal inhibitors, while WA alone decreased the levels of Akt, Cdk4 and GR. In addition, we carried out RT-PCR to examine whether WA affects the mRNA levels of these three genes. Figure 2.5B shows that WA treatment did not change the mRNA levels of these three genes. These data suggest that WA induced Hsp90 client protein degradation is proteasome-dependent and WA did not affect the

transcriptional level of Hsp90 client proteins.

Withaferin A does not block ATP binding to Hsp90.

Most of current Hsp90 inhibitors, including geldanamycin, 17-AAG, IPI-504 and 17-DMAG, bind to the Hsp90 ATP binding pocket which prevents client protein refolding (23, 27). To investigate whether WA also change the ATP binding to Hsp90, an ATP-sepharose beads pull down assay was performed. As shown in Figure 2.6, 5 μM 17-AAG completely blocked ATP beads binding to Hsp90; in contrast, 5, 10, and 20 μM WA did not block ATP beads binding to Hsp90. As a negative control, 20 μM celastrol did not block ATP beads binding to Hsp90, which is consistent with previous study (35).

Withaferin A dissociates Hsp90-Cdc37 complex in pancreatic cancer cells.

Since Hsp90 forms a superchaperone complex with other cochaporones, including Hsp70, P23, Cdc37, Hop and immunophilins, we further tested the alteration of Hsp90 superchaperone complexes in response to WA treatment by using co-immunoprecipitation (coIP) assay in Panc-1 cells. Panc-1 cells were treated with 10 μM WA for 1, 6, 12, and 24 h, coIP Hsp90 was carried out. The coIP samples were then immunobloted with anti-Cdc37 antibody. Figure 2.7A shows that 10 μM WA completely disrupted the Hsp90-Cdc37 complex as early as 1 h post treatment. In contrast, the Hsp90-Hop complex was not decreased by WA treatment. Figure 2.7B shows the dose-dependence of WA on disrupting the Hsp90-Cdc37 complex. After exposure to WA for 24 h, 1 μM WA decreased the amount of Cdc37 by 2.04-folds, which was pulled down by Hsp90. WA (5 μM) completely blocked the Hsp90-Cdc37 complex. To investigate whether the

decreased levels of Cdc37 in the coIP results were due to the expression level alteration of Cdc37, western blotting was carried out to examine the protein level of Cdc37 without coIP. Figure 2.7C shows that WA did not change the Cdc37 protein level. These data further confirmed that the decreased level of Cdc37 by WA in coIP Hsp90 samples was due to the dissociation of Hsp90-Cdc37 complex.

P23 has been demonstrated to bind directly to Hsp90 when it is in the ATP bound conformation (45). Classical Hsp90 inhibitors like geldanamycin (GA) and PU24FCl bind to the ATP binding pocket and lock the Hsp90 in the intermediate superchaperone complex (46, 47), hence Hsp90 will no longer be available to bind to p23. As shown in Figure 2.7D, coIP with P23 showed that WA did not change Hsp90-P23 association, resulting in equal amount of Hsp90 pulled down by P23. In contrast, 17-AAG decreased the Hsp90-P23 interaction dramatically, which was consistent with ATP binding assay (Fig 2.7D).

Withaferin A exhibits anticancer activity in pancreatic cancer xenografts.

The data described above showed that WA is an Hsp90 inhibitor by binding to Hsp90, which resulted in Hsp90 client protein degradation and apoptosis in pancreatic cancer cells *in vitro*. We next examined WA's therapeutic efficacy *in vivo*. Pancreatic cancer (Panc-1) xenografts were generated in female nude mice. When the tumors reached 100 mm^3, the mice were randomly divided into three groups (n=6). The mice were treated i.p. with either vehicle control or WA at 3.0 mg/kg or 6.0 mg/kg. After 70 days, control tumors grew to an average size of 1014±176 mm^3. In contrast, tumors from 3.0 mg/kg and 6.0 mg/kg WA-treatment group grew to an average size of 701±268 and 422±95 mm^3, corresponding to 30%

and 58% inhibition, respectively ($P < 0.05$; Figure .8A). Systemic toxicity of WA was analyzed by measuring the animal weights. As shown in Figure 2.8B, the higher dose (6 mg/kg) WA treatment group had negligible weight loss (<10%) during the first week treatment, regained their weight from the second week, and had a 12% increase in body weight increase after 70 days. Meanwhile, mice in control group and the 3 mg/kg WA treatment group did not display weight loss. These data demonstrated WA shows potential anticancer effect against pancreatic cancer *in vivo* without significant toxicity.

Discussion

In the present study, we evaluated the anticancer efficacy of WA against pancreatic cancer. WA treatment significantly induced antiproliferative effects against Panc-1, BxPc3 and MiaPaca2 pancreatic cancer cells in cell culture and exhibited potent tumor growth inhibition of pancreatic cancer xenografts. Our data showed that WA directly binds to Hsp90 and leads to the degradation of Hsp90 client proteins through an ATP independent mechanism.

Hsp90 is crucial for maintaining the native conformation of proteins. It was found to be highly expressed in various cancerous tissues compared to the non-cancerous tissue (48, 49), which provides cancer cells selectivity by Hsp90 inhibitor (22, 50). For instance, 17-AAG binding affinity to Hsp90 in cancer cells is 100-fold higher than that to Hsp90 in normal cells (22). Therefore, inhibiting the Hsp90 chaperone activity emerged as a new molecular target for developing anticancer agents because of its high selectivity and simultaneous knockdown of

various oncogenic proteins. Several Hsp90 inhibitors have been developed and tested in preclinical and clinical models for their anticancer activity including 17-AAG, 17-DMAG and IPI-504 (23-26).

In addition to ATP binding blockage of Hsp90, researchers have also identified other Hsp90 inhibition mechanisms. For example, the histone deacetylase inhibitors (hydroxamic acid analogue, LAQ 824 and LBH589) were shown to induce the hyperacetylation of Hsp90, resulting in inhibition of ATP binding and attenuation of chaperone activity (51). In this study, we demonstrated that WA inhibited Hsp90 chaperone activity to induce Hsp90 client protein degradation. However, unlike the classical Hsp90 inhibitor, WA directly binds to Hsp90 C-terminus. These were evidenced by the pull-down assay of WA-Biotin to C-terminus Hsp90 containing cysteine residues but not N-terminus Hsp90 or yeast Hsp90 (without cysteine residues). In addition, the binding of WA-biotin to Hsp90 could be competitively inhibited by unlabeled WA. Furthermore, ATP-sepharose beads pull down assay did not show any inhibition of WA to ATP binding to Hsp90. These data also further suggest that WA inhibition of Hsp90 is not through an ATP dependent mechanism, which is different from the classical Hsp90 inhibitors.

To further confirm that WA binds to Hsp90 reactive cysteine residues, we examined whether exogenous thiols in cell culture would rescue the WA-inhibition to Hsp90. N-acetylcysteine (NAC) is a natural sulfur-containing amino acid derivative and is a thiol antioxidant (52). Preincubation of Panc-1 cells with NAC reversed WA induced Hsp90 aggregation (data not shown), whereas NAC

failed to reverse a mild oxidant, hydrogen peroxide (H_2O_2) induced Hsp90 aggregation. Although geldanamycin and its derivatives were shown to be able to produce ROS (53), 17-AAG was unable to induce Hsp90 aggregation. In addition, WA induced Hsp90 client protein degradation and Hsp70 induction were also rescued by NAC pretreatment (Data not shown). Regardless the mechanism of NAC in reverse WA effects (chemical reaction or cellular response), these data suggest that WA may inhibit Hsp90 function through cysteine of the C-terminal Hsp90. However, the specific cysteine residues that WA binds to need to be further elucidated.

One interesting phenomenon we observed is that WA disrupts Hsp90-Cdc37 complex. Cdc37 is believed to play a central role in regulating kinase client proteins in the intermediate Hsp90 superchaperone complex. A client protein first binds the Hsp70/Hsp40 chaperone complex and then interacts with Cdc37. Hsp90 is subsequently recruited to the complex via p60/Hop (54). Similar to Hsp90, Cdc37 is also upregulated in cancer cells. Cdc37 is highly expressed in all prostate tumors and absent from normal prostate epithelium. Transgenic mice expressing Cdc37 in the prostate epithelium have displayed dramatic proliferative disorders in the prostate, including epithelial hyperplasia and dysplasia (55). Hepatocellular carcinoma also overexpresses Cdc37 and Hsp90 compared to normal and surrounding tissues (56). Previous study showed that Celastrol inhibited Hsp90 chaperone activity by blocking Hsp90-Cdc37 interactions and led to Hsp90 client protein degradation for its anticancer activity (35). Celastrol also binds to C-terminus of Hsp90 (Zhang *et al.*, unpublished data). In the present

study, we found that WA disrupts Hsp90-Cdc37 complex. WA blockage of Hsp90-Cdc37 complex might be a result of WA binding-induced conformational change of Hsp90 or other unknown mechanisms. Further study is warranted to elucidate these mechanisms. It is worth noting that WA inhibition of Hsp90 chaperone activity should not be solely due to the disruption of Hsp90-Cdc37 association. As described earlier, Cdc37 helps load its client proteins onto the Hsp90 chaperone complex. The client proteins of Cdc37 include many kinases, such as Raf-1, Akt and Src family kinases, and steroid receptors such as androgen receptor but not the closely related glucocorticoid receptor (GR) (57). However, our data showed that WA treatment could also induce the degradation of GR. These data suggest that WA inhibits Hsp90 chaperone activity might be also due to the direct binding of WA to Hsp90.

Furthermore, P23 and Cdc37 were demonstrated to bind to the same sites on the N-terminus of Hsp90, and binding of P23 and Cdc37 to Hsp90 is mutually exclusive (35, 58). Cdc37 and P23 bind to Hsp90 at different stages of the chaperone cycle: Cdc37 binds to Hsp90 in the intermediate complex; whereas P23 binds to Hsp90 in the mature complex in which Hsp90 adopts a different conformation from the intermediate complex. Classical Hsp90 inhibitors such as geldanamycin and 17-AAG lock Hsp90 in the intermediate complex, hence preventing P23 binding to Hsp90 (35). Our data showed that WA did not interfere with the Hsp90-P23 interaction, while 17-AAG induced Hsp90-P23 dissociation. There are two possible mechanisms for WA induced Hsp90-Cdc37 dissociation but not Hsp90-P23 dissociation: one is that WA binds directly to the cysteine

residues on the C-terminus of Hsp90, resulting in a conformational change of Hsp90 which preventing Cdc37 but not P23 from binding; another is that besides Hsp90, WA also reacts with cysteines in Cdc37 which contributes to the disruption of Hsp90-Cdc37 interaction, however, although cysteine residues are present in P23, they are not accessible to WA, thus providing a selectivity of action. It is important to note that this is rather speculative and needs to be further confirmed.

Previous studies have shown that the 4β-hydroxy-5β, 6β-epoxy-2-en-1-one moiety and unsaturated lactone are critical for WA's biological function (59). The epoxide within B ring and the unsaturated lactone ring were demonstrated to be involved in Michael addition thioalkylation reactions (43, 44, 60). In addition, the ketone containing unsaturated A-ring could also react with thiol-nucleophiles and act as Michael acceptor (59). Thus these three functional groups could be crucial for the interaction between WA and Hsp90. Gedunin and aforementioned Celastrol are two natural products exhibiting Hsp90 inhibitory activity. They modulate Hsp90 activity by a mechanism different from classical Hsp90 inhibitors such as GA, since they do not competitively bind to the ATP-binding pocket of Hsp90 (47). The exact mechanism how Gedunin inhibits Hsp90 is still unknown. Gedunin also possesses a ketone containing unsaturated A ring and an additional epoxide which are similar to WA. Although the preliminary structure-activity studies of Gedunin revealed that the α, β-unsaturated ketone within the A ring of Gedunin does not behave as a Michael acceptor (61), the epoxide on Gedunin might act as a Michael acceptor and thus Gedunin might also inhibit

Hsp90 in a way similar to WA. On the other hand, Celastrol also has electrophilic sites within the unsaturated A and B ring and was shown to react with thiols in proteins (62, 63). Our unpublished data by Zhang et al. indicate that Celastrol binds to C-terminus Hsp90; hence, it would not be surprised if Celastrol inhibits Hsp90 via binding to reactive cysteine residues of Hsp90 (64).

Withaferin A belongs to a large family of natural products steroidal lactone triterpenoids, the withanolides, which are major constituents purified from medicinal plant *Withania somnifera* and its related solanaceae species such as *Physalis*, *Nicandra*, *Dunalia*, *Datura*, *Jaborosa*, and *Acnistus* (65). The withanolides are demonstrated to have antitumor, antibacterial, anti-inflammatory, antidepressant, antioxidant, antiulcer, cytotoxic, quinone reductase induction, antileishmanial, antitrypanosomal, immunosuppressive, cognition-enhancing and memory-improving effects, as well as hypotensive, bradycardic and respiratory-stimulant action (66-68). As a prototype of the withanolides, Withaferin A has been studied extensively. Up to date, over 130 withanolides are known and more than 40 withanolides are isolated (69). The individual withanolides were purified and evaluated for their biological functions. For instance, some newly isolated withanolides have been shown to have cytotoxic activity, including Withangulatin B, Withangulatin C, Withangulatin G, Withangulatin H, and Withangulatin I (68). The structure-activity studies further confirmed that the unsaturated A ring and epoxide are important for the cytotoxic activity of withanolides (67). Another Withanolide, Withangulatin A was shown to inhibit topoisomerase II and induce heat shock response (70, 71). Although DNA damage mediated by

topoisomerase II inhibitors has been shown to induce heat shock response (72), another topoisomerase II inhibitor VM-26 could not induce heat shock response in the same cell line as Withangulatin A (71). Therefore, Withangulatin A induces heat shock response through a way other than topoisomerase II inhibition mediated DNA damage. Considering the quasi identical structure (the same unsaturated ketone containing A ring, epoxide containing B ring and unsaturated lactone ring) of Withangulatin A to Withaferin A, Withangulatin A might induce heat shock response by inhibition of Hsp90 (73). In addition, Tubocapsenolide A (TA), another withanolide possessing the three key functional groups, showed high cytotoxicity against cancer cells and exhibited Hsp90 inhibitory activity (37). TA induces Hsp90 client protein degradation and induces Hsp90 dimer formation. Although there's no direct evidence that TA binds to Hsp90, TA could inhibit Hsp90 through binding to the reactive cysteine residues of Hsp90 like WA.

In conclusion, our data suggest that withaferin A represents a new type of Hsp90 inhibitor. It directly binds Hsp90, inhibits Hsp90 with an ATP-independent mechanism, induces Hsp90 client protein degradation and disrupts the Hsp90-Cdc37 interaction. These Hsp90 inhibition mechanisms of withaferin A may partially contribute to its anticancer activity in vitro pancreatic cancer cell lines and in vivo pancreatic cancer xenografts. These data provide a potential of withaferin A as a novel Hsp90 inhibitor for use against pancreatic cancers.

References

1. Bardeesy N, DePinho RA. Pancreatic cancer biology and genetics. Nat Rev Cancer 2002; 2: 897-909.
2. Jemal A, Siegel R, Ward E, Murray T, Xu J, Thun MJ. Cancer statistics, 2007. CA Cancer J Clin 2007; 57: 43-66.
3. Di Costanzo F, Carlini P, Doni L, et al. Gemcitabine with or without continuous infusion 5-FU in advanced pancreatic cancer: a randomised phase II trial of the Italian oncology group for clinical research (GOIRC). British Journal of Cancer 2005; 93: 185-9.
4. Kindler HL, Dugan WM, Hochster H, et al. Phase II study of pemetrexed plus gemcitabine in advanced pancreatic cancer. American Journal of Cancer (Auckland, New Zealand) 2005; 4: 185-91.
5. Xiong HQ. Molecular targeting therapy for pancreatic cancer. Cancer Chemother Pharmacol 2004; 54 Suppl 1: S69-77.
6. Buchler P, Reber HA, Buchler M, et al. Hypoxia-inducible factor 1 regulates vascular endothelial growth factor expression in human pancreatic cancer. Pancreas 2003; 26: 56-64.
7. Michaud DS. Epidemiology of pancreatic cancer. Minerva Chir 2004; 59: 99-111.
8. Schnall SF, Macdonald JS. Chemotherapy of adenocarcinoma of the pancreas. Semin Oncol 1996; 23: 220-8.
9. Newman DJ, Cragg GM, Snader KM. Natural products as sources of new drugs over the period 1981-2002. J Nat Prod 2003; 66: 1022-37.
10. Shohat B, Gitter S, Abraham A, Lavie D. Antitumor activity of withaferin A (NSC-101088). Cancer chemotherapy reports 1967; 51: 271-6.
11. Mohan R, Hammers HJ, Bargagna-Mohan P, et al. Withaferin A is a potent inhibitor of angiogenesis. Angiogenesis 2004; 7: 115-22.
12. Srinivasan S, Ranga RS, Burikhanov R, Han SS, Chendil D. Par-4-dependent apoptosis by the dietary compound withaferin A in prostate cancer cells. Cancer Res 2007; 67: 246-53.
13. Yang H, Shi G, Dou QP. The tumor proteasome is a primary target for the natural anticancer compound Withaferin A isolated from "Indian winter cherry". Mol Pharmacol 2007; 71: 426-37.
14. Stan SD, Hahm ER, Warin R, Singh SV. Withaferin A causes FOXO3a- and Bim-dependent apoptosis and inhibits growth of human breast cancer cells in vivo. Cancer Res 2008; 68: 7661-9.
15. Malik F, Kumar A, Bhushan S, et al. Reactive oxygen species generation and mitochondrial dysfunction in the apoptotic cell death of human myeloid leukemia HL-60 cells by a dietary compound withaferin A with concomitant protection by N-acetyl cysteine. Apoptosis 2007; 12: 2115-33.
16. Devi PU, Kamath R, Rao BS. Radiosensitization of a mouse melanoma by withaferin A: in vivo studies. Indian J Exp Biol 2000; 38: 432-7.
17. Kaileh M, Vanden Berghe W, Heyerick A, et al. Withaferin a strongly elicits IkappaB kinase beta hyperphosphorylation concomitant with potent inhibition of its kinase activity. J Biol Chem 2007; 282: 4253-64.

18. Bargagna-Mohan P, Hamza A, Kim YE, et al. The tumor inhibitor and antiangiogenic agent withaferin A targets the intermediate filament protein vimentin. Chem Biol 2007; 14: 623-34.
19. Falsey RR, Marron MT, Gunaherath GM, et al. Actin microfilament aggregation induced by withaferin A is mediated by annexin II. Nat Chem Biol 2006; 2: 33-8.
20. Rowlands MG, Newbatt YM, Prodromou C, Pearl LH, Workman P, Aherne W. High-throughput screening assay for inhibitors of heat-shock protein 90 ATPase activity. Anal Biochem 2004; 327: 176-83.
21. Prodromou C, Roe SM, O'Brien R, Ladbury JE, Piper PW, Pearl LH. Identification and structural characterization of the ATP/ADP-binding site in the Hsp90 molecular chaperone. Cell 1997; 90: 65-75.
22. Kamal A, Thao L, Sensintaffar J, et al. A high-affinity conformation of Hsp90 confers tumour selectivity on Hsp90 inhibitors. Nature 2003; 425: 407-10.
23. Chiosis G. Targeting chaperones in transformed systems--a focus on Hsp90 and cancer. Expert Opin Ther Targets 2006; 10: 37-50.
24. Adams J, Elliott PJ. New agents in cancer clinical trials. Oncogene 2000; 19: 6687-92.
25. Egorin MJ, Zuhowski EG, Rosen DM, Sentz DL, Covey JM, Eiseman JL. Plasma pharmacokinetics and tissue distribution of 17-(allylamino)-17-demethoxygeldanamycin (NSC 330507) in CD2F1 mice1. Cancer Chemother Pharmacol 2001; 47: 291-302.
26. Ramanathan RK, Trump DL, Eiseman JL, et al. Phase I pharmacokinetic-pharmacodynamic study of 17-(allylamino)-17-demethoxygeldanamycin (17AAG, NSC 330507), a novel inhibitor of heat shock protein 90, in patients with refractory advanced cancers. Clin Cancer Res 2005; 11: 3385-91.
27. Neckers L. Development of small molecule Hsp90 inhibitors: utilizing both forward and reverse chemical genomics for drug identification. Curr Med Chem 2003; 10: 733-9.
28. Janin YL. Heat shock protein 90 inhibitors. A text book example of medicinal chemistry? J Med Chem 2005; 48: 7503-12.
29. Taldone T, Sun W, Chiosis G. Discovery and development of heat shock protein 90 inhibitors. Bioorg Med Chem 2009; 17: 2225-35.
30. Powers MV, Workman P. Inhibitors of the heat shock response: biology and pharmacology. FEBS Lett 2007; 581: 3758-69.
31. Whitesell L, Lindquist SL. HSP90 and the chaperoning of cancer. Nat Rev Cancer 2005; 5: 761-72.
32. Amin K, Ip C, Jimenez L, Tyson C, Behrsing H. In vitro detection of differential and cell-specific hepatobiliary toxicity induced by geldanamycin and 17-allylaminogeldanamycin using dog liver slices. Toxicol Sci 2005; 87: 442-50.
33. Schnur RC, Corman ML, Gallaschun RJ, et al. erbB-2 oncogene inhibition by geldanamycin derivatives: synthesis, mechanism of action, and structure-activity relationships. Journal of Medicinal Chemistry 1995; 38: 3813-20.
34. Grenert JP, Sullivan WP, Fadden P, et al. The amino-terminal domain of heat shock protein 90 (hsp90) that binds geldanamycin is an ATP/ADP switch

domain that regulates hsp90 conformation. Journal of Biological Chemistry 1997; 272: 23843-50.
35. Zhang T, Hamza A, Cao X, et al. A novel Hsp90 inhibitor to disrupt Hsp90/Cdc37 complex against pancreatic cancer cells. Mol Cancer Ther 2008; 7: 162-70.
36. Cao X, Bloomston M, Zhang T, et al. Synergistic antipancreatic tumor effect by simultaneously targeting hypoxic cancer cells with HSP90 inhibitor and glycolysis inhibitor. Clin Cancer Res 2008; 14: 1831-9.
37. Chen WY, Chang FR, Huang ZY, Chen JH, Wu YC, Wu CC. Tubocapsenolide A, a novel withanolide, inhibits proliferation and induces apoptosis in MDA-MB-231 cells by thiol oxidation of heat shock proteins. J Biol Chem 2008; 283: 17184-93.
38. Blagosklonny MV. Hsp-90-associated oncoproteins: Multiple targets of geldanamycin and its analogs. Leukemia 2002; 16: 455-62.
39. Banerji U, Walton M, Raynaud F, et al. Pharmacokinetic-pharmacodynamic relationships for the heat shock protein 90 molecular chaperone inhibitor 17-allylamino, 17-demethoxygeldanamycin in human ovarian cancer xenograft models. Clin Cancer Res 2005; 11: 7023-32.
40. Cumming RC, Andon NL, Haynes PA, Park M, Fischer WH, Schubert D. Protein disulfide bond formation in the cytoplasm during oxidative stress. J Biol Chem 2004; 279: 21749-58.
41. Nardai G, Sass B, Eber J, Orosz G, Csermely P. Reactive cysteines of the 90-kDa heat shock protein, Hsp90. Arch Biochem Biophys 2000; 384: 59-67.
42. Martinez-Ruiz A, Villanueva L, Gonzalez de Orduna C, et al. S-nitrosylation of Hsp90 promotes the inhibition of its ATPase and endothelial nitric oxide synthase regulatory activities. Proc Natl Acad Sci U S A 2005; 102: 8525-30.
43. Fuska J, Fuskova A, Rosazza JP, Nicholas AW. Novel cytotoxic and antitumor agents. IV. Withaferin A: relation of its structure to the in vitro cytotoxic effects on P388 cells. Neoplasma 1984; 31: 31-6.
44. Oh JH, Lee TJ, Park JW, Kwon TK. Withaferin A inhibits iNOS expression and nitric oxide production by Akt inactivation and down-regulating LPS-induced activity of NF-kappaB in RAW 264.7 cells. Eur J Pharmacol 2008; 599: 11-7.
45. Sullivan W, Stensgard B, Caucutt G, et al. Nucleotides and two functional states of hsp90. J Biol Chem 1997; 272: 8007-12.
46. Johnson JL, Toft DO. A novel chaperone complex for steroid receptors involving heat shock proteins, immunophilins, and p23. J Biol Chem 1994; 269: 24989-93.
47. Hieronymus H, Lamb J, Ross KN, et al. Gene expression signature-based chemical genomic prediction identifies a novel class of HSP90 pathway modulators. Cancer Cell 2006; 10: 321-30.
48. Yufu Y, Nishimura J, Nawata H. High constitutive expression of heat shock protein 90 alpha in human acute leukemia cells. Leuk Res 1992; 16: 597-605.

49. Ogata M, Naito Z, Tanaka S, Moriyama Y, Asano G. Overexpression and localization of heat shock proteins mRNA in pancreatic carcinoma. Journal of Nippon Medical School 2000; 67: 177-85.
50. Plescia J, Salz W, Xia F, et al. Rational design of shepherdin, a novel anticancer agent. Cancer Cell 2005; 7: 457-68.
51. Nimmanapalli R, Fuino L, Bali P, et al. Histone deacetylase inhibitor LAQ824 both lowers expression and promotes proteasomal degradation of Bcr-Abl and induces apoptosis of imatinib mesylate-sensitive or -refractory chronic myelogenous leukemia-blast crisis cells. Cancer Res 2003; 63: 5126-35.
52. Deneke SM. Thiol-based antioxidants. Curr Top Cell Regul 2000; 36: 151-80.
53. Fukuyo Y, Inoue M, Nakajima T, et al. Oxidative stress plays a critical role in inactivating mutant BRAF by geldanamycin derivatives. Cancer Res 2008; 68: 6324-30.
54. Mandal AK, Lee P, Chen JA, et al. Cdc37 has distinct roles in protein kinase quality control that protect nascent chains from degradation and promote posttranslational maturation. J Cell Biol 2007; 176: 319-28.
55. Stepanova L, Yang G, DeMayo F, et al. Induction of human Cdc37 in prostate cancer correlates with the ability of targeted Cdc37 expression to promote prostatic hyperplasia. Oncogene 2000; 19: 2186-93.
56. Pascale RM, Simile MM, Calvisi DF, et al. Role of HSP90, CDC37, and CRM1 as modulators of P16(INK4A) activity in rat liver carcinogenesis and human liver cancer. Hepatology 2005; 42: 1310-9.
57. MacLean M, Picard D. Cdc37 goes beyond Hsp90 and kinases. Cell Stress Chaperones 2003; 8: 114-9.
58. Siligardi G, Hu B, Panaretou B, Piper PW, Pearl LH, Prodromou C. Co-chaperone regulation of conformational switching in the Hsp90 ATPase cycle. J Biol Chem 2004; 279: 51989-98.
59. Yokota Y, Bargagna-Mohan P, Ravindranath PP, Kim KB, Mohan R. Development of withaferin A analogs as probes of angiogenesis. Bioorg Med Chem Lett 2006; 16: 2603-7.
60. Liang MC, Bardhan S, Pace EA, et al. Inhibition of transcription factor NF-kappaB signaling proteins IKKbeta and p65 through specific cysteine residues by epoxyquinone A monomer: correlation with its anti-cancer cell growth activity. Biochem Pharmacol 2006; 71: 634-45.
61. Brandt GE, Schmidt MD, Prisinzano TE, Blagg BS. Gedunin, a novel hsp90 inhibitor: semisynthesis of derivatives and preliminary structure-activity relationships. J Med Chem 2008; 51: 6495-502.
62. Lee JH, Koo TH, Yoon H, et al. Inhibition of NF-kappa B activation through targeting I kappa B kinase by celastrol, a quinone methide triterpenoid. Biochem Pharmacol 2006; 72: 1311-21.
63. Trott A, West JD, Klaic L, et al. Activation of heat shock and antioxidant responses by the natural product celastrol: transcriptional signatures of a thiol-targeted molecule. Mol Biol Cell 2008; 19: 1104-12.
64. Zhang T, Li Y, Yu Y, Zou P, Jiang Y, Sun D. Characterization of celastrol to inhibit hsp90 and cdc37 interaction. J Biol Chem 2009; 284: 35381-9.

65. Kuroyanagi M, Arakawa T, Hirayama Y, Hayashi T. Antibacterial and antiandrogen flavonoids from Sophora flavescens. J Nat Prod 1999; 62: 1595-9.
66. Mirjalili MH, Moyano E, Bonfill M, Cusido RM, Palazon J. Steroidal lactones from Withania somnifera, an ancient plant for novel medicine. Molecules 2009; 14: 2373-93.
67. Damu AG, Kuo PC, Su CR, et al. Isolation, structures, and structure - cytotoxic activity relationships of withanolides and physalins from Physalis angulata. J Nat Prod 2007; 70: 1146-52.
68. Lee SW, Pan MH, Chen CM, Chen ZT. Withangulatin I, a new cytotoxic withanolide from Physalis angulata. Chem Pharm Bull (Tokyo) 2008; 56: 234-6.
69. Tursunava RN, Maslennikova VA, NK A. Withanolides in the vegetable kingdom Chem Nat Comp 1977; 13: 131-8.
70. Juang JK, Huang HW, Chen CM, Liu HJ. A new compound, withangulatin A, promotes type II DNA topoisomerase-mediated DNA damage. Biochem Biophys Res Commun 1989; 159: 1128-34.
71. Lee WC, Lin KY, Chen CM, Chen ZT, Liu HJ, Lai YK. Induction of heat-shock response and alterations of protein phosphorylation by a novel topoisomerase II inhibitor, withangulatin A, in 9L rat brain tumor cells. J Cell Physiol 1991; 149: 66-76.
72. Krueger JH, Walker GC. groEL and dnaK genes of Escherichia coli are induced by UV irradiation and nalidixic acid in an htpR+-dependent fashion. Proc Natl Acad Sci U S A 1984; 81: 1499-503.
73. Zaarur N, Gabai VL, Porco JA, Jr., Calderwood S, Sherman MY. Targeting heat shock response to sensitize cancer cells to proteasome and Hsp90 inhibitors. Cancer Res 2006; 66: 1783-91.

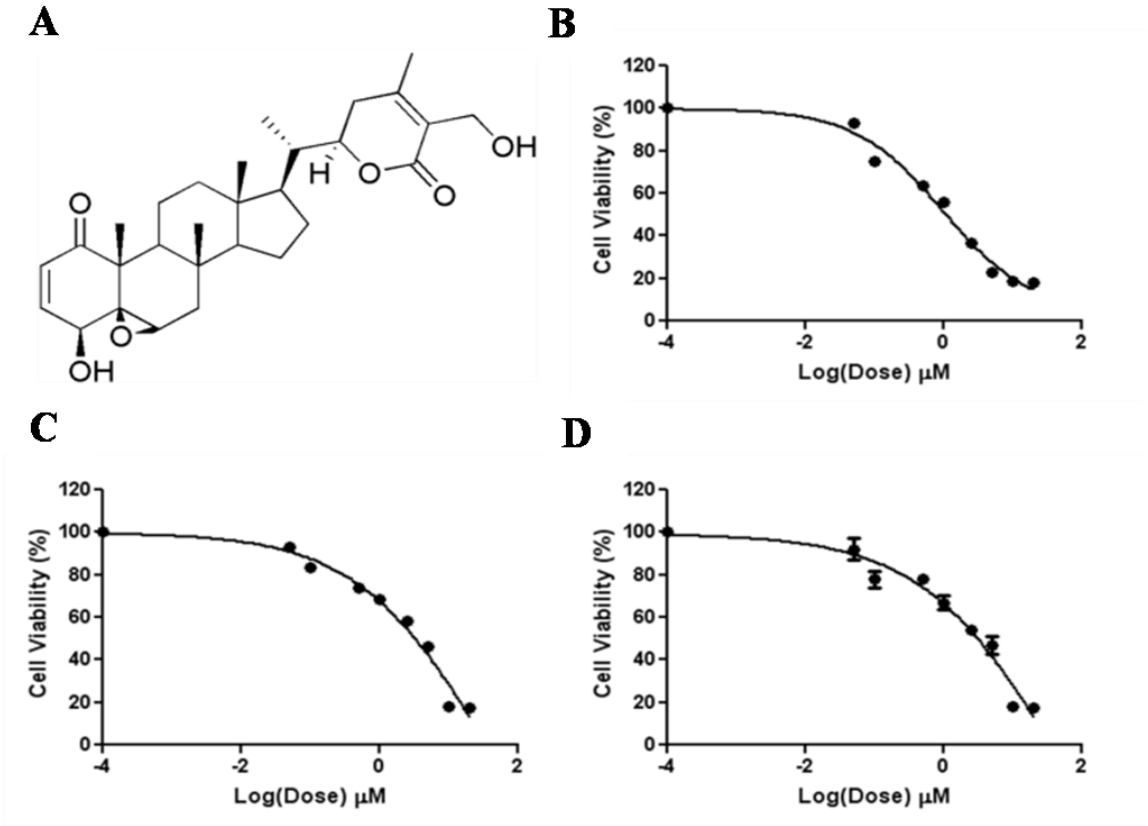

Figure 2.1 Anticancer effect of withaferin A in pancreatic cancer cells. A. Chemical structure of WA. B. Effect of WA treatment on viability of Panc-1 cells. Panc-1 cells were seeded in 96-well plates at a density of 5000 cells per well. 24 hours later the cells were subjected to WA treatment with concentrations of 0.05, 0.1, 0.5, 1.0, 2.5, 5, 10, and 20 μM. MTS assay was performed to assess cell viability after 48 h incubation. **C. Effect of WA treatment on viability of MiaPaCa-2 cells.** Viability of MiaPaCa2 cells after WA treatment was assessed similar to B. **D. Effect of WA treatment on viability of BxPc-3 cells.** Viability of BxPc3 cells after WA treatment was assessed similar to B.

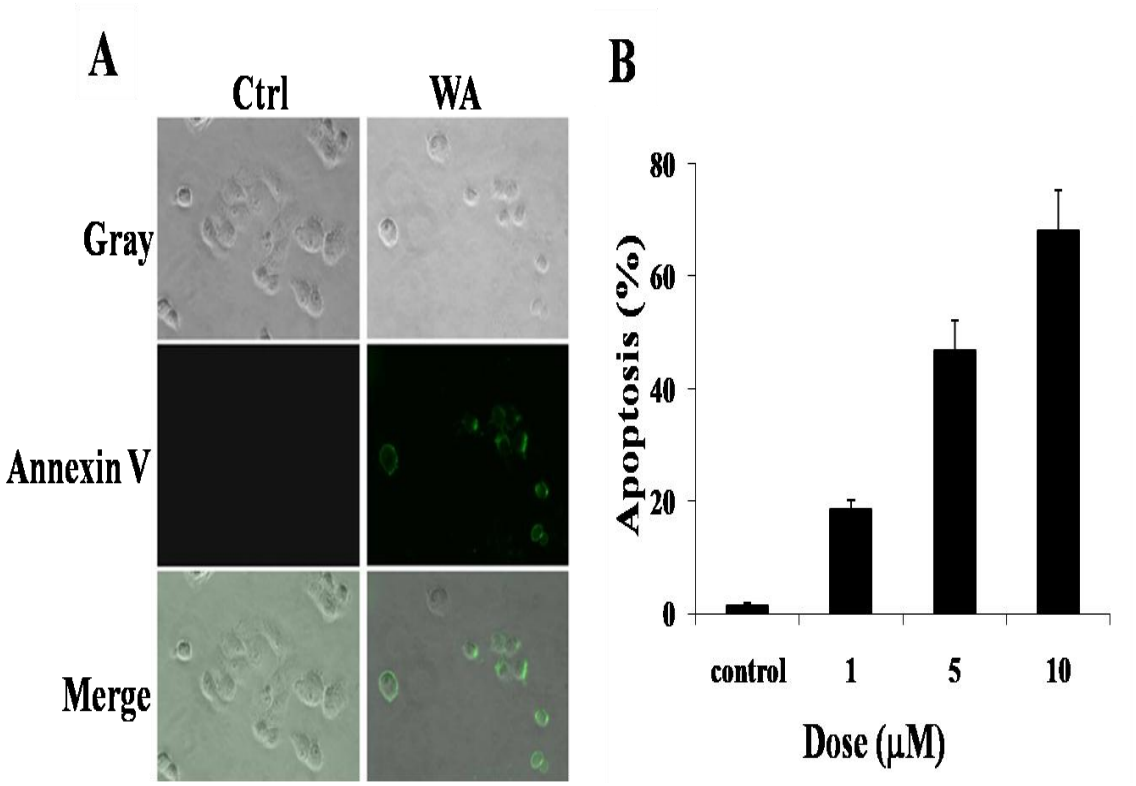

Figure 2.2 Withaferin A induces apoptosis in pancreatic cancer cells. A. Representative images from one of four independent experiments. Panc-1 cells were treated with 1, 5, and 10 μM WA for 12 h. Cells were stained with Annexin V-EGFP (green). Apoptotic cells were observed under fluorescent microscope. **B. Quantification of WA induced apoptotic cells.** The percentage of apoptotic cells were calculated as Annexin-EGFP positive cells divided by the total cancer cells.

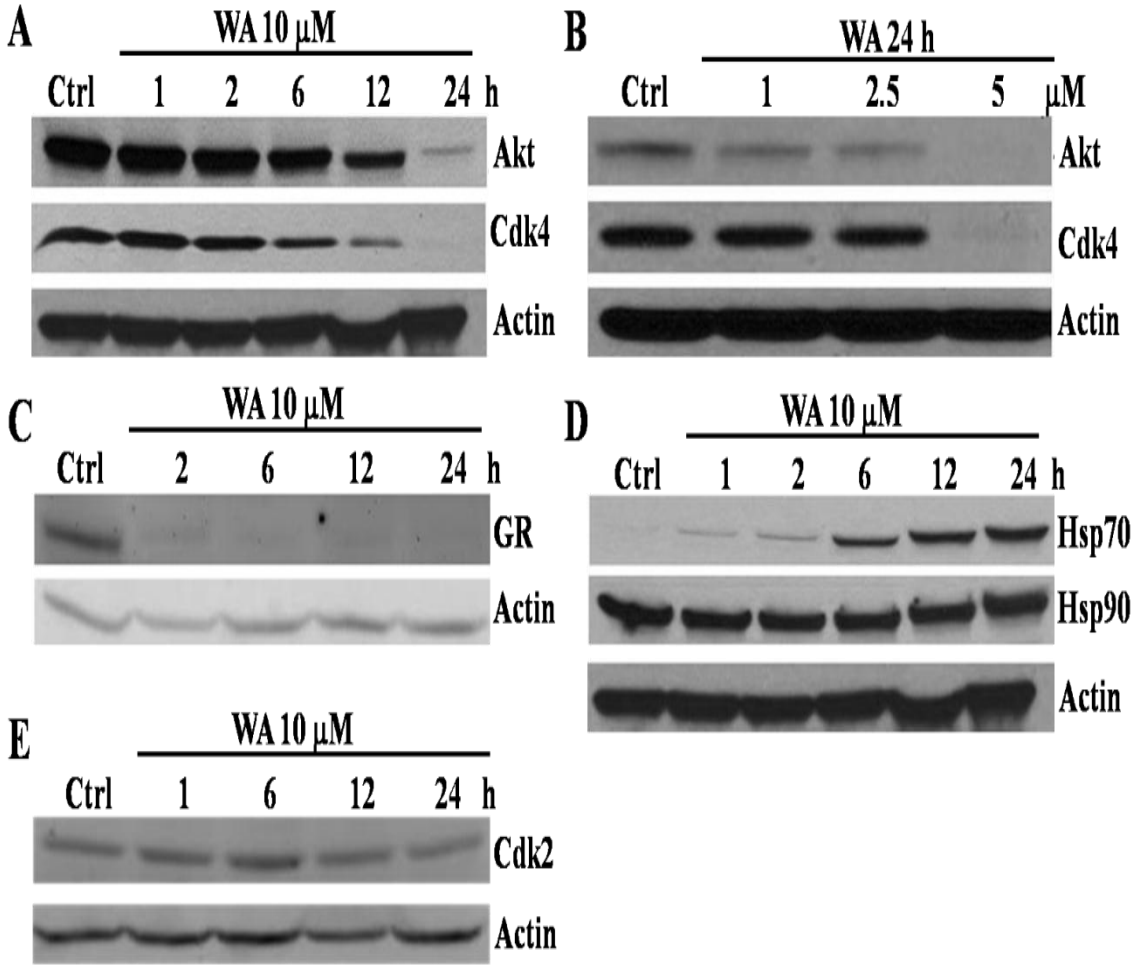

Figure 2.3 Withaferin A induces Hsp90 client protein degradation and Hsp70 upregulation. A and B. WA induces Hsp90 client protein Akt and Cdk4 degradation in Panc-1 cells in a time- and dose-dependent manner. Panc-1 cells were treated with different concentrations of WA for different times. Cell lysates (50 μg protein in each lane) were analyzed by western blot analysis with specific antibodies to Akt, Cdk4 and Actin. Actin was served as internal standard. **C. WA induces Hsp90 client protein GR degradation.** Panc-1 cells were treated with10 μM WA for different times. Cell lysates (50 μg protein in each lane) were analyzed by western blot analysis with specific antibodies to GR and Actin. Actin was served as internal standard. **D. WA induces expression of Hsp70.** Panc-1 cells were treated with10 μM WA for different times. Cell lysates (50 μg protein in each lane) were analyzed by western blot analysis with specific antibodies to Hsp70 and Actin. Actin was served as internal standard. **E. WA does not change the Cdk2 protein level.** Panc-1 cells were treated with10 μM WA for different times. Cell lysates (50 μg protein in each lane) were analyzed by western blot analysis with specific antibodies to Cdk2 and Actin. Actin was served as internal standard.

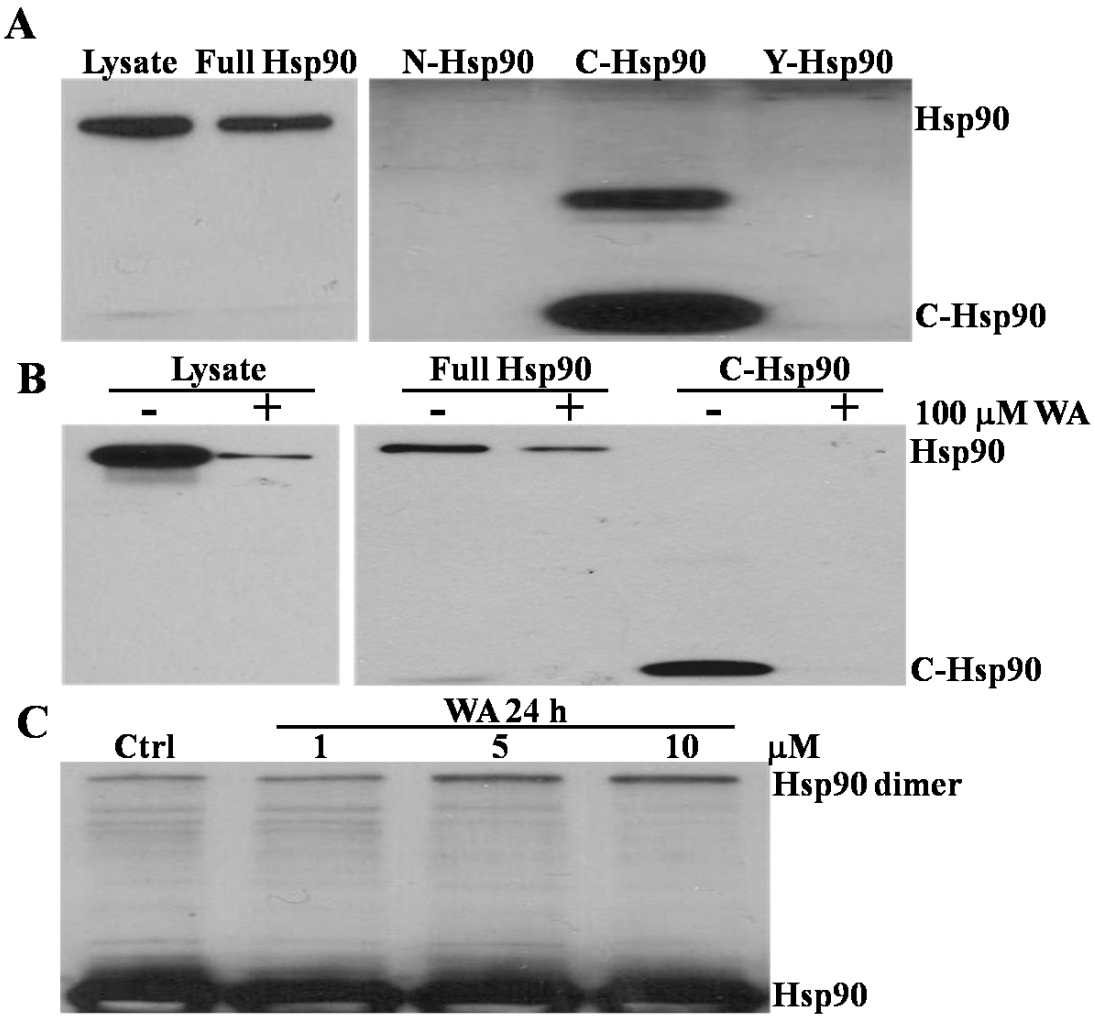

Figure 2.4 Withaferin A binds to Hsp90 and induces Hsp90 aggregation. A. WA-Biotin Hsp90 pull down assay. 1 mg of Panc-1 cell lysates (Lysate), 5 μg of purified full length human Hsp90β (Full Hsp90) 5 μg of N-terminus human Hsp90β (N-Hsp90), 5 μg of C-terminus human Hsp90β (C-Hsp90) and 5 μg of yeast Hsp90 (Y-Hsp90) were used to carry out the WA-Biotin pull down assay. The WA-Biotin pull down protein were subjected to western blot analysis with specific antibodies to Hsp90. **B. WA competes with WA-Biotin binding to Hsp90.** The samples (Lysate, Full Hsp90 and C-Hsp90) were preincubated with 100 μM WA for 1 h before subject to WA-Biotin binding assay. The WA-Biotin pull down protein were subjected to western blot analysis with specific antibodies to Hsp90. **C. WA induces Hsp90 aggregation in a dose dependent manner.** Panc-1 cells were treated with 1, 5 and 10 μM WA for 24 h. Cell lysates (50 μg protein in each lane) were subjected to non-reducing gel electrophoresis and then analyzed by western blot with specific antibodies to Hsp90.

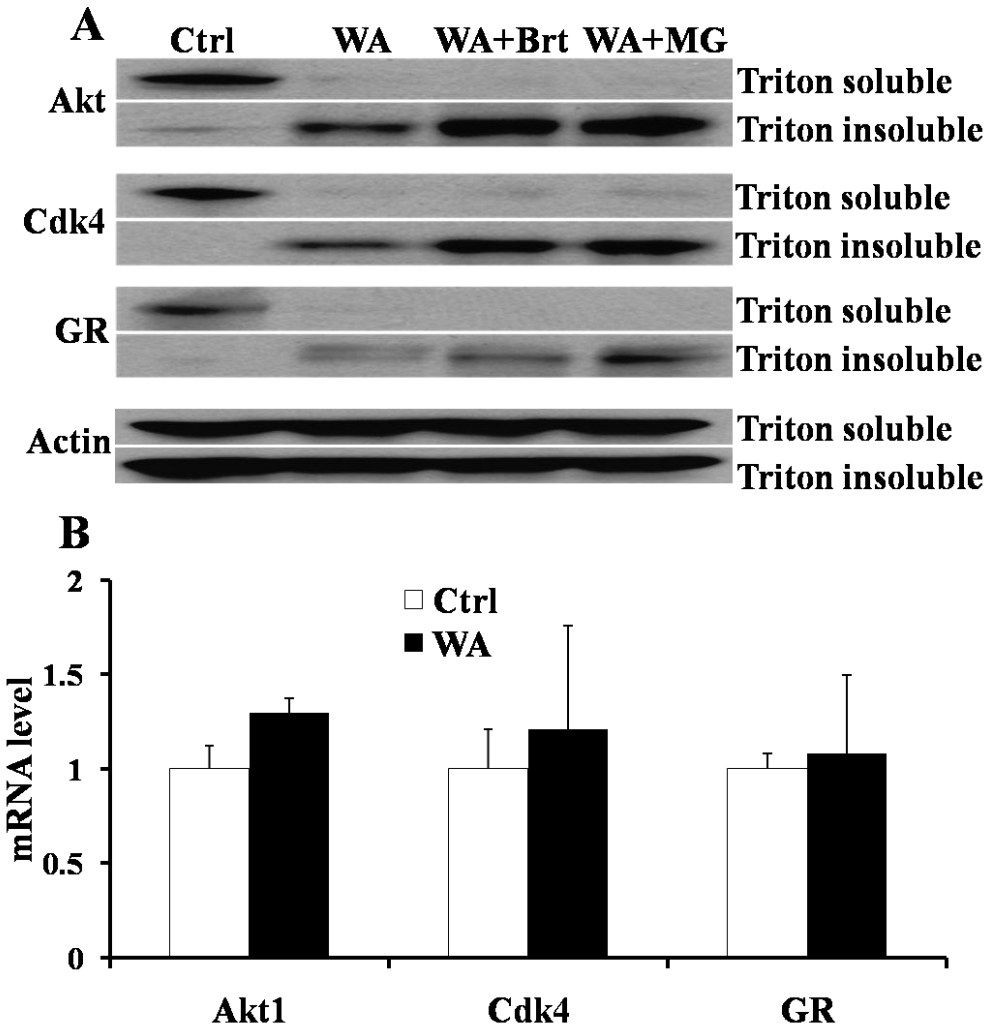

Figure 2.5 Withaferin A induced Hsp90 client protein degradation is proteasome-dependent. A. WA induced Hsp90 client protein degradation is reversed by proteasome inhibitors. Panc-1 cells were preincubated with 10 μM Bortezomib (Brt) or MG132 (MG) for 1 h, and then were treated with 5 μM WA for another 12 h. Cells were collected and proteins were isolated as triton soluble part and triton insoluble part. Proteins (both triton soluble and triton insoluble parts) were subjected to western blot analysis with specific antibodies to Akt, Cdk4, GR and Actin. Actin was served as internal standard. **B. mRNA levels of Hsp90 client protein in Panc-1 cells after WA treatment.** Panc-1 cells were treated with 5 μM WA for 12 h, and the total mRNAs were isolated. RT-PCR was carried out to examine the mRNA levels of Akt, Cdk4 and GR using the specific primers of Akt, Cdk4, GR and Actin. Actin was served as internal standard.

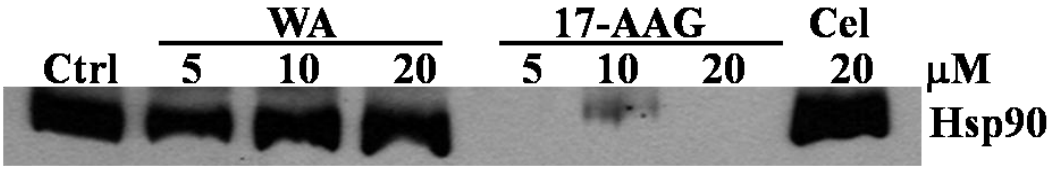

Figure 2.6 WA does not inhibit ATP binding to Hsp90. 5 μg of purified human Hsp90β was incubated with WA, 17-AAG and Celastrol (Cel) for 30 min. 25 μl ATP-sepharose beads were added to the samples to pull down Hsp90. Western blot was used to detect Hsp90 using specific antibody to Hsp90.

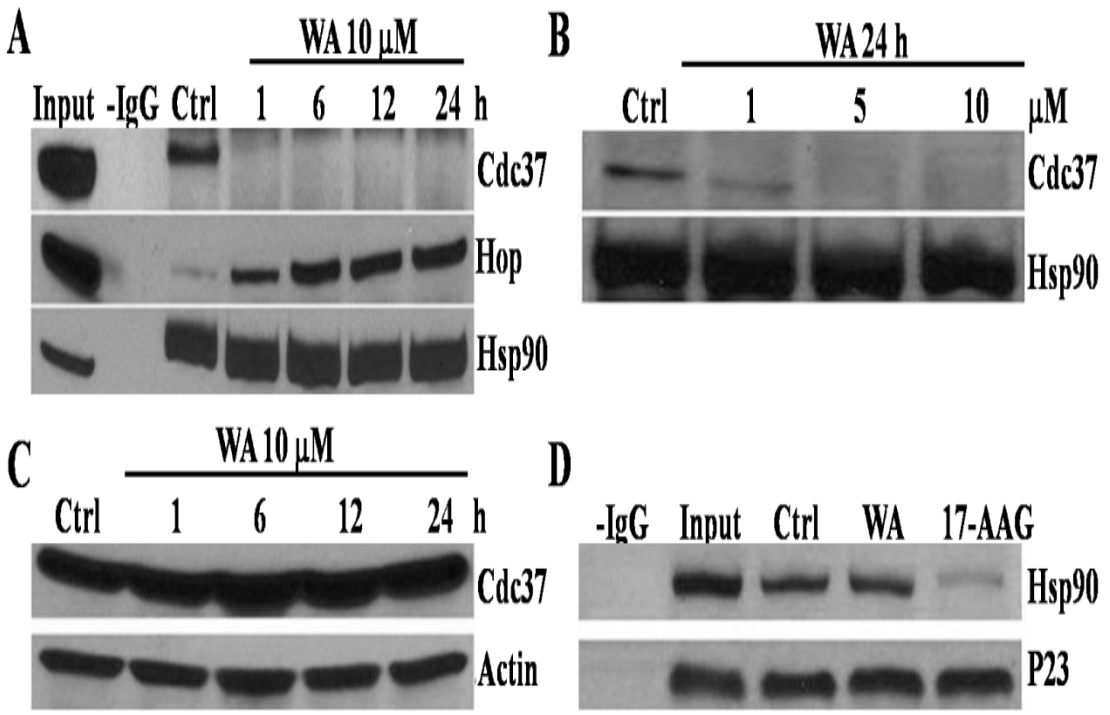

Figure 2.7 WA disrupts Hsp90-Cdc37 complex in Panc-1 cells. A and B. Co-immunoprecipitation (coIP) Hsp90. Cell lysates (500 μg total protein) were immunoprecipitated with Hsp90 antibody. Western blot was performed to detect Cdc37, Hop and Hsp90 using specific antibodies to Cdc37, Hop and Hsp90. A. Panc-1 cells were treated with 10 μM WA for 0 to 24 h. B. Panc-1 cells were treated with 1, 5, and 10 μM WA for 24 h. Input, total cell lysate; -IgG, without adding antibody. **C. Western blot analysis of Cdc37 expression level.** Panc-1 cells were treated with 10 μM WA for different times. Cell lysates (50 μg protein in each lane) were analyzed by western blot with specific antibodies to Cdc37 and Actin. Actin was served as internal standard. **D. CoIP P23.** Cell lysates (500 μg total protein) were immunoprecipitated with P23 antibody, then western blot was performed to detect Hsp90 and P23 using specific antibodies to Hsp90 and P23.

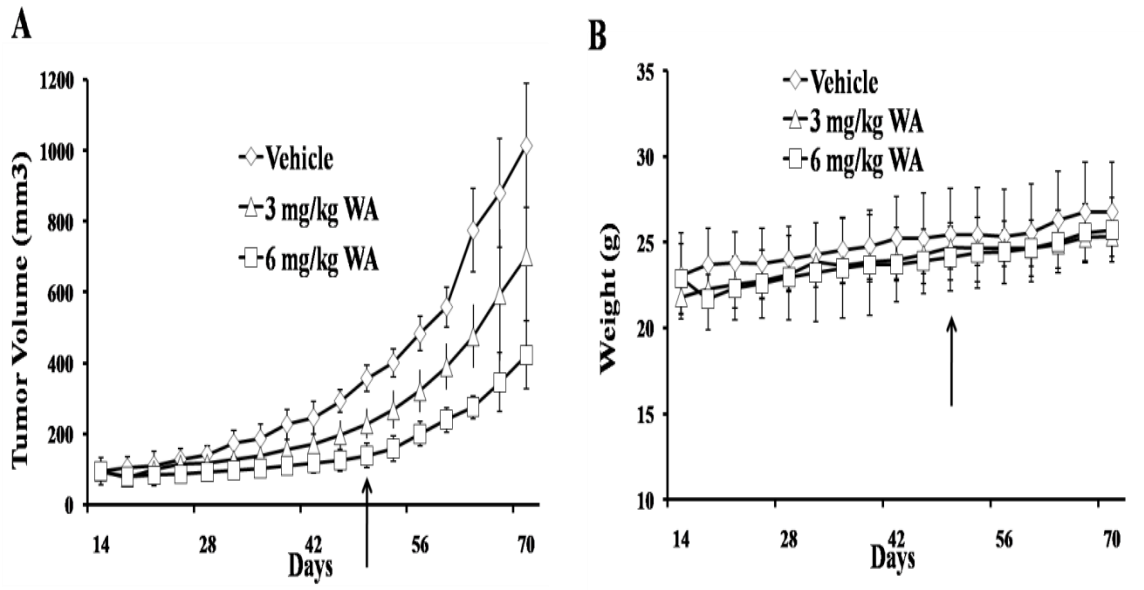

Figure 2.8 Antitumor effect of Withaferin A in Panc-1 pancreatic cancer xenografts. A. Tumor growth curves. The pancreatic tumor xenograft mouse model was generated by injecting the Panc-1 cancer cells s.c. to the right and left flanks of the nude mice. When the tumors reached 100 mm^3, mice were divided randomly into three groups (n= 6/group) to receive vehicle, 3 mg/kg or 6 mg/kg WA treatment as scheduled. Tumor sizes and body weights were measured twice a week. Drug treatment was stopped after 30 days' treatment, and tumor sizes and body weights were monitored until 70 days. *Arrows* indicate the date that stops treatment. **B. Body weight of mice.** Body weights of mice were monitored twice per week.

CHAPTER III

SYNERGISTIC EFFECT OF WITHAFERIN A AND MYRICETIN IN PANCREATIC CANCER CELLS

Abstract

Withaferin A (WA) has shown anticancer effect against pancreatic cancers through inhibition of Hsp90. However, WA induced Hsp70 upregulation which has anti-apoptotic effect. The purpose of this study is to investigate inhibition of Hsp70 by myricentin (MY) sensitize WA against pancreatic cancer cells. MY (5 μM) combination treatment with WA decreased IC_{50} of WA by 2.19-, 2.65-, and 3.93-folds compared to WA treatment alone in pancreatic cancer Panc-1, MiaPaca-2, and BxPc-3 cells, respectively. WA (1 μM) treatment alone induced 2.3-fold increases in caspase-3 activity compared to control, while the combination of WA (1 μM) and MY (5 μM) induced 4-fold increases in Caspase-3 activity while 5 μM MY alone treatment had minimal effect on Caspase-3 activity. Western-blot showed that combination of WA (1 μM) and MY (10 μM) decreased WA-induced Hsp70 expression by 3-fold compared to WA treatment alone. WA and MY acted synergistically in downregulating Hsp90 client proteins including

mutated P53, Akt, and Cdk4. SiRNA of Hsp70 (siHsp70) was further employed to confirm that knockdown of Hsp70 could sensitize pancreatic cancer cells to WA treatment. siHsp70 decreased WA-induced Hsp70 mRNA and protein levels by 2.5 and 6.5-fold, respectively. Combination of siHsp70 and WA treatment increased Caspase-3 activity by 2.7-fold compared to WA treatment alone. Furthermore, combined 4 mg/kg WA and 50 mg/kg MY treatment showed further inhibition of tumor growth compared to WA treatment alone in pancreatic cancer xenografts. These data suggest that Myricetin may be used to sensitize Hsp90 inhibitors against pancreatic cancer cells.

Key words: Withaferin A; Myricetin; Pancreatic cancer; Hsp90; Hsp70;

Introduction

Pancreatic cancer is among the most aggressive cancers to treat due to the late diagnosis and lack of effective therapies. Although the incidence of pancreatic cancer is relatively low, pancreatic cancer is the fourth leading cause of cancer death in the United States with five-year survival of less than 5%(1). Pancreatic cancer is highly resistant to conventional chemotherapy (2-5). Gemcitabine, the standard therapeutic drug for pancreatic cancer, only improves the disease symptoms with no significant five-year survival benefits. Therefore, novel agents for prevention and treatment of pancreatic cancers are highly desired.

In our previous report, a natural product withaferin A (WA) was demonstrated potent antiproliferative activity against various pancreatic cancer cells in vitro (6). The anticancer effect of WA was also confirmed in vivo against pancreatic cancer cell Panc-1 xenografts with inhibition of tumor growth by 58% at a dosage of 6 mg/kg. Further study elucidated that the anticancer effect of WA was partially through the inhibition of Hsp90 chaperoning activity by covalently binding to the C-terminus, which resulted in Hsp90 client protein degradation and cancer cell apoptosis.

Despite WA exhibited potent anticancer effect against pancreatic cancer cells, WA elicited extensive Hsp70 upregulation. Hsp70 is an ATP-dependent molecular chaperone assisting nascent polypeptides folding, assembly and translocation (7). In normal cells, the expression of Hsp70 is at basal level; under heat shock response, Hsp70 is upregulated and assists in the recovery from stress and promoting cell survival (8). Hsp70 also acts as Hsp90 cochaperone (9). Studies have shown that Hsp70 exhibits antiapoptotic effects, which is related to heat shock response. Hsp70 inhibits the mitochondrial pathway of apoptosis by associating with apoptotic protease activating factor 1 (Apaf-1), blocking the assembly of functional apoptosomes (10), and suppressing the activity of caspase-3 (11, 12). In addition, Hsp70 also inhibits caspase-independent death effecter apoptosis inducing factor (AIF) by directly binding to AIF, which prevents its translocation into nucleus and induces chromatin condensation and DNA fragmentation (12-14). Hsp70 is constitutively expressed in most cancer cells and human cancer tissues from various origins (15-17). The

high Hsp70 expression in various human cancers has been demonstrated to associate with metastasis, poor prognosis and resistance to radiation therapy or chemotherapy (18-24).

Considering the antiapoptotic role of Hsp70, the upregulation of Hsp70 after WA treatment could undermine the anticancer effect of WA. Thus, we proposed that inhibition of Hsp70 would sensitize pancreatic cancer cells to WA treatment. Our previous study have shown that a natural product flavonol myricetin (MY) inhibits human Hsp70 ATPase activity with IC_{50} about 12 μM and decreases levels of Hsp70 protein, tau, and Akt (25, 26). In the present study, we intend to investigate that Myricetin (MY) inhibits Hsp70 to sensitize Withaferin A (WA) efficacy inhibiting Hsp90 in pancreatic cancer cells.

Materials and methods

Cell culture and reagents

Human pancreatic cancer cell lines BxPc-3, Panc-1, and MiaPaca-2 were cultured in Dulbecco's Modified Eagle Medium (DMEM) or RPMI-1640 Medium supplemented with 10% FBS and 1% P/S at 37^{o}C and 5% CO_2. Withaferin A was a kind gift from Dr. A. A. Leslie Gunatilaka (The University of Arizona, Tucson, AZ). Myricetin was purchased from Sigma-Aldrich, Inc. (St. Louis, MO). The following antibodies were used for western blot: Akt (Cell Signaling, Beverly, MA), mutated P53, Hsp70, Cdk4, and beta-Actin (Santa Cruz, Santa Cruz, CA).

MTS assay

MTS assay was carried out to evaluate the cytotoxicity of single agent

treatment or combination treatment. Pancreatic cancer cells were seeded in 96-well plates at a density of 3000 - 5000 cells per well for 24 hours. For single agent treatment, myricetin (MY, 0.5 to 50 μM) and withaferin A (WA, 0.01 to 5 μM) were added to the cells. For combination treatment, 5 μM MY together with varied concentrations of WA (0.01 to 5 μM) were added to the cells. Cells were treated for 48 hours and cell viabilities were measured. The IC_{50} values of the different treatments for cytotoxicity were estimated by WinNonlin software (Pharsight, Mountain View, CA).

For siRNA treatment, the cells are first transfected with siHsp70 with lipofectamine 2000 for 24 hours with 5 pmol per well. 24 hours later the cells are replaced with fresh medium and treated with increasing concentrations of WA (0.05 - 2 μM). After additional 48 hours incubation, cell viabilities were measured.

Apoptosis study

Cancer cell apoptosis was evaluated by caspase-3 activity assay. Caspase-3 assay kit (MBL International Corporation, Woburn, MA) was used as described in manufacturer protocol. Briefly, after the cancer cells were treated, proteins were isolated and incubated with caspase-3 substrate chromophore *p*-nitroanilide (*p*NA) labeled DEVD-*p*NA. Active caspase-3 cleaves peptide (after D) and releases *p*NA with absorbance at 405 nm which can be detected by a microtiter plate reader.

Western-Blot

siRNA of Hsp70 (siHsp70) and control siRNA (siCtrl) were purchased from Dharmacon (Lafayette, CO). siHsp70 has the sequence of 5'-TCA TCA GCG

GAC TGT ACCA-3' (27). siCtrl has the sequence of 5'-AAT TCT CCG AAC GTG TCA CGT-3' (28). Pancreatic cancer BxPc-3 cells were transfected with a total of 600 pmol of siRNA of Hsp70 (siHsp70) or control siRNA (siCtrl) with lipofectamine 2000 reagents for 24 hours in a 100 mm cell culture dish. Then 2.5 μM Withaferin A (WA) was added to the dish with fresh medium to treat for another 24 hours. After drug treatment, cells were washed with cold PBS, collected and lysed in RIPA lysis buffer (Cell signaling, Danvers, MA) for 30 min on ice. Samples were centrifuged at 14,000 rpm for 15 min at 4°C. The supernatants were collected and added with 2 × Laemmli sample buffer, boiled for 5 min. Then 30 μg of protein was subjected to electrophoresis in 10% SDS-polyacrylamide gel (Bio-Rad, Hercules, CA). The protein was transferred to nitrocellulose membrane, blocked and incubated with intended protein primary antibodies and β-actin antibody (as internal standard) with 1:1000 dilutions in 5% milk Tris-buffered saline with 0.1% tween-20 (TBS-T) at room temperature for 2 hours. The membrane was washed 3 times with TBS-T for 10 min, and then incubated with horseradish peroxidase-conjugated secondary antibody for 1 hour at room temperature. An enhanced chemiluminescence system ECL (Amersham, Piscataway, NJ) was used to detect the protein levels.

Real-time PCR assay

RT-PCR was carried out as described previously (6). Briefly, pancreatic cancer BxPc-3 cells were transfected with a total of 200 pmol of siHsp70 or siCtrl with lipofectamine 2000 reagents (Invitrogen, Carsbad, CA) for 24 hours in a 60 mm cell culture dish. Then 2.5 μM WA was added to the dish with fresh medium to

treat for another 12 hours. TRIzol reagents (Invitrogen, Carsbad, CA) were used to extract total cellular RNAs as described in protocol provided by manufacturer. Superscript III first strand synthesis kit from Invitrogen was used to reverse transcribe the cDNA. Then the real-time PCR was carried out in ABI PRISM 7900T real-time PCR system (PerkinElmer, Branchburg, NJ) with SYBR Green PCR Master Mix (Applied Biosystems). The primers used in RT-PCR were as follows: Hsp70, forward, 5'-TGT TCC GTT TCC AGC CCC CAA-3'; reverse, 5'-GGG CTT GTC TCC GTC GTT GAT-3'. Internal standard β-actin, forward, 5'-GCT CGT CGT CGA CAA CGG CTC-3'; reverse, 5'-CAA ACA TGC TCT GGG TCA TCT TCT C-3'. mRNA level was calculated as fold change of control. After completion of the RT-PCR, Ct values (cycle numbers in which signal intensity equal to the threshold value) were obtained from the software. For each samples, ΔCt was calculated as $\Delta Ct = Ct_{hsp70} - Ct_{actin}$. Then ΔΔCt was calculated as $\Delta\Delta Ct = \Delta Ct_{treatment} - \Delta Ct_{control}$. The fold change of the Hsp70 mRNA level relative to control group was calculated as $2^{-\Delta\Delta Ct}$.

Evaluate the synergistic effect of combination treatment

The synergistic effect was determined by the combination index (CI) (29). Combination index was calculated as $CI_{50}=IC50_{WA\ combination}/IC50_{WA\ alone} + IC50_{MYcombination}/IC50_{MYalone}$. Where $IC50_{MYcombination}$ is the IC50 of MY in combination treatment with WA; $IC50_{WA\ combination}$ is the IC50 of the WA after combined treatment with MY; $IC50_{WA\ alone}$, and $IC50_{MYalone}$ are the IC50s of the WA and My treatment alone. The synergism, additivity, and antagonism of the

combination effect would be represented by the CI values less than, equal to, or more than 1.0, respectively.

Pancreatic cancer mice xenograft model

The pancreatic tumor xenograft mouse model was established to examine the in vivo synergistic anticancer activity of WA and MY. 4 to 6-week old nu/nu athymic female mice were obtained from Charles River Laboratories (Charles River, Wilmington, MA). BxPc-3 pancreatic cancer cells ($5\text{-}10\times10^6$) were mixed with reconstituted basement membrane (Collaborative Research, Bedford, MA) and inoculated s.c. to the right and left flanks of the mice. When the tumors reach ~100 mm^3, mice were randomly divided into four different groups for treatment (n= 6/group): vehicle, WA treatment alone group, MY treatment alone group, and combined WA and MY treatment group. WA and MY were dissolved in the vehicle (10% DMSO, 40% Cremophor/ethanol (3:1), and 50% PBS). Different groups of mice were treated with vehicle, 4 mg/kg WA alone, 50 mg/kg MY alone, and combined 4 mg/kg WA and 50 mg/kg MY, respectively, by i.p. injection daily for two weeks. Tumor sizes were monitored twice a week.

Statistical analysis

Statistical analysis was performed with one-way ANOVA or Student's *t*-test. Each experiment was conducted independently at least three times. Data are presented as mean ± SD. A probability level of $P < 0.05$ was considered statistically significant.

Results

Withaferin A induces Hsp90 client protein degradation and Hsp70 upregulation in pancreatic cancer cells

Withaferin A (WA) was shown to bind to Hsp90, inhibit the chaperoning activity of Hsp90, induce Hsp90 client protein degradation and cancer cell death (6). Western-blot confirmed that WA induced Hsp90 client protein (Akt, Cdk4 and mutated P53) degradation in pancreatic cancer BxPc-3 cells. As shown in Figure 3.1, 2.5 μM WA treatment for 24 hours completely abolished the expression levels of Akt, Cdk4 and mutated P53. Whereas, Hsp70 was increased by 5.66 fold compared to control.

Myricetin decreases Hsp70 level in pancreatic cancer cells

Our previous report demonstrated that 10 μM myricetin (MY) treatment slightly decreased Hsp70 level in Hela cells and the IC_{50} determined for the inhibition of Hsp70 ATPase activity was 12 ± 1 μM (25). Here, we examined whether MY reduces the protein level of Hsp70 in pancreatic cancer BxPc-3 cells. Figure 3.2 showed that Hsp70 exhibited time-dependent decrease after MY treatment. After exposure to 50 μM MY for 3 hours, Hsp70 was decreased by 3.3-fold, which was maintained during the 24 hours treatment. Mutated P53 was decreased by 6.8-fold after 50 μM MY treatment as early as 1 hour time point. Akt level was decreased 2.2-fold at 3 hours time point after MY treatment and back to normal level at 24 hours time point which was consistent with our earlier finding in Hela cells, in which 50 μM MY induced Akt level reduction in 1 to 6 hours but not after 24 hours (26).

Synergistic anticancer effect of Withaferin A and Myricetin against pancreatic cancer cells

As shown above, withaferin A (WA) inhibited Hsp90 chaperoning activity, induced Hsp90 client protein degradation and Hsp70 upregulation, whereas myricetin (MY) inhibited Hsp70 activity and decreased Hsp70 level. Thus, we proposed that MY treatment would sensitize pancreatic cancer cells to WA treatment due to the reduction of WA induced Hsp70. To confirm the synergistic anticancer effect of the combination treatment of WA and MY in pancreatic cancer cells, MY and WA were combined to treat pancreatic cancer BxPc-3, MiaPaca-2 and Panc-1 cells. The concentration of MY was chosen as 5 μM at which MY exhibited no significant cell killing effects against the three pancreatic cancer cell lines (Figure 3.3A). Our previous data showed that MY (5 μM) decreased Hsp70 ATPase activity by 34% (25). The combination of WA and MY showed a significant synergistic effect (Table 3.1). The IC_{50}s of WA in the combination treatment with MY were decreased by 3.93-, 2.65- and 2.19-folds compared to WA treatment alone in BxPc-3, MiaPaca-2 and Panc-1 cells, respectively. Table 3.1 summarizes the IC_{50}s of WA against different pancreatic cancer cell lines and under different treatment conditions. To better illustrate the synergism of combination treatment, the combination index (CI) values were calculated. CI values less than, equal to, and greater than 1.0 suggests synergy, additivity, and antagonism, respectively (29). The CI values of combination use of WA and MY were from 0.35 to 0.56 in the three pancreatic cancer cell lines, indicating significant synergistic effect between MY and WA (In calculation, IC_{50}

of MY was chosen as 50 μM at which the pancreatic cancer cell survival was over 60%).

Next, we further examined the combination effect of WA and MY on the induction of apoptosis in pancreatic cancer BxPc-3 cells using caspase-3 activity assay. As shown in Figure 3.3B, 1 μM WA induced 2.3-fold increase in caspase-3 activity compared to control; 5 μM MY slightly induced caspase-3 activity with 1.4 fold of control which was not statistically significant; whereas, the combination of 1 μM WA and 5 μM MY treatment induced 4-fold increase in caspase-3 activity. Therefore, WA and MY exhibited synergism to induce apoptosis in pancreatic cancer cells.

Myricetin decreases withaferin A induced Hsp70 upregulation

As we have shown that withaferin A (WA) and myricetin (MY) exhibited synergism in antiproliferative activity and apoptosis induction in pancreatic cancer cells, we further examined the underlying mechanism. Western-blot was performed to evaluate Hsp70 and Hsp90 client protein levels after combined treatment of MY and WA. As shown in Figure 3.4A, 1 μM WA treatment alone for 24 hours increased Hsp70 level by 4.6-fold, whereas 5 μM MY treatment alone had no effect on Hsp70 level, however, combination treatment of 1 μM WA and 5 μM MY still showed increased Hsp70 level by 3.8-fold, which was similar to 1 μM WA treatment alone. To further confirm that MY could reduce WA-induced Hsp70 upregulation, we increased MY concentration to 50 μM. Figure 3.4B shows that 10 μM MY decreased WA-induced Hsp70 expression by 3-fold compared to WA treatment alone.

We also investigated Hsp90 client protein levels under combination treatment of WA and MY. As shown in Figure 3.4A, 1 μM WA alone and 5 μM MY alone for 24 hours did not decrease the protein level of mutated P53, whereas combination treatment of 1 μM WA and 5 μM MY together decreased mutated P53 by 3.4-folds. Higher concentrations of MY further synergized with WA to induce Hsp90 client protein degradation. For instance, combination treatment of 10 μM MY and 1 μM WA decreased Akt level by 2.8-folds compared to 1 μM WA treatment alone; in addition, combination treatment of 25 μM MY and 1 μM WA decreased Cdk4 level by 3.7-folds compared to 1 μM WA treatment alone (Figure 3.4B).

siRNA of Hsp70 sensitize pancreatic cancer cells to withaferin A treatment

As we have proved that withaferin A (WA) and myricetin (MY) acted synergistically against pancreatic cancer cells which was partially through the inhibition of Hsp70, we further utilized siRNA of Hsp70 (siHsp70) to knockdown Hsp70 to confirm that inhibition of Hsp70 sensitizes pancreatic cancer cells to WA treatment. To evaluate the knockdown efficiency of siHsp70, RT-PCR and Western-blot were performed to examine the Hsp70 mRNA level and protein level after siHsp70 and WA treatment. BxPc-3 pancreatic cancer cells (1×10^6) were seeded in the 10 cm cell culture dishes. When cancer cells were confluent, cells were transfected with siHsp70 or siCtrl (600 pmol per dish) for 24 hours. Then, cancer cells were treated with 2.5 μM WA for another 12 hours. RNA was isolated and RT-PCR was carried out to measure the Hsp70 levels. Hsp70 mRNA levels were normalized to control group without WA treatment. As shown in Fig 3.5A, siCtrl has no effect on Hsp70 mRNA level, while siHsp70 decreased

Hsp70 mRNA by 2.5-folds. After WA treatment, Hsp70 mRNA in WA treatment alone and combination of WA and siCtrl treatment groups increased more than 2-folds compared to control, whereas Hsp70 mRNA in combination of WA and siHsp70 group was only 81% of control, which was 42% of WA treatment alone.

Western-blot was further carried out to examine whether siHsp70 could knockdown WA-induced Hsp70 protein expression. BxPc-3 pancreatic cancer cells were transfected with siHsp70 for 24 hours and then treated with 2.5 μM WA for another 24 hours. Proteins were isolated and western-blot was carried out to examine the Hsp70 level. As shown in Figure 3.5B, without WA treatment, siHsp70 decreased Hsp70 level by 2.6-fold; After WA treatment, the level of Hsp70 was dramatically increased in Ctrl and siCtrl groups, while in siHsp70 group, there was only minor increase in Hsp70 expression.

As we have confirmed that siHsp70 could successfully knockdown both the mRNA and protein levels of Hsp70, we used MTS assay to examine the antiproliferative effect of combination of siHsp70 and WA treatment. Pancreatic cancer cells were seeded in the 96-well plate in a density of 3000 cells per well. Cells were transfected with siCtrl or siHsp70 (10 pmol per well) by lipofectamine 2000 for 24 hours and then treated with indicated concentrations of WA for another 48 hours. Figure 3.6 shows that the transfection of siHsp70 further increased the antiproliferative activity of WA compared to Ctrl and siCtrl groups. Caspase-3 activity assay was further employed to estimate the apoptotic cells after combination of siHsp70 and WA treatment. siHsp70 and siCtrl induced 1.8-fold caspase-3 activity compared to control, whereas WA treatment alone and

combination treatment of WA and siCtrl induced 4.7-foldcaspase-3 activity as compared to control. Combination treatment of WA and siHsp70 induced caspase-3 activity by 13.0-folds compared to control.

The protein levels of Hsp90 client protein including Akt, Cdk4 and Glucocorticoid receptor (GR) were also examined after siHsp70 and WA treatment. Figure 3.7 shows that siHsp70 alone did not significantly alter the protein levels of Akt, Cdk4, and GR, whereas combination of siHsp70 and WA treatment completely abolished these Hsp90 client proteins.

Withaferin A and myricetin exhibited synergistic antitumor effect in pancreatic cancer xenograft

The previous data indicated withaferin A (WA) and myricetin (MY) acted synergistically in inducing apoptosis of pancreatic cancer cells and inhibiting cell proliferation in vitro, we next addressed whether WA and MY would show synergistic anticancer activity in vitro. Therefore, BxPc-3 pancreatic cancer xenograft mouse model was established, and the mice bearing tumor were randomly divided into four groups, treated with vehicle, 4 mg/kg WA alone, 50 mg/kg MY alone, and combined 4 mg/kg WA and 50 mg/kg MY treatment, respectively. After i.p., daily treatment for two weeks, 4 mg/kg WA treatment alone showed significant tumor growth inhibition compared to vehicle treatment group, whereas, 50 mg/kg MY treatment alone showed minor effect without statistical significance (Figure 3.8). In addition, combined 4 mg/kg WA and 50 mg/kg MY treatment showed further inhibition of tumor growth compared to WA

treatment alone with *p* value < 0.05 (Figure 3.8). The result indicated WA and MY showed synergistic anticancer effect both in vitro and in vivo.

Discussion

Natural products represent a large resource for the discovery and development of new drugs. About 40% of the newly approved drugs in the past years are either natural products or their derivatives and analogues (30, 31) including some well-known drugs such as paclitaxel (Taxol) and pentostatin (Nipent) (31, 32).

Withaferin A is a steroidal lactone isolated from the roots of the Indian medicinal plant *Withania somnifera* (*W. somnifera*) (6). *W. somnifera* is widely cultivated in the India and has been used in Ayurvedic and indigenous medicine for over 3,000 years (33). Different formulations of *W. somnifera* including decoctions, infusions, ointments, powder, and syrup were applied to treat various physiological disorders including burns, wounds, infections, gastrointestinal diseases, infertility, and cutaneous abscesses (34). As one of the major active constituents of *W. somnifera*, Withaferin A was shown to have anti-inflammatory, anti-angiogenesis, anti-tumor, and radio-sensitizing activity (35, 36).

Myricetin (MY) is a phenolic compound naturally occurring in grapes, onions, broccoli, berries, garlic, black tea, bell pepper (37-39). MY was demonstrated to have antioxidant, anticarcinogenic, antiangiogenesis, antiviral, topoisomerase II repressor, analgesic, antithrombotic, antiartherosclerotic and antidiabetic activity (40-44). From prevention perspective, intake of MY was correlated with lower

prostate cancer incidence with the relative risk (RR) of 0.43 (45). Another study carried out by Nöthlings *et al.* have shown the benefit of the intake of three flavonols including myricetin, kaempferol, and quercetin in treating pancreatic cancer (46). A reduced pancreatic cancer risk (RR = 0.77) was observed with the intake of total flavonols. MY intake was associated with reduced pancreatic cancer incidence in female and Caucasian populations with RR 0.72 and 0.59, respectively. In addition, intake of MY dramatically decreased pancreatic cancer incidence among current smokers with RR 0.55 (46).

We have shown that withaferin A (WA) had Hsp90 inhibitory activity and myricetin (MY) had Hsp70 inhibitory activity (6, 25, 26). In the present study, we demonstrated that these two natural products withaferin A and myricetin acted synergistically against pancreatic cancer cells which was partially through MY's inhibition of Hsp70 as evidenced by the reduction of the Hsp70 induced by WA. In addition, MY and WA worked synergistically in mediating Hsp90 client protein degradation. Finally, we utilized siHsp70 which knockdown Hsp70 to further confirm that inhibition of Hsp70 sensitized pancreatic cancer cells to WA treatment. The synergistic effect of MY and WA on pancreatic cancer cells indicates the potential chemopreventive and therapeutic effect of MY and WA against pancreatic cancer.

Recently, Hsp90 has emerged as an exciting molecular target for developing anticancer drugs. Hsp90 inhibitors have two advantages: 1, Hsp90 inhibitors simultaneously downregulate various oncogenes which are directly involved in cancer development; 2, Hsp90 inhibitors showed high selectivity on cancer cells

as they rely more on the function of Hsp90 and oncogenic protiens. Currently, Hsp90 inhibitors have been tested in preclinical and clinical models for their anticancer activity including 17-AAG, 17-DMAG, IPI-504 and LAQ824 against various tumors (47-53).

However, the clinical efficacy of Hsp90 inhibitor as single agent in treatment of cancer is still under investigation (47-51, 53, 54). Some limitations may hinder the development of Hsp90 inhibitors: 1, Hsp90 inhibitors such as 17-AAG showed dose limiting toxicity (hepatotoxicity), which limits the dose escalation in clinical trials; 2, drug induced heat shock response may undermine its efficacy. Heat shock response is mediated by the transcriptional regulator heat shock factor 1 (Hsf1). Hsf1 transiently binds to Hsp90 in cytosol and its transcriptional activity is sequestered by Hsp90 (55). Under stress such as heat, oxidative stress and massive mutant protein presence or inhibition of Hsp90 by Hsp90 inhibitors, Hsf1 is released from Hsp90 complex, hyperphosphorylated, homotrimerized and translocated into nucleus to bind to the heat shock elements (HSE) in the promoter of *hsp70* gene and activate its transcription (55-57). Heat shock response induced by Hsp90 inhibitors was demonstrated to contribute to the development of drug resistance to Hsp90 inhibitors (12, 18, 58-60).

Researchers have conducted many studies to explore the possibility of targeting heat shock response to sensitize cancer cells to Hsp90 inhibitors. For example, KNK437 and quercetin, which inhibited the DNA binding and transcriptional activation of Hsf1, were found to sensitize multidrug resistant cancer cells against hyperthermal therapy and chemotherapeutic drugs including

17-AAG (15, 57, 61, 62). However, KNK437 and quercetin exhibit low inhibitory efficiency of Hsf1 (at 200 μM level and require multiple dosing). In addition, knockdown Hsp70 expression by siHsp70 was also shown to enhance the anticancer activity of classical Hsp90 inhibitors such as GA, 17-AAG and EC78 (59, 60).

In the current study, we demonstrated that myricetin (MY) as low as 5 μM potentiates the anticancer effect of withaferin A (WA) although the IC_{50}s of MY on pancreatic cancer cells were over 50 μM. Our data indicate myricetin (MY) may be used to sensitize Hsp90 inhibitors for pancreatic cancer therapy.

Reference

1. Dunphy, E. P. *Clin J Oncol Nurs* 2008, 12, (5), 735-41.
2. Ghaneh, P.; Costello, E.; Neoptolemos, J. P. *Postgrad Med J* 2008, 84, (995), 478-97.
3. Ghaneh, P.; Smith, R.; Tudor-Smith, C.; Raraty, M.; Neoptolemos, J. P. *Eur J Surg Oncol* 2008, 34, (3), 297-305.
4. Shore, S.; Raraty, M. G.; Ghaneh, P.; Neoptolemos, J. P. *Aliment Pharmacol Ther* 2003, 18, (11-12), 1049-69.
5. Sultana, A.; Smith, C. T.; Cunningham, D.; Starling, N.; Neoptolemos, J. P.; Ghaneh, P. *J Clin Oncol* 2007, 25, (18), 2607-15.
6. Yu, Y.; Hamza, A.; Zhang, T.; Gu, M.; Zou, P.; Newman, B.; Li, Y.; Gunatilaka, A. A.; Zhan, C. G.; Sun, D. *Biochem Pharmacol* 2010, 79, (4), 542-51.
7. Beckmann, R. P.; Mizzen, L. E.; Welch, W. J. *Science* 1990, 248, (4957), 850-4.
8. Jolly, C.; Morimoto, R. I. *J Natl Cancer Inst* 2000, 92, (19), 1564-72.
9. Arlander, S. J.; Felts, S. J.; Wagner, J. M.; Stensgard, B.; Toft, D. O.; Karnitz, L. M. *J Biol Chem* 2006, 281, (5), 2989-98.
10. Beere, H. M.; Wolf, B. B.; Cain, K.; Mosser, D. D.; Mahboubi, A.; Kuwana, T.; Tailor, P.; Morimoto, R. I.; Cohen, G. M.; Green, D. R. *Nat Cell Biol* 2000, 2, (8), 469-75.
11. Jaattela, M.; Wissing, D.; Kokholm, K.; Kallunki, T.; Egeblad, M. *EMBO J* 1998, 17, (21), 6124-34.
12. Guo, F.; Sigua, C.; Bali, P.; George, P.; Fiskus, W.; Scuto, A.; Annavarapu, S.; Mouttaki, A.; Sondarva, G.; Wei, S.; Wu, J.; Djeu, J.; Bhalla, K. *Blood* 2005, 105, (3), 1246-55.
13. Ravagnan, L.; Gurbuxani, S.; Susin, S. A.; Maisse, C.; Daugas, E.; Zamzami, N.; Mak, T.; Jaattela, M.; Penninger, J. M.; Garrido, C.; Kroemer, G. *Nat Cell Biol* 2001, 3, (9), 839-43.
14. Gurbuxani, S.; Schmitt, E.; Cande, C.; Parcellier, A.; Hammann, A.; Daugas, E.; Kouranti, I.; Spahr, C.; Pance, A.; Kroemer, G.; Garrido, C. *Oncogene* 2003, 22, (43), 6669-78.
15. Creagh, E. M.; Sheehan, D.; Cotter, T. G. *Leukemia* 2000, 14, (7), 1161-73.
16. Garrido, C.; Brunet, M.; Didelot, C.; Zermati, Y.; Schmitt, E.; Kroemer, G. *Cell Cycle* 2006, 5, (22), 2592-601.
17. Parcellier, A.; Gurbuxani, S.; Schmitt, E.; Solary, E.; Garrido, C. *Biochem Biophys Res Commun* 2003, 304, (3), 505-12.
18. Schmitt, E.; Maingret, L.; Puig, P. E.; Rerole, A. L.; Ghiringhelli, F.; Hammann, A.; Solary, E.; Kroemer, G.; Garrido, C. *Cancer Res* 2006, 66, (8), 4191-7.
19. Brondani Da Rocha, A.; Regner, A.; Grivicich, I.; Pretto Schunemann, D.; Diel, C.; Kovaleski, G.; Brunetto De Farias, C.; Mondadori, E.; Almeida, L.; Braga Filho, A.; Schwartsmann, G. *Int J Oncol* 2004, 25, (3), 777-85.

20. Vargas-Roig, L. M.; Gago, F. E.; Tello, O.; Aznar, J. C.; Ciocca, D. R. *Int J Cancer* 1998, 79, (5), 468-75.
21. Nanbu, K.; Konishi, I.; Mandai, M.; Kuroda, H.; Hamid, A. A.; Komatsu, T.; Mori, T. *Cancer Detect Prev* 1998, 22, (6), 549-55.
22. Sliutz, G.; Karlseder, J.; Tempfer, C.; Orel, L.; Holzer, G.; Simon, M. M. *Br J Cancer* 1996, 74, (2), 172-7.
23. Samali, A.; Cotter, T. G. *Exp Cell Res* 1996, 223, (1), 163-70.
24. Creagh, E. M.; Cotter, T. G. *Immunology* 1999, 97, (1), 36-44.
25. Jinwal, U. K.; Miyata, Y.; Koren, J., 3rd; Jones, J. R.; Trotter, J. H.; Chang, L.; O'Leary, J.; Morgan, D.; Lee, D. C.; Shults, C. L.; Rousaki, A.; Weeber, E. J.; Zuiderweg, E. R.; Gestwicki, J. E.; Dickey, C. A. *J Neurosci* 2009, 29, (39), 12079-88.
26. Koren, J., 3rd; Jinwal, U. K.; Jin, Y.; O'Leary, J.; Jones, J. R.; Johnson, A. G.; Blair, L. J.; Abisambra, J. F.; Chang, L.; Miyata, Y.; Cheng, A. M.; Guo, J.; Cheng, J. Q.; Gestwicki, J. E.; Dickey, C. A. *J Biol Chem* 2010, 285, (4), 2498-505.
27. McCollum, A. K.; Teneyck, C. J.; Sauer, B. M.; Toft, D. O.; Erlichman, C. *Cancer Res* 2006, 66, (22), 10967-75.
28. Zhang, X.; Chen, Z. G.; Choe, M. S.; Lin, Y.; Sun, S. Y.; Wieand, H. S.; Shin, H. J.; Chen, A.; Khuri, F. R.; Shin, D. M. *Clin Cancer Res* 2005, 11, (17), 6261-9.
29. Zhao, L.; Wientjes, M. G.; Au, J. L. *Clin Cancer Res* 2004, 10, (23), 7994-8004.
30. Cragg, G. M.; Newman, D. J.; Snader, K. M. *J Nat Prod* 1997, 60, (1), 52-60.
31. Tietze, L. F.; Bell, H. P.; Chandrasekhar, S. *Angew Chem Int Ed Engl* 2003, 42, (34), 3996-4028.
32. Newman, D. J.; Cragg, G. M. *J Nat Prod* 2007, 70, (3), 461-77.
33. Mirjalili, M. H.; Moyano, E.; Bonfill, M.; Cusido, R. M.; Palazon, J. *Molecules* 2009, 14, (7), 2373-93.
34. Kaileh, M.; Vanden Berghe, W.; Heyerick, A.; Horion, J.; Piette, J.; Libert, C.; De Keukeleire, D.; Essawi, T.; Haegeman, G. *J Biol Chem* 2007, 282, (7), 4253-64.
35. Shohat, B.; Gitter, S.; Abraham, A.; Lavie, D. *Cancer chemotherapy reports* 1967, 51, (5), 271-6.
36. Mohan, R.; Hammers, H. J.; Bargagna-Mohan, P.; Zhan, X. H.; Herbstritt, C. J.; Ruiz, A.; Zhang, L.; Hanson, A. D.; Conner, B. P.; Rougas, J.; Pribluda, V. S. *Angiogenesis* 2004, 7, (2), 115-22.
37. McDonald, M. S.; Hughes, M.; Burns, J.; Lean, M. E.; Matthews, D.; Crozier, A. *J Agric Food Chem* 1998, 46, (2), 368-375.
38. Hakkinen, S. H.; Karenlampi, S. O.; Heinonen, I. M.; Mykkanen, H. M.; Torronen, A. R. *J Agric Food Chem* 1999, 47, (6), 2274-9.
39. Miean, K. H.; Mohamed, S. *J Agric Food Chem* 2001, 49, (6), 3106-12.
40. Larson, R. A. *Phytochemistry* 1988, 27, (4), 969-978.
41. Ong, K. C.; Khoo, H. E. *Gen Pharmacol* 1997, 29, (2), 121-6.

42. Maggiolini, M.; Recchia, A. G.; Bonofiglio, D.; Catalano, S.; Vivacqua, A.; Carpino, A.; Rago, V.; Rossi, R.; Ando, S. *J Mol Endocrinol* 2005, 35, (2), 269-81.
43. Tong, Y.; Zhou, X. M.; Wang, S. J.; Yang, Y.; Cao, Y. L. *Arch Pharm Res* 2009, 32, (4), 527-33.
44. Jung, S. K.; Lee, K. W.; Byun, S.; Lee, E. J.; Kim, J. E.; Bode, A. M.; Dong, Z.; Lee, H. J. *Carcinogenesis* 2010, 31, (5), 911-7.
45. Knekt, P.; Kumpulainen, J.; Jarvinen, R.; Rissanen, H.; Heliovaara, M.; Reunanen, A.; Hakulinen, T.; Aromaa, A. *Am J Clin Nutr* 2002, 76, (3), 560-8.
46. Nothlings, U.; Murphy, S. P.; Wilkens, L. R.; Henderson, B. E.; Kolonel, L. N. *Am J Epidemiol* 2007, 166, (8), 924-31.
47. Weigel, B. J.; Blaney, S. M.; Reid, J. M.; Safgren, S. L.; Bagatell, R.; Kersey, J.; Neglia, J. P.; Ivy, S. P.; Ingle, A. M.; Whitesell, L.; Gilbertson, R. J.; Krailo, M.; Ames, M.; Adamson, P. C. *Clin Cancer Res* 2007, 13, (6), 1789-93.
48. Modi, S.; Stopeck, A. T.; Gordon, M. S.; Mendelson, D.; Solit, D. B.; Bagatell, R.; Ma, W.; Wheler, J.; Rosen, N.; Norton, L.; Cropp, G. F.; Johnson, R. G.; Hannah, A. L.; Hudis, C. A. *J Clin Oncol* 2007, 25, (34), 5410-7.
49. Solit, D. B.; Osman, I.; Polsky, D.; Panageas, K. S.; Daud, A.; Goydos, J. S.; Teitcher, J.; Wolchok, J. D.; Germino, F. J.; Krown, S. E.; Coit, D.; Rosen, N.; Chapman, P. B. *Clin Cancer Res* 2008, 14, (24), 8302-7.
50. de Bono, J. S.; Kristeleit, R.; Tolcher, A.; Fong, P.; Pacey, S.; Karavasilis, V.; Mita, M.; Shaw, H.; Workman, P.; Kaye, S.; Rowinsky, E. K.; Aherne, W.; Atadja, P.; Scott, J. W.; Patnaik, A. *Clin Cancer Res* 2008, 14, (20), 6663-73.
51. Ronnen, E. A.; Kondagunta, G. V.; Ishill, N.; Sweeney, S. M.; Deluca, J. K.; Schwartz, L.; Bacik, J.; Motzer, R. J. *Invest New Drugs* 2006, 24, (6), 543-6.
52. Ramanathan, R. K.; Trump, D. L.; Eiseman, J. L.; Belani, C. P.; Agarwala, S. S.; Zuhowski, E. G.; Lan, J.; Potter, D. M.; Ivy, S. P.; Ramalingam, S.; Brufsky, A. M.; Wong, M. K.; Tutchko, S.; Egorin, M. J. *Clin Cancer Res* 2005, 11, (9), 3385-91.
53. Holzbeierlein, J. M.; Windsperger, A.; Vielhauer, G. *Curr Oncol Rep* 12, (2), 95-101.
54. Tse, A. N.; Klimstra, D. S.; Gonen, M.; Shah, M.; Sheikh, T.; Sikorski, R.; Carvajal, R.; Mui, J.; Tipian, C.; O'Reilly, E.; Chung, K.; Maki, R.; Lefkowitz, R.; Brown, K.; Manova-Todorova, K.; Wu, N.; Egorin, M. J.; Kelsen, D.; Schwartz, G. K. *Clin Cancer Res* 2008, 14, (20), 6704-11.
55. Zou, J.; Guo, Y.; Guettouche, T.; Smith, D. F.; Voellmy, R. *Cell* 1998, 94, (4), 471-80.
56. Nakai, A.; Tanabe, M.; Kawazoe, Y.; Inazawa, J.; Morimoto, R. I.; Nagata, K. *Mol Cell Biol* 1997, 17, (1), 469-81.
57. Guo, F.; Rocha, K.; Bali, P.; Pranpat, M.; Fiskus, W.; Boyapalle, S.; Kumaraswamy, S.; Balasis, M.; Greedy, B.; Armitage, E. S.; Lawrence, N.; Bhalla, K. *Cancer Res* 2005, 65, (22), 10536-44.
58. Zaarur, N.; Gabai, V. L.; Porco, J. A., Jr.; Calderwood, S.; Sherman, M. Y. *Cancer Res* 2006, 66, (3), 1783-91.
59. Powers, M. V.; Clarke, P. A.; Workman, P. *Cancer Cell* 2008, 14, (3), 250-62.

60. McCollum, A. K.; TenEyck, C. J.; Stensgard, B.; Morlan, B. W.; Ballman, K. V.; Jenkins, R. B.; Toft, D. O.; Erlichman, C. *Cancer Res* 2008, 68, (18), 7419-27.
61. Mello, C. C.; Conte, D., Jr. *Nature* 2004, 431, (7006), 338-42.
62. Koishi, M.; Yokota, S.; Mae, T.; Nishimura, Y.; Kanamori, S.; Horii, N.; Shibuya, K.; Sasai, K.; Hiraoka, M. *Clin Cancer Res* 2001, 7, (1), 215-9.

Table 3.1 Synergistic anticancer effect of withaferin A and myricetin in pancreatic cancer cells.

Cells	IC_{50} of WA alone (μM)	IC_{50} of WA when combined with 5 μM MY (μM)	Combination index
Bx-Pc3	1.89 ± 0.21	0.48 ± 0.11	0.35 ± 0.15
MiaPaca-2	0.61 ± 0.13	0.23 ± 0.08	0.48 ± 0.12
Panc-1	1.14 ± 0.15	0.52 ± 0.12	0.56 ± 0.14

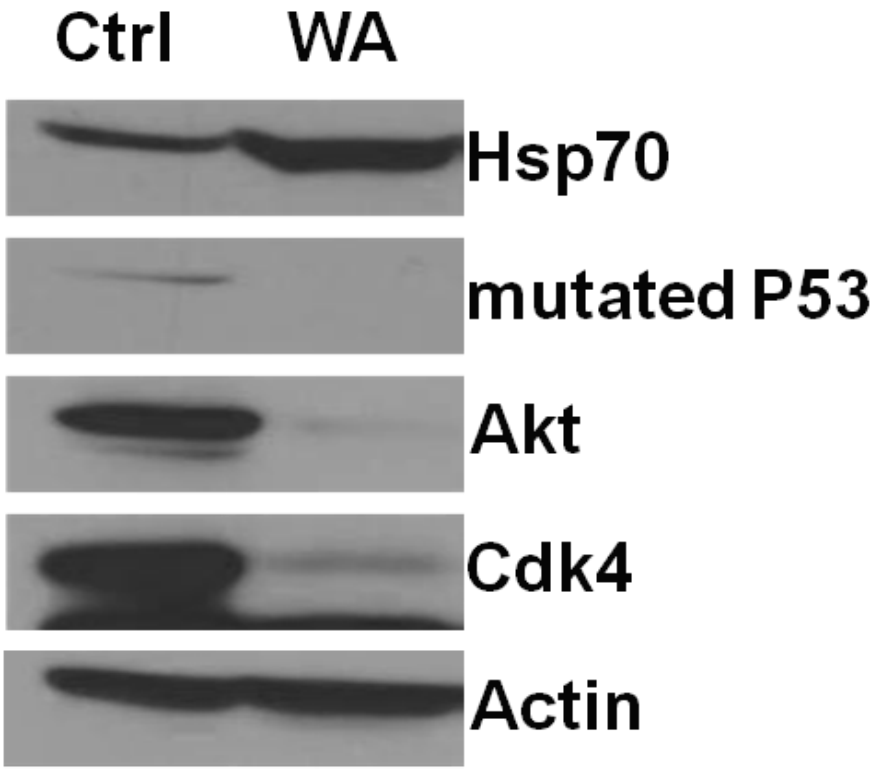

Figure 3.1 Protein level changes after withaferin A treatment in BxPc-3 cells. BxPc-3 pancreatic cancer cells were treated with 2.5 μM WA for 24 hours. Cell lysates (50 μg protein in each lane) were analyzed by western blot analysis with specific antibodies to Akt, Cdk4, Hsp70, mutated P53 and Actin. Actin was served as internal standard.

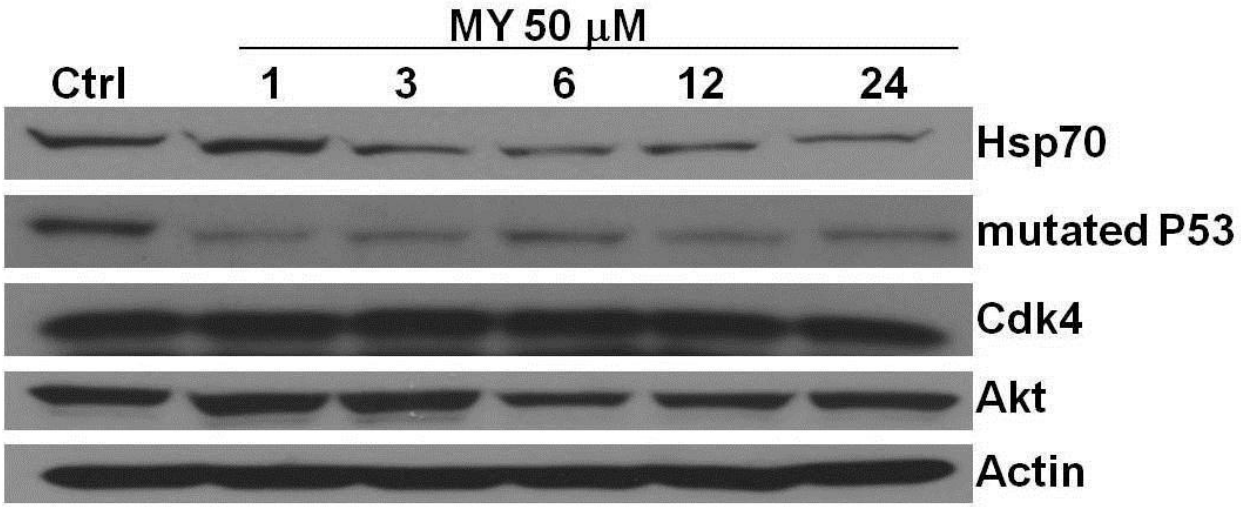

Figure 3.2 Protein level changes after myricetin treatment in BxPc-3 cells. BxPc-3 pancreatic cancer cells were treated with varied concentrations of MY for 24 hours or 50 μM MY for different time points. Cell lysates (50 μg protein in each lane) were analyzed by western blot analysis with specific antibodies to Akt, Hsp70, mutated P53 and Actin. Actin was served as internal standard.

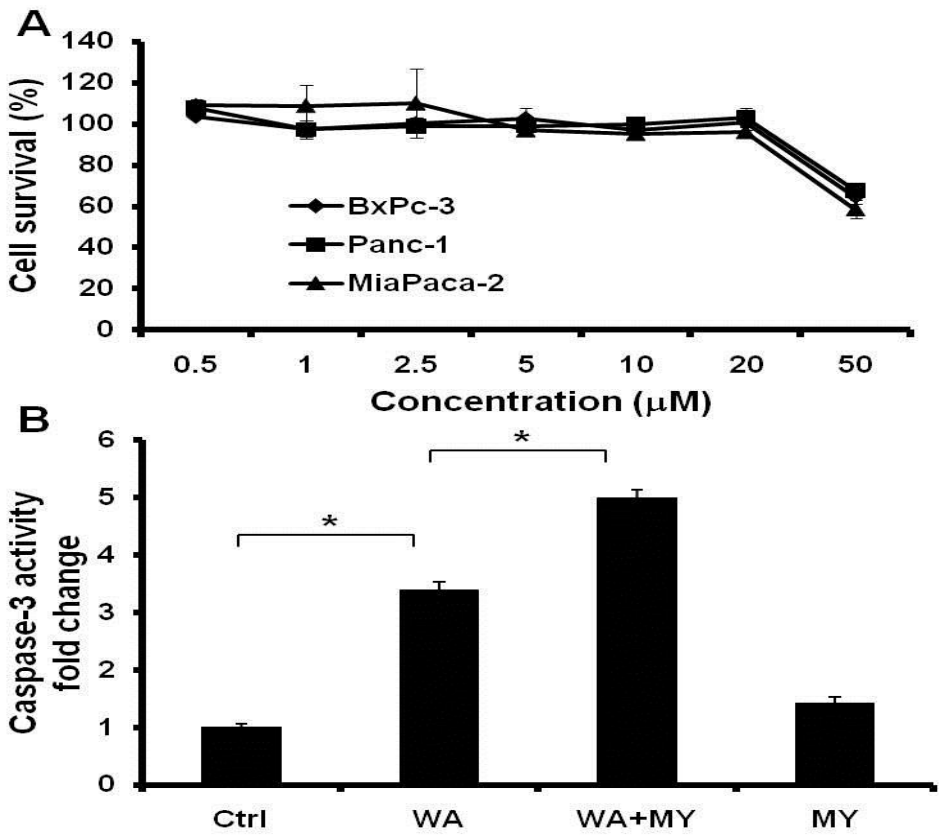

Figure 3.3 Anticancer effect of myricetin and withaferin A against pancreatic cancer cells. A, effect of MY treatment on viability of pancreatic cancer BxPc-3, MiaPaca-2 and Panc-1 cells. BxPc-3, MiaPaca-2 or Panc-1 cells were seeded in 96-well plates at a density of 5000 cells per well. 24 hours later the cells were subjected to MY treatment with concentrations of 0.5, 1.0, 2.5, 5, 10, 20 and 50 μM. MTS assay was performed to assess cell viability after 48 h incubation. B, apoptosis induced by WA and MY treatment against BxPc-3 cancer cells. Cancer cell apoptosis was evaluated by caspase-3 activity assay. BxPc-3 cancer cells were treated with 5 μM MY, 1 μM WA or combined 5 μM MY and 1 μM WA for 24 hours, proteins were isolated and analyzed with Caspase-3 assay kit (MBL International Corporation, Woburn, MA) for caspase-3 activity. The measured caspase-3 activities were normalized to control group, and were represented as fold change. *, $P < 0.05$.

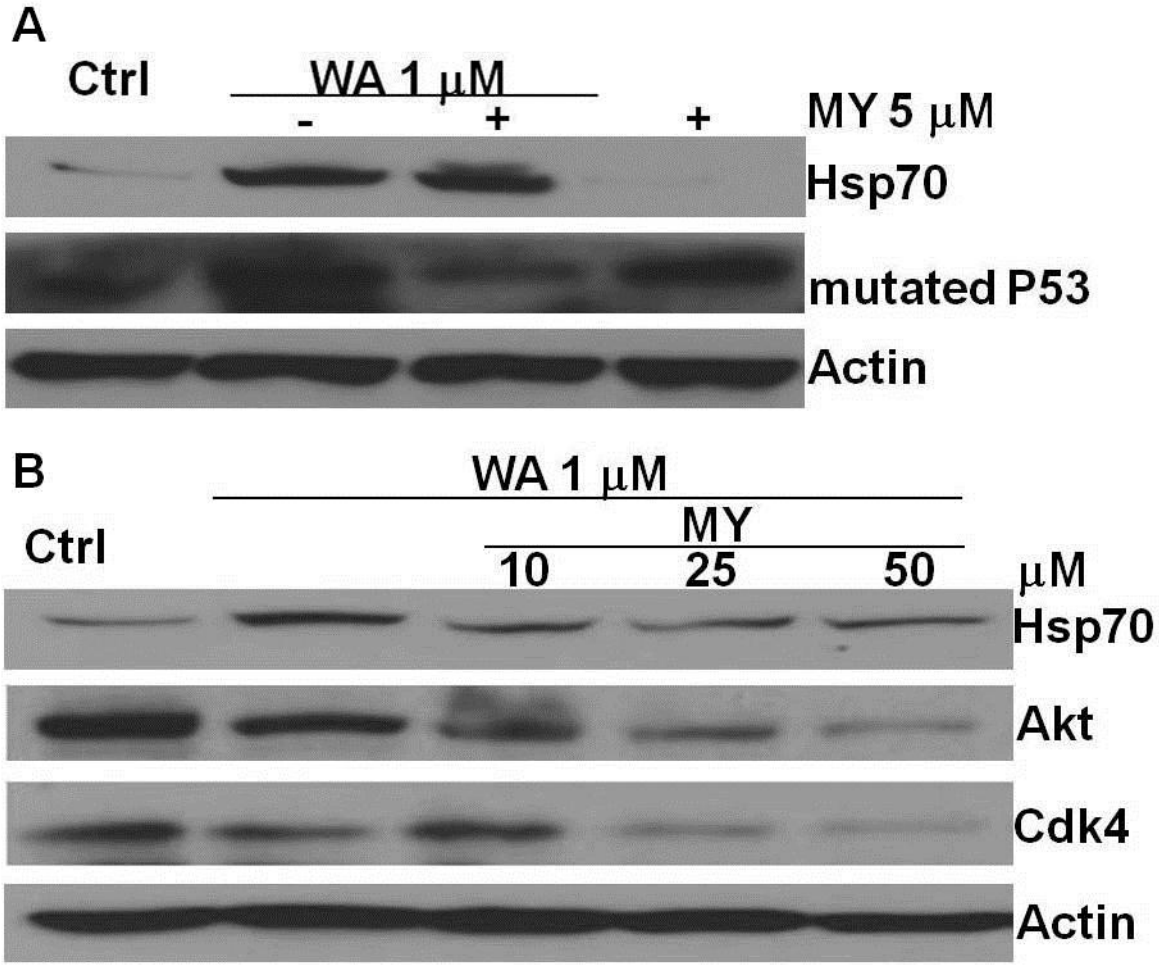

Figure 3.4 Protein level changes after myricetin and withaferin A treatment in BxPc-3 cells. BxPc-3 pancreatic cancer cells were treated with 1 μM WA for 24 hours, or treated with combined 1 μM WA and varied concentrations of MY. Cell lysates (50 μg protein in each lane) were analyzed by western blot analysis with specific antibodies to Akt, Cdk4, Hsp70, mutated P53 and Actin. Actin was served as internal standard.

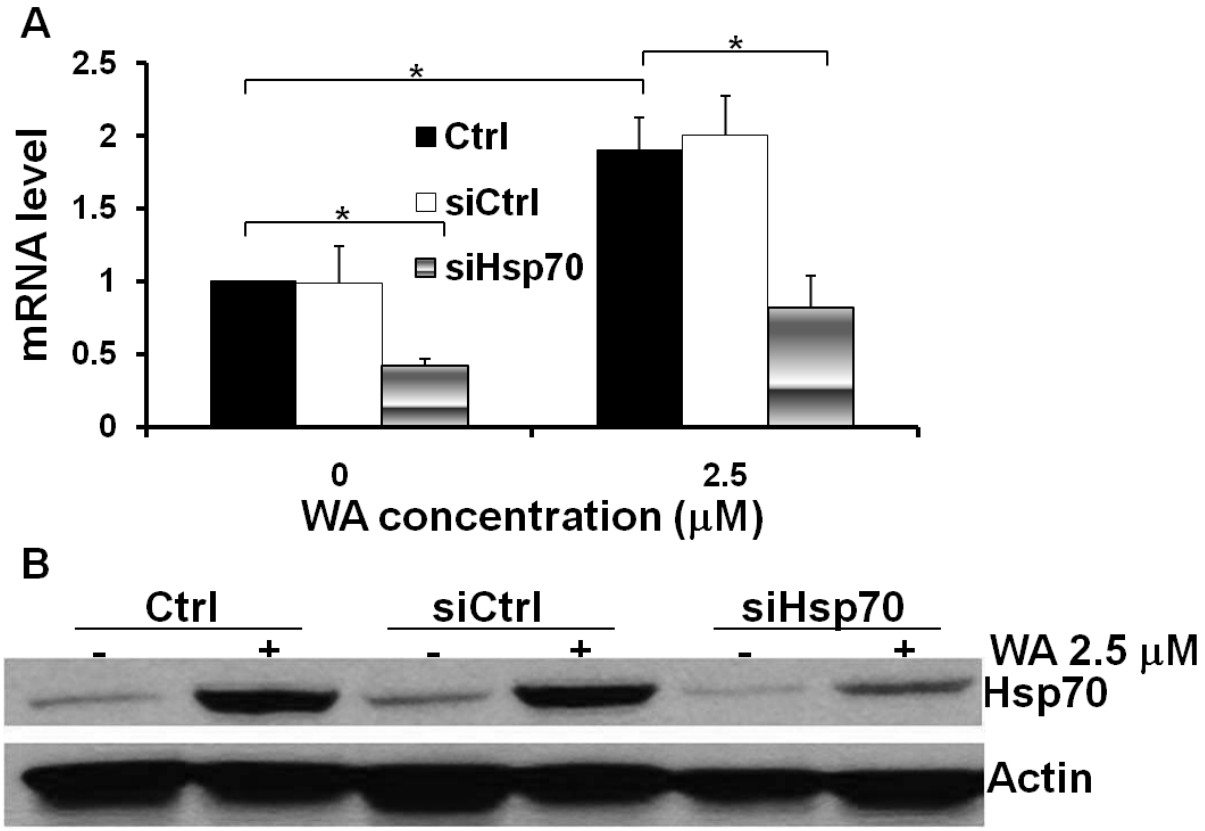

Figure 3.5 mRNA and protein level of Hsp70 after siHsp70 and withaferin A treatment in BxPc-3 cells. BxPc-3 pancreatic cancer cells were transfected with siHsp70 or siCtrl (600 pmol per dish) for 24 hours. Then, cancer cells were treated with 2.5 μM WA for another 12 hours for isolation of RNA or for another 24 hours for isolation of proteins. RNAs were used to carry out RT-PCR to measure Hsp70 mRNA level, which was normalized to control and calculated as fold change of control. Proteins were analyzed by western blot analysis with specific antibodies to Hsp70 and Actin. Actin was served as internal standard.

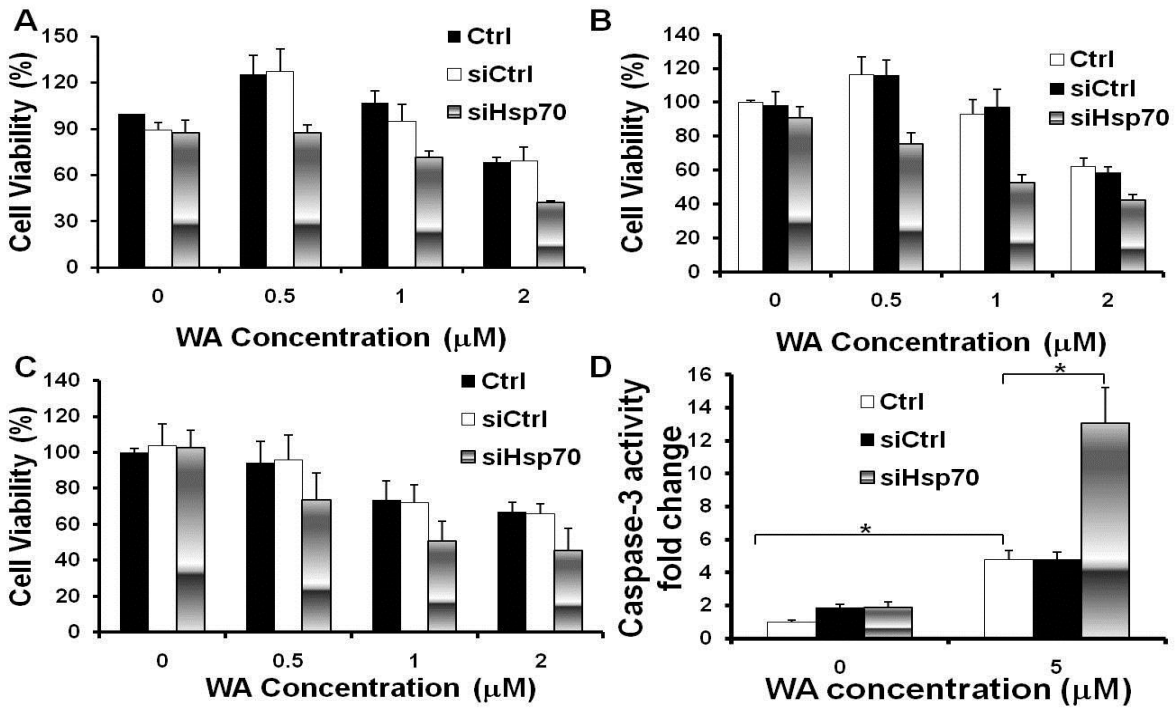

Figure 3.6 Anticancer effect of siHsp70 and withaferin A against pancreatic cancer cells. A, effect of siHsp70 and WA treatment on viability of pancreatic cancer BxPc-3. BxPc-3 cells were seeded in 96-well plates at a density of 5000 cells per well. BxPc-3 cells were first transfected with siHsp70 with lipofectamine 2000 for 24 hours with 5 pmol per well. 24 hours later the cells are replaced with fresh medium and treated with increasing concentrations of WA (0.05 - 2 μM). After additional 48 hours incubation, cell viabilities were measured. B, effect of siHsp70 and WA treatment on viability of pancreatic cancer MiaPaca-2. Viability of MiaPaca-2 cells after siRNA and WA treatment was assessed similar to A. C, effect of siHsp70 and WA treatment on viability of pancreatic cancer Panc-1 cells. Viability of Panc-1 cells after siRNA and WA treatment was assessed similar to A. D, apoptosis induced by siHsp70 and WA treatment against BxPc-3 cancer cells. Pancreatic cancer BxPc-3 cells were transfected with a total of 600 pmol of siRNA of Hsp70 (siHsp70) or control siRNA (siCtrl) with lipofectamine 2000 reagents for 24 hours in a 100 mm cell culture dish. Then 5 μM Withaferin A (WA) was added to the dish with fresh medium to treat for another 12 hours. Proteins were isolated and analyzed with Caspase-3 assay kit for caspase-3 activity similar to Figure 3B.

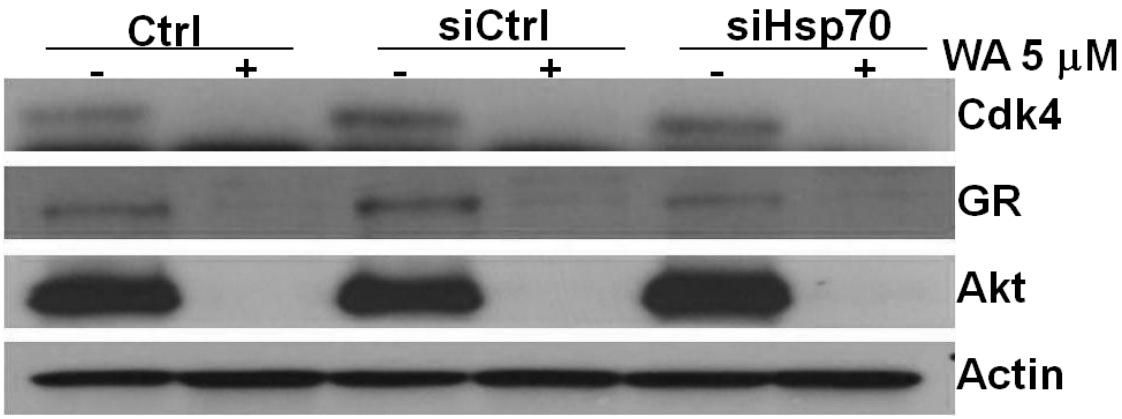

Figure 3.7 Protein level changes after siHsp70 and withaferin A treatment in BxPc-3 cells. BxPc-3 pancreatic cancer cells were transfected with siHsp70 or siCtrl for 24 hours. Then, cancer cells were treated with 5 μM WA for another 24 hours for isolation of proteins to carry out western-blot. Cell lysates (50 μg protein in each lane) were analyzed by western blot analysis with specific antibodies to Akt, Cdk4, GR and Actin. Actin was served as internal standard.

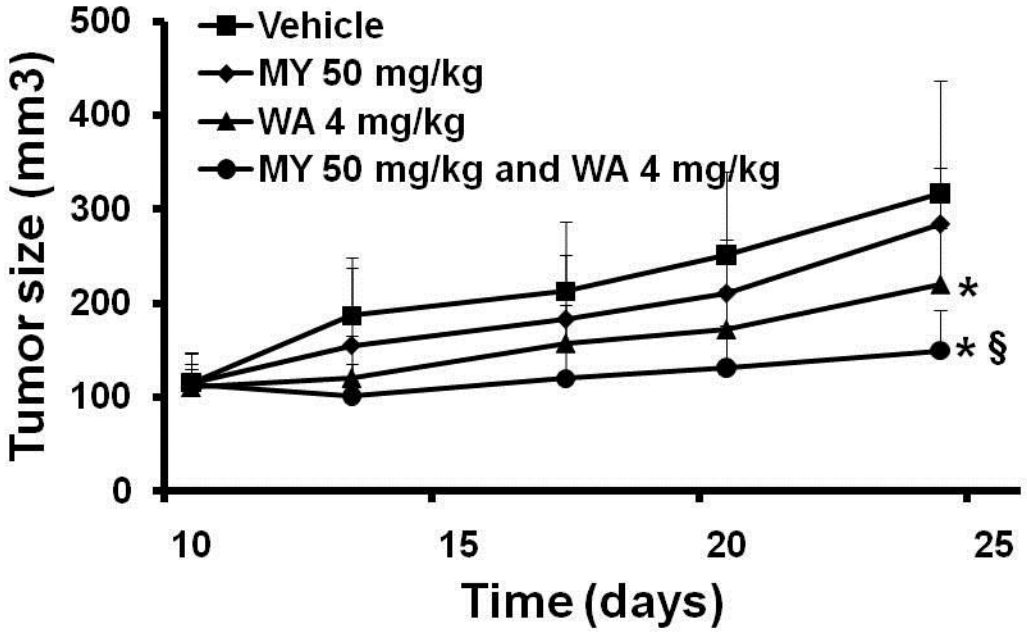

Figure 3.8 Withaferin A and myricetin exhibited synergistic effect in pancreatic cancer xenograft model. 5-10×10^6 BxPc-3 pancreatic cancer cells were mixed with reconstituted basement membrane and inoculated s.c. to the right and left flanks of the 4 to 6-week old nu/nu athymic female mice. When the tumors reach ~100 mm^3, mice were randomly divided into four different groups for treatment (n= 6/group). Mice were treated with vehicle, 4 mg/kg WA alone, 50 mg/kg MY alone, and combined 4 mg/kg WA and 50 mg/kg MY, respectively, by i.p. injection daily for two weeks. Tumor sizes were monitored twice a week. *, $p < 0.05$ comparing to Ctrl; §, $p < 0.05$ when comparing to WA treatment alone.

CHAPTER IV

STRUCTURE-ACTIVITY RELATIONSHIP (SAR) OF WITHANOLIDES TO INHIBIT HSP90 FOR ITS ACTIVITY IN PANCREATIC CANCER CELLS

Abstract

Withaferin A (WA), a triterpenoid of the withanolides, directly binds to Hsp90 and leads to the degradation of Hsp90 client protein. The purpose of this study is to investigate the structure activity relationship (SAR) of withanolides for its inhibition of Hsp90 and anti-proliferative activities in pancreatic cancer cells. In pancreatic cancer Panc-1 cells, withaferin A (WA) and four analogues withanolide E (WE), 4β-hydroxywithanolide E (HWE), 3-aziridinylwithaferin A (AzWA) inhibited cell proliferation with IC50s ranged from 1.05 to 2.76 μM. WA, WE, HWE, and AzWA also induced caspase-3 activity by 21- , 6- , 11- and 15-fold, respectively, in pancreatic cancer cells, while withaperuvin (WP) did not show any activity. The data showed that WA, WE, HWE, and AzWA, but not WP, all directly bound to Hsp90 and induced Hsp90 aggregation in pancreatic cancer cells. Western blotting assay showed that WA, WE, HWE, AzWA, but not WP, inhibited Hsp90 chaperone activity to induce degradation of Hsp90 client protein Akt and Cdk4 through proteasome-dependent pathway in pancreatic cancer cells.

However, only WA, HWE and AzWA disrupted Hsp90-Cdc37 complexes but not WE and WP. SAR study suggests that the C-5, 6 epoxy functional group contributes considerably for withanolide to bind to Hsp90, inhibit Hsp90 chaperon activity, and result in Hsp90 client protein depletion. Meanwhile, the hydroxyl group at C-4 within ketone unsaturated A ring may enhance withanolide to inhibit Hsp90 activity and disrupt Hsp90-Cdc37 interaction whereas the steric bulk substitution at C-3 may reduce its activity. These data provide detailed SAR mechanisms for withanolide to inhibit Hsp90 and exhibit anti-proliferative efficacy.

Key words: Withanolide; Hsp90; Cdc37; Structure-activity relationship; Pancreatic cancer

Introduction

The active constituents from *Withania somnifera* (WS), including alkaloids and withanolides, have been studied extensively for their biological activities (1, 2). Withaferin A (WA), one of the major active components of withanolides, was reported to have anti-angiogenesis, anti-tumor, and radio-sensitizing activities in various cancer cell lines (3-6). It has been reported that withaferin A suppressed nuclear factor kappa B (NF-κB) activation (7), covalently bound to annexin II, altered cytoskeletal architecture (8), and inhibited tumor necrosis factor-induced activation of IκB kinase via a thioalkylation-sensitive redox mechanism (9). Previously, we also showed that withaferin A (WA) exhibited anti-proliferative activity via Hsp90 inhibition in pancreatic cancer cells (10). Unlike classical

Hsp90 inhibitors (such as geldanamycin) that block the Hsp90 ATP binding site, WA directly binds to Hsp90 C-terminus and induces Hsp90-dependent client protein degradation. In addition, WA also disrupted Hsp90-Cdc37 complex, which is also different from classic Hsp90 inhibitors.

The 90 kDa heat-shock protein (Hsp90) has emerged as a promising target for drug discovery (11, 12). Studies revealed that Hsp90 is associated with the folding, stabilization, activation, and maturation of many important oncogenic client proteins in cancer cells (13-15). Since Hsp90 regulates many cellular processes in cancer cells, such as proliferation, cell cycle progression, survival, invasion, angiogenesis and metastasis (16), inhibition of Hsp90 by small molecules leads to simultaneous degradation of multiple oncogenic proteins, and inhibits these cellular processes of cancer cells (17, 18).

Hsp90 chaperone activity is regulated by numerous co-chaperones, such as Hsp70, Hop, Cdc37, and driven by a cycle of N-terminal ATP/ADP exchange through ATP hydrolysis at N-terminal ATP binding site (19). Several natural products including geldanamycin (GA) and its derivatives 17-AAG, 17-DMAG inhibit Hsp90 ATPase activity through competitively blockage of the N-terminal ATP binding pocket and cause proteasomal degradation of client proteins (20-24). Another type of Hsp90 inhibitor, novobiocin (and its derivatives) targets the C-terminal ATP binding pocket, inducing similar cellular responses as N-terminal ATP pocket inhibitors (25, 26). In addition to the inhibition of ATPase activity of Hsp90, other Hsp90 inhibition mechanisms have also been characterized. For instance, epilgallocatechin-3-gallate (EGCG) was reported to directly bind Hsp90

C-terminal and impair the Hsp90's association with its co-chaperones p23 and Hsc70 (18). However, EGCG had little effect on ATPase activity (27). Since Hsp90 is known to interact with various co-chaperones to assemble a superchaperone complex for its protein folding and maturation, disruption of Hsp90 complex may provide additional mechanisms to inhibit Hsp90 for cancer therapy.

Withaferin A (WA) binds to Hsp90 C-terminus and also blocks Hsp90-Cdc37 complex in cancer cells. However, it remains unclear what is the functional group of withaferin A which contributes to the inhibition of Hsp90 chaperoning activity. Previous studies have shown that the 4 β-hydroxy-5 β, 6 β epoxy-2-en-1 moiety and unsaturated lactone are critical for WA's biological function (28). In this study, we intend to investigate different structures of withaferin A (WA) and its four analogues for their mechanisms to inhibit Hsp90 and efficacy of anti-proliferative activity in pancreatic cancer cells. The data suggest that the C-5, 6 epoxy functional group of withanolides is required to bind Hsp90, induce Hsp90 aggregation, and induce Hsp90 client protein degradation, and eventually show anti-proliferative activity. The substitution of C-2, 3 position may hinder withanolides to inhibit Hsp90 activity while the C-4 hydroxyl group within ketone unsaturated A ring of withanolide may enhance its activity to inhibit Hsp90 and disrupt Hsp90-Cdc37 interaction.

Materials and methods

Compounds and antibodies

Withaferin A (Figure 4.1) was purchased from Calbiochem Inc. (San Diego, CA). 3-Aziridinylwithaferin A (AzWA, NSC339665, Figure 4.1), withanolide E (WE, NSC179834, Figure 4.1), 4β-hydroxywithanolide E (HWE, NSC212509, Figure 4.1), and Withaperuvin (WP, NSC334387, Figure 4.1) were kindly provided by The NCI/DTP Open Chemical Repository (http://dtp.cancer.gov). The following antibodies were used for Western blot: Akt, PARP (Cell Signaling, Beverly, MA), Hsp70 (StressGen, Victoria, BC, Canada), Cdk4, β-Actin, Cdc37 and Hsp90 (Santa Cruz, Santa Cruz, CA). Monoclonal Hsp90 antibody H9010 for immunoprecipitation was purchased from Alexis Biochemicals (San Diego, CA). Pan-caspase inhibitor (Z-VAD-FMK) was purchased from Promega (Madison, WI).

MTS assay

Human pancreatic cancer cell line Panc-1 was cultured in 10% FBS RPMI-1640 at 37 °C and 5% CO_2. Pancreatic cancer cells were seeded in 96-well microplates at a density of 3,000 to 5,000 cells per well and cultured for overnight. The cells were treated with different drugs at various concentrations in DMSO (0.5% DMSO final concentration) for 48h. The cell proliferation was assessed using MTS assay (Promega, Madison, WI) according to the manufacturer's manual. The number of living cells in the culture is directly proportional to the absorbance at 490 nm by a formazan product bioreduced from MTS in living cells. The IC_{50} value for cytotoxicity was estimated by WinNonlin software (Pharsight, Mountain View, CA).

Caspase-3 activity assay.

Panc-1 cells were treated with 10μM Withaferin A (WA), withanolide E (WE), 4β-hydroxywithanolide E (HWE), 3-Aziridinylwithaferin A (AzWA), and Withaperuvin (WP), respectively for 48h. The Caspase-3 activity assay was performed according to the manufacturer's instruction of Caspase-3/CPP32 Fluorometric Assay Kit (Biovision Research Products, Mountain View, CA). Cellular protein was extracted with the supplied lysis buffer and protein concentration was measured using BCA Protein Assay Reagents (Pierce, Rockford, IL). The cleavage of DEVD-AFC, a substrate of caspase-3, was quantified using a fluorescence microtiter plate reader with a 400 nm excitation filter and a 505 nm emission filter.

Withaferin A-Biotin pull down assay

Biotinyl-Withaferin A (WA-biotin) was prepared and used in the pull down assay as described previously (8). Briefly, Panc-1 pancreatic cancer cell whole cell extract was prepared in TNEK buffer (5 mM Tris, pH 7.4; NP-40 1%; EDTA 2 mM; KCl 200 mM) supplemented with protease inhibitors. Aliquots of cell lysate containing equal amounts of total protein were precleared with NeutrAvidin beads (Pierce) before incubation with equal concentration of different drugs for 1h at 4 °C, respectively. Then equal amounts of immobilized WA-biotin were added to each sample and incubated for 2 h at 4 °C with constant agitation. The beads were then washed with TNEK buffer for three times, and were boiled in loading buffer for 4 min to dissociate the bound proteins. Western blot was carried out to determine the levels of Hsp90 proteins.

Western-blot

The procedure for Western blotting analysis was performed as previously described (29). Briefly, after treated with different drugs for the 24-48 hr, Panc-1 cells were washed twice with ice-cold PBS, collected in RIPA lysis buffer (20 mM Tris-HCl, 150 mM NaCl, 1% NP-40, 5mM EDTA, 1 mM Na3VO4, pH 7.5) supplemented with a protease inhibitor mixture (Sigma-Aldrich, St. Louis, MO), and incubated on ice for 20 min. Afterward cell lysate was centrifuged at 14,000 × rpm for 10 min, and the pellet was diluted in SDS sample buffer. Isolation of triton-soluble and triton-insoluble proteins was performed as described by Chen et al.(30) . Protein concentration was determined using BCA Protein Reagents (Pierce, Rockford, IL). The protein was separated by SDS-PAGE and electrotransferred onto a PVDF membrane (BioRad, Richmond, CA). Bolts were then probed with appropriate antibodies.

To analyze the disulfide-bonded protein, non-reducing SDS-PAGE was employed. Briefly, drug-treated cells were washed twice with ice-cold and then incubated in ice-cold PBS with 40 mM iodoacetamide (IA) for 5 min to prevent thiol-disulfide exchange and inhibit postlysis oxidation of free cysteines (31). Afterwards, sample was diluted in SDS-sample buffer without reducing agents before loading onto SDS-PAGE.

Co-immunoprecipitation assay

The general procedure for co-immunoprecipitation was described as follows. The drug-treated Panc-1 cells were harvested and lysed in RIPA lysis buffer supplemented with a protease inhibitor mixture (Sigma-Aldrich, St. Louis, MO). After centrifugation pellet was collected and protein was quantified using BCA

protein assay reagents (Pierce, Rockford, IL). Each of protein samples (500 μg) was first incubated with 5 μl H9010 anti-Hsp90 antibody (Axxora, San Diego, CA) for 1 h at 4 °C, rotating, and then added with 30 μl protein G agarose (Pierce, Rockford, IL) followed by incubation of another 2 h at 4 °C. The beads were washed three times with PBS plus protease inhibitors and boiled in loading buffer for 4 min to isolate the bound proteins. The protein was separated by SDS-PAGE. Western blot was performed to determine the levels of co-immunoprecipitated proteins.

Results

Withaferin A (WA), and its analogs withanolide E (WE), 4β-hydroxywithanolide E (HWE), and 3-Aziridinylwithaferin A (AzWA) inhibit cell proliferation and induce apoptosis in pancreatic cancer Panc-1cells

To investigate the cytotoxicity of WA, WE, HWE, AzWA and WP, pancreatic cancer Panc-1 cells were incubated with increasing concentrations of WA and its derivatives for 48 h, respectively. Cell viability was examined by MTS assay. As shown in Figure 4.2A, WA, WE and HWE exhibited dose-dependent cytotoxicity against Panc-1 with IC_{50}s of 1.05, 1.46 and 1.21 μM, respectively; whereas AzWA showed relatively weaker inhibitory effect on Panc-1 with IC_{50} of 2.76 μM. In contrast, WP did not inhibit cell viability even at a concentration up to 50 μM.

One of the primary events in apoptosis is activation of caspase-3 (32). To study whether WA and its derivatives induced apoptosis, caspase-3 activity was measured in Panc-1 cells with WA, AzWA, WE, HWE and WP treatment. As

shown in Figure 4.2B, 10 μM WA, AzWA, WE and HWE for 48 h treatment increased caspase-3 activity by 21.3-, 5.8-, 11.6- and 15.3-fold, respectively, in comparison with untreated cells. In contrast, 10 μM WP did not induce apoptosis in Panc-1 cells. Similarly, PARP protein level also showed that WA, AzWA, WE and HWE decreased PARP level and resulted in the occurrence of cleaved PARP, whereas WP did not (Figure 4.2C).

WA's analogues WE, HWE and AzWA decrease cellular levels of Hsp90 client proteins

Previously, WA was shown to bind Hsp90 and induce Hsp90 client protein degradation. Since WA's analogues WE, HWE and AzWA exhibited potent anti-proliferative activity and induced apoptosis in Panc-1 cells similarly to WA, we also tested if WE, HWE and AzWA would also interact with Hsp90 and cause simultaneous down-regulation of multiple oncogenic proteins. To examine this, we investigated a panel of cancer-associated Hsp90 client proteins level in response to 10 μM WA, AzWA, WE, HWE or WP for 24 h treatment, respectively. The levels of Hsp90 client protein Akt and Cdk4 were down-regulated by 5-, 4-, 2-, 4-fold, and 6-, 3-,3-, 3-fold, respectively, upon incubation with WA, WE, HWE or AzWA. However, WP did not cause significant alterations of the protein levels of Akt and Cdk4 (Figure 4.3A).

Because the induction of Hsp70 is another molecular signature in response to Hsp90 inhibition (33), we also determined the Hsp70 protein level after WA, AzWA, WE, HWE or WP treatment. As shown in Figure 4.3B, 10 μM WA, AzWA, WE or HWE increased the protein level of Hsp70 by 2- to 3-fold after 24 h

treatment while they did not change the Hsp90 protein level (Figure 4.3C), whereas WP failed to increase Hsp70 protein level. These data suggested that WA, AzWA, WE and HWE may inhibit Hsp90 chaperone activity, which might contribute to their anti-proliferative activity in pancreatic cancer cells. However, WP has no effect on the inhibition of Hsp90 activity.

WA's analogues AzWA, WE and HWE induced Hsp90 client proteins degradation is proteasome-dependent

It was reported that WA induced Hsp90 client protein degradation was proteasome-mediated (10). Since WA's analogues AzWA, WE and HWE also decreased Hsp90 client protein levels, we further examined whether AzWA, WE and HWE induced Hsp90 client proteins via proteasome-dependent pathway. WP served as a negative control. MG132 was used as proteasome inhibitor to reverse the protein degradation. WA, AzWA, WE or HWE treatment alone decreased the level of Akt and Cdk4. To better characterize the protein level change, the total protein were divided into two fractions: triton soluble and triton insoluble fraction. For proteins whose fate is proteasome mediated degradation, the proteins would be encapsulated into the vehicle, and underwent ubiquitination and followed by proteasome degradation. The vehicle encapsulated proteins are recovered in the triton insoluble fraction but not in the triton soluble fraction. When cells were treated with 10 μM MG132 combined with 10 μM WA, AzWA, WE or HWE, respectively, the Akt and Cdk4 proteins were disappeared from the triton-soluble fraction (Figure 4.4B) but accumulated by 1-, 7-, 4-, 2-fold and 1-, 7-, 3-, 4-fold, respectively, in the triton-insoluble fraction

(Figure 4.4A). Whereas, pre-incubation with pan-caspase inhibitor (Z-VAD-FMK) for 1 h and then treated with WA, WE, HWE, AzWA and WP for 24 h did not show accumulation of Akt or Cdk4 in the combined treatment group compared to WA and its analogues treatment alone in the triton insoluble fraction indicating caspase was not involved in the protein degradation of Akt and Cdk4 (Figure 4.4D). These results indicate that WA, AzWA, WE and HWE may inhibit Hsp90 to induce proteasome-mediated client proteins aggregation, while WP did not inhibit Hsp90.

WA's analogues AzWA, WE or HWE directly binds to Hsp90 and cause Hsp90 aggregation

It has been reported that Hsp90 chaperone proteins are sensitive to cellular redox conditions and tend to form disulfide bonds under stress conditions (30, 31). WA has also exhibited high reactivity with cysteine residues in proteins such as Annexin II (8) and vimentin (34). Moreover, previous studies have shown that WA may directly bind to Hsp90 and cause disulfide-linked high molecular weight conformers of Hsp90 (10). Therefore, we tested whether WA's analogues AzWA, WE, HWE and WP bind to Hsp90 using competition with biotinyl-withaferin A pull down assay. As shown in Figure 4.5A, WA-biotin successfully pulled down Hsp90 from cell lysate. Preincubation with 100 μM of unlabeled WE, HWE or AzWA were able to compete against the WA-biotin binding to Hsp90 in cell lysate, while WP did not compete with biotin-WA for its binding to Hsp90. Furthermore, we used nonreducing gel electrophoresis to determine the Hsp90 aggregates in WA and its derivatives AzWA, WE, HWE or WP-treated cells. When Panc-1 cells

were incubated with 10 μM WA, AzWA, WE or HWE for 24 h, respectively, the formation of Hsp90 aggregates was detected, exhibited as slower migration and higher molecular weight band (Figure 4.5B). However, WP did not induce Hsp90 aggregation.

WA, HWE, AzWA, but not WE or WP interrupt Hsp90-Cdc37 association in pancreatic cancer cells

In cancer cells, Hsp90 requires an array of co-chaperones to assemble a superchaperone complex, which catalyzes the conformational maturation of various client proteins (35). It was reported that Hsp90-Cdc37 complex played a significant role in regulating protein kinases in cancer cells (36). In our previous study, we have shown that withaferin A dissociated Hsp90-Cdc37 in a time and dose dependent manner, and 5 μM withaferin A treatment could completely block Hsp90-Cdc37 interaction (10). To further characterize whether WA's analogues AzWA, WE, HWE or WP could block the Hsp90-Cdc37 interaction, co-immunoprecipitation (co-IP) assay was employed. After incubation with 10 μM WA, AzWA, WE, HWE or WP for 24h, respectively, Panc-1 cells were collected for total cellular protein. Co-IP Hsp90 was carried out, and the Cdc37 protein levels were detected by immunoblotting in precipitated Hsp90 complexes. The result showed that AzWA, WE, HWE or WP all failed to disrupt the interaction of Hsp90-Cdc37 (Figure 4.6A). Further increasing the drug treatment concentration to 20 μM, co-IP of Hsp90 showed that WA, HWE and AzWA can decrease Cdc37 interaction to Hsp90 but not WE and WP (Figure 4.6B). Meanwhile, western blotting was carried out to analyze the total cellular protein level of Cdc37

(without co-IP). As shown in Figure 4.6C, WA, AzWA, WE, HWE or WP did not change the total cellular Cdc37 protein level. These data indicate that the absent of Cdc37 band after drug treatment in co-IP result was not due to the expression level alteration of Cdc37 protein. These data further confirmed that only WA, but not AzWA, WE, HWE or WP was able to block Hsp90-Cdc37 interaction.

Discussion

Withanolides, a large family of natural steroidal lactone triterpenoids, are major constituents purified from medicinal plant W. somnifera and its related Solanaceae species such as Physalis, Nicandra, Dunalia,Datura, Jaborosa, and Acnistus (28). Withaferin A, a prototype of the natural products withanolides, is reported to have antitumor, antibacterial, anti-inflammatory, antidepressant, antioxidant, immunosuppressive activities (37, 38). Previous studies indicated that withaferin A (WA) represents as a novel Hsp90 inhibitor against pancreatic cancers both in vitro and in vivo. WA inhibited Hsp90 activity through directly binding to Hsp90, induced Hsp90 client protein degradation and dissociated the Hsp90–Cdc37 interaction. The purpose of our current study is to investigate the structure and activity relationship inhibiting Hsp90 of withaferin A and its analogs withanolide E (WE), 4β-hydroxywithanolide E (HWE), and 3-aziridinylwithaferin A (AzWA).

To date, several studies have identified the potential pharmacophores of withaferin A for its activities. The data showed that the 4 β-hydroxy-5 β, 6 β-epoxy-2-en-1-one moiety and unsaturated lactone side chains are critical for

biological activity (39). The 5 β, 6 β-epoxide group within B ring was reported to react with 2-mercaptoethanol, which is a biochemical thiol-oxidizer (40) to be involved in Michael addition thioalkylation reactions (41-43). An earlier study also demonstrated that the epoxide functionality at C-5,6 acts as a Michael acceptor is essential for withaferin A anticancer activities in P-388 lymphocytic leukemia (44). In addition, the ketone containing unsaturated A ring is also readily alkylated by thiol-nucleophiles and undergoes Michael addition (39). Although it was reported that the C-27 hydroxyl group in unsaturated lactone was considered to be dispensable (45), it may have some contributions to withaferin A's activity (46). Furthermore, the preliminary structure–activity studies of newly identified withanolides also confirmed that the ketone unsaturated A ring and epoxide are important for their cytotoxic activity, including withangulatin B,withangulatin C, withangulatin G, withangulatin H, and withangulatin I (38, 47).

This study showed that withaferin A (WA), withanolide E (WE), 4 β-hydroxywithanolide E (HWE) and 3-aziridinyl-withaferin A (AzWA) all share the 5 β, 6 β-epoxide group. These compounds resulted in similar anti-proliferative activity and apoptosis induction against pancreatic cancer cell Panc-1. In contrast, up to 50 μM withaperuvin (WP) which does not have 5 β, 6 β-epoxide group within B ring, was unable to significantly decrease the cell viability and induce apoptosis in Panc-1 cells. These results suggest that the 5 β, 6 β-epoxide group within B ring plays an important role in the anti-proliferative activity of withaferin A against pancreatic cells. Indeed, these finding was confirmed by the previous

studies, which reported that the loss or replacement of epoxy functional group at C- 5, 6 of withafeirn A abrogated its biological function (40, 41).

In addition, the substituent group at C-2, 3 in the unsaturated A ring also impacts the biological function of withaferin A. In our study, 3-aziridinyl-withaferin A (AzWA) demonstrated relatively weak anti-proliferative activity and apoptosis induction in Panc-1 cells as compared to withaferin A. Similar results have been revealed that the activity of withaferin A was decreased when it was converted to 3-methoxy-2,3-dihydrowithaferin A (45). Furthermore, the anti-proliferative activity and apoptosis induction of 4 β-hydroxywithanolide E (HWE), which contained a hydroxyl substituent at C-4, slightly increased compared to withanolide E, which lacked the 4 β-hydroxy group. Previous data also confirmed that hydroxyl group at C-4 within ketone unsaturated A ring contributed to the inhibition of cell viability of withanolides (46).

Our study showed that withaferin A (WA) and its analogs may also inhibit Hsp90 by direct binging to Hsp90 without affecting its ATP binding site. We further explored the structure-activity relationship of WA and its analogs to inhibit Hsp90 chaperone machinery.

In mammalian cells, Hsp90 plays a critical role as molecular chaperons for the stability, maturation and activation of oncogenic client proteins such as Raf, Akt, v-Src, Her2, Cdk4, mutant p53, focal adhesion kinase, vascular endothelial growth factor receptor, and telomerase, which are crucial for oncogenesis and malignant progression (48, 49). Drug-mediated inhibition of Hsp90 leads to simultaneous misfolding and aggregation of various client protein, which results

in degradation via ubiquitin-proteasome pathway (50, 51). In addition, Hsp90 was considered to be over expressed in cancerous tissue and existed as altered superchaperone complex, which inherently results in greater drug selectivity to cancer cells (52, 53). Therefore, Hsp90 has emerged as a promising therapeutic target for cancer therapeutics. Recently, several drugs have been developed to inhibit Hsp90 and validated in clinical trials including 17-AAG, 17-DMAG and IPI-504, which are all derivatives or analogues based on the structure of geldanamycin (GA), a potent Hsp90 inhibitor from natural products (54-58).

In order to assess whether epoxy group at C-5, 6 within B ring, the substituent groups at C-3 and the hydroxyl group at C-4 of withanolide affect Hsp90 inhibition, we examined the protein levels of Akt and Cdk4, two well identified Hsp90 client proteins, and Hsp70 a molecular signature in response to Hsp90 inhibition in cancer cells in response to the treatment of WA and its analogs (49). Consistent with the results of cytotoxicity and apoptosis, withanolide E (WE), 4 β-hydroxy-withanolide E (HWE), 3-aziridinyl-withaferin A (AzWA), which all contain the 5 β, 6 β-epoxide group induced the Akt and Cdk4 degradation as well as HSP70 up-regulation, whereas withaperuvin (WP) showed little effects. In addition, 4 β-hydroxywithanolide E (HWE), with an additional hydroxyl group at C-4 decreased protein levels of Akt and Cdk4 more than that of withanolide E (WE). Furthermore, 3-aziridinylwithaferin A (AzWA), with an additional aziridinyl group at C-3 induced much less of Hsp90 client protein degradation compared to withaferin A (WA). In the presence of proteasome inhibitor MG132, both Akt and Cdk4 accumulated in Triton-insoluble fraction of drug-treated cells, suggesting

that withanolide E (WE), 4 β-hydroxywithanolide E (HWE) or 3-aziridinylwithaferin A (AzWA) triggered proteasome-dependent degradation of misfolded/aggregated Hsp90 client protein. The alteration of these important signaling molecules suggest that the epoxy group at C-5, 6 within B ring, the substituent group at C-3 and the hydroxyl group at C-4 within ketone unsaturated A ring contributed considerably to the inhibition of Hsp90 activity.

The competition of Biotinyl-withaferin A pull down assay by other withaferin analogs provide structure-activity relationship for withanolide to bind Hsp90. In our previous study, we have shown that withaferin A directly binds to the C-terminus Hsp90 but not N-terminus Hsp90, which might be though the interaction with the reactive cysteine residues. Since only C-terminus Hsp90 contains reactive cysteine residues whereas N-terminus Hsp90 not. In addition, withaferin A biotin failed to pull down full length yeast Hsp90 which did not contain reactive cysteine residues (10). In the present study, we demonstrated that withanolide E (WE), 4 β-hydroxywithanolide E (HWE) and 3-aziridinylwithaferin A (AzWA) were able to compete for biotin-WA binding to Hsp90 in cell lysate, whereas withaperuvin (WP) failed to inhibit biotin-WA binding. These results suggest that epoxide functional group at C-5, 6 plays an important role in withanolide interacting with the C-terminus of Hsp90.

Previous studies revealed that Hsp90 chaperone proteins containing cysteine residues are sensitive to cellular redox conditions and form intermolecular disulfide bonds in stress conditions, hence cause the formation of high molecular weight aggregate of Hsp90 (59, 60). Withaferin A (WA),

withanolide E (WE), 4 β-hydroxywithanolide E (HWE) and 3-aziridinylwithaferin A (AzWA) all induced Hsp90 aggregates, which suggests the importance of epoxide functional group at C-5, 6 to induce Hsp90 aggregation.

Cdc37, a cochaperone of Hsp90 is crucial in loading protein kinase to Hsp90 superchaperone complex (61, 62). Cdc37 associated with a large subset of Hsp90 client proteins, which are essential in signal transduction, cell proliferation and survival (62). Cdc37 was found to be highly expressed in cancer cells and may contribute the malignant phenotype (63, 64). 10 μM Withaferin A was observed to disrupt Hsp90-Cdc37 complex. In addition, 20 μM 4β-hydroxy-withanolide E (HWE), and 3-aziridinyl-withaferin A (AzHA) were also demonstrated to be able to inhibit Hsp90-Cdc37 interaction. Whereas, 20 μM withanolide E (WE) or withaperuvin (WP) did not disrupt the Hsp90-Cdc37 interaction in pancreatic cancer cell lysate. Further examining the structures of WA, HWE, AzWA which can disrupt Hsp90-Cdc37 interaction whereas WE and WP cannot, WA, HWE and AzWA share the same C-5, C-6 epoxide group and C-4 hydroxyl group, whereas WE contains C-5, C-6 epoxide group but not C-4 hydroxyl group, and WP contains C-4 hydroxyl group but not C-5, C-6 epoxide group, indicating both C-5, C-6 epoxide group and C-4 hydroxyl group might be crucial for disruption of Hsp90-Cdc37 interaction.

In summary, various withaferin A analogs were investigated for their anticancer activity and mechanisms to inhibit Hsp90. The data suggest that the epoxy functional group at C-5, 6 of withanolides is required to bind Hsp90, induce Hsp90 aggregation, and induce Hsp90 client protein degradation, and eventually

show anti-proliferative activity. The substitution of C-2, 3 position may hinder withanolides to inhibit Hsp90 activity while the hydroxyl group at C-4 within ketone unsaturated A ring of withanolide may enhance its activity to inhibit Hsp90 and induce Hsp90 client protein degradation, and disrupt Hsp90-Cdc37 interaction. These structure-activity relationships of withanolides provide detailed mechanism for this class of compounds to inhibit Hsp90 for their anticancer activity.

References

1. Davis L, Kuttan G. Effect of Withania somnifera on DMBA induced carcinogenesis. J Ethnopharmacol 2001; 75: 165-8.
2. Mishra LC, Singh BB, Dagenais S. Scientific basis for the therapeutic use of Withania somnifera (ashwagandha): a review. Altern Med Rev 2000; 5: 334-46.
3. Mohan R, Hammers HJ, Bargagna-Mohan P, et al. Withaferin A is a potent inhibitor of angiogenesis. Angiogenesis 2004; 7: 115-22.
4. Srinivasan S, Ranga RS, Burikhanov R, Han SS, Chendil D. Par-4-dependent apoptosis by the dietary compound withaferin A in prostate cancer cells. Cancer Res 2007; 67: 246-53.
5. Malik F, Kumar A, Bhushan S, et al. Reactive oxygen species generation and mitochondrial dysfunction in the apoptotic cell death of human myeloid leukemia HL-60 cells by a dietary compound withaferin A with concomitant protection by N-acetyl cysteine. Apoptosis 2007; 12: 2115-33.
6. Stan SD, Hahm ER, Warin R, Singh SV. Withaferin A causes FOXO3a-and Bim-dependent apoptosis and inhibits growth of human breast cancer cells in vivo. Cancer Res 2008; 68: 7661-9.
7. Ichikawa H, Takada Y, Shishodia S, Jayaprakasam B, Nair MG, Aggarwal BB. Withanolides potentiate apoptosis, inhibit invasion, and abolish osteoclastogenesis through suppression of nuclear factor-kappaB (NF-kappaB) activation and NF-kappaB-regulated gene expression. Mol Cancer Ther 2006; 5: 1434-45.
8. Falsey RR, Marron MT, Gunaherath GM, et al. Actin microfilament aggregation induced by withaferin A is mediated by annexin II. Nat Chem Biol 2006; 2: 33-8.
9. Kaileh M, Vanden Berghe W, Heyerick A, et al. Withaferin a strongly elicits IkappaB kinase beta hyperphosphorylation concomitant with potent inhibition of its kinase activity. J Biol Chem 2007; 282: 4253-64.
10. Yu Y, Hamza A, Zhang T, et al. Withaferin A targets heat shock protein 90 in pancreatic cancer cells. Biochem Pharmacol; 79: 542-51.
11. Powers MV, Workman P. Inhibitors of the heat shock response: biology and pharmacology. FEBS Lett 2007; 581: 3758-69.
12. Chaudhury S, Welch TR, Blagg BS. Hsp90 as a target for drug development. ChemMedChem 2006; 1: 1331-40.
13. Westerheide SD, Morimoto RI. Heat shock response modulators as therapeutic tools for diseases of protein conformation. J Biol Chem 2005; 280: 33097-100.
14. McClellan AJ, Xia Y, Deutschbauer AM, Davis RW, Gerstein M, Frydman J. Diverse cellular functions of the Hsp90 molecular chaperone uncovered using systems approaches. Cell 2007; 131: 121-35.
15. Kamal A, Boehm MF, Burrows FJ. Therapeutic and diagnostic implications of Hsp90 activation. Trends Mol Med 2004; 10: 283-90.
16. Workman P. Combinatorial attack on multistep oncogenesis by inhibiting the Hsp90 molecular chaperone. Cancer Lett 2004; 206: 149-57.

17. Blagosklonny MV. Hsp-90-associated oncoproteins: multiple targets of geldanamycin and its analogs. Leukemia 2002; 16: 455-62.
18. Hostein I, Robertson D, DiStefano F, Workman P, Clarke PA. Inhibition of signal transduction by the Hsp90 inhibitor 17-allylamino-17-demethoxygeldanamycin results in cytostasis and apoptosis. Cancer Res 2001; 61: 4003-9.
19. Obermann WM, Sondermann H, Russo AA, Pavletich NP, Hartl FU. In vivo function of Hsp90 is dependent on ATP binding and ATP hydrolysis. J Cell Biol 1998; 143: 901-10.
20. Neckers L. Development of small molecule Hsp90 inhibitors: utilizing both forward and reverse chemical genomics for drug identification. Curr Med Chem 2003; 10: 733-9.
21. Roe SM, Prodromou C, O'Brien R, Ladbury JE, Piper PW, Pearl LH. Structural basis for inhibition of the Hsp90 molecular chaperone by the antitumor antibiotics radicicol and geldanamycin. J Med Chem 1999; 42: 260-6.
22. Supko JG, Hickman RL, Grever MR, Malspeis L. Preclinical pharmacologic evaluation of geldanamycin as an antitumor agent. Cancer Chemother Pharmacol 1995; 36: 305-15.
23. Egorin MJ, Lagattuta TF, Hamburger DR, et al. Pharmacokinetics, tissue distribution, and metabolism of 17-(dimethylaminoethylamino)-17-demethoxygeldanamycin (NSC 707545) in CD2F1 mice and Fischer 344 rats. Cancer Chemother Pharmacol 2002; 49: 7-19.
24. Glaze ER, Lambert AL, Smith AC, et al. Preclinical toxicity of a geldanamycin analog, 17-(dimethylaminoethylamino)-17-demethoxygeldanamycin (17-DMAG), in rats and dogs: potential clinical relevance. Cancer Chemother Pharmacol 2005; 56: 637-47.
25. Allan RK, Mok D, Ward BK, Ratajczak T. Modulation of chaperone function and cochaperone interaction by novobiocin in the C-terminal domain of Hsp90: evidence that coumarin antibiotics disrupt Hsp90 dimerization. J Biol Chem 2006; 281: 7161-71.
26. Marcu MG, Chadli A, Bouhouche I, Catelli M, Neckers LM. The heat shock protein 90 antagonist novobiocin interacts with a previously unrecognized ATP-binding domain in the carboxyl terminus of the chaperone. J Biol Chem 2000; 275: 37181-6.
27. Li Y, Zhang T, Jiang Y, Lee HF, Schwartz SJ, Sun D. (-)-Epigallocatechin-3-gallate inhibits Hsp90 function by impairing Hsp90 association with cochaperones in pancreatic cancer cell line Mia Paca-2. Mol Pharm 2009; 6: 1152-9.
28. M K, K S, K U. Cell differentiation inducing steroids from Withania somnifera L. Chem Pharm Bull 1999; 47: 1646-9.
29. Zhang T, Hamza A, Cao X, et al. A novel Hsp90 inhibitor to disrupt Hsp90/Cdc37 complex against pancreatic cancer cells. Mol Cancer Ther 2008; 7: 162-70.
30. Chen WY, Chang FR, Huang ZY, Chen JH, Wu YC, Wu CC. Tubocapsenolide A, a novel withanolide, inhibits proliferation and induces

apoptosis in MDA-MB-231 cells by thiol oxidation of heat shock proteins. J Biol Chem 2008; 283: 17184-93.
31. Cumming RC, Andon NL, Haynes PA, Park M, Fischer WH, Schubert D. Protein disulfide bond formation in the cytoplasm during oxidative stress. J Biol Chem 2004; 279: 21749-58.
32. Khan N, Afaq F, Saleem M, Ahmad N, Mukhtar H. Targeting multiple signaling pathways by green tea polyphenol (-)-epigallocatechin-3-gallate. Cancer Res 2006; 66: 2500-5.
33. Banerji U, Walton M, Raynaud F, et al. Pharmacokinetic-pharmacodynamic relationships for the heat shock protein 90 molecular chaperone inhibitor 17-allylamino, 17-demethoxygeldanamycin in human ovarian cancer xenograft models. Clin Cancer Res 2005; 11: 7023-32.
34. Bargagna-Mohan P, Hamza A, Kim YE, et al. The tumor inhibitor and antiangiogenic agent withaferin A targets the intermediate filament protein vimentin. Chem Biol 2007; 14: 623-34.
35. Kamal A, Thao L, Sensintaffar J, et al. A high-affinity conformation of Hsp90 confers tumour selectivity on Hsp90 inhibitors. Nature 2003; 425: 407-10.
36. Roe SM, Ali MM, Meyer P, et al. The Mechanism of Hsp90 regulation by the protein kinase-specific cochaperone p50(cdc37). Cell 2004; 116: 87-98.
37. Mirjalili MH, Moyano E, Bonfill M, Cusido RM, Palazon J. Steroidal lactones from Withania somnifera, an ancient plant for novel medicine. Molecules 2009; 14: 2373-93.
38. Damu AG, Kuo PC, Su CR, et al. Isolation, structures, and structure - cytotoxic activity relationships of withanolides and physalins from Physalis angulata. J Nat Prod 2007; 70: 1146-52.
39. Yokota Y, Bargagna-Mohan P, Ravindranath PP, Kim KB, Mohan R. Development of withaferin A analogs as probes of angiogenesis. Bioorg Med Chem Lett 2006; 16: 2603-7.
40. Misra L, Lal P, Chaurasia ND, Sangwan RS, Sinha S, Tuli R. Selective reactivity of 2-mercaptoethanol with 5beta,6beta-epoxide in steroids from Withania somnifera. Steroids 2008; 73: 245-51.
41. Fuska J, Fuskova A, Rosazza JP, Nicholas AW. Novel cytotoxic and antitumor agents. IV. Withaferin A: relation of its structure to the in vitro cytotoxic effects on P388 cells. Neoplasma 1984; 31: 31-6.
42. Oh JH, Lee TJ, Park JW, Kwon TK. Withaferin A inhibits iNOS expression and nitric oxide production by Akt inactivation and down-regulating LPS-induced activity of NF-kappaB in RAW 264.7 cells. Eur J Pharmacol 2008; 599: 11-7.
43. Liang MC, Bardhan S, Pace EA, et al. Inhibition of transcription factor NF-kappaB signaling proteins IKKbeta and p65 through specific cysteine residues by epoxyquinone A monomer: correlation with its anti-cancer cell growth activity. Biochem Pharmacol 2006; 71: 634-45.
44. Ray AB, Gupta M. Withasteroids, a growing group of naturally occurring steroidal lactones. Fortschr Chem Org Naturst 1994; 63: 1-106.
45. Bargagna-Mohan P, Ravindranath PP, Mohan R. Small molecule anti-angiogenic probes of the ubiquitin proteasome pathway: potential application to choroidal neovascularization. Invest Ophthalmol Vis Sci 2006; 47: 4138-45.

46. Jayaprakasam B, Zhang Y, Seeram NP, Nair MG. Growth inhibition of human tumor cell lines by withanolides from Withania somnifera leaves. Life Sci 2003; 74: 125-32.
47. Lee SW, Pan MH, Chen CM, Chen ZT. Withangulatin I, a new cytotoxic withanolide from Physalis angulata. Chem Pharm Bull (Tokyo) 2008; 56: 234-6.
48. Hartl FU, Hayer-Hartl M. Molecular chaperones in the cytosol: from nascent chain to folded protein. Science 2002; 295: 1852-8.
49. Wegele H, Muller L, Buchner J. Hsp70 and Hsp90--a relay team for protein folding. Rev Physiol Biochem Pharmacol 2004; 151: 1-44.
50. Mimnaugh EG, Chavany C, Neckers L. Polyubiquitination and proteasomal degradation of the p185c-erbB-2 receptor protein-tyrosine kinase induced by geldanamycin. J Biol Chem 1996; 271: 22796-801.
51. An WG, Schulte TW, Neckers LM. The heat shock protein 90 antagonist geldanamycin alters chaperone association with p210bcr-abl and v-src proteins before their degradation by the proteasome. Cell Growth Differ 2000; 11: 355-60.
52. Workman P. Altered states: selectively drugging the Hsp90 cancer chaperone. Trends Mol Med 2004; 10: 47-51.
53. Plescia J, Salz W, Xia F, et al. Rational design of shepherdin, a novel anticancer agent. Cancer Cell 2005; 7: 457-68.
54. Chiosis G, Rodina A, Moulick K. Emerging Hsp90 inhibitors: from discovery to clinic. Anticancer Agents Med Chem 2006; 6: 1-8.
55. Usmani SZ, Bona R, Li Z. 17 AAG for HSP90 inhibition in cancer--from bench to bedside. Curr Mol Med 2009; 9: 654-64.
56. Ramanathan RK, Egorin MJ, Eiseman JL, et al. Phase I and pharmacodynamic study of 17-(allylamino)-17-demethoxygeldanamycin in adult patients with refractory advanced cancers. Clin Cancer Res 2007; 13: 1769-74.
57. Janin YL. Heat shock protein 90 inhibitors. A text book example of medicinal chemistry? J Med Chem 2005; 48: 7503-12.
58. Chiosis G. Targeting chaperones in transformed systems--a focus on Hsp90 and cancer. Expert Opin Ther Targets 2006; 10: 37-50.
59. Nardai G, Sass B, Eber J, Orosz G, Csermely P. Reactive cysteines of the 90-kDa heat shock protein, Hsp90. Arch Biochem Biophys 2000; 384: 59-67.
60. Clark CB, Rane MJ, El Mehdi D, Miller CJ, Sachleben LR, Jr., Gozal E. Role of oxidative stress in geldanamycin-induced cytotoxicity and disruption of Hsp90 signaling complex. Free Radic Biol Med 2009; 47: 1440-9.
61. Smith JR, Workman P. Targeting CDC37: an alternative, kinase-directed strategy for disruption of oncogenic chaperoning. Cell Cycle 2009; 8: 362-72.
62. Pearl LH. Hsp90 and Cdc37 -- a chaperone cancer conspiracy. Curr Opin Genet Dev 2005; 15: 55-61.
63. Schwarze SR, Fu VX, Jarrard DF. Cdc37 enhances proliferation and is necessary for normal human prostate epithelial cell survival. Cancer Res 2003; 63: 4614-9.
64. Stepanova L, Yang G, DeMayo F, et al. Induction of human Cdc37 in prostate cancer correlates with the ability of targeted Cdc37 expression to promote prostatic hyperplasia. Oncogene 2000; 19: 2186-93.

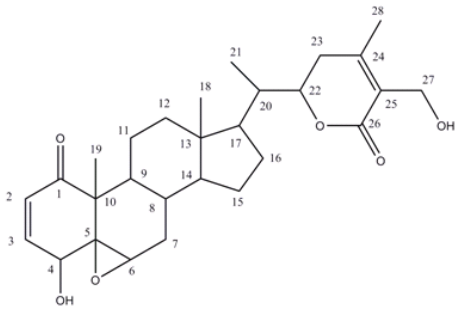

1. Withaferin A (WA)

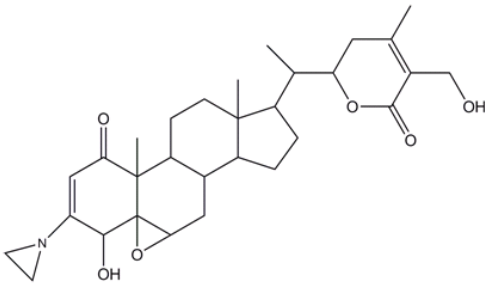

2. 3-Aziridinylwithaferin A (AzWA)

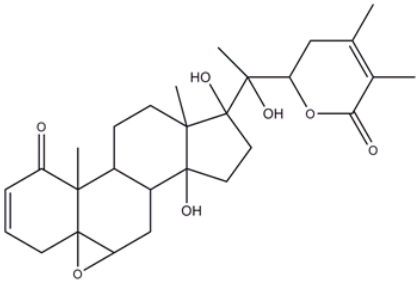

3. Withanolide E (WE)

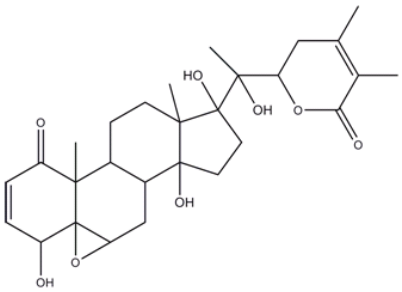

4. 4β-Hydroxywithanolide E (HWE)

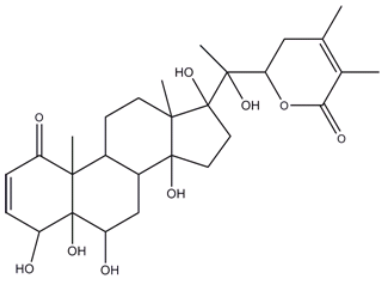

5. Withaperuvin (WP)

Figure 4.1 Chemical structure of withaferin A (WA), withanolide E (WE), 4β-hydroxywithanolide E (HWE), 3-Aziridinylwithaferin A (AzWA) and Withaperuvin (WP).

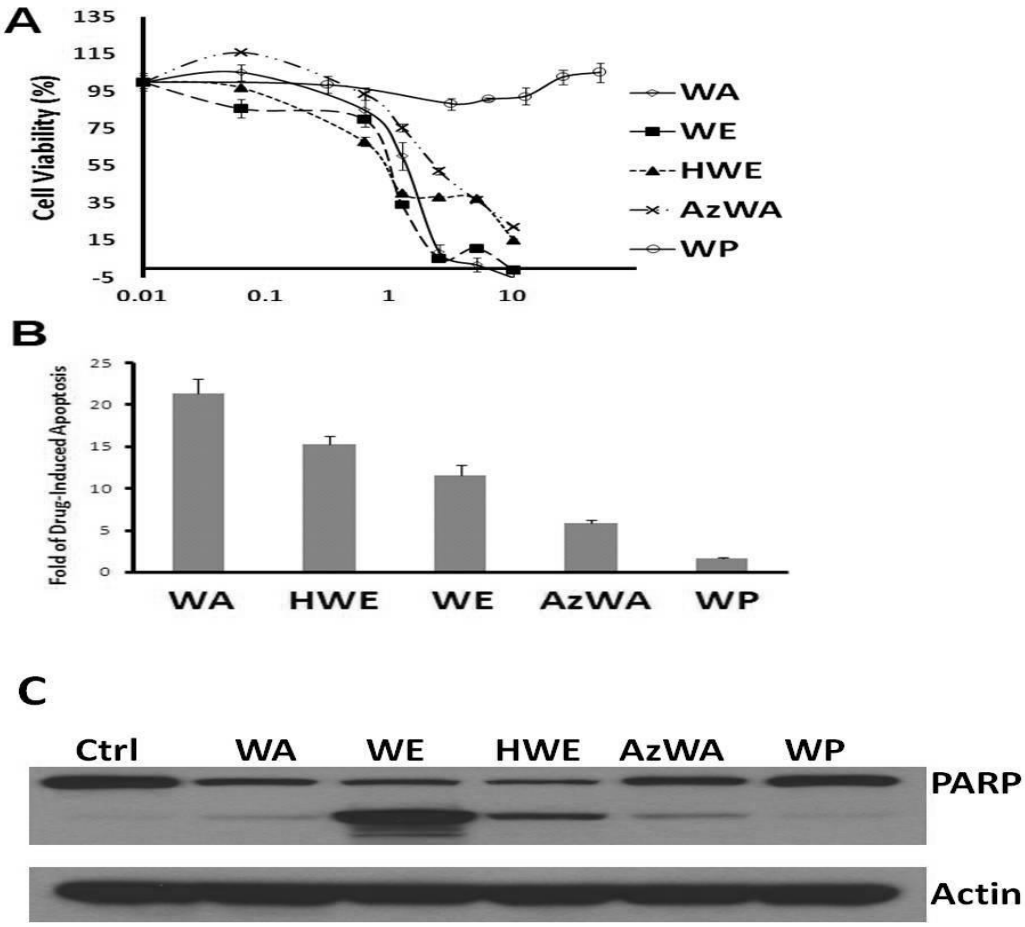

Figure 4.2 Effect of WA, WE, HWE, AzWA, and WP on cytotoxixty and apoptosis induction in Panc-1 cells. A. Dose-response curve of withaferin A (WA) and its analogues, withanolide E (WE), 4β-hydroxywithanolide E (HWE), 3-Aziridinylwithaferin A (AzWA) and withaperuvin (WP), on cell cytotoxity in Panc-1 cells. Cells were grown in log phase and treated with increasing concentrations of WA, WE, HWE, AzWA or WP for 48 h, respectively. The cytotoxicity of those compounds were measured by MTS assay. B. Caspase-3 activity in Panc-1 cells after WA, WE, HWE, AzWA or WP treatment. Cells were treated with WA, WE, HWE, AzWA or WP, respectively and harvested at the indicated time. Cell lysates were prepared for caspase-3 activity assay. Results are expressed as arbitrary fluorescent units (AFU) normalized to milligram of cytosolic protein. Data are presented as mean ± SD (n = 3). C. PARP protein level in Panc-1 cells after WA, WE, HWE, AzWA or WP treatment. Cells were treated with 10 μM WA, WE, HWE, AzWA or WP, respectively for 24 h. Equal amounts of protein (50 μg/lane) were subjected to SDS-PAGE and analyzed by Western blot with specific antibodies to PARP and Actin. Actin was served as internal standard. Results are representative of three independent experiments.

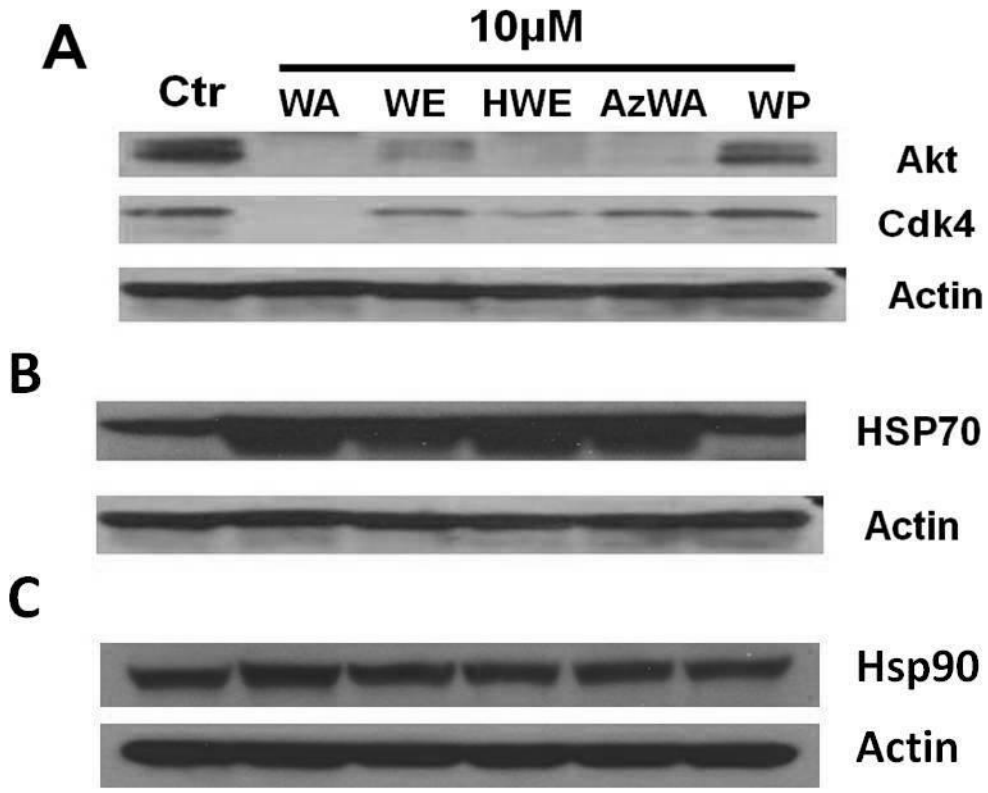

Figure 4.3 WA, WE, HWE, and AzWA but not WP induced Hsp90 client protein degradation and Hsp70 upregulation in Panc-1 cells. A. HSP90 client protein degradation in Panc-1 cells induced by withaferin A (WA) and its analogues, withanolide E (WE), 4β-hydroxywithanolide E (HWE), 3-Aziridinylwithaferin A (AzWA) and Withaperuvin (WP). Panc-1 cells were treated with 10 μM WA or its analogues for 24h, respectively. Equal amounts of protein (50 μg/lane) were subjected to SDS-PAGE and analyzed by Western blot with specific antibodies to Akt, Cdk4 and Actin. Actin was served as internal standard. Results are representative of three independent experiments. B. WA, WE, HWE or AzWA unregulated Hsp70 protein level. Equal amounts of protein (50 μg/lane) were subjected to SDS-PAGE and analyzed by Western blot with specific antibodies to Hsp70 and Actin. Actin was served as internal standard. Results are representative of three independent experiments. C. WA, WE, HWE or AzWA did not affect Hsp90 protein level. Equal amounts of protein (50 μg/lane) were subjected to SDS-PAGE and analyzed by Western blot with specific antibodies to Hsp90 and Actin. Actin was served as internal standard. Results are representative of three independent experiments.

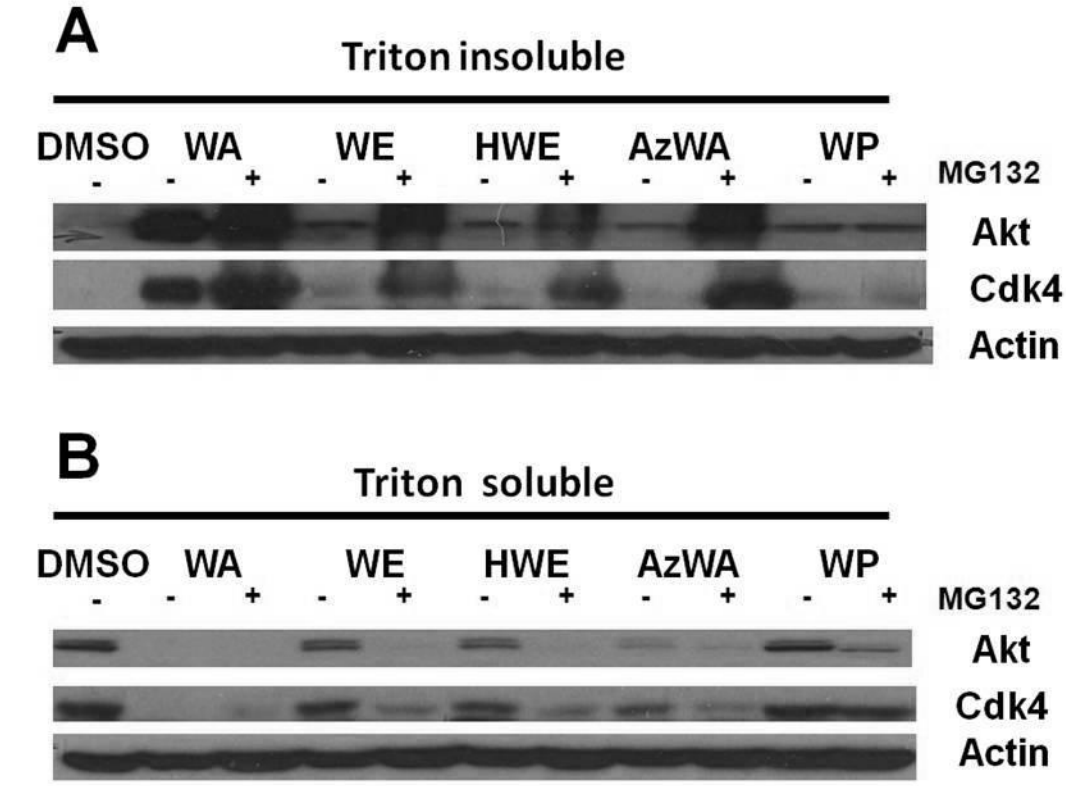
A
Triton insoluble
DMSO
WA
WE
HWE
AzWA
WP
- - + - + - + - + - +
MG132
Akt
Cdk4
Actin
B
Triton soluble
DMSO
WA
WE
HWE
AzWA
WP
- - + - + - + - + - +
MG132
Akt
Cdk4
Actin

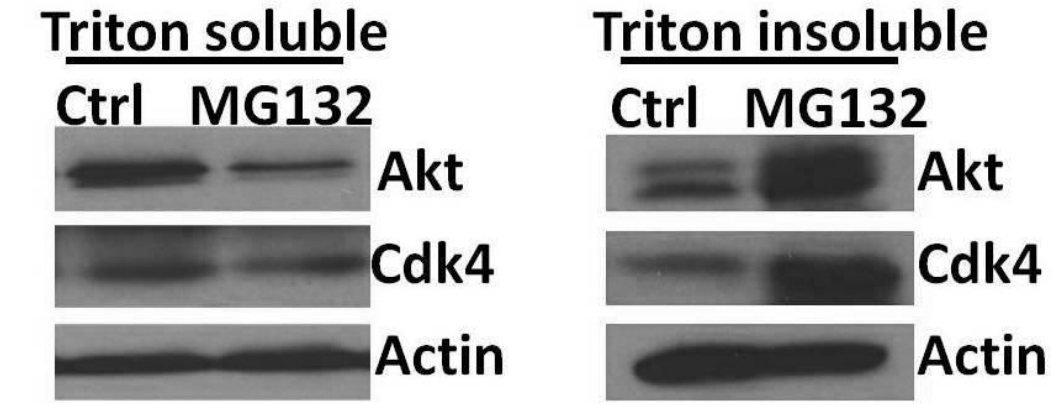
C
Triton soluble
Ctrl MG132
Akt
Cdk4
Actin
Triton insoluble
Ctrl MG132
Akt
Cdk4
Actin

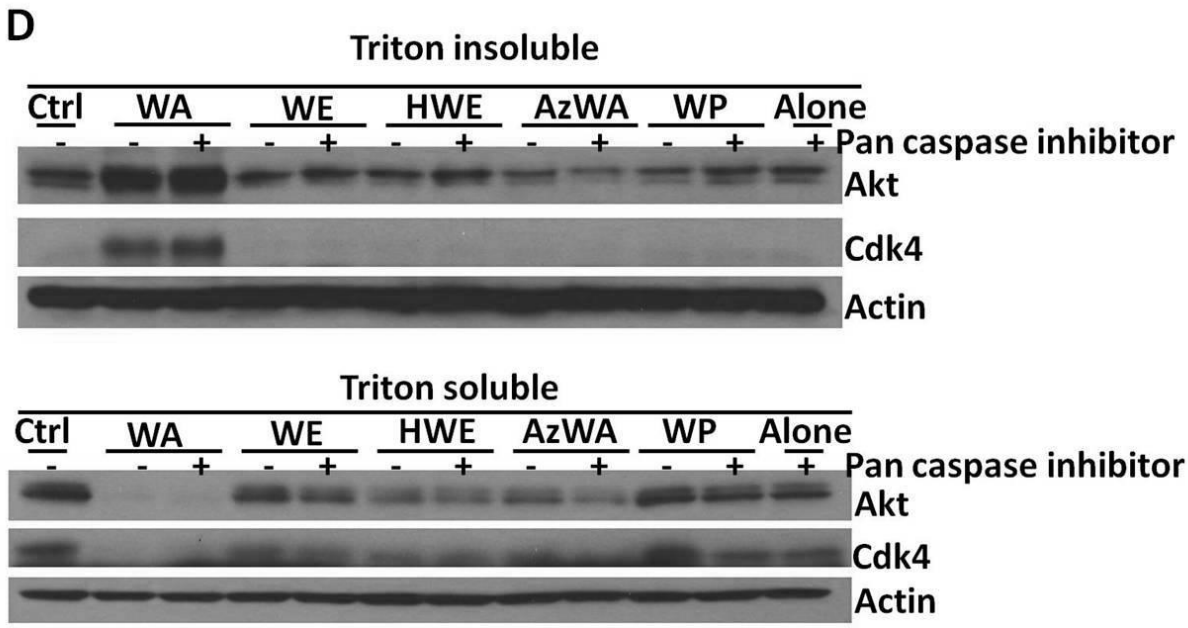

Figure 4.4 Withaferin A (WA) and its analogues induced Hsp90 client protein degradation through proteasome-dependent pathway. Panc-1 cells were preincubated with 10 μM MG132 for 1 h, and then were treated with 5 μM WA for another 24h. Cells were harvested and were lysed in Triton X-100 buffer, and the Triton X-100-insoluble fraction was resolubilized in 2% SDS. Proteins (both triton-soluble and triton-insoluble parts) were subjected to Western blot analysis with specific antibodies to Akt, Cdk4 and Actin. Actin was served as internal standard. Results are representative of three independent experiments. A. Triton insoluble part; B. Triton soluble part; C. Panc-1 cells were treated with 10 μM MG132 for 25 h; D. Panc-1 cells were preincubated with 15 μM Pan-caspase inhibitor for 1 h, and then were treated with 5 μM WA for another 24h.

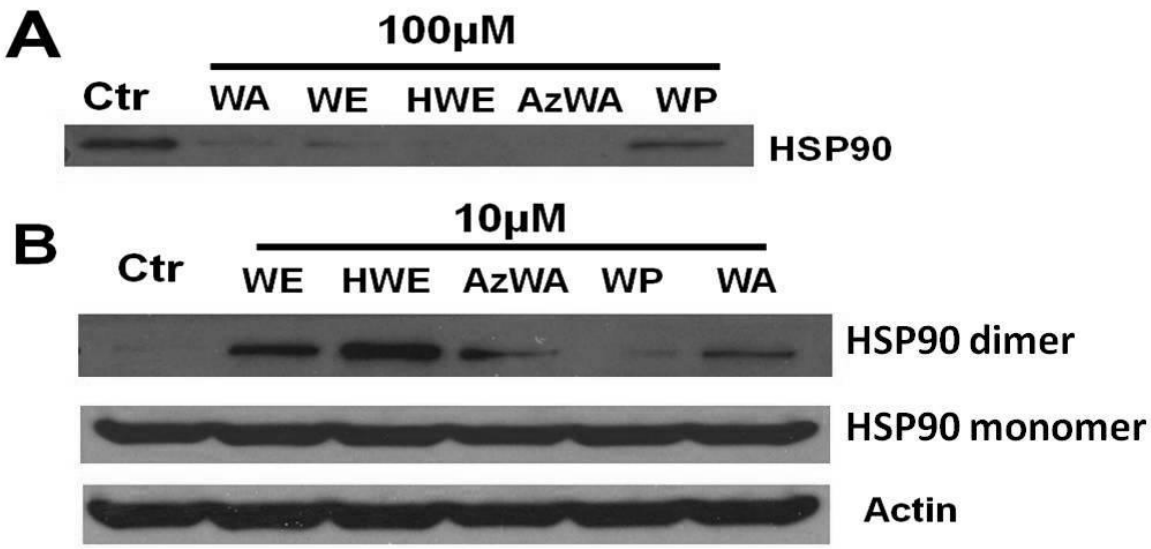

Figure 4.5 Withaferin A and its analogues directly bind to Hsp90 and induce Hsp90 aggregation. A. Withaferin A (WA) and its analogues, withanolide E (WE), 4β-hydroxywithanolide E (HWE), 3-Aziridinylwithaferin A (AzWA) and Withaperuvin (WP) compete with WA-biotin binding to Hsp90. One mg cell lysate was preincubated with 100 μM WA or its analogues for 1 h, respectively before subject to WA-biotin pull down assay. The WA-biotin pull down protein were subjected to Western blot analysis with specific antibodies to Hsp90. B. WA, WE, HWE or AzWA induces Hsp90 aggregation. Panc-1 cells were treated with 10 μM WA or its analogues for 24 h, respectively. Equal amounts of protein (50 μg/lane) were subjected to non-reducing gel electrophoresis and then analyzed by Western blot with specific antibodies to Hsp90 and Actin, Actin was served as internal standard. Results are representative of three independent experiments.

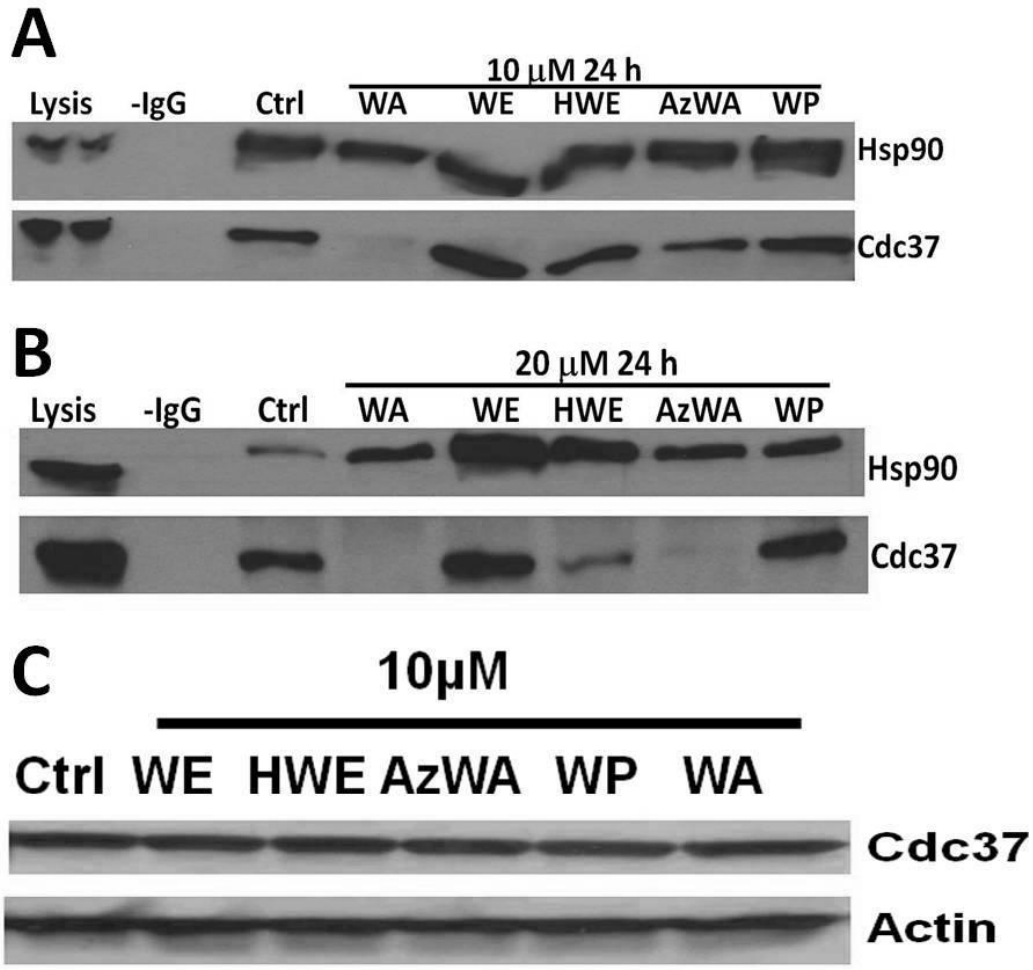

Figure 4.6 Disruption of Hsp90-Cdc37 in Panc-1 cells by withaferin A (WA) and its analogues. A. Immunoprecipitation of Hsp90 and Cdc37 complex. Cell lysates (500 μg total protein) were immunoprecipitated with Hsp90 antibody. Western blot was performed to detect Cdc37 and Hsp90 using specific antibodies. Panc-1 cells were treated with 10 μM WA, WE, HWE, AzWA or WP for 24 h, respectively. Lysis, total cell lysate; IgG, without antibody. B. Panc-1 cells were treated with 20 μM WA, WE, HWE, AzWA or WP for 24 h, respectively. C. Total expression levels of Cdc37 in Panc-1 cells. Panc-1 cells were treated with WA, WE, HWE, AzWA or WP for 24 h, respectively. Equal amounts of protein (50 μg/lane) were subjected to SDS-PAGE and analyzed by Western blot with specific antibodies to Cdc37 and Actin. Actin was served as internal standard. Results are representative of three independent experiments.

CHAPTER V

SUMMARY

The purpose of this study is to investigate the anticancer activity and Hsp90 inhibitory mechanism of withaferin A, to investigate the enhanced anticancer effect of combined withaferin A and myricetin treatment, and to identify the functional groups in withanolides for its anticancer activity and Hsp90 inhibitory activity in pancreatic cancer cells.

In the present study, withaferin A was demonstrated to exhibit potent anticancer activity against pancreatic cancer cells both *in vitro* and *in vivo*. MTS assay showed that withaferin A inhibited pancreatic cancer cell growth with IC_{50}s below 3 μM in three pancreatic cancer cell lines Panc-1, MiaPaca-2 and BxPc-3. WA-Biotin pull-down assay was employed to show that WA can specifically bind to C-terminus Hsp90. The binding of WA to Hsp90 inhibited Hsp90 chaperoning activity and induced Hsp90 client protein including Akt, Cdk4, and glucocorticoid receptor (GR) degradation as shown by western-blot, which was reversed by proteasome inhibitors (MG132 and bortezomib), indicating WA induced Hsp90 client protein degradation was mediated by proteasome. ATP sepharose binding assay showed that withaferin A did not compete with ATP binding to Hsp90 in

contrast to classical Hsp90 inhibitor 17-AAG. In addition, examining the Hsp90 superchaperone complex by co-immunoprecipitation (co-IP) showed that withaferin A did not affect Hsp90-P23 association whereas 17-AAG treatment resulted in Hsp90-P23 dissociation. Interestingly, withaferin A disrupted Hsp90-Cdc37 interaction whereas 17-AAG could not, further indicating withaferin A inhibited Hsp90 in a way different from classical Hsp90 inhibitors. The antitumor effect of withaferin A was also confirmed in the pancreatic cancer xenograft models as administration of withaferin A could result in significant tumor growth inhibition compared to control.

Inhibition of Hsp90 by withaferin A induced Hsp70 upregulation, which was shown to have antiapoptotic activity. Therefore, myricetin, another natural product which was demonstrated to be Hsp70 inhibitor, was employed to examine whether inhibition of Hsp70 by myricetin could sensitize pancreatic cancer cells to withaferin A treatment. MTS assay showed that myricetin could enhance the anti-proliferative activity of withaferin A by decreasing the IC_{50}s of withaferin A by 2.19-, 2.65-, and 3.93-fold compared to withaferin A treatment alone in pancreatic cancer Panc-1, MiaPaca-2, and BxPc-3 cells, respectively. Caspase-3 activity assay also showed that combined treatment of withaferin A and myricetin dramatically increased caspase-3 activity compared with either withaferin A or myricetin treatment alone. Western-blot confirmed that myricetin could decrease withaferin A induced Hsp70 upregulation. In addition, myricetin and withaferin A acted synergistically in downregulating Hsp90 client protein (mutated P53, Akt, and Cdk4). Combined withaferin A and myricetin treatment

also showed significant advantage in tumor growth inhibition in pancreatic cancer xenografts compared to either withaferin A or myricetin treatment alone.

Finally, WA and four analogues withanolide E (WE), 4β-hydroxywithanolide E (HWE), 3-aziridinylwithaferin A (AzWA) were examined for their anticancer activity and Hsp90 inhibitory activity in pancreatic cancer cells to assess the structure activity relationship (SAR) of withanolides. WA, WE, HWE, and AzWA demonstrated anti-proliferative activity against pancreatic cancer cells whereas WP did not. In addition, all the compounds except WA could bind to Hsp90, induce Hsp90 aggregation, and induce Hsp90 client protein degradation. WA, HWE and AzWA could disrupt Hsp90-Cdc37 interaction with varied potency, whereas WE and WP could not. The SAR analysis indicated that the C-5, 6 epoxy functional group was responsible for Hsp90 inhibition and anticancer activity; whereas, the hydroxyl group at C-4 might enhance Hsp90 inhibitory activity and induce Hsp90-Cdc37 complex dissociation; in contrast, the steric bulk substitution at C-3 may reduce their activity.

In conclusion, withaferin A was shown to have potent anticancer activity in pancreatic cancer cells both *in vitro* and *in vivo*. Withaferin A was also demonstrated to inhibit Hsp90 by directly binding to the C-terminus, which was different from classical Hsp90 inhibitors, and thus proposing a new mechanism for developing Hsp90 inhibitors. Combined withaferin A and myricetin treatment was shown to have enhanced anticancer efficacy in pancreatic cancer cells. SAR analysis demonstrated the key functional groups in withanolides for their

anticancer effect and Hsp90 inhibitory activity, which could be the guidance for future Hsp90 inhibitor and anticancer agent development.

APPENDIX I

EXAMINATION OF THE PHARMACOKINETICS OF SEVERAL ACTIVE INGREDIENTS OF GINGER IN HUMANS

Abstract

Ginger extracts or powders have been studied in various clinical trials for different indications. However, little information regarding the pharmacokinetics of the ginger active constituents in human biological matrices is available. This study aims to develop a LC-MS/MS method for simultaneous determination of 6, 8, 10-gingerols and 6-shogaol and study their pharmacokinetics in human plasma and colon tissues. A sensitive LC-MS/MS method was established and validated with low limit of quantification (LLOQ) in a range of 2 – 5 ng/ml for the four analytes. The intra- and inter-day accuracy ranged from -7.3 to 10.4% and from -9.4 to 9.8%, respectively. The intra- and inter-day precision ranged from 0.9 to 10.9% and from 2.0 to 12.4%, respectively. To measure the metabolic conjugates (glucuronide and sulfate) of 6, 8, 10-gingerols and 6-shogaol, the samples were pretreated with β-glucuronidase and sulfatase hydrolysis. After oral dosing of 2.0 gram ginger extracts capsules in human, free 10-gingerol and 6-shogaol were detected in plasma with peak concentrations (9.5 ± 2.2 and 13.6 ± 6.9 ng/ml, respectively) at 1 h after oral administration, but no free 6-gingerol

and 8-gingerol were detected in plasma from 0.25-24 h. The peak concentrations of glucuronide metabolites of 6, 8, 10-gingerols and 6-shogaol were 0.47 ± 0.31, 0.17 ± 0.14, 0.37 ± 0.19, 0.73 ± 0.54 μg/ml at 1 h, respectively. The peak concentrations of the sulfate metabolites of 6, 8, 10-gingerols and 6-shogaol were 0.28 ± 0.15, 0.027 ± 0.018, 0.018 ± 0.006, 0.047 ± 0.035 μg/ml at 1 h, respectively. Very low concentrations (2 to 3 ng/ml) of 10-gingerol glucuronide and sulfate were found in colon tissues. Pharmacokinetic analysis performed using WinNonlin showed that half lives of these four analytes and their metabolites were 1-3 h in human plasma. No accumulation was observed for 6, 8, 10-gingerols and 6-shogaol and their metabolites after multiple daily dosing.
Keywords: 6-gingerol, 8-gingerol, 10-gingerol and 6-shogaol, LC-MS/MS, glucuronide, sulfate, pharmacokinetics

Introduction

The antioxidative, anti-inflammatory, and antitumor properties of ginger (*Zingiber officinale* Roscoe, Zingiberaceae) have been recognized in previous studies (1-5). Various clinical trials involving ginger powders or extracts have been conducted to evaluate the lipid lowering effect (6), treatment of arthritis (7, 8), prevention of nausea and vomiting (9-11), and relief of pain in women with primary dysmenorrhea (12). However, clinical studies using ginger extracts or powders produced mixed or moderate/marginal benefits. For instance, Chaiyakunapruk et al. demonstrated that administration of ginger at a fixed dose

of 1 g was more effective than placebo for the prevention of postoperative nausea and vomiting and postoperative vomiting (13). Whereas Betz et al. concluded that there was no clear evidence for the efficacy of ginger in the treatment of postoperative nausea and vomiting and of kinetosis (14). Bliddal et al. showed that 170 mg daily dosing for 3 weeks of ginger extract did not show significant benefit over placebo in relieving pain in patients with osteoarthritis (15). In contrast, a 6-week treatment period with 510 mg of ginger extract daily dosing produced moderate effect on knee pain in patients with osteoarthritis (16).

In most of the clinical trials, no substantial information regarding the composition of the ginger extract or powders was demonstrated. The use of non-standardized ginger products throughout the clinical studies might partly explain the mixed results of the clinical studies in addition to the different study design and dose regimens. Nevertheless, a study carried out by Schwertner et al. determined the variation in 6-gingerol, 6-shogaol, 8-gingerol, and 10-gingerol concentrations and labeling of different brands of ginger root dietary supplements (7). It was found that large variations were present in the gingerol composition of ginger root powders from different manufacturers, as 6-gingerol ranged from 0.00 to 9.43 mg/g, 6-shogaol ranged from 0.16 to 2.18 mg/g, 8-gingerol ranged from 0.00 to 1.10 mg/g, and 10 gingerol ranged from 0.00 to 1.40 mg/g.

Ginger contains volatile oils (~1 to 3%) and non-volatile pungent components oleoresin (1). A variety of active components were identified in the oleoresin portion of ginger including gingerols and shogaols. Gingerols are series of homologues with varied unbranched alkyl chain length; whereas, shogaols are

series of homologues derived from gingerols with dehydration at the C-5 and C-4 during long-term storage or thermal processing. In addition, other active compounds from oleoresin portion of ginger were also reported, such as [6]-paradol, [6]- and [10]-dehydrogingerdione, [6]- and [10]-gingerdione, [4]-, [6]-, [8]-, and [10]-gingerdiol, [6]-methylgingerdiol, zingerone, [6]-hydroxyshogaol, [6]-, [8]-, [10]-dehydroshogaol, and diarylheptanoids (17-19). Among these compounds, gingerols and shogaols are the major constituents of oleoresin; while the other compounds are present in a limited amount, accounting for 1-10 % of the overall amount of gingerols and shogaols (19). Gingerols (especially 6-gingerol) are the major components in the fresh ginger rhizome. The amount of shogaols is increased in the dried ginger, as evidenced by the reduction of the ratio of 6-gingerol to 6-shogaol from 10:1 in fresh ginger to 1:1 in dried ginger (17, 18, 20).

As ginger powders or extracts contain various components, it would be valuable to identify certain compounds which are responsible for their pharmacological effects. It was demonstrated that 6, 8, 10-gingerols and 6-shogaol had varied efficacy in anti-inflammatory, antibacterial, antipyretic, antilipidemic, antitumorigenic, and antiangiogenic effects (5, 21-27). 6-gingerol was shown to inhibit the enzymatic activity of leukotriene A_4 hydrolase (LTA_4H) and suppress anchorage-independent cancer cell growth in HCT116 and HT29 colorectal cancer cells with IC50s around 50 μM, and 35 μM, respectively (28). Whereas, Sang et al. demonstrated that shogaols (6-, 8-, and 10-) exhibited much higher antiproliferative potency than gingerols (6-, 8-, and 10-) against H-1299 human lung cancer cells with IC50s of 8 μM for 6-shogaol, and 150 μM for

6-gingerol (19). In addition, 10-gingerol was the most potent among the gingerols (19). Furthermore, Dugasani et al. evaluated the antioxidative activity of gingerols and shogaol, and found that 6-shogaol was the strongest with an IC50 of about 8 μM, while 6, 8, and 10-gingerols had the IC50s of 28, 20, and 12 μM, respectively (29).

Despite the numerous studies of the pharmacological effects of the ginger extracts or powders in the human clinical trials, there are limited studies of the pharmacokinetics of the ginger active constituents in human biological matrices. The concentrations of 6, 8, 10-gingerols and 6-shogaol required to show efficacy in vivo are still largely unknown. In our previous study, we developed a HPLC method to determine the concentrations of 6, 8, 10-gingerols and 6-shogaol in healthy human subjects who received p.o. dose of ginger powder capsules at 2.0 g per day (1). However, due to the low sensitivity of the HPLC method with LLOQ ranged from 0.10 to 0.25 μg/ml for the four analytes, we did not detect any of these four compounds in the plasma, although we detected the glucuronide conjugates of the four analytes. No sulfate conjugates of 8-gingerol, 10-gingerol and 6-shogaol were detected. Thus, a more sensitive method for the quantification of the 6, 8, 10-gingerols and 6-shogaol and their metabolite conjugates is desired to characterize the pharmacokinetics of the active ingredients of ginger in human.

In this study, we developed and validated a LC-MS/MS method for the quantification of the 6, 8, 10-gingerols and 6-shogaol simultaneously with the LLOQ ranged from 2 to 5 ng/ml. We further utilized this method to analyze

human plasma samples and detected low concentrations of free 10-gingerol and 6-shogaol, while most of 6, 8, 10-gingerols and 6-shogaol existed in plasma as glucuronide and sulfate metabolites. The pharmacokinetics of the 6, 8, 10-gingerols and 6-shogaol and their metabolites were analyzed. The half lives of all compounds and their metabolites were between 1-3 h.

Materials and Methods

Chemicals and reagents

The ginger product used in this study was manufactured by Pure Encapsulations® (Sudbury, MA) (batch #ZO/06006). A 250 mg dry extract of ginger root capsule contained 6.60 mg (2.64%) 6-gingerol, 1.58 mg (0.63%) 8-gingerol, 3.05 mg (1.22%) 10-gingerol, and 5.63 mg (2.25%) 6-shogaol. The enzymes β-glucuronidase (Type IX-A from *Escherichia coli*) and sulfatase (Type H-1 from *Helix pomatia*) were purchased from Sigma-Aldrich Inc. Sodium phosphate and sodium acetate (American Chemical Society certified) were purchased from Fisher Scientific. 6, 8, 10-gingerols, and 6-shogaol were purchased from Chromadex. Pelargonic acid vanillylamide (PAV), the internal standard, was obtained from Sigma and is >97% pure. Acetonitrile (HPLC grade), methanol (HPLC grade) were purchased from Fisher Scientific (Fisher Scientific Co., Pittsburgh, PA). Formic acid (analytical grade) was from Sigma (Sigma Chemical Company, St. Louis, MO). Water was purified with a Milli- Q water system (Millipore, Bedford, MA).

Clinical trial design

Three studies were conducted in healthy volunteers, single dose in normal risk participants, multiple doses in normal risk and high risk participants. In common to all three studies, participants were 18 years or older and in good health as defined by an unremarkable medical history, physical and screening blood work, and no chronic medication use. Exclusion criteria for the study included: anyone with (1) a history of peptic ulcer disease, gastrointestinal bleeding from gastric or duodenal ulcers, or gastrin secreting tumors; (2) pregnant or lactating women; (3) history of cardiovascular disease; (4) lactose intolerance; (5) or an allergy to ginger. Participants were asked to avoid all foods containing ginger within the 14 days prior to drug administration and completed a food checklist to verify that they were not consuming any ginger-rich foods such as ginger ale or Japanese food. All study procedures were administered at the University of Michigan General Clinical Research Center (GCRC) after the participant gave written, informed consent, and the study was approved by the University of Michigan Institutional Review Board.

Single dose in healthy volunteers

Nine healthy volunteers received 2 gram oral dose of the ginger capsules. Blood was drawn from the participants at baseline, 15, 30, and 45 minutes as well as at 1, 2, 4, 6, 10, 24, 48 and 72 hours after ingestion of the ginger capsules. The plasma fraction was separated from blood immediately, and kept at -70ºC until assayed.

Multiple doses in normal risk participants

A total of 30 participants were enrolled and recruited. Participants to be eligible were assessed as being at normal-risk for developing colorectal cancer. Normal-risk was defined as having had no history of either familial colorectal cancer syndromes or first-degree relatives with colon cancer diagnosed before the age of 60. Normal-risk individuals also could not have a personal history of colorectal cancer or resection of a villous adenoma >1 cm in size or any adenoma containing carcinoma in situ. Participants were randomized (16 to placebo and 14 to ginger) to receive eight 250 mg ginger capsules of study medication taken daily for 28 days. Blood for gingerols/shogaol analysis was drawn at baseline and within 24 hours of the last study medication dose. Participants underwent two flexible sigmoidoscopies, one before drug treatment and the second, 28 days after drug treatment commenced. The second procedure was performed at a time as close as possible to 24 h after the participant took the final ginger dose. The participants were not prepared for the procedure with any enemas. Tissue samples were taken by opening and pressing the biopsy forceps perpendicular to the mucosal surface with mild pressure. Each biopsy specimen was taken ~2 cm or more from other biopsy sites in distal sigmoid colonic mucosa that had no visual appearance of trauma or recent biopsy.

Biopsy samples were placed into a sterile 1.5-ml eppendorf tube and frozen in liquid nitrogen at exactly 50 s after the time the biopsy forceps were closed. The specimens were stored at -70°C until immediately before analysis. The plasma fraction was separated from blood immediately, and kept at -20ºC until assayed.

Multiple doses in high risk subjects

This trial involved 20 participants who were at high risk for developing colorectal cancer (CRC). Participants were randomized, 10 in each group, to receive either eight 250 mg capsules of ginger or placebo (lactose powder) daily for 28 days. High risk for colorectal cancer was defined as having a 1st degree relative diagnosed with CRC before the age of 60; and/or a prior history of a colon adenoma; and/or resected early (Dukes A, B or C) colon cancer previously. Otherwise the trial in people at high risk for CRC was identical to the study in individuals at normal risk for CRC.

Equipment

The quantitative LC-MS/MS analysis was performed on an API 3200 hybrid triple quadrupole/Linear Ion Trap mass spectrometer coupled with an Agilent 1200 HPLC system (Applied Biosystems, MDS Sciex Toronto, Canada).

Liquid chromatography parameters

The chromatography was performed using a 1.8 µm Agilent Zorbax StableBond-C_{18} column (4.6 mm × 50 mm *i.d.*). The injection volume was 10 µl and the flow rate was kept constantly at 300 µl/min. Mobile phase A and B were water containing 0.1% formic acid (v/v) and ACN, respectively. The flow gradient was initially 38 : 62 v/v of A : B for 3 min, linearly ramped to 0 : 100 over 1.5 min, held at 0 : 100 for 3.4 min, and then returned to 38 : 62 over 0.1min. This condition was held for a further 5 min prior to the injection of another sample.

MS/MS parameters

The mass spectrometer was operated at ESI positive ion mode and detection of the ions was performed in the multiple reaction monitoring (MRM) mode. The

analytes and IS were first characterized by Q1 MS (Q1) scan and enhanced product ion (EPI) scan to determine the precursor ions and product ions used in MRM mode. Figure 2 shows the EPI spectra of the analytes and IS. The MS/MS transitions selected were: 6-gingerol, m/z 295.2 precursor ion [M+H]+ to the m/z 137.1 product ion; 8-gingerol, m/z 323.2 precursor ion [M+H]+ to the m/z 137.1 product ion; 10-gingerol, m/z 351.2 precursor ion [M+H]+ to the m/z 137.1 product ion; 6-shogaol, m/z 277.2 precursor ion [M+H]+ to the m/z 137.1 product ion; IS, m/z 294.2 precursor ion [M+H]+ to the m/z 137.1 product ion. The ion spray voltage was set at 5000 V. Ionization temperature was set as 400 °C. CAD was set as Medium. Ihe was set as OFF. The instrument parameters, curtain gas, Gas 1 and Gas 2 (auxillary gas), were set at 10, 60 and 40, respectively. Compounds parameters, declustering potential (DP), collision energy (CE), entrance potential (EP), collision entrance energy (CEP) and collision exit potential (CXP) were 33, 27, 5, 18.4, 2 V for 6-gingerol; 33, 27, 5,19.19, 2 V for 8-gingerol; 33, 27, 5, 19.97, 2 V for 10-gingerol; 44, 18, 5, 17.9, 2 V for 6-shogaol; and 33, 27, 5, 18.38, 2 V for internal standard PAV, respectively. Data acquisition and quantitation were performed using analyst software version 1.4.2 (Applied Biosystems, MDS Sciex Toronto, Canada).

Preparation of stock solution, calibration standard and quality control samples

The stock solutions of 6, 8, 10-gingerols, 6-shogaol and PAV were prepared in methanol with concentrations of 1 mg/ml individually. A series of working standard of the four analytes mixture containing 0.04, 0.1, 0.2, 0.4, 1, 2, 4, 10, 40

μg/ml of the four analytes was prepared by dilution from the stock solutions with methanol. Internal standard PAV working solution was prepared by diluting the stock solution with methanol to the final concentration of 2 μg/ml. Low, medium and high concentration quality control working stock solutions (0.3, 5, 20 μg/ml, respectively) were prepared in methanol using separately weighed stock solutions of the four analytes. Nine calibration standard solutions at 0.002, 0.005, 0.01, 0.02, 0.05, 0.1, 0.2, 0.5, and 2 μg/ml were prepared by spiking blank plasma with appropriate amounts of working standards. QC plasma samples at 0.015, 0.25, 1 μg/ml were prepared in the same way as calibration standard. Blank plasma sample without analytes and internal standard and zero plasma sample with internal standard but not analytes were also prepared and analyzed. All the standard solutions were stored at 4 °C.

Sample preparation

Plasma samples (100 μl) were transferred to microcentrifuge tubes. Then 5 μl internal standard PAV working solution (2 μg/mL) was added to the plasma and the mixture was added with 295 μl ACN and vortexed for 1 min at high speed. The tubes were centrifuged at 13,000 rpm for 10 min to precipitate protein. The clear supernatants were transferred to vial inserts and 10 μl was injected into LC-MS/MS.

To analyze the metabolic conjugates (glucuronide and sulfate) of 6, 8, 10-gingerols and 6-shogaol, the plasma samples were pre-incubated with the enzymes β-glucuronidase and sulfatase as described previously (1, 30). Briefly, 100 μl plasma samples were added with either 10 μl β-glucuronidase (500 units)

in sodium-phosphate buffer (0.1 M, pH 6.8) or 10 μl sulfatase (60 units) in sodium-acetate buffer (0.1 M, pH 5.0), and incubated at 37 °C for 1 h. The samples were then extracted as described above.

Method validation

Specificity: specificity of the analytical method was investigated by the analysis of blank plasma samples from six different sources to avoid potential endogenous interferences at the retention times of the analytes and IS.

Extraction recovery: extraction recovery was determined in triplicate by comparing the peak areas of analytes determined in QC samples spike-pre-extraction and QC samples spike-after-extraction.

Linearity and LLOQ: linearity was evaluated in triplicate for 6, 8, and 10-gingerols in a concentration range from 0.005 to 2 μg/ml, while in a concentration range from 2 to 2000 ng/ml for 6-shogaol. The lower limit of quantification was determined as the lowest concentrations of the analytes which had a signal-to-noise ratio (*S/N*) over 10 and had acceptable accuracy within ±20% (% bias) and precision were less than 20% (% R.S.D).

Accuracy and Precision: accuracy was calculated as the mean percentage deviation of measured concentrations of the three QC samples and LLOQ sample from their nominal concentrations. Precision was calculated as the coefficient of variation (CV) of multiple determinations. Both the inter-day and intra-day results were determined for the accuracy and precision.

Pharmacokinetic analysis

Pharmacokinetic analysis of the plasma analytes concentration – time profile was carried out by Winnolin software (Pharsight, Mountain View, CA).

Results

LC-MS/MS analysis

Blank plasma samples from six different sources were analyzed and found to be free of the interference at the retention times and the mass transitions as the analytes and IS. Figure A1.3 shows representative chromatograms of the blank plasma, blank plasma spiked with analytes and IS, and real plasma sample obtained 1 h after oral administration of ginger powder capsules. The retention time was 4.03 min for 6-gingerol, 7.16 min for 8-gingerol, 9.42 min for 10-gingerol, 8.35 min for 6-shogaol and 4.80 min for IS. Despite the isotope of IS resulted in a peak at 4.82 min in the 6-gingerol channel, all the analytes and IS achieved baseline separation from each other.

Linearity and LLOQ

Calibration curves were constructed from the peak-area ratios of analytes to IS vs plasma concentrations using quadratic regression with a 1/x weighting. Table A1.1 shows linear range, coefficient (*r*) and LLOQ. The LLOQ of 6, 8, 10-gingerols and 6-shogaol were determined as 5 ng/ml, 5 ng/ml, 5 ng/ml, and 2 ng/ml, respectively.

Extraction recovery

Extraction recoveries of the established method ranged from 84.4% to 97.6% for 6-gingerol, from 81.7% to 94.7% for 8-gingerol, from 80.4% to 92.2% for 10-

gingerol, and from 81.8% to 93.6% for 6-shogaol, respectively (Table A1.2). Overall, the extraction recovery was efficient and consistent at different concentration levels of analytes.

Accuracy and Precision

The results for intra-day and inter-day accuracy and precision are listed in Table A1.3. The intra- and inter-day accuracy (expressed as percentage bias against the nominal concentration) ranged from -7.3 to 10.4% and from -9.4 to 9.8%, respectively. The intra- and inter-day precision (expressed as R.S.D.) ranged from 0.9 to 10.9% and from 2.0 to 12.4%, respectively. Therefore, the accuracy and precision for this quantification method are acceptable.

Stability

As the single dose study involved re-analysis of samples that were previously collected and analyzed by HPLC, we set out to examine the stability of the glucuronide and sulfate conjugates of the 6, 8, 10-gingerols and 6-shogaol. Because of the lack of gingerol and shogaol glucuronide or sulfate conjugates standard, we were not able to determine the stability of the conjugates directly. We reanalyzed the samples 6 months after our original quantification. The concentrations determined were within 90 to 110% of the original quantification determined values by using LC-MS/MS. In addition, the concentrations of the 6, 8, 10-ginerols and 6-shogaol conjugate metabolites were within 85 to 115% of the concentrations determined by HPLC which was performed 1.5 years ago.

Pharmacokinetic study

Concentrations of 6, 8, 10-gingerols and 6-shogaol in the plasma after the single dose of ginger powder capsules

In the present study, we applied LC-MS/MS method to quantify the concentrations of 6, 8, 10-gingerols and 6-shogaol, as well as their glucuronide and sulfate conjugates. Free 10-gingerol was detected in plasma with peak concentration of 9.5 ± 2.2 ng/ml at 1 h, which was undetectable after 2 h post dosing. Free 6-shogaol was detected in plasma at peak concentration of 13.6 ± 6.9 ng/ml at 1h, which was undetectable after 4 h post dosing (Figure A1.4). No free 6-gingerol or 8-gingerol were detected in the plasma samples from 0- 24 h time post dosing. The terminal half lives of 10-gingerol and 6-shogaol were 2.1 and 1.3 h, respectively. Other pharmacokinetic parameters were listed in table A1.4.

Glucuronide conjugates of 6, 8, 10-gingerols and 6-shogaol in the plasma after single dose of ginger powder capsules

As gingerols were predominantly present in the form of glucuronide conjugates in the plasma samples after oral dosing (1), we further analyzed the glucuronide conjugates of 6, 8, 10-gingerols and 6-shogaol . The plasma samples were first subjected to the β-glucuronidase hydrolysis, then followed by liquid-liquid extraction as described previously (1). 6-gingerol glucuronide conjugate was detected from 0.25 to 10 h with peak concentration of 0.47 ± 0.31 μg/ml at 1 h. 8-gingerol glucuronide conjugate was observed from 0.25 to 10 h with peak concentration of 0.17 ± 0.14 μg/ml at 1 h. 10-gingerol glucuronide conjugate was observed from 0.25 to 10 h with peak concentration of 0.37 ± 0.19 μg/ml at 1 h.

6-shogaol glucuronide conjugate was observed from 0.25 to 8 h with peak concentration of 0.073 ± 0.054 μg/ml at 1 h (Figure A1.4). To analyze the pharmacokinetic parameters of glucuronide conjugates, the concentrations were calculated with subtraction of free analytes concentrations, since the concentrations of glucuronides were measured after conversion of metabolites to free analytes. The pharmakinetic parmameters were summarized in table A1.4. The half lives of glucuronide conjugates of 6, 8, 10-gingerols and 6-shogaol were 1.6, 1.0, 2.1, and 1.5 h, respectively.

Sulfate conjugates of 6, 8, 10-gingerols and 6-shogaol in the plasma after single dose of ginger powder capsules

The sulfate conjugates of 6, 8, 10-gingerols and 6-shogaol were also determined after the sulfatase hydrolysis. 6-gingerol sulfate conjugate was detected from 0.25 to 8 h with peak concentration of 0.28 ± 0.15 μg/ml at 1 h. 8-gingerol sulfate conjugate was observed from 0.5 to 4 h with peak concentration of 0.28 ± 0.18 μg/ml at 1 h. 10-gingerol sulfate conjugate was observed from 0.25 to 10 h with peak concentration of 0.017 ± 0.007 μg/ml at 1 h. 6-shogaol sulfate conjugate was observed from 0.25 to 6 h with peak concentration of 0.047 ± 0.035 μg/ml at 1 h (Figure A1.4).

Similarly, to analyze the pharmacokinetic parameters of sulfate conjugates, the concentrations were calculated with subtraction of free analytes concentrations. The pharmacokinetic parameters of the sulfate metabolites of 6, 8, 10-gingerols and 6-shogaol were shown in table A1.4. Their half lives were 1.8, 1.3, 3.2, and 1.4 h, respectively.

Concentrations of 6, 8, 10-gingerols and 6-shogaol and their conjugate metabolites in the plasmas after multiple dose of ginger powder capsules

Total of 23 healthy human subjects received either placebo (n=11) or ginger powder capsules 2.0 g/day (n=12) for 24 days. Their plasmas were drawn within 24 h of the last dose. Free 6, 8, 10-gingerols and 6-shogaol and their conjugate metabolites were determined. Due to their short half lives, no free 6, 8, 10-gingerols and 6-shogaol were detected in the plasma of all the subjects in 24 hours after last dosing. These data suggest that no accumulation of free 6, 8, 10-gingerols and 6-shogaol in plasma after multiple daily dosing. Low levels of 6-gingerol glucuronide (ranged from 5.43 to 13.6 ng/ml), 6-gingerol sulfate (ranged from 6.19 to 7.29 ng/ml) and 10-gingerol glucuronide (ranged from 6.96 to 9.33 ng/ml) were observed in 4 subjects who received ginger powder capsules. The levels of 10-gingerol sulfate, 8-gingerol glucuronide, 8-gingerol sulfate, 6-shogaol gluruconide and 6-shogaol sulfate were below the detection limits in all the participants. These data demonstrated no accumulation of 6, 8, 10-gingerols and 6-shogaol or their conjugate metabolites in plasma after 24 days' multiple daily dosing regimen due to their short half lives and fast clearance.

Concentrations of 6, 8, 10-gingerols and 6-shogaol and their conjugate metabolites in the colon tissues after multiple doses of ginger powder capsules in normal and high risk colon cancer subjects

Although 6-gingerol was shown to have high concentration in gastrointestinal tract after p.o. dosing (31), no free 6-gingerol and its metabolites were detected in the colon tissues at 24 h after multiple daily dose ginger powder capsules.

Only marginal levels of 10-gingerol glucuronide and sulfate conjugates were detected at 24 h after multiple daily dosing of ginger powder capsules which ranged from 1.72 to 2.76 ng/ml.

Discussion

In a previous study, Wang et al. developed a HPLC/MS method to quantify 6, 8, 10-gingerols and 6-shogaol in rat plasma after oral administration of ginger oleoresin (3). The LLOQ ranged from 3.57 to 10.4 ng/ml for 6, 8, 10-gingerols and 6-shogaol. Free 6, 8, 10-gingerols and 6-shogaol were detected in rat plasma with varied concentrations at dose 300 mg/kg (p.o.). However, only glucuronide conjugate of 6-gingerol was detected in rat plasma, whereas the levels of the glucuronide conjugates of 8, 10-gingerols and 6-shogaol were under LLOQ. Another study at p.o. dosing 30 mg/kg of purified 6-gingerol in rats failed to detect free 6-gingerol in rat plasma (32).

In the current study, we developed a LC-MS/MS method for the simultaneous quantification of 6, 8, 10-gingerols and 6-shogaol with LLOQ ranged from 2 to 5 ng/ml, which was more sensitive compared to the LC/MS method developed by Wang et al. In addition, we analyzed pharmacokinetics of these 4 analytes and their glucuronide and sulfate metabolites in human plasma. Our data indicate that only free 10-gingerol and 6-shogaol were detected in the human plasma, whereas, the majority of the 6, 8, 10-gingerols and 6-shogaol existed as glucuronide and sulfate metabolites after oral dosing of 2 gram ginger powder capsules. Furthermore, due to the short half lives of the 4 analytes, no

accumulation was observed in the plasma after multiple daily doses. Moreover, no analytes or their conjugates were detected in the colon tissues at 24 h after multiple dosing.

Our data suggest both the glucuronide and sulfate conjugates of 6, 8, 10-gingerols and 6-shogaol are present in human plasma. No free 6-gingerol was detected in plasma despite it was the most abundant component of the ginger powder capsule (2.64%). In comparison, although 6-shogaol makes up 2.25% and 10-gingerol only accounts for 1.22% of the ginger powder capsule, 6-shogaol and 10-gingerol free compounds were detected in the human plasma. Whether 6-gingerol conversion to 6-shogaol in gastro-intestinal tract needs to be further explored, as previous report demonstrated that 6-gingerol and 6-shogaol inter-converted to each other in simulated gastric fluid (33). Overall, all the 6-gingerol, 8-gingerol and the majority of 10-gingerol and 6-shogaol were present as either the glucuronide conjugate or sulfate conjugate, and only small amount of 10-gingerol and 6-shogaol were present as the free drugs, therefore, the pharmacological efficacy of 6-shogaol and 10-gingerol needs to be further validated. In fact, reports showed that 6-shogaol and 10-gingerol were much more pharmacologically active than 6-gingerol or 8-gingerol (19, 29, 34). However, the peak concentrations determined for 10-gingerol and 6-shogaol were 9.5 ± 2.2 ng/ml (0.027 ± 0.006 μM) and 13.6 ± 6.9 ng/ml (0.049 ± 0.025 μM), which were less than the IC_{50}s of 10-gingerol and 6-shogaol (12 μM and 8 μM, respectively). Although gingerols and shogaol might be higher in colon tissues (31), in the present study, only limited amount of 10-gingerol glucuronide and

sulfate conjugates were detected at 24 h after multiple daily dosing in several subjects. To better understand the pharmacokinetics of the gingerols and shogaol in colon tissues and correlate pharmacokinetic to pharmacodynamic effect, early sampling time would be required to quantify the drug concentrations in colon tissues in future clinical studies.

In the present study, we measured 6, 8, 10-gingerols, 6-shogaol and their glucuronide and sulfate conjugates in human plasma and colon tissues. However, it is worth noting that other metabolites of the gingerols and shogaol might also have pharmacological activity. For instance, *rac*-6-dihydroparadol (6-DHP), a mammalian metabolite of 6-gingerol and 6-shogaol which was chemically and metabolically stable, was shown to inhibit IκB-α degradation and NF-κB nuclear translocation, thus decreased iNOS protein expression and suppressed NO synthesis in murine macrophage, finally led to anti-inflammatory effect (35). In addition, the other components of ginger powders or extracts such as paradols were not quantified due to the lack of commercially available standards. Paradols have shown pharmacological effects similar to gingerols and shogaols (36-39). All these components warrant future studies.

Conclusion

In conclusion, this study developed and validated a sensitive LC-MS/MS method for the simultaneous quantification of 6, 8, 10-gingerols and 6-shogaol in the human plasma. Low levels of free 10-gingerol and 6-shogaol were detected in human plasma, whereas most of the 6, 8, 10-gingerols and 6-shogaol existed

in the form of glucuronide or sulfate conjugates. The pharmacokinetics of the 6, 8, 10-gingerols and 6-shogaol and their metabolites were analyzed. The half lives of all compounds and their metabolites are between 1-3 h in human plasma.

References

1. Zick SM, Djuric Z, Ruffin MT, et al. Pharmacokinetics of 6-gingerol, 8-gingerol, 10-gingerol, and 6-shogaol and conjugate metabolites in healthy human subjects. Cancer Epidemiol Biomarkers Prev 2008; 17: 1930-6.
2. Kawai T, Kinoshita K, Koyama K, Takahashi K. Anti-emetic principles of Magnolia obovata bark and Zingiber officinale rhizome. Planta Med 1994; 60: 17-20.
3. Wang W, Li CY, Wen XD, Li P, Qi LW. Simultaneous determination of 6-gingerol, 8-gingerol, 10-gingerol and 6-shogaol in rat plasma by liquid chromatography-mass spectrometry: Application to pharmacokinetics. J Chromatogr B Analyt Technol Biomed Life Sci 2009; 877: 671-9.
4. Shukla Y, Singh M. Cancer preventive properties of ginger: a brief review. Food Chem Toxicol 2007; 45: 683-90.
5. Surh YJ. Anti-tumor promoting potential of selected spice ingredients with antioxidative and anti-inflammatory activities: a short review. Food Chem Toxicol 2002; 40: 1091-7.
6. Alizadeh-Navaei R, Roozbeh F, Saravi M, Pouramir M, Jalali F, Moghadamnia AA. Investigation of the effect of ginger on the lipid levels. A double blind controlled clinical trial. Saudi Med J 2008; 29: 1280-4.
7. Schwertner HA, Rios DC, Pascoe JE. Variation in concentration and labeling of ginger root dietary supplements. Obstet Gynecol 2006; 107: 1337-43.
8. Tao Y, Li W, Liang W, Van Breemen RB. Identification and quantification of gingerols and related compounds in ginger dietary supplements using high-performance liquid chromatography-tandem mass spectrometry. J Agric Food Chem 2009; 57: 10014-21.
9. Apariman S, Ratchanon S, Wiriyasirivej B. Effectiveness of ginger for prevention of nausea and vomiting after gynecological laparoscopy. J Med Assoc Thai 2006; 89: 2003-9.
10. Chittumma P, Kaewkiattikun K, Wiriyasiriwach B. Comparison of the effectiveness of ginger and vitamin B6 for treatment of nausea and vomiting in early pregnancy: a randomized double-blind controlled trial. J Med Assoc Thai 2007; 90: 15-20.
11. Hickok JT, Roscoe JA, Morrow GR, Ryan JL. A Phase II/III Randomized, Placebo-Controlled, Double-Blind Clinical Trial of Ginger (Zingiber officinale) for Nausea Caused by Chemotherapy for Cancer: A Currently Accruing URCC CCOP Cancer Control Study. Support Cancer Ther 2007; 4: 247-50.
12. Ozgoli G, Goli M, Moattar F. Comparison of Effects of Ginger, Mefenamic Acid, and Ibuprofen on Pain in Women with Primary Dysmenorrhea. J Altern Complement Med 2009; 15: 129-32.
13. Chaiyakunapruk N, Kitikannakorn N, Nathisuwan S, Leeprakobboon K, Leelasettagool C. The efficacy of ginger for the prevention of postoperative nausea and vomiting: a meta-analysis. Am J Obstet Gynecol 2006; 194: 95-9.
14. Betz O, Kranke P, Geldner G, Wulf H, Eberhart LH. [Is ginger a clinically relevant antiemetic? A systematic review of randomized controlled trials]. Forsch Komplementarmed Klass Naturheilkd 2005; 12: 14-23.

15. Bliddal H, Rosetzsky A, Schlichting P, et al. A randomized, placebo-controlled, cross-over study of ginger extracts and ibuprofen in osteoarthritis. Osteoarthritis Cartilage 2000; 8: 9-12.
16. Altman RD, Marcussen KC. Effects of a ginger extract on knee pain in patients with osteoarthritis. Arthritis Rheum 2001; 44: 2531-8.
17. Govindarajan VS. Ginger--chemistry, technology, and quality evaluation: part 1. Crit Rev Food Sci Nutr 1982; 17: 1-96.
18. Govindarajan VS. Ginger-chemistry, technology, and quality evaluation: part 2. Crit Rev Food Sci Nutr 1982; 17: 189-258.
19. Sang S, Hong J, Wu H, et al. Increased growth inhibitory effects on human cancer cells and anti-inflammatory potency of shogaols from Zingiber officinale relative to gingerols. J Agric Food Chem 2009; 57: 10645-50.
20. Wu H, Hsieh MC, Lo CY, et al. 6-Shogaol is more effective than 6-gingerol and curcumin in inhibiting 12-O-tetradecanoylphorbol 13-acetate-induced tumor promotion in mice. Mol Nutr Food Res 2010; 54: 1296-306.
21. Mascolo N, Jain R, Jain SC, Capasso F. Ethnopharmacologic investigation of ginger (Zingiber officinale). J Ethnopharmacol 1989; 27: 129-40.
22. Kim EC, Min JK, Kim TY, et al. [6]-Gingerol, a pungent ingredient of ginger, inhibits angiogenesis in vitro and in vivo. Biochem Biophys Res Commun 2005; 335: 300-8.
23. Yagihashi S, Miura Y, Yagasaki K. Inhibitory effect of gingerol on the proliferation and invasion of hepatoma cells in culture. Cytotechnology 2008; 57: 129-36.
24. Lee TY, Lee KC, Chen SY, Chang HH. 6-Gingerol inhibits ROS and iNOS through the suppression of PKC-alpha and NF-kappaB pathways in lipopolysaccharide-stimulated mouse macrophages. Biochem Biophys Res Commun 2009; 382: 134-9.
25. Akoachere JF, Ndip RN, Chenwi EB, Ndip LM, Njock TE, Anong DN. Antibacterial effect of Zingiber officinale and Garcinia kola on respiratory tract pathogens. East Afr Med J 2002; 79: 588-92.
26. Ficker C, Smith ML, Akpagana K, et al. Bioassay-guided isolation and identification of antifungal compounds from ginger. Phytother Res 2003; 17: 897-902.
27. Park M, Bae J, Lee DS. Antibacterial activity of [10]-gingerol and [12]-gingerol isolated from ginger rhizome against periodontal bacteria. Phytother Res 2008; 22: 1446-9.
28. Jeong CH, Bode AM, Pugliese A, et al. [6]-Gingerol suppresses colon cancer growth by targeting leukotriene A4 hydrolase. Cancer Res 2009; 69: 5584-91.
29. Dugasani S, Pichika MR, Nadarajah VD, Balijepalli MK, Tandra S, Korlakunta JN. Comparative antioxidant and anti-inflammatory effects of [6]-gingerol, [8]-gingerol, [10]-gingerol and [6]-shogaol. J Ethnopharmacol; 127: 515-20.
30. Asai A, Miyazawa T. Occurrence of orally administered curcuminoid as glucuronide and glucuronide/sulfate conjugates in rat plasma. Life Sci 2000; 67: 2785-93.

31. Jiang SZ, Wang NS, Mi SQ. Plasma pharmacokinetics and tissue distribution of [6]-gingerol in rats. Biopharm Drug Dispos 2008; 29: 529-37.
32. Wang W, Li CY, Wen XD, Li P, Qi LW. Plasma pharmacokinetics, tissue distribution and excretion study of 6-gingerol in rat by liquid chromatography-electrospray ionization time-of-flight mass spectrometry. J Pharm Biomed Anal 2009; 49: 1070-4.
33. Bhattarai S, Tran VH, Duke CC. Stability of [6]-gingerol and [6]-shogaol in simulated gastric and intestinal fluids. J Pharm Biomed Anal 2007; 45: 648-53.
34. Rhode J, Fogoros S, Zick S, et al. Ginger inhibits cell growth and modulates angiogenic factors in ovarian cancer cells. BMC Complement Altern Med 2007; 7: 44.
35. Aktan F, Henness S, Tran VH, Duke CC, Roufogalis BD, Ammit AJ. Gingerol metabolite and a synthetic analogue Capsarol inhibit macrophage NF-kappaB-mediated iNOS gene expression and enzyme activity. Planta Med 2006; 72: 727-34.
36. Tjendraputra E, Tran VH, Liu-Brennan D, Roufogalis BD, Duke CC. Effect of ginger constituents and synthetic analogues on cyclooxygenase-2 enzyme in intact cells. Bioorg Chem 2001; 29: 156-63.
37. Chung WY, Jung YJ, Surh YJ, Lee SS, Park KK. Antioxidative and antitumor promoting effects of [6]-paradol and its homologs. Mutat Res 2001; 496: 199-206.
38. Nurtjahja-Tjendraputra E, Ammit AJ, Roufogalis BD, Tran VH, Duke CC. Effective anti-platelet and COX-1 enzyme inhibitors from pungent constituents of ginger. Thromb Res 2003; 111: 259-65.
39. Oyagbemi AA, Saba AB, Azeez OI. Molecular targets of [6]-gingerol: Its potential roles in cancer chemoprevention. Biofactors 2010; 36: 169-78.

Table A1.1 Calibration curve, linear range and LLOQ of 6-gingerol; 8-gingerol; 10-gingerol; 6-shogaol in plasma.

Compounds	*r*	Linear range (ng/ml)	LLOQ (ng/ml)
6-gingerol	0.998	5 – 2000	5
8-gingerol	0.999	5 – 2000	5
10-gingerol	0.999	5 – 2000	5
6-shogaol	0.999	2 - 2000	2

Table A1.2 Extraction recovery for 6-gingerol; 8-gingerol; 10-gingerol; 6-shogaol in human plasma, expressed as Mean ± R.S.D. (%).

QC (ng/ml)	6-gingerol	8-gingerol	10-gingerol	6-shogaol
15	96.6 ± 7.2	87.1 ± 2.1	82.4 ± 9.0	85.7 ± 0.6
250	84.4 ± 2.4	81.7 ± 4.1	80.4 ± 7.6	81.8 ± 2.9
1000	97.6 ± 2.7	94.7 ± 2.0	92.2± 4.8	93.6 ± 3.2

Table A1.3 Precision and accuracy of LC/MS/MS analysis of 6-gingerol; 8-gingerol; 10-gingerol; 6-shogaol.

Analyte	Nomical concentration (ng/ml)	Intra-day			Inter-day		
		Measured concentration (ng/ml)	Precision (% R.S.D.)	Accuracy (% bias)	Measured concentration (ng/ml)	Precision (% R.S.D.)	Accuracy (% bias)
6-gingerol	15	16.5	1.0	10.0	16.1	9.0	7.1
	250	245	2.3	-2.0	249	6.2	-0.1
	1000	926	5.7	-7.3	904	3.0	-9.5
8-gingerol	15	15.9	2.0	6.2	15.8	4.4	5.3
	250	235	10.9	-5.9	267	4.0	7.2
	1000	941	2.5	-5.8	978	12.4	-3.2
10-gingerol	15	16.5	1.3	9.8	15.9	2.0	6.4
	250	248	2.6	-5.5	274	5.4	9.8
	1000	992	5.2	-0.7	1025	9.4	2.5
6-shogaol	15	16. 6	0.9	10.4	15.3	4.1	2.2
	250	242	1. 6	-3.3	269	2.4	7.6
	1000	966	4.3	-3.4	969	6.5	-3.1

Table A1.4 Estimated plasma phamacokinetic parameters after single oral administration of 2.0 g ginger extracts.

Parameter	6-gingerol			8-gingerol			10-gingerol			6-shogaol		
	Free	Glucuronide	Sulfate	Free	Glucuronide	Sulfate	Free	Glucuronide	Sulfate	Free	Glucuronide	Sulfate
AUC(0-t) (μg*h/mL)	N/A	0.74 ± 0.56	0.43 ± 0.26	N/A	0.26 ± 0.27	0.036 ± 0.035	0.008 ± 0.004	0.88 ± 0.60	0.059 ± 0.015	0.024 ± 0.013	0.11 ± 0.08	0.079 ± 0.044
MRT(0-t) (h)	N/A	1.61 ± 0.34	1.77 ± 0.34	N/A	1.34 ± 0.36	1.05 ± 0.36	0.93 ± 0.28	2.04 ± 0.34	2.94 ± 1.03	1.18 ± 0.36	1.48 ± 0.52	1.58 ± 0.40
T1/2 (h)	N/A	1.64 ± 0.88	1.79 ± 0.99	N/A	1.03 ± 0.34	1.25 ± 0.26	1.79 ± 0.32	2.09 ± 0.44	3.24 ± 1.83	1.32 ± 0.44	1.54 ± 0.66	1.40 ± 0.36
Tmax (h)	N/A	1.03 ± 0.41	1.03 ± 0.41	N/A	1.06 ± 0.40	1.03 ± 0.38	1.11 ± 0.40	1.19 ± 0.51	1.14 ± 0.52	1.00 ± 0.41	1.03 ± 0.41	1.06 ± 0.37
Cmax (μg/ml)	N/A	0.45 ± 0.25	0.26 ± 0.13	N/A	0.16 ± 0.11	0.027 ± 0.015	0.009 ± 0.002	0.41 ± 0.24	0.017 ± 0.006	0.011 ± 0.007	0.080 ± 0.057	0.049 ± 0.026
CL/F (L/h/kg)	N/A	1.32 ± 0.58	1.77 ± 0.84	N/A	0.70 ± 0.44	2.16 ± 0.84	14.5 ± 0.6	0.82 ± 0.61	5.98 ± 2.56	2.75 ± 0.71	1.14 ± 0.69	1.30 ± 0.59

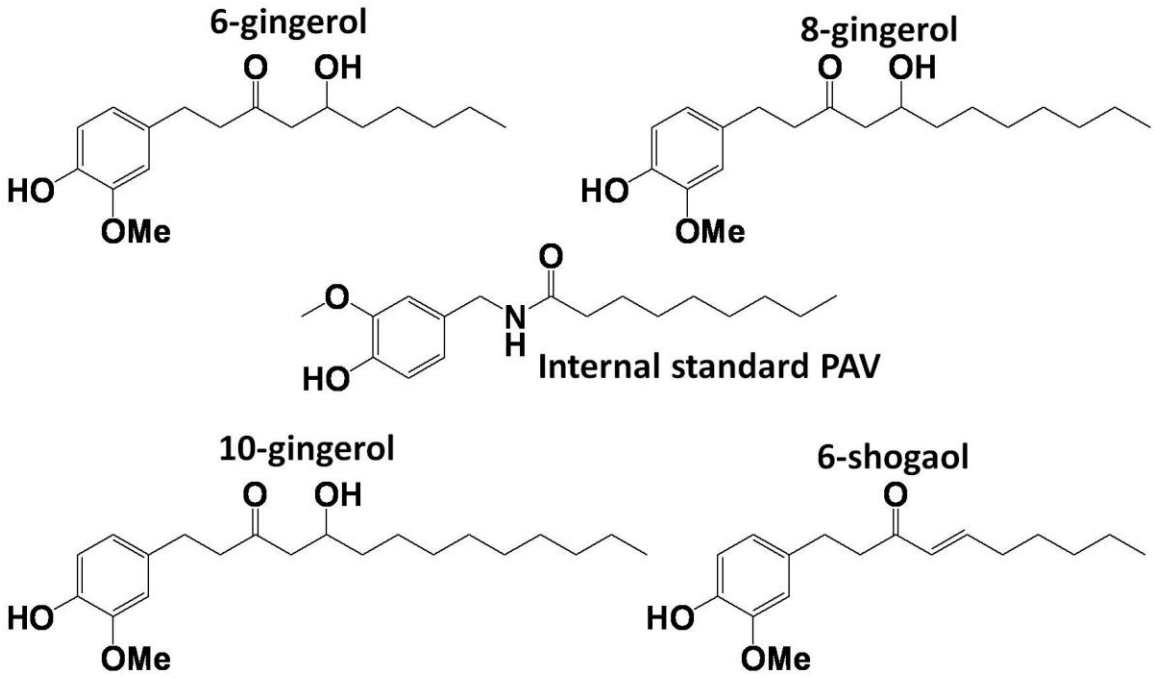

Figure A1.1 Chemical Structures of 6-, 8-, 10-gingerols, 6-shogaol and internal standard Pelargonic acid vanillylamide (PAV).

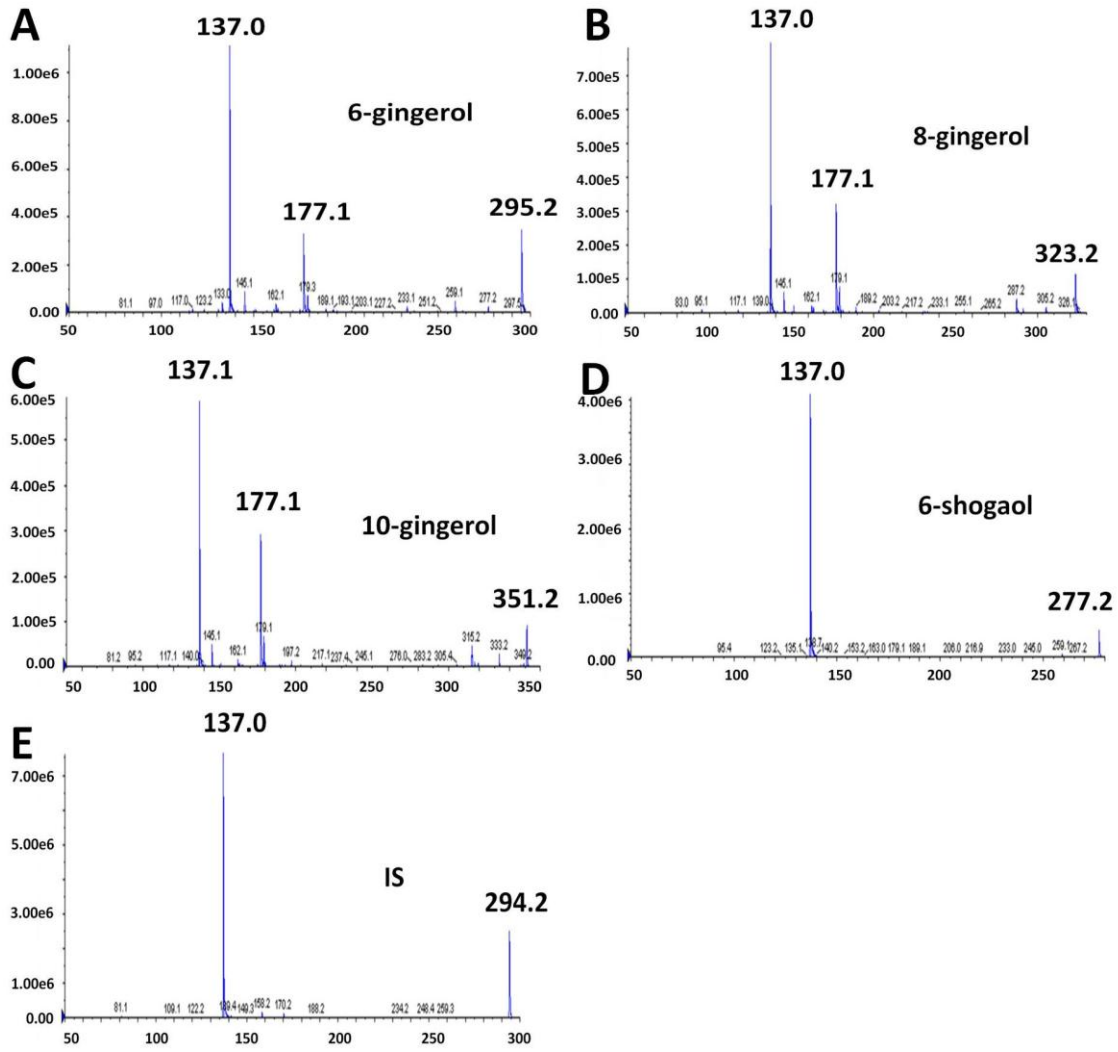

Figure A1.2 Enhanced product ion (EPI) mass spectra of the analytes and internal standard. A, EPI of 6-gingerol; B, EPI of 8-gingerol; C, EPI of 10-gingerol; D, EPI of 6-shogaol; E, EPI of IS.

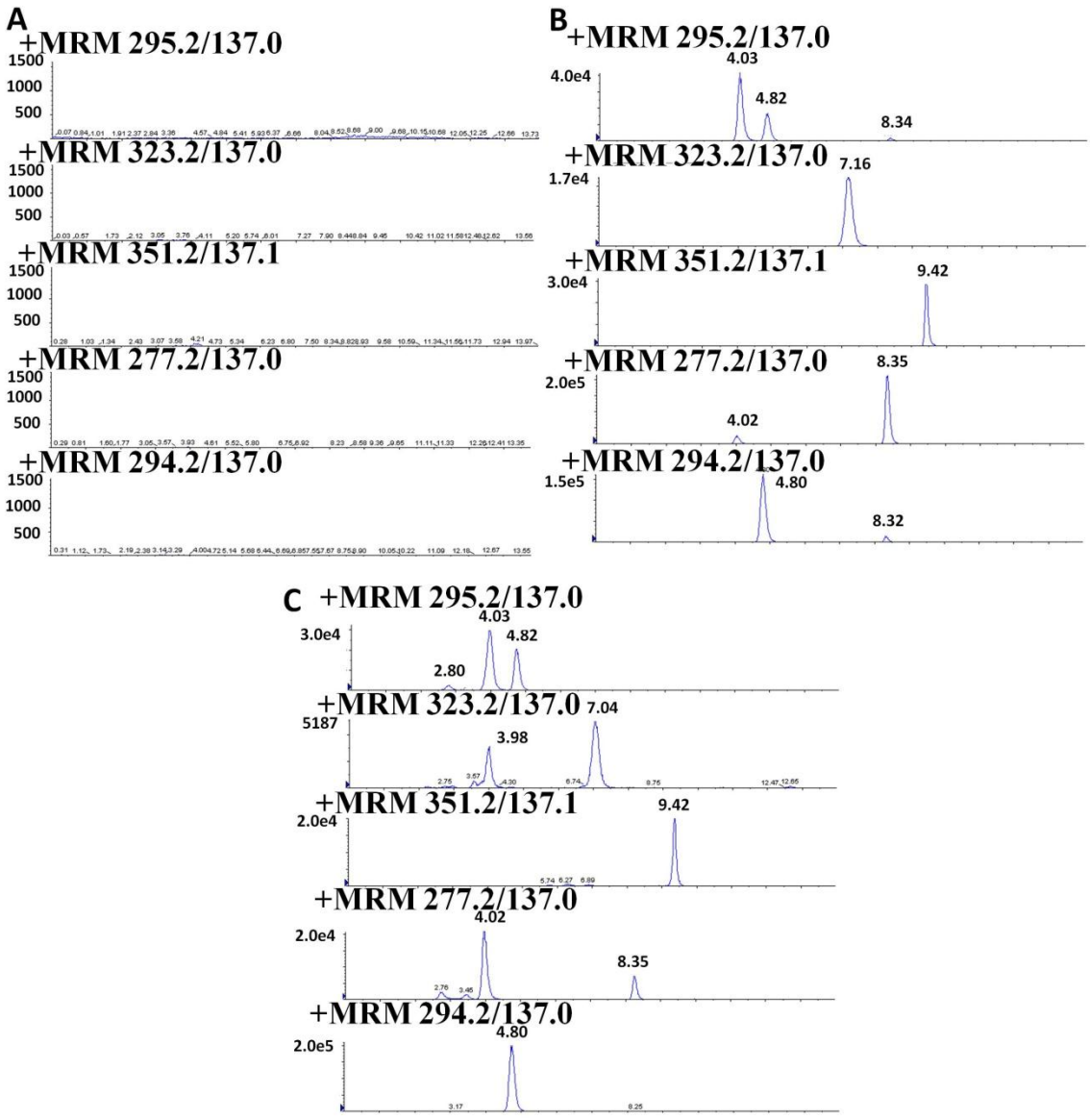

Figure A1.3 Representative MRM chromatograms of the analytes and internal standard. 6-gingerol, 295.2/137.0; 8-gingerol 323.2/137.0; 10-gingerol, 351.2/137.0; 6-shogaol, 277.2/137.0; Internal standard PAV, 294.2/137.0. A, blank plasma sample; B, blank plasma sample spiked with four analytes and IS; C, plasma sample obtained 1 h after oral administration of ginger powder.

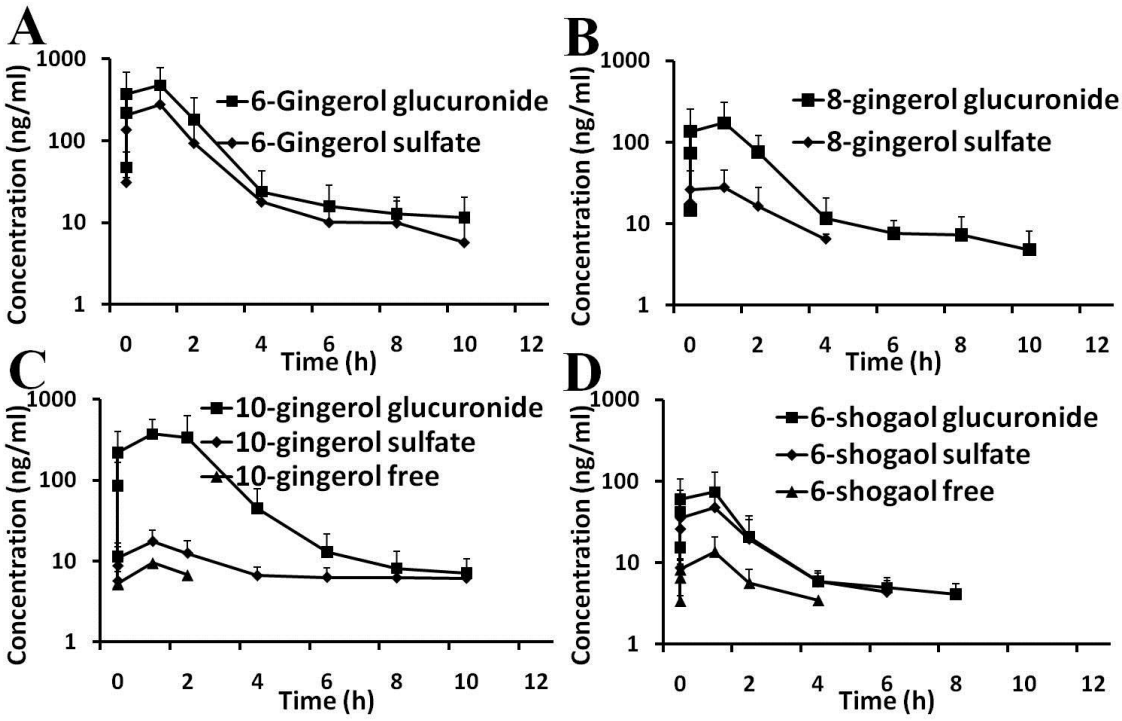

Figure A1.4 Mean plasma concentration-time profiles of 6-gingerol; 8-gingerol; 10-gingerol; 6-shogaol, and their glucuronide, and sulfate conjugates in human plasma after oral administration of 2.0 g ginger powders (n=8). A, 6-gingerol; B, 8-gingerol; C, 10-gingerol; D, 6-shogaol.

APPENDIX II

SUPERPARAMAGNETIC IRON OXIDE NANOPARTICLE (SPIO) "THERANOSTICS" FOR MULTIMODALITY TUMOR IMAGING, GENE DELIVERY, TARGETED DRUG AND PRODRUG DELIVERY

Abstract

The superparamagnetic iron oxide nanoparticle (SPIOs) "theranostics", which contain imaging probes for tumor diagnosis and therapeutic compounds for therapy in a single nanoparticle, might provide significant benefits compared to exiting tumor imaging and therapeutic strategies. In this review, we summarize the progress of SPIOs "theranostics" that integrate tumor targeting, multimodality imaging, and gene delivery, or targeted drug and prodrug delivery. This review describes various methods of SPIOs synthesis, surface coating, and characterization. Different tumor targeting strategies such as antibody fragments, nucleotides, receptor ligands are discussed to improve SPIOs delivery for multimodality imaging. We also examine the utility of SPIOs for gene, siRNA delivery and imaging. Several methods for drug encapsulation and conjugation onto SPIOs are compared for targeted drug delivery, site-specific release, and imaging-guided drug delivery. Finally, we also review pharmacokinetics (including biodistribution) of SPIOs based on their characteristics.

Keywords: SPIOs, theranostics, multimodality imaging, gene delivery, prodrug, targeted drug delivery

Cancer remains to be the second leading cause of death in the United States after heart disease. For people under 85 years, cancer causes more deaths than heart disease despite much progress in cancer treatment in the last three decades (1). The estimated occurrence of cancer incidence and mortality were 1,479,350 new cancer cases and 562,340 deaths, respectively in 2009 (1). Hence, the development of novel approaches for early detection, diagnosis and effective cancer treatment and prevention strategies are critical to decrease cancer incidence and increase cancer patient survival.

Nanotechnology has been applied in our daily lives, ranging from carbon soot or carbon black in ink, cosmetics, to delicate nanoparticles drug delivery systems (2, 3). The progress in nanotechnology and nanomedicine may contribute to the successful management of some diseases including cancer. Wagner *et al.* recently summarized the application of nanoparticles in medicine, which included drug delivery and drug therapy, imaging and diagnostics, biomaterials and implants (4). Nanoparticles may be generated from a variety of materials for medical use. Liposome, the first nanotechnology drug delivery system, can be traced back to 1960s (5, 6). Subsequently, a variety of nanoparticles made from different biomaterials including organic dedrimers, carbon, silicon, semiconductors, gold, and iron oxide were fabricated and tested for tumor imaging, diagnosis and therapy (2, 7). The advantages of nanoparticles in drug

delivery and molecular imaging have been well recognized. The advances include targeted delivery of therapeutic agents to the specific disease sites (8, 9), delivery of physicochemically unfavorable drugs, *e.g.*, water-insoluble drugs (10, 11), non-invasive and real-time monitoring of the sites of drug release, and assessment of drug efficacy (12).

Recently, one of the significant advances of nanoparticles is to integrate targeting, imaging, and drug delivery into one single nanoparticle (12-15). The development of these nano “theranostics”, which combines drug therapy and diagnostic imaging using the carrier nanoparticles, might provide significant benefits over exiting tumor imaging and chemotherapy strategies.

Superparamagnetic iron oxide nanoparticles (SPIOs) emerged as a feasible nano “theranostics” for tumor imaging and drug delivery owing to their distinct characteristics. The superparamagnetic nature of SPIOs makes them excellent magnetic resonance imaging (MRI) contrast agents. The ability of SPIOs to convert the energy absorbed from an oscillating magnetic field to the thermal energy can be used to destroy local tumor tissues for cancer therapy (hyperthermia effect) (10, 16). In addition, the large surface area of SPIOs makes the functional modifications of the SPIOs feasible, which enables the conjugation of the targeting moiety, drug molecules and imaging agents (15). For example, Liong and colleagues synthesized multifunctional mesoporous silica nanoparticles with the SPIOs core encapsulated in the esostructured silica spheres for multiple modality imaging and cancer therapy (14). The SPIOs core was used for MRI imaging. The surface mesoporous silicate was further modified

by using folic acid for tumor targeting, conjugated with fluorescein isothiocyanate (FITC) for optical fluorescent imaging, and loaded with either camptothecin (CPT) or paclitaxel (TXL) for anticancer efficacy (14).

This review summarizes the progress in SPIOs theranostics that integrates multimodality tumor imaging, gene delivery, and drug delivery. The focus of this review is on their synthesis and characterization, distinct role in MRI imaging, application in multimodality imaging, gene delivery, targeted drug and prodrug delivery for cancer therapy. We also summarize the pharmacokinetic, biodistribution, and toxicity profile of SPIOs.

Synthesis and characterization of SPIOs

Synthesis of SPIOs

SPIOs consist of an iron oxide core and a hydrophilic surface coating. The ferromagnetic substances have intrinsic magnetic properties due to the aligned unpaired electron spins; whereas SPIOs have no net magnetic field without external magnetic field (17). In the presence of an external magnetic field, the iron oxide particles generate local field inhomogeneities that promote the relaxation of the transverse magnetization (T2 and/or $T2^*$) thereby resulting in MRI signal loss. Typically, the larger the iron core and/or hydrated particle size, the greater the $T2/T2^*$ effects. The iron oxide cores are typically composed of either magnetite (Fe_3O_4) or maghemite (γFe_2O_3) (18). γFe_2O_3 could be converted from synthesized Fe_3O_4 through oxidation by exposure to oxygen or oxidizing agents, and these two iron oxide structures share similar magnetic properties (18). A conventional chemical method for synthesizing magnetite is

coprecipitation, by adding a base to the Fe^{2+} and Fe^{3+} aqueous salt solutions (19). Different pH, ionic strength, temperature, Fe^{2+} and Fe^{3+} ratio, and different salts could result in different size, shape and composition of nanoparticles (19-21). Although the coprecipitation technique is simple and efficient to yield a large amount of nanoparticles per batch, the nanoparticles produced are polydispersed with a broad particle size distribution. To produce monodispersed nanoparticles, some other methods were developed including microemulsion, ultrasound irradiation, sol-gel syntheses, electrospray syntheses, hydrothermal synthesis (18, 21, 22). For instance, Hyeon *et al.* synthesized highly crystalline and monodisperse maghemite nanocrystallites by using thermal decomposition (23). The uniformity of the nanoparticles was confirmed by the transmission electron microscopic (TEM) images, and the nanoparticles exhibited 2-dimensional and 3-dimensional assembly of the particles. The advantage of this method is that the procedure omits the exhaustive size selection step. By adjusting the experimental parameters, nanoparticles can be easily produced with size of 4-16 nm.

Surface coating of SPIOs

The surface coating of SPIOs is critical for the stability (with respect to aggregation) as well as for the biodistribution and pharmacokinetics of the SPIOs. Without surface coating, the large hydrophobic surfaces of the SPIOs would induce the hydrophobic interactions between the particles, resulting in aggregation and precipitation. In addition, the surface coating of the SPIOs can protect them from uptake by the reticular endothelial system (RES) such as

macrophages, and therefore prolong their circulation in plasma for *in vivo* use (24). Furthermore, the functional groups of the surface coating of the SPIOs make the surface modification possible for the manufacturing of the multifunctional SPIO nanoparticles. A variety of materials have been applied to coat the SPIOs including both inorganic components (such as silica (25), gold, gadolinium, carbon (26)) and organic shells (such as polymers) (22). Silica has been widely used to coat iron oxide nanoparticles because of its favorable properties including compatibility, hydrophilicity, controllable coating density, and the terminal silanol group available for bioconjugation (27-29). For instance, Zhang and colleagues coated SPIOs with silica without significantly increasing the particle sizes. The coated SPIOs showed no cytotoxicity and exhibited high T2 relaxivity after internalized by the immortalized Rat progenitor cells (25). There are a variety of polymers used to coat SPIOs, including poly (lactic-*co*-glycolic acid) (PLGA), dextran, chitosan, poly (vinyl alcohol) (PVA), poly (vinylpyrrolidone) (PVP), poly (ethyleneglycol) (PEG) (19, 30-32). The surface coating of the newly synthesized SPIOs can be carried out during synthesis or post-synthesis. The post-synthesis might be preferred since the former procedure would change the physical characteristics of the resulting nanoparticles (33).

Characterization of SPIOs

According to the overall diameter of SPIOs (including both iron oxide core and surface coating), SPIOs can be categorized into the following subgroups (18, 34): oral SPIOs (large SPIOs > 300 nm, including clinically used AMI-121 and OMP);

standard SPIOs (SSPIOs 60 – 150 nm, including clinically used AMI-25 and SHU 555A); ultrasmall SPIOs (USPIOs 10-40 nm, including clinically used AMI-277 and NC100150) and monocrystalline iron oxide nanoparticles (MION with size 2.8 ± 9 nm). The former three groups are being clinically used for imaging of various organs and physiological functions including bowel, liver/spleen, lymph node, bone marrow, perfusion imaging and MRI angiography. Due to its monocrystallinity and small size, MION can pass through capillary fenestra to reach the extravascular space for targeted MRI imaging and magnetically labeled cell probe MRI imaging (34, 35).

The superparamagnetic properties, stability and biological functions of SPIOs largely depend on their structural and physicochemical factors including particle size, particle shape, crystal structure, charge and surface coating (21, 34). For instance, Sato *et al.* determined that the critical size of magnetization for iron oxide nanoparticles was 25 nm. Below 25 nm, with the decrease in the particle size, the saturation magnetization of iron oxide nanocrystals reduced sharply, which was probably due to the surface effects such as the appearance of a magnetically inactive layer (36). Although the magnetic properties of iron oxides (at room temperature) are determined primarily by the size, shape and purity of the iron oxide core, the surface coating may also influence the magnetic properties of the particles. Zhang *et al.* synthesized three SPIOs coating with silica-, APTMS-, and AEAPTMS, respectively. Subsequent characterization of the three SPIOs revealed that silica-coated SPIOs exhibited highest T_2 relaxivity of 339.80 ± 0.22 $s^{-1}mM^{-1}$, and APTMS- and AEAPTMS-coated SPIOs exhibited

much less T_2 relaxivity of 134.40 ± 0.01 and 84.79 ± 0.02 $s^{-1}mM^{-1}$ s^{-1}, respectively (25). In addition, there is a tradeoff between large crystal/particle size and good T_2/T_2^* effects and optimal tumor uptake. Typically, particles over 100 nm exhibit high magnetization (and T_2/T_2^* effects), but have poor uptake into non-RES tissue. However, smaller particles (<25 nm) exhibit good uptake (via diffusion through non-normal endothelium) but lower magnetizations (lower T_2/T_2^* effects).

Therefore, before application of the SPIOs, the characterization of the physicochemical parameters of the SPIOs is indispensable. Various techniques are currently used to characterize the SPIOs including transmission electron microscopy (TEM), high resolution TEM (HRTEM), X-ray diffraction (XRD), Infra red spectroscopy, photon correlation spectroscopy (PCS)/dynamic light scattering (DLS), Mossbauer spectroscopy, relaxometry (NMRD profiles), and vibrating sample magnetometry (VSM)(37-41). Typically, TEM, HRTEM and XRD are used to evaluate the iron oxide core size and core size distribution. PCS/DLS and NMRD analysis maybe used to determine the hydrated particle size. The magnetization is generally evaluated using VSM or NMRD analysis.

TEM: is a microscopy technique with higher resolution than light microscopes. It utilizes a beam of electrons to transmit through and interact with the specimens to obtain the image. It is generally used to obtain the morphology and size distribution of the nanoparticles.

HRTEM: is an imaging mode of the TEM with much higher resolution. It can be employed to image the local microstructure (such as glide plane, lattice

fringes, screw axis, lattice vacancies and defects) of the nanoparticles at an atomic scale (42, 43).

PCS/DLS: is a method to derive dynamic information about particles' movement in solution. It is also used to determine the hydrodynamic size of the nanoparticles (the total size of the particle comprising both iron oxide core and the surrounding coating materials and water molecules) (44).

VSM: is widely used to measure the magnetic properties of a variety of materials. The samples are placed in a uniform magnetic field to induce a dipole moment. Then the samples are vibrated sinusoidally to induce electrical signal in the pick-up coil. The signal produced is proportional to the sample's magnetic moment. Therefore, the magnetic property of the material can be determined by measuring the induced electrical signal in the pick-up coil.

Zeta-potential is another important parameter for the nanoparticles as it is related to the stability of the colloidal dispersions. In addition, zeta potential is also critical for biodistribution of SPIOs and attachment of DNA to the particle surface. When the zeta-potential is large (both negative and positive), there is large repulsion between particles, hence, particles resist aggregation, whereas when the zeta-potential is low (near zero), the particles are rapidly coagulated or flocculated due to the overwhelming attraction forces (Van der Waals). Zeta-potential is determined by the surface charge density, surface structure and shear plane location (42). Zeta-potential can be calculated from different experimental techniques including microelectrophoresis, electric conductivity, and electrophoretic mobility (42, 45).

SPIOs for multimodality tumor imaging

SPIOs for MRI imaging

Since the acquisition of the first MRI image by Lauterbur (46) (who shared Nobel Prize with Mansfield for their contribution in MRI development), MRI has become one of the major imaging modalities to visualize the internal organs and physiological functions of the body. MRI utilizes an external magnetic field, an intermittent radiofrequency pulse and a gradient magnetic field to generate the MRI signal. MRI images are formed when the patient is placed in an external applied magnetic field. Water protons may align with or against the applied field. The small excess of water protons aligned with the field represent the net proton magnetization that rotates in the direction of applied field at a given frequency (determined by the applied field strength). Radio-frequency energy (rf) is applied at the rotational frequency of the water protons causing the net magnetization to move away from equilibrium (aligned with the field). Once the rf is removed the net magnetization returns to equilibrium at rates defined by the longitudinal and transverse magnetization decay. Gradients are used to define the imaging location or slice (in 2D or 3D space) and the resultant native soft tissue contrast is due to endogenous variations in the proton densities and longitudinal and transverse relaxation times associated with the different tissues. Although MRI can utilize the endogenous water protons (normally hydrogen nuclei) to produce the signal, a contrast agent is often used to improve sensitivity and specificity. The contrast agent itself does not produce the image, rather, it affect the magnetic resonance relaxation properties of the protons surrounding it. For

instance, the paramagnetic Gadolinium (Gd) chelates which are commonly used as contrast agent clinically, induce shortening of T1 relaxation (longitudinal or spin-lattice relaxation) resulting in increased signal intensity on a T1-weighted image. However, Gadolinium chelates suffered from relatively low contrast capacity (the detection limit is approximately 10^{-5} moles/L), short retention time *in vivo* with half life about 1.5 hr, and potential renal toxicity in renal function impaired patients (47-50). Although the generation of high relaxivity lipid based Gadolinium agents (micelles and lipoproteins) has proven effective for targeted molecular imaging (51), the clinical utility of these materials has yet to be determined since a large percent of the injected Gadolinium dose (<10%) may be retained and/or metabolized. As a result, safety issues may limit clinical translation of these agents. More recently, SPIOs have been applied to act as contrast agents. Unlike gadolinium chelates, SPIOs are negative contrast agents since they induce shortening of T_2/T_2^* relaxation (transverse or spin-spin relaxation/effective transverse), which produces decreased signal intensity on a T_2/T_2^* weighted image (52). SPIOs are more efficient than gadolinium chelates as signal contrasts and have a detection limit of approximately 10^{-6} moles/L (53, 54). In addition, due to the fact that the iron is an endogenous metal ion and that most cells may safely take up, metabolize and excrete iron oxide particles, SPIOs are generally preferred as molecular imaging probes (15, 55). In fact, different sized iron oxide nanoparticles have been used for bowel contrast, liver/spleen imaging, lymph node imaging, bone marrow imaging, perfusion imaging and MRI angiography (34). For tumor imaging, SPIOs have been extensively employed for

detection of hepatic and splenic tumor, nodal metastases, bone tumor, brain tumor (56-61). The above imaging of tumors utilizes the physiological process of SPIOs in circulation including the uptake of SPIOs by RES cells to accumulate in certain organs including liver, spleen and lymph node as well as enhanced permeation and retention (EPR) effect due to the leaky vasculature in tumor tissues for passive targeting of tumors (62, 63). For instance, large SPIOs (such as clinically used Feridex, >90 nm) are used for liver imaging indications since healthy liver Kupffer cells are able to quickly take up circulating SPIOs. As a result, normal liver appears dark and tumors (that do not have normal Kupffer cells) appear bright. However, imaging of the lymphatic system, bone marrow, and atherosclerotic plaque requires the use of smaller iron oxide particles (<25 nm) that exhibit prolonged circulation, limited RES uptake, and the ability to diffuse through non-normal endothelium.

As negative contrast agents, one challenge for SPIOs in MRI is the fact that it is difficult to separate signal loss due to the SPIOs and signal loss from MRI imaging artifacts such as motion, pari-vascular effects, and partial voluming effects. Recently, several positive-contrast techniques have been developed to generate signal hyperintensity (signal gain) in the vicinity of SPIOs such as white marker imaging (64, 65), GRASP (gradient echo acquisition for superparamagnetic particles) (66), IRON (inversion recovery on-resonance water suppression) (67), and SGM (susceptibility-gradient mapping) (68-70). For instance, Liu *et al.* used white marker imaging, IRON and SGM to detect the SPIO-labeled C6 glioma cells in an experimental flank tumor model by MRI (69).

They found that these three positive-contrast techniques produced hyperintensities in areas around the labeled flank tumors against a dark background, and provided greater sensitivities than the T_2^*- weighted images. Furthermore, the three positive-contrast techniques also provided better accuracy since it's easier to differentiate the hyperintense regions from other signal voids such as blood flow observed on T_2^*- weighted images. In addition, SGM technique exhibited the highest sensitivity among the three positive-contrast techniques. Overall, the new advances in positive-contrast techniques might allow for more sensitive and accurate detection of iron oxide particles.

Targeting

Targeting SPIOs to tumors with antibody

Although SPIOs show increased contrast efficiency to gadolinium chelates in MRI imaging, the detection limit of 10^{-6} moles/L of SPIOs in MRI is still much less than the detection limit of 10^{-8} moles/L of fluorescence detection in optical imaging system and of 10^{-11} moles/L of PET/SPECT (53, 71). Thus, strategies still need to be developed to increase the sensitivity and specificity of SPIOs.

One method is to incorporate a targeting moiety to actively deliver SPIOs to tumor tissues rather than the passive EPR effect to increase the local concentration of SPIOs in the tumor tissues to enhance the contrast. A variety of targeting moieties have been used, including antibodies and their fragments, peptides, aptamers, and specific ligands. Antibodies are commonly used targeting groups utilizing the high affinity and high specificity between antibody-antigen bindings. For example, Chen *et al.* immobilized Herceptin, the

monoclonal antibody against HER2/neu receptors which are overexpressed in 15 to 25% of breast cancer patients, to the surface of SPIOs and evaluated the targeted SPIOs endocytosis by different breast cancer cells resulting MRI images (72). The internalization of the Herceptin-SPIO was observed in four HER2/neu receptor positive cells (BT-474, SKBR3, MDA-MB-231 and MCF7) by fluorescence microscopy while the internalization of Herceptin-SPIO was not observed in HER2/neu negative KB cell line. The magnetic resonance contrast was observed, with the enhancement proportionally to the HER2/neu expression levels in the four HER2/neu receptor positive cell lines. The targeting capacity of Herceptin-SPIO was further confirmed in breast cancer cell xenografts. Herceptin-SPIO was found to decrease the average enhancement of positive tumor (SKBR3 cell) and negative tumor (KB cell) by about 45.7 ± 1.9 and 3.3 ± 1.2 %, respectively, indicating the specific targeting of Herceptin-SPIO to the HER2/new expressing cells. Some other antibodies were also used, such as antibody against prostate-specific membrane antigen (PSMA) (73), and antibody against carcinoembryonic antigen (CEA) (74). Although antibody showed promise as targeting moiety, there are still some drawbacks for antibody targeting. First, immunogenicity of antibody from non-human source might generate immune response. Although humanized monoclonal antibodies are developed to minimize immunogenicity, they might still cause immune reactions in a small population (53); second, the high molecular weight of intact antibody (150 kDa, 15 nm) might limit the SPIO-antibody's penetration through the vasculature and tumor tissues (15). An alternative approach is to utilize antibody

fragments, including Fab' and scFv with relatively low molecular weight while maintaining comparable antigen binding affinity. For instance, Natarajan *et al.* conjugated anti-MUC-1 antibody fragments di-scFv-c (50 kD) to iron oxide nanoparticles. The conjugates can specifically target to aberrant MUC-1, a protein abundantly expressed in most human epithelial cell adenocarcinomas (16). Because of the smaller size of antibody fragment, they managed to conjugate 20-30 molecules of di-scFv-c to one nanoparticle compared to 4-5 intact monoclonal antibodies per nanoparticle. The anti-MUC-1 di-scFv-c conjugated nanoparticles showed specific binding to MUC-1 expressing cancer cells both *in vitro* and *in vivo*. A single chain anti-EGFR antibody (ScFvEGFR, 25 kD) was also successfully conjugated to SPIOs. The conjugates specifically bound to and were internalized by EGFR expressing tumor cells for enhanced MRI contrast (75). Small peptides are also used as targeting moieties, including AGKGTPSLETTP peptide specific for human hepatocellular carcinoma cells (76), Chlorotoxin (a 36-amino acid peptide) with high selectivity and binding affinity for membrane matrix metalloproteinase-2 (MMP-2) in a variety cancer cells (77), RGD peptide for $\alpha_v\beta_3$ integrins as a biomarker of angiogenesis in tumor (78).

Targeting SPIOs to tumors with nucleotides

Aptamers, short strands of oligonucleotides, may bind to various molecular targets, such as nucleic acid, proteins, small molecules. The small size, limited immunogenicity, high selectivity, and easy production make the aptamers favorable candidates for targeting groups. Wang and his colleagues used an A10 RNA aptamer (Apt) as targeting group which can specifically recognize the

extracellular domain of PSMA (79). Since PSMA is highly expressed in prostate cancer cells, the engineered SPIO-Apt nanoparticles can be differentially taken up by PSMA-expressing prostate cancer LNCaP cells compared to non-PSMA-expressing prostate cancer PC3 cells. The uptake of SPIO-Apt nanoparticles by LNCaP cells led to a dramatic decrease in the transverse relaxation time (T2) from 104.2 ± 1.4 to 26.6 ± 0.4 ms, while SPIO-Apt nanoparticles incubated with PC3 cells did not affect the T2 relaxation time, which further indicates the specific uptake of SPIO-Apt nanoparticles by the PSMA-expressing LNCaP cells.

Targeting SPIOs to tumors with receptor ligands

Many receptors are aberrantly expressed on the cancer cell surface due to the high proliferation nature of cancer cells, such as epithelial growth factor receptor (EGFR), vascular endothelial growth factor receptor (VEGFR), and folate receptor, which makes their corresponding ligands or ligand analogs as innate targeting moieties. For example, folic acid has been extensively used as a targeting ligand for delivery of anticancer agents, proteins, and genes to the cancer cells via folate receptor (80-83). Landmark *et al.* conjugated folic acid to the SPIO nanoparticles, and SPIO-folic acid nanoparticles showed selective binding and uptake by the folate expressing KB tumor cells (84). Octreaotide (OCT), a somatostatin (SST) analog binding to somatostatin receptors (SSTRs) expressed on breast cancer cells, was utilized by Li *et al.* to direct SPIOs for target specific MRI imaging (85). OCT-SPIO was able to specifically bind to SSTR expressing MCF-7 cells and decreased the T2 relaxation time dramatically. The OCT-SPIO targeted contrast ability was further confirmed *in vivo* with the

signal intensity of the tumor decreased in a T2-weighted image. A ligand fragment ATF (amino-terminal fragment of urokinase plasminogen activator, residue 1-135) was used as target to systemically deliver SPIOs to pancreatic tumor tissues since its receptor uPAR is highly expressed in more than 86% of pancreatic cancer tissues. The SPIO-ATF exhibited selective accumulation in tumors and enhanced MRI contrast (86). Transferrin has also been used as target to direct SPIOs to tumor cells by ways of transferring receptor pathway (87, 88).

Multimodality imaging using labeled SPIOs

Benefit from its multifunctionality surface, SPIOs may be developed for multimodality tumor imaging. For instance, bioconjugate fluorescent dye on to the SPIOs surface to integrate both MRI and fluorescent imaging, or bioconjugate radioactive tracers (*e.g.*, ^{124}I) to integrate both MRI and PET, or all of the three. As there are hundreds of functional groups on the surface of SPIOs, it's possible to conjugate dozens of fluorescent dye molecules or radioactive tracers to SPIOs to further increase their sensitivity. A key issue for multimodality imaging is that multimodal imaging systems need to be clinically available to acquire images from different morphologic or functional contrast agents simultaneously or sequentially. Therefore, an integration software would also be required to integrate these acquired multimodality images to better illustrate the information. Although difficulties exist, multimodality imaging shows advantages by complementing the individual imaging modality to give better detection, more accurate diagnosis, and capability to monitor the molecular level events.

Clinicians have studied the possibility of PET/MRI fusion imaging by taking advantage of high sensitivity of PET and high anatomical resolution of MRI (89-91). The fusion images of PET and MRI showed better sensitivity and specificity than the single modality, as well as providing important diagnostic information (92). Automated software for analysis of fusion images (93) and integrated single machine for detection of both MRI and PET (53) have been developed, which made the multimodality imaging more feasible. Another example is a triple labeled SPIO nanoparticle developed by Lewin *et al.* which was conjugated with FITC fluorescent dye and diethylenetriamine pentaacetic acid (DTPA) for ^{111}In labeling achieving triple imaging modalities (magnetic resonance, fluorescent, and nuclear imaging) (94). The multimodality imaging was able to track single cells in tissue samples.

As MRI lacks real time information while ultrasound (US) gives excellent real time information. Researchers have tried to combine these two imaging modalities together. Yang *et al.* fabricated a novel encapsulated microbubble (EMB) construct with SPIOs embedded in the polymer shell of the microbubble (95). Such microbubble vesicles showed enhanced magnetic susceptibility while maintaining echogenicity to be US contrast agents which were acoustically active to generate sonoporation under US exposure. This microbubble vesicle showed potential for developing US and MRI dual contrast agents.

SPIOs for targeted gene delivery and multimodality imaging

In addition to conventional cancer treatment such as chemotherapy, radiotherapy and surgery, gene therapy appears to be another promising option

for cancer treatment with several products entering phase III clinical trials, such as Advexin (targeting tumor suppressor gene p53), Rexin-G (targeting cell cycle control gene cyclin G) (96-98). Cancer gene therapy is featured by the transfer and expressing of exogenous genetic materials (plasmid DNA, siRNA, microRNA) in cancer cells to express certain proteins (*e.g.*, Advexin expresses wild-type p53 to promote cancer cells undergo apoptosis) or knockdown the specific proteins (*e.g.*, siRNA against oncogene mutant K-ras to induce K-ras protein degradation and hence promote cancer cell death). Currently, the majority of delivery vectors are viral, which show high efficiency but have safety concerns (98). The viruses can induce immune responses which lead to the neutralization of viruses, or the exaggerated immune reactions could produce severe side effects. Another disadvantage is that the mis-incorporation of the viral genome to the host genome probably would lead to oncogene expression, which was the case for the occurrence of leukemia in some children who received gene therapy. Thus, some non-viral gene delivery strategies are developed including electroporation (99), sonoporation (100), gene gun utilizing the gold nanoparticles (101), and a variety of carriers such as bacteria (102), Peptide (103), antibody-protamine fusion protein (104), polymers (105), and liposomes (106).

SPIO –DNA complex for gene delivery

SPIOs have also been used to deliver genetic materials into cancer cells. SPIOs based gene deliveries either utilize the surface positive charges of SPIOs to interact with the negatively charged genetic materials to form complex or through chemical conjugation. Li *et al.* coated SPIOs with poly-L-lysine to convert

the negatively charged SPIOs surface to positively charged, which could be used to condense negatively charged pNM23-GFP plasmid DNA to form complexes (107). The protein NM-H1 expressed by pNM23-GFP plasmid DNA shows anti-metastasis ability in a variety of cancers. They found that the administration of SPIO-PLL/pNM23-GFP complex would suppress the tumor metastasis in a pulmonary metastasis model, whereas administration of pNM23-GFP plasmid DNA alone did not affect the tumor growth and metastasis, which indicate the effective transfection of the pNM23-GFP plasmid DNA. The administration of SPIO-PLL/pNM23-GFP complex prolonged the survival of the tumor bearing mice in a pattern similar to conventional chemotherapeutic agent cyclophosphamide treat group. The combination group of SPIO-PLL/pNM23-GFP complex treatment and cyclophosphamide produced even longer survival in tumor bearing mice. The SPIO-PLL mediated pNM23-GFP delivery provides following advantages: (1) the naked plasmid DNA is subject to nuclease digestion in the blood circulation and uptake by the mononuclear phagocytic system, which limit the circulation time of plasmid DNA and efficient targeting to cancer cells (108); (2) the nanoparticles protect plasmid DNA from enzymatic degradation, probably due to that the positive charges on nanoparticles surface repels Mg^{2+} which is required for enzyme cleavage and the conformational change of DNA structure which limits the enzyme susceptible sites (109, 110); (3) the positively charged SPIO-PLL nanoparticles would facilitate the uptake of plasmid DNA by cancer cells (111); (4) the EPR effect would allow the SPIO-PLL/pNM23-GFP complex accumulation in the tumor tissues and thus achieve

passive targeting. However, one challenge for cellular delivery of DNA via SPIOs is that most SPIOs transport the DNA to endosomes/lysosomes thereby limiting gene delivery efficiency. For effective gene delivery, some of the DNA must be released within the cellular cytosol so that it can migrate to the nucleus.

SPIO-siRNAs conjugates for siRNAs delivery and multimodality imaging

Medarova and his colleagues utilized chemical conjugation to conjugate the synthetic siRNAs duplex to the SPIOs (13). In addition, they further conjugated Cy5.5 dye for the purpose of near-infrared optical imaging (NIRF), and a myristoylated polyarginine peptide for membrane translocation. They chose two candidate siRNAs for delivery, siGFP (for imaging) and siSurvivin (for therapy). They found that the conjugated MN-NIRF-siGFP could be efficiently uptake by the cancer cells to show efficient gene silencing effect which was indicated by the decrease in GFP fluorescence. *In vivo* test of MN-NIRF-siGFP also confirmed the ability of conjugated nanoparticles to target to tumor tissues as evidenced by the decrease of T2 relaxation times in tumor tissues in MRI image and strong fluorescent signal observed by NIRF. The gene silencing effect was proved by RT-PCR demonstrating the decrease of GFP mRNA levels. When they replaced the siGFP with siSurvivin (survivin, an anti-apoptotic protein, knockdown survivin by siRNAs can induce cancer cell death), they found that MN-NIRF-siSurvivin significantly increased the cancer cell apoptosis and necrosis, and survivin mRNA level was also decreased as expected. Therefore, MN-NIRF-siSurvivin conjugates combining siRNA delivery with dual imaging modality (MRI and NIRF) were feasible for multimodality imaging and targeted gene delivery. Several

points are worthy of noting: Myristoylated polyarginine peptide was used as membrane translocation enhancer, whereas no tumor targeting moiety was conjugated to the nanoparticles; although the cell uptake of the conjugate was increased, the accumulation of conjugates in tumor tissues was mediated by the passive accumulation (EPR effect) only, therefore, the incorporation of a tumor targeting ligand probably would further increase tumor targeting ability and minimize the toxicity. In addition, siRNAs were conjugated to iron oxide nanoparticles through a stable thioether bond; although the chemical conjugation was shown not to affect siRNAs' silencing efficiency significantly, the relatively large SPIO nanoparticle would probably have sterical hindrance, and thus affect siRNAs recognition to the target mRNA and its process by RNA-induced silencing complex (RISC). These would compromise the silencing efficiency of siRNA (112). Lee *et al.* used similar strategy as Medarova but conjugated manganese-doped magnetism-engineered iron oxide (MnMEIO) nanoparticles with a cancer specific targeting moiety RGD peptide (specifically binds to tumor expressing $\alpha_v\beta_3$ integrin) and Cy5 dye-labeled siGFP through a disulfide bond, which can be cleaved in the cytoplasm to release the siGFP (113). The constructed MnMEIO-siGFP-Cy5/PEG-RGD conjugate showed specific internalization by $\alpha_v\beta_3$ integrin expressing breast cancer MDA-MB-435 cells while not by lung carcinoma A549 cells (deficient in $\alpha_v\beta_3$ integrin) by both MRI and fluorescence confocal microscopy. The target gene silencing ability of the MnMEIO-siGFP-Cy5/PEG-RGD conjugate was proved by its dose dependent knockdown of the GFP in MDA-MB-435-GFP cells while no significant change

was observed in A549-GFP cells. In addition, MnMEIO-siGFP-Cy5 without targeting group also showed no gene silencing effect on either MDA-MB-435-GFP or A549-GFP cells.

SPIOs for prodrug and targeted drug delivery

Site specific drug release from SPIOs

SPIOs based prodrug strategy achieves site specific delivery of the chemotherapeutic drug molecules to increase local concentration in tumor tissues and minimize the unwanted toxicity to the normal tissues. Drug molecules are either entrapped in the SPIOs surface layer using physical interactions (electrostatic interaction or hydrophobic interaction) or chemically conjugated to SPIOs surface functional groups for controlled release in target cells through pH dependent release or enzymatic cleavage (11, 76, 79, 114, 115).

Jain *et al.* developed an oleic acid (OA)-pluronic-coated iron oxide magnetic nanoparticles to load water-insoluble basic compound doxorubicin (DOX) (11). DOX molecules partitioned into the hydrophobic OA shell with an encapsulation efficiency of 82%. The release kinetics of DOX from nanoparticles was determined in vitro in PBS buffer (pH 7.4). Sustained release was observed, with 28% cumulative drug release occurring in 2 days and about 80% cumulative drug release occurring in over 2 weeks. The DOX loaded nanoparticles showed cytotoxic effect in cancer cells. Yang *et al.* also used DOX as model chemotherapeutic agent to evaluate their SPIOs' drug delivery ability (114). DOX were incorporated onto the amphiphilic block polymer coated IO nanoparticles with 85% loading efficiency for 5 nm IO nanoparticles and 95% loading efficiency

for 10 nm IO nanoparticles. ATF peptide was also conjugated to the nanoparticles for targeted delivery to the uPAR-expressing breast cancer cells. They further examined pH-dependent release of DOX from nanoparticles as the amine group of DOX is converted to a charged molecule at low pH, and thus become water soluble. Indeed, increased release of DOX was observed with decrease of pH in the incubation buffer. At pH 4.0, 70 to 80% of DOX was released after 2 hr incubation, while 20-30% was released at pH 6.0. This pH dependent release of DOX from nanoparticles might mimic the actual release mechanism in cells. After ATF-IO-DOX was taken up by cells through the ATF-receptor mediated endocytosis, the low pH environment in the endosome (pH 5.5-6.0) and lysosomes (pH 4.5-5.0) facilitates the release of DOX from nanoparticles. The ATF-IO-DOX showed favorable delivery efficiency than IO-DOX and exhibited highest cytotoxicity against breast cancer cells, whereas free DOX showed marginal cell uptake and least cytotoxicity.

Targeted prodrug delivery

Hwu and his colleagues used chemical conjugation to covalently attach the anticancer agent paclitaxel molecules to the IO nanoparticles through a phosphodiester bond (prodrug) (116). The paclitaxel molecules (parent drugs) were expected to be released from the nanoparticles by the intracellular phosphodiesterase. The *in vitro* drug release confirmed that 91% of paclitaxel were hydrolyzed and released as free drugs by phosphodiesterase after 10 days from paclitaxel-IO (prodrug). The paclitaxel-IO showed selective cytotoxicity

against human cancer cells (OECM1), while it had much lower effect against human normal cells (HUVEC).

Methotrexate, a folic acid analog served as both therapeutic agent and targeting moiety to the folate receptor overexpressing cancer cells, was chemically conjugated to the SPIOs via a peptide bond (117). The authors postulated that MTX (parent drug) would not be released from the nanoparticles-MTX (prodrug) under intravenous conditions, while MTX would be cleaved in the cellular lysosomal compartment (low pH and the presence of lysozymes), and thus achieve cell specific delivery and decrease off-target effects. *In vitro* release kinetics showed that MTX release was in a pH-dependent manner in the presence of proteases, with higher release under lower pH. In addition, methotrexate-SPIOs exhibited specific uptake by the folate-receptor overexpressing breast cancer MCF-7 cells (approximately 20-folds higher than the primary cardiomyocyte cells with low folate-receptor expression). The majority of the methotrexate-SPIOs were internalized and resided in the lysosomes of the cells. The methotrexate-SPIOs efficacy was validated against MCF-7 cells and human cervical cancer cells.

Imaging-guided drug delivery

In addition, SPIOs were also applied in drug delivery and controlled drug release since they were able to rupture the thermal sensitive phospholipids outshell to release the encapsulated drugs when they were exposed to an exogenous magnetic field (118-120). Barbincova *et al.* first tested the possibility of this strategy for use in controlled drug release. Both DOX and SPIOs were

encapsulated in the liposomes. After applying the AC-magnetic field with a frequency of ~ 1 MHz, DOX was immediately released from the liposomes (118). The magnetic field induced SPIOs to generate heat for controlled drug release. At these frequencies, heat was produced exclusively from the Néel relaxation, thus, the adjacent normal tissues were not heated to minimize the side effect (121). Hu *et al.* constructed $(Fe_3O_4/PAH)_4$ microcapsules with iron oxide nanoparticles distributed throughout the polyelectrolyte shell (120). They found that the FITC-dextran or DOX molecules can be released from the $(Fe_3O_4/PAH)_4$ microcapsules in the presence of a high-frequency magnetic field (HFMF, 50-100 kHz). In the absence of HFMF, the cumulative released amount of DOX was 9%, whereas in the presence of HFMF, the cumulative released amount of DOX was increased to about 67% in 30 minutes, indicating the deterioration of the outshell of the $(Fe_3O_4/PAH)_4$ microcapsules which resulted in the fast release. This approach can be adapted for imaging-guided drug delivery.

Biodistribution, pharmacokinetics and toxicology of SPIOs

The biodistribution and pharmacokinetics of SPIOs depend on their size, charge and surface coating. Normally, nanoparticles with a small size less than 10 nm will be quickly removed by renal clearance and extravasation, while the nanoparticles with large size over 200 nm are sequestered by liver and spleen by macrophage uptake (122). Thus the SPIOs with an intermediate size would favorably used since they have longer half lives and circulation time to reach the target site. However, larger SPIOs may also be used due to specific purpose. For instance, oral SPIO agents such as AMI-121 (crystal core 10 nm, hydrodynamic

diameter 300 nm) and OMP (crystal core 50 nm, hydrodynamic diameter 3.5 μm) have been clinically applied for the evaluation of bowel function (34). These nanoparticles are coated with nonbiodegradable and insoluble matrix (*e.g.*, polystyrene) to protect them from being absorbed by GI tract hence become excellent contrast agents for bowel abnormalities.

After *i.v.* administration of SPIOs, nanoparticles are extensively taken up by macrophages in the liver (Küpffer cells), spleen and bone marrow (44). For instance, a pharmacokinetic study of clinically used SPIO AMI-25 with an average diameter of 80 nm using ^{59}Fe radiotracer in rats showed that ^{59}Fe-AMI-25 was predominantly located in the liver and spleen, with 6.3 ± 0.52%ID/g and 10.9 ± 7.56%ID/g (percentage of injected dose per gram of tissue), respectively at 1 hr post injection, indicating early RES macrophage uptake (123). Minimal amounts of ^{59}Fe were detected in other organs including kidney, lung and brain. The human blood half-lives of the various clinically used SPIOs for MRI imaging have been determined to be from 1 hr to 36 hrs, e.g., AMI-25 has the blood half life of 2 hrs (44).

By modifying particle size, particle surface coating and charge, macrophage uptake of SPIOs can be controlled. In general, larger size and charged nanoparticles would have higher macrophage uptake relative to smaller particles and electrically neutral particles (124-126). SPIOs surface properties could also contribute to the uptake by phagocytic cells. Matuszewski *et al.* found that carboxyl dextran-coated SPIOs (of equal or even smaller sizes) exhibited higher uptake by macrophages than dextran-coated SPIOs (127). To minimize

macrophage uptake and increase circulation time, some strategies were proposed. For instance, MG-CoA reductase inhibitor lovastatin which downregulates class A types I and II macrophage scavenger receptors was used to decrease macrophage uptake; and decoy particles Ni-liposome were used to eliminate plasma opsonins (15, 128, 129).

Although gadolinium agents have been associated with toxicity (such as nephrogenic systemic fibrosis (NSF) in renally impaired patients), clinically used SPIOs as MRI contrast agents exhibited high biocompatibility and low toxicity (130). SPIOs were generally metabolized in lysosomal compartment in macrophage and endothelial cells, and the resulting iron molecules were incorporated into hemoglobin as body iron supplements (30, 123, 131). Therefore, the administration of SPIOs was shown to reverse iron deficiency anemia. Singh *et al.* demonstrated Ferumoxytol, a carbohydrate-coated SPIOs, was well tolerated and had a safety profile comparable to placebo in anemic patients with chronic kidney disease (CKD) (132).

Macrophage plays an important role in the immune system acting in both innate immunity and adaptive immunity. Upon phagocytose pathogens, macrophage would release a variety of substances including enzymes, complement proteins, growth factors and cytokines, such as interleukin-1, to initiate immune response or develop inflammation. Titania particles have been shown to induce IL-1 production from macrophage, while uptake of SPIOs by macrophages elicited minimal IL-1 secretion indicating a low pro-inflammatory potential of SPIOs (124). In addition, Medarova *et al.* showed that the

administration of SPIO conjugated siRNAs exhibited no immunostimulatory properties with comparable levels of interferon (IFN)-α and inflammatory cytokine IL–6 to control groups, whereas immunogenicity for *in vivo* delivery of siRNAs was still a challenge (13). Iron oxide nanoparticles also did not provoke inflammatory response in human aortic endothelial cells (HAECs). In contrast, yttrium oxide (Y_2O_3) and zinc oxide (ZnO) nanoparticles induced inflammatory response characterized by the secretion of inflammatory markers intra-cellular cell adhesion molecule-1, IL-8, and monocyte chemotactic protein-1 (133).

Although SPIOs exhibited high biocompatibility, more studies might be warranted to ensure the safe use of SPIOs based on the following reasons: (1) reactive oxygen species (ROS) generation: SPIOs were shown to induce reactive oxygen species (ROS) to increase the cell membrane permeability, which probably contribute to their internalization by cells (134). *In vivo* study demonstrated that lipid hydroperoxide (LHPO, as a measure of oxidative stress) level was increased in liver, spleen and kidney after SPIOs administration, and then gradually back to normal (135). There were no significant changes in other organs such as lung, brain and heart. Further histological analysis of the liver, spleen and kidney showed no significant change in the cellular structure. (2) neurotoxicity: PC12 cells exhibited diminished viability and capacity to differentiate in response to nerve growth factor when exposed to dimercaptosuccinic acid (DMSA) coated iron oxide nanoparticles (136). (3) toxicity profile of surface modification: Cationic surface coating exhibited more toxicity than uncoated nanoparticles and anionic coated nanoparticles (137).

Dextran coated magnetite inhibited cell proliferation similar to uncoated magnetite, whereas albumin coated magnetite even stimulated cell proliferation (138). Overall, the toxicity of specific SPIOs still needs to be tested for their various compositions and physical chemical properties.

Other inorganic nanoparticle

Besides iron oxide nanoparticles, other inorganic nanoparticles have been used for the purpose of imaging, gene delivery and drug delivery, which include quantum dot (112, 139), silica (110, 140), silver (141), and gold (142-145).

Quantum dot, semiconductor nanocrystals with exceptional photostability, is extensively used in imaging both *in vitro* and *in vivo* animal model. A typical quantum dot fluorophore is made of CdSe cores coated with a layer of ZnS. Quantum dots exhibit size tunable fluorescent emission capacity and have broad excitation spectra which distinguished them from organic dyes (146). Quantum dots have also been used in gene delivery (112). However, quantum dots suffered from high toxicity, which might limit their future applications (147).

Gold nanoparticles, based on their specific geometries, can be further divided into gold nanospheres, gold nonobelts, gold nanocages, gold nanoprisms, gold nanostars, and gold nanorods (145). Gold nanoparticles showed distinct optical properties due to the excitation of local surface plasmon resonances (LSPRs). The fluorescent properties of gold nanoparticles have been applied to label DNA strands to investigate the complementary DNA hybridization events as the fluorescent spectra intensity would be sharply decreased when the oligos hybridize, which leads to the aggregates of DNA linked gold nanoparticles (148).

Furthermore, gold nanoparticles can also act as fluorescence or Raman spectrum enhancer. It was shown that adsorbed molecules on gold surface enhanced fluorescence or surface Raman scattering (149, 150). The intrinsic Raman enhancement factors can be as high as 10^{14} to 10^{15}, which makes single molecule detection possible (151). Gold nanoparticles have also been implicated in tumor imaging (152), gene delivery (143) and drug delivery (153, 154). Similar to SPIOs, gold nanoparticles can be used in cancer hyperthermal therapy (155). The antiangiogenic role of gold nanoparticles, mediated by the inhibition of vascular permeability factor/vascular endothelial growth factor (VPF/VEGF) –165 and basic fibroblast growth factor (bFGF), has also been recognized for their potential use in angiogenesis inhibition (156). The radiotherapy enhancement was achieved by the administration of gold nanoparticles through the mechanism of high-Z radioenhancement (144). Gold nanoparticle and SPIOs were found to degrade the MDR1 level in Pgp overexpressing K562/A02 cells when combining with anticancer drug daunorubicin (DN), and thus increased the cellular accumulation of DNR and increased cancer cell death (157). Gold nanoparticles might also be a potential X-ray or CT contrast agent (158). The easy preparation, surface modification and low toxicity of gold nanoparticles make them as potential candidates for tumor imaging, therapy, gene delivery, and drug delivery.

References

1. Jemal A, Siegel R, Ward E, Hao Y, Xu J, Thun MJ. Cancer statistics, 2009. CA Cancer J Clin 2009.
2. Sanvicens N, Marco MP. Multifunctional nanoparticles--properties and prospects for their use in human medicine. Trends Biotechnol 2008; 26: 425-33.
3. Petri-Fink A, Hofmann H. Superparamagnetic iron oxide nanoparticles (SPIONs): from synthesis to in vivo studies--a summary of the synthesis, characterization, in vitro, and in vivo investigations of SPIONs with particular focus on surface and colloidal properties. IEEE Trans Nanobioscience 2007; 6: 289-97.
4. Wagner V, Dullaart A, Bock AK, Zweck A. The emerging nanomedicine landscape. Nat Biotechnol 2006; 24: 1211-7.
5. Bangham AD, Standish MM, Watkins JC. Diffusion of univalent ions across the lamellae of swollen phospholipids. J Mol Biol 1965; 13: 238-52.
6. Farokhzad OC, Langer R. Impact of nanotechnology on drug delivery. ACS Nano 2009; 3: 16-20.
7. Rao J. Shedding light on tumors using nanoparticles. ACS Nano 2008; 2: 1984-6.
8. Leserman LD, Barbet J, Kourilsky F, Weinstein JN. Targeting to cells of fluorescent liposomes covalently coupled with monoclonal antibody or protein A. Nature 1980; 288: 602-4.
9. Heath TD, Fraley RT, Papahdjopoulos D. Antibody targeting of liposomes: cell specificity obtained by conjugation of F(ab')2 to vesicle surface. Science 1980; 210: 539-41.
10. Gil PR, Parak WJ. Composite nanoparticles take aim at cancer. ACS Nano 2008; 2: 2200-5.
11. Jain TK, Morales MA, Sahoo SK, Leslie-Pelecky DL, Labhasetwar V. Iron oxide nanoparticles for sustained delivery of anticancer agents. Mol Pharm 2005; 2: 194-205.
12. Ferrari M. Cancer nanotechnology: opportunities and challenges. Nat Rev Cancer 2005; 5: 161-71.
13. Medarova Z, Pham W, Farrar C, Petkova V, Moore A. In vivo imaging of siRNA delivery and silencing in tumors. Nat Med 2007; 13: 372-7.
14. Liong M, Lu J, Kovochich M, et al. Multifunctional inorganic nanoparticles for imaging, targeting, and drug delivery. ACS Nano 2008; 2: 889-96.
15. Peng XH, Qian X, Mao H, et al. Targeted magnetic iron oxide nanoparticles for tumor imaging and therapy. Int J Nanomedicine 2008; 3: 311-21.

16. Natarajan A, Xiong CY, Gruettner C, DeNardo GL, DeNardo SJ. Development of multivalent radioimmunonanoparticles for cancer imaging and therapy. Cancer Biother Radiopharm 2008; 23: 82-91.
17. Bonnemain B. Superparamagnetic agents in magnetic resonance imaging: physicochemical characteristics and clinical applications. A review. J Drug Target 1998; 6: 167-74.
18. Thorek DL, Chen AK, Czupryna J, Tsourkas A. Superparamagnetic iron oxide nanoparticle probes for molecular imaging. Ann Biomed Eng 2006; 34: 23-38.
19. Gupta AK, Gupta M. Synthesis and surface engineering of iron oxide nanoparticles for biomedical applications. Biomaterials 2005; 26: 3995-4021.
20. Sjogren CE, Briley-Saebo K, Hanson M, Johansson C. Magnetic characterization of iron oxides for magnetic resonance imaging. Magn Reson Med 1994; 31: 268-72.
21. Laurent S, Forge D, Port M, et al. Magnetic iron oxide nanoparticles: synthesis, stabilization, vectorization, physicochemical characterizations, and biological applications. Chem Rev 2008; 108: 2064-110.
22. Lu AH, Salabas EL, Schuth F. Magnetic nanoparticles: synthesis, protection, functionalization, and application. Angew Chem Int Ed Engl 2007; 46: 1222-44.
23. Hyeon T, Lee SS, Park J, Chung Y, Na HB. Synthesis of highly crystalline and monodisperse maghemite nanocrystallites without a size-selection process. J Am Chem Soc 2001; 123: 12798-801.
24. Gaur U, Sahoo SK, De TK, Ghosh PC, Maitra A, Ghosh PK. Biodistribution of fluoresceinated dextran using novel nanoparticles evading reticuloendothelial system. Int J Pharm 2000; 202: 1-10.
25. Zhang C, Wangler B, Morgenstern B, et al. Silica- and alkoxysilane-coated ultrasmall superparamagnetic iron oxide particles: a promising tool to label cells for magnetic resonance imaging. Langmuir 2007; 23: 1427-34.
26. Ma Y, Manolache S, Denes FS, Thamm DH, Kurzman ID, Vail DM. Plasma synthesis of carbon magnetic nanoparticles and immobilization of doxorubicin for targeted drug delivery. J Biomater Sci Polym Ed 2004; 15: 1033-49.
27. Philipse AP, Vanbruggen MPB, Pathmamanoharan C. Magnetic Silica Dispersions - Preparation and Stability of Surface-Modified Silica Particles with a Magnetic Core. Langmuir 1994; 10: 92-9.
28. Yang HH, Zhang SQ, Chen XL, Zhuang ZX, Xu JG, Wang XR. Magnetite-containing spherical silica nanoparticles for biocatalysis and bioseparations. Anal Chem 2004; 76: 1316-21.
29. Ulman A. Formation and Structure of Self-Assembled Monolayers. Chem Rev 1996; 96: 1533-54.
30. Arbab AS, Wilson LB, Ashari P, Jordan EK, Lewis BK, Frank JA. A model of lysosomal metabolism of dextran coated superparamagnetic iron oxide (SPIO) nanoparticles: implications for cellular magnetic resonance imaging. NMR Biomed 2005; 18: 383-9.

31. Kaushik A, Khan R, Solanki PR, et al. Iron oxide nanoparticles-chitosan composite based glucose biosensor. Biosens Bioelectron 2008; 24: 676-83.
32. Cheong SJ, Lee CM, Kim SL, et al. Superparamagnetic iron oxide nanoparticles-loaded chitosan-linoleic acid nanoparticles as an effective hepatocyte-targeted gene delivery system. Int J Pharm 2009; 372: 169-76.
33. Bee A, Massart R, Neveu S. Synthesis of Very Fine Maghemite Particles. Journal of Magnetism and Magnetic Materials 1995; 149: 6-9.
34. Wang YX, Hussain SM, Krestin GP. Superparamagnetic iron oxide contrast agents: physicochemical characteristics and applications in MR imaging. Eur Radiol 2001; 11: 2319-31.
35. Weissleder R, Lee AS, Khaw BA, Shen T, Brady TJ. Antimyosin-labeled monocrystalline iron oxide allows detection of myocardial infarct: MR antibody imaging. Radiology 1992; 182: 381-5.
36. Sato T, Iijima T, Seki M, Inagaki N. Magnetic-Properties of Ultrafine Ferrite Particles. Journal of Magnetism and Magnetic Materials 1987; 65: 252-6.
37. Lovely GR, Brown AP, Evans SD, Brydson R. HRTEM characterisation of surface effects in iron oxide nanoparticles. Electron Microscopy and Analysis 2003 2004: 479-82.
38. Miser DE, Li P, Hajaligol MR. High-resolution TEM characterization of a nanoparticle iron oxide catalyst and reaction products. Abstracts of Papers of the American Chemical Society 2002; 224: U47-U.
39. Herrera LK, Cotte M, de Haro MCJ, Duran A, Justo A, Perez-Rodriguez JL. Characterization of iron oxide-based pigments by synchrotron-based micro X-ray diffraction. Applied Clay Science 2008; 42: 57-62.
40. Di Marco M, Port M, Couvreur P, Dubernet C, Ballirano P, Sadun C. Structural characterization of ultrasmall superparamagnetic iron oxide (USPIO) particles in aqueous suspension by energy dispersive X-ray diffraction (EDXD). J Am Chem Soc 2006; 128: 10054-9.
41. Bonetti E, Savini L, Deriu A, Albanese G, Moya J. X-ray diffraction and Mossbauer spectroscopy of the core/shell iron/iron oxide system. Journal of Magnetism and Magnetic Materials 2003; 262: 132-5.
42. Di Marco M, Sadun C, Port M, Guilbert I, Couvreur P, Dubernet C. Physicochemical characterization of ultrasmall superparamagnetic iron oxide particles (USPIO) for biomedical application as MRI contrast agents. Int J Nanomedicine 2007; 2: 609-22.
43. Rose HH. Optics of high-performance electron microscopes. Science and Technology of Advanced Materials 2008; 9: -.
44. Corot C, Robert P, Idee JM, Port M. Recent advances in iron oxide nanocrystal technology for medical imaging. Adv Drug Deliv Rev 2006; 58: 1471-504.
45. Kunzelmann U, Jacobasch HJ, Reinhard G. Investigations of the Influence of Vapor-Phase Inhibitors on the Surface-Charge of Iron-Oxide Particles by Zeta-Potential Measurements. Werkstoffe Und Korrosion-Materials and Corrosion 1989; 40: 723-8.
46. Lauterbu.Pc. Image Formation by Induced Local Interactions - Examples Employing Nuclear Magnetic-Resonance. Nature 1973; 242: 190-1.

47. Oksendal AN, Hals PA. Biodistribution and toxicity of MR imaging contrast media. J Magn Reson Imaging 1993; 3: 157-65.
48. Runge VM, Wells JW. Update - Safety, New Applications, New Mr Agents. Topics in Magnetic Resonance Imaging 1995; 7: 181-95.
49. Shellock FG, Kanal E. Safety of magnetic resonance imaging contrast agents. Jmri-Journal of Magnetic Resonance Imaging 1999; 10: 477-84.
50. Frangioni JV. New technologies for human cancer imaging. J Clin Oncol 2008; 26: 4012-21.
51. Briley-Saebo KC, Geninatti-Crich S, Cormode DP, et al. High-relaxivity gadolinium-modified high-density lipoproteins as magnetic resonance imaging contrast agents. J Phys Chem B 2009; 113: 6283-9.
52. Nelson KL, Runge VM. Basic Principles of Mr Contrast. Topics in Magnetic Resonance Imaging 1995; 7: 124-36.
53. Debbage P, Jaschke W. Molecular imaging with nanoparticles: giant roles for dwarf actors. Histochem Cell Biol 2008; 130: 845-75.
54. Weissleder R, Elizondo G, Wittenberg J, Rabito CA, Bengele HH, Josephson L. Ultrasmall superparamagnetic iron oxide: characterization of a new class of contrast agents for MR imaging. Radiology 1990; 175: 489-93.
55. Bradbury M, Hricak H. Molecular MR imaging in oncology. Magn Reson Imaging Clin N Am 2005; 13: 225-40.
56. Weissleder R, Hahn PF, Stark DD, et al. Superparamagnetic iron oxide: enhanced detection of focal splenic tumors with MR imaging. Radiology 1988; 169: 399-403.
57. Weissleder R, Stark DD, Rummeny EJ, Compton CC, Ferrucci JT. Splenic lymphoma: ferrite-enhanced MR imaging in rats. Radiology 1988; 166: 423-30.
58. Seneterre E, Taourel P, Bouvier Y, et al. Detection of hepatic metastases: ferumoxides-enhanced MR imaging versus unenhanced MR imaging and CT during arterial portography. Radiology 1996; 200: 785-92.
59. Anzai Y, Brunberg JA, Lufkin RB. Imaging of nodal metastases in the head and neck. Jmri-Journal of Magnetic Resonance Imaging 1997; 7: 774-83.
60. Bush CH, Mladinich CR, Montgomery WJ. Evaluation of an ultrasmall superparamagnetic iron oxide in MRI in a bone tumor model in rabbits. J Magn Reson Imaging 1997; 7: 579-84.
61. Enochs WS, Harsh G, Hochberg F, Weissleder R. Improved delineation of human brain tumors on MR images using a long-circulating, superparamagnetic iron oxide agent. J Magn Reson Imaging 1999; 9: 228-32.
62. Bremer C, Allkemper T, Baermig J, Reimer P. RES-specific imaging of the liver and spleen with iron oxide particles designed for blood pool MR-angiography. J Magn Reson Imaging 1999; 10: 461-7.
63. Maeda H, Sawa T, Konno T. Mechanism of tumor-targeted delivery of macromolecular drugs, including the EPR effect in solid tumor and clinical overview of the prototype polymeric drug SMANCS. J Control Release 2001; 74: 47-61.
64. Seppenwoolde JH, Viergever MA, Bakker CJ. Passive tracking exploiting local signal conservation: the white marker phenomenon. Magn Reson Med 2003; 50: 784-90.

65. Seppenwoolde JH, Vincken KL, Bakker CJ. White-marker imaging--separating magnetic susceptibility effects from partial volume effects. Magn Reson Med 2007; 58: 605-9.
66. Mani V, Briley-Saebo KC, Itskovich VV, Samber DD, Fayad ZA. Gradient echo acquisition for superparamagnetic particles with positive contrast (GRASP): sequence characterization in membrane and glass superparamagnetic iron oxide phantoms at 1.5T and 3T. Magn Reson Med 2006; 55: 126-35.
67. Stuber M GW, Schaer M, Bulte JW, Kraichman DL. Shedding light on the dark spot with IRON: a method that generates positive contrast in the presence of superparamagnetic nanoparticles. In *Proceedings of the International Society of Magnetic Resonance in Medicine* 2005; Miami Beach: Abstract no: 2608.
68. Dahnke H LW, Frank JA, Schaeffter T. . Optimal positive contrast of labeled cells via conventional 3D imaging. In *Proceedings of the International Society of Magnetic Resonance in Medicine* 2006; Seattle: Abstract no: 361.
69. Liu W, Dahnke H, Jordan EK, Schaeffter T, Frank JA. In vivo MRI using positive-contrast techniques in detection of cells labeled with superparamagnetic iron oxide nanoparticles. NMR Biomed 2008; 21: 242-50.
70. Mani V, Adler E, Briley-Saebo KC, et al. Serial in vivo positive contrast MRI of iron oxide-labeled embryonic stem cell-derived cardiac precursor cells in a mouse model of myocardial infarction. Magn Reson Med 2008; 60: 73-81.
71. Ter-Pogossian MM. PET, SPECT, and NMRI: competing or complementary disciplines? J Nucl Med 1985; 26: 1487-98.
72. Chen TJ, Cheng TH, Chen CY, et al. Targeted Herceptin-dextran iron oxide nanoparticles for noninvasive imaging of HER2/neu receptors using MRI. J Biol Inorg Chem 2009; 14: 253-60.
73. Serda RE, Adolphi NL, Bisoffi M, Sillerud LO. Targeting and cellular trafficking of magnetic nanoparticles for prostate cancer imaging. Mol Imaging 2007; 6: 277-88.
74. Tiefenauer LX, Tschirky A, Kuhne G, Andres RY. In vivo evaluation of magnetite nanoparticles for use as a tumor contrast agent in MRI. Magn Reson Imaging 1996; 14: 391-402.
75. Yang L, Mao H, Wang YA, et al. Single chain epidermal growth factor receptor antibody conjugated nanoparticles for in vivo tumor targeting and imaging. Small 2009; 5: 235-43.
76. Yang Y, Jiang JS, Du B, Gan ZF, Qian M, Zhang P. Preparation and properties of a novel drug delivery system with both magnetic and biomolecular targeting. J Mater Sci Mater Med 2009; 20: 301-7.
77. Sun C, Veiseh O, Gunn J, et al. In vivo MRI detection of gliomas by chlorotoxin-conjugated superparamagnetic nanoprobes. Small 2008; 4: 372-9.
78. Zhang C, Jugold M, Woenne EC, et al. Specific targeting of tumor angiogenesis by RGD-conjugated ultrasmall superparamagnetic iron oxide particles using a clinical 1.5-T magnetic resonance scanner. Cancer Res 2007; 67: 1555-62.
79. Wang AZ, Bagalkot V, Vasilliou CC, et al. Superparamagnetic iron oxide nanoparticle-aptamer bioconjugates for combined prostate cancer imaging and therapy. ChemMedChem 2008; 3: 1311-5.

80. Lee D, Lockey R, Mohapatra S. Folate receptor-mediated cancer cell specific gene delivery using folic acid-conjugated oligochitosans. J Nanosci Nanotechnol 2006; 6: 2860-6.
81. Stella B, Arpicco S, Peracchia MT, et al. Design of folic acid-conjugated nanoparticles for drug targeting. J Pharm Sci 2000; 89: 1452-64.
82. Ginobbi P, Geiser TA, Ombres D, Citro G. Folic acid-polylysine carrier improves efficacy of c-myc antisense oligodeoxynucleotides on human melanoma (M14) cells. Anticancer Res 1997; 17: 29-35.
83. Low PS, Henne WA, Doorneweerd DD. Discovery and development of folic-acid-based receptor targeting for imaging and therapy of cancer and inflammatory diseases. Acc Chem Res 2008; 41: 120-9.
84. Landmark KJ, Dimaggio S, Ward J, et al. Synthesis, characterization, and in vitro testing of superparamagnetic iron oxide nanoparticles targeted using folic Acid-conjugated dendrimers. ACS Nano 2008; 2: 773-83.
85. Li X, Du X, Huo T, Liu X, Zhang S, Yuan F. Specific Targeting of Breast Tumor by Octreotide-Conjugated Ultrasmall Superparamagnetic Iron Oxide Particles Using a Clinical 3.0-Tesla Magnetic Resonance Scanner. Acta Radiol 2009: 1-12.
86. Yang L, Mao H, Cao Z, et al. Molecular Imaging of Pancreatic Cancer in a Preclinical Animal Tumor Model Using Targeted Multifunctional Nanoparticles. Gastroenterology 2009.
87. Kresse M, Wagner S, Pfefferer D, Lawaczeck R, Elste V, Semmler W. Targeting of ultrasmall superparamagnetic iron oxide (USPIO) particles to tumor cells in vivo by using transferrin receptor pathways. Magn Reson Med 1998; 40: 236-42.
88. Hogemann-Savellano D, Bos E, Blondet C, et al. The transferrin receptor: a potential molecular imaging marker for human cancer. Neoplasia 2003; 5: 495-506.
89. Ledezma CJ, Chen W, Sai V, et al. (18)F-FDOPA PET/MRI fusion in patients with primary/recurrent gliomas: Initial experience. Eur J Radiol 2008.
90. Ruf J, Lopez Hanninen E, Bohmig M, et al. Impact of FDG-PET/MRI image fusion on the detection of pancreatic cancer. Pancreatology 2006; 6: 512-9.
91. Malesci A, Balzarini L, Chiti A, Lucignani G. Pancreatic cancer or chronic pancreatitis? An answer from PET/MRI image fusion. Eur J Nucl Med Mol Imaging 2004; 31: 1352.
92. Lemke AJ, Niehues SM, Amthauer H, Rohlfing T, Hosten N, Felix R. [Clinical use of digital retrospective image fusion of CT, MRI, FDG-PET and SPECT -- fields of indications and results]. Rofo 2004; 176: 1811-8.
93. Nakano Y, Fujibuchi T, Isobe T, et al. [Assessment of whole body PET/MRI fusion imaging using automated software: usefulness of partial body fusion]. Nippon Hoshasen Gijutsu Gakkai Zasshi 2006; 62: 822-31.
94. Lewin M, Carlesso N, Tung CH, et al. Tat peptide-derivatized magnetic nanoparticles allow in vivo tracking and recovery of progenitor cells. Nat Biotechnol 2000; 18: 410-4.

95. Yang F, Li Y, Chen Z, Zhang Y, Wu J, Gu N. Superparamagnetic iron oxide nanoparticle-embedded encapsulated microbubbles as dual contrast agents of magnetic resonance and ultrasound imaging. Biomaterials 2009.
96. Senzer N, Nemunaitis J. A review of contusugene ladenovec (Advexin) p53 therapy. Curr Opin Mol Ther 2009; 11: 54-61.
97. Morse M. Technology evaluation: Rexin-G, Epeius Biotechnologies. Curr Opin Mol Ther 2005; 7: 164-9.
98. Brower V. Cancer gene therapy steadily advances. J Natl Cancer Inst 2008; 100: 1276-8.
99. Mazda O, Kishida T. Molecular therapeutics of cancer by means of electroporation-based transfer of siRNAs and EBV-based expression vectors. Front Biosci (Elite Ed) 2009; 1: 316-31.
100. Li YS, Davidson E, Reid CN, McHale AP. Optimising ultrasound-mediated gene transfer (sonoporation) in vitro and prolonged expression of a transgene in vivo: potential applications for gene therapy of cancer. Cancer Lett 2009; 273: 62-9.
101. Uchida M, Li XW, Mertens P, Alpar HO. Transfection by Particle Bombardment: Delivery of Plasmid DNA into Mammalian Cells Using Gene Gun. Biochim Biophys Acta 2009.
102. Innocentin S, Guimaraes V, Miyoshi A, et al. Lactococcus lactis Expressing either Staphylococcus aureus Fibronectin-Binding Protein A or Listeria monocytogenes Internalin A can efficiently internalize and deliver DNA in human epithelial cells. Appl Environ Microbiol 2009.
103. Crombez L, Morris MC, Dufort S, et al. Targeting cyclin B1 through peptide-based delivery of siRNA prevents tumour growth. Nucleic Acids Res 2009.
104. Song E, Zhu P, Lee SK, et al. Antibody mediated in vivo delivery of small interfering RNAs via cell-surface receptors. Nat Biotechnol 2005; 23: 709-17.
105. Jere D, Arote R, Jiang HL, Kim YK, Cho MH, Cho CS. Bioreducible polymers for efficient gene and siRNA delivery. Biomed Mater 2009; 4: 25020.
106. Chen JL, Hu Y, Shuai WP, Chen HL, Liang WQ, Gao JQ. Telomerase-targeting antisense oligonucleotides carried by polycation liposomes enhance the growth inhibition effect on tumor cells. J Biomed Mater Res B Appl Biomater 2009; 89: 362-8.
107. Li Z, Xiang J, Zhang W, et al. Nanoparticle delivery of anti-metastatic NM23-H1 gene improves chemotherapy in a mouse tumor model. Cancer Gene Ther 2009; 16: 423-9.
108. Kaul G, Amiji M. Tumor-targeted gene delivery using poly(ethylene glycol)-modified gelatin nanoparticles: in vitro and in vivo studies. Pharm Res 2005; 22: 951-61.
109. He XX, Wang K, Tan W, et al. Bioconjugated nanoparticles for DNA protection from cleavage. J Am Chem Soc 2003; 125: 7168-9.
110. He XX, Wang KM, Li D, et al. A novel DNA-enrichment technology based on amino-modified functionalized silica nanoparticles. Journal of Dispersion Science and Technology 2003; 24: 633-40.

111. Dellian M, Yuan F, Trubetskoy VS, Torchilin VP, Jain RK. Vascular permeability in a human tumour xenograft: molecular charge dependence. Br J Cancer 2000; 82: 1513-8.
112. Derfus AM, Chen AA, Min DH, Ruoslahti E, Bhatia SN. Targeted quantum dot conjugates for siRNA delivery. Bioconjug Chem 2007; 18: 1391-6.
113. Lee JH, Lee K, Moon SH, Lee Y, Park TG, Cheon J. All-in-one target-cell-specific magnetic nanoparticles for simultaneous molecular imaging and siRNA delivery. Angew Chem Int Ed Engl 2009; 48: 4174-9.
114. Lily Yang ZC, Hari Krishna Sajja, Hui Mao, Liya Wang, Huaying Geng, Hengyi Xu, Tieshan Jiang, Willian C. Wood, Shuming Nie, and Y. Andrew Wang. Development of Receptor Targeted Magnetic Iron Oxide Nanoparticles for Efficieny Drug Delivery and Tumor Imaging. Journal of Biomedical Nanotechnology 2008; 4: 1-11.
115. Cengelli F, Grzyb JA, Montoro A, Hofmann H, Hanessian S, Juillerat-Jeanneret L. Surface-Functionalized Ultrasmall Superparamagnetic Nanoparticles as Magnetic Delivery Vectors for Camptothecin. ChemMedChem 2009; 4: 988-97.
116. Hwu JR, Lin YS, Josephrajan T, et al. Targeted Paclitaxel by conjugation to iron oxide and gold nanoparticles. J Am Chem Soc 2009; 131: 66-8.
117. Kohler N, Sun C, Wang J, Zhang M. Methotrexate-modified superparamagnetic nanoparticles and their intracellular uptake into human cancer cells. Langmuir 2005; 21: 8858-64.
118. Babincova M, Cicmanec P, Altanerova V, Altaner C, Babinec P. AC-magnetic field controlled drug release from magnetoliposomes: design of a method for site-specific chemotherapy. Bioelectrochemistry 2002; 55: 17-9.
119. Liu TY, Hu SH, Liu KH, Shaiu RS, Liu DM, Chen SY. Instantaneous drug delivery of magnetic/thermally sensitive nanospheres by a high-frequency magnetic field. Langmuir 2008; 24: 13306-11.
120. Hu SH, Tsai CH, Liao CF, Liu DM, Chen SY. Controlled rupture of magnetic polyelectrolyte microcapsules for drug delivery. Langmuir 2008; 24: 11811-8.
121. M. Babincova PC, P. Babinec, V. Altanerova, C. Altaner, . Magnetoliposomes mediated local electromagnetic hyperthermia. Radio Eng 2000; 9: 12-3.
122. Gupta AK, Wells S. Surface-modified superparamagnetic nanoparticles for drug delivery: preparation, characterization, and cytotoxicity studies. IEEE Trans Nanobioscience 2004; 3: 66-73.
123. Weissleder R, Stark DD, Engelstad BL, et al. Superparamagnetic iron oxide: pharmacokinetics and toxicity. AJR Am J Roentgenol 1989; 152: 167-73.
124. Raynal I, Prigent P, Peyramaure S, Najid A, Rebuzzi C, Corot C. Macrophage endocytosis of superparamagnetic iron oxide nanoparticles: mechanisms and comparison of ferumoxides and ferumoxtran-10. Invest Radiol 2004; 39: 56-63.
125. Chouly C, Pouliquen D, Lucet I, Jeune JJ, Jallet P. Development of superparamagnetic nanoparticles for MRI: effect of particle size, charge and surface nature on biodistribution. J Microencapsul 1996; 13: 245-55.

126. Villanueva A, Canete M, Roca AG, et al. The influence of surface functionalization on the enhanced internalization of magnetic nanoparticles in cancer cells. Nanotechnology 2009; 20: 115103.
127. Matuszewski L, Persigehl T, Wall A, et al. Cell tagging with clinically approved iron oxides: feasibility and effect of lipofection, particle size, and surface coating on labeling efficiency. Radiology 2005; 235: 155-61.
128. Rogers WJ, Basu P. Factors regulating macrophage endocytosis of nanoparticles: implications for targeted magnetic resonance plaque imaging. Atherosclerosis 2005; 178: 67-73.
129. Simberg D, Duza T, Park JH, et al. Biomimetic amplification of nanoparticle homing to tumors. Proc Natl Acad Sci U S A 2007; 104: 932-6.
130. Neuwelt EA, Hamilton BE, Varallyay CG, et al. Ultrasmall superparamagnetic iron oxides (USPIOs): a future alternative magnetic resonance (MR) contrast agent for patients at risk for nephrogenic systemic fibrosis (NSF)? Kidney Int 2009; 75: 465-74.
131. Briley-Saebo K, Bjornerud A, Grant D, Ahlstrom H, Berg T, Kindberg GM. Hepatic cellular distribution and degradation of iron oxide nanoparticles following single intravenous injection in rats: implications for magnetic resonance imaging. Cell Tissue Res 2004; 316: 315-23.
132. Singh A, Patel T, Hertel J, Bernardo M, Kausz A, Brenner L. Safety of ferumoxytol in patients with anemia and CKD. Am J Kidney Dis 2008; 52: 907-15.
133. Gojova A, Guo B, Kota RS, Rutledge JC, Kennedy IM, Barakat AI. Induction of inflammation in vascular endothelial cells by metal oxide nanoparticles: effect of particle composition. Environ Health Perspect 2007; 115: 403-9.
134. Apopa PL, Qian Y, Shao R, et al. Iron oxide nanoparticles induce human microvascular endothelial cell permeability through reactive oxygen species production and microtubule remodeling. Part Fibre Toxicol 2009; 6: 1.
135. Jain TK, Reddy MK, Morales MA, Leslie-Pelecky DL, Labhasetwar V. Biodistribution, clearance, and biocompatibility of iron oxide magnetic nanoparticles in rats. Mol Pharm 2008; 5: 316-27.
136. Pisanic TR, 2nd, Blackwell JD, Shubayev VI, Finones RR, Jin S. Nanotoxicity of iron oxide nanoparticle internalization in growing neurons. Biomaterials 2007; 28: 2572-81.
137. Hilger I, Fruhauf S, Linss W, et al. Cytotoxicity of selected magnetic fluids on human adenocarcinoma cells. Journal of Magnetism and Magnetic Materials 2003; 261: 7-12.
138. Berry CC, Wells S, Charles S, Curtis ASG. Dextran and albumin derivatised iron oxide nanoparticles: influence on fibroblasts in vitro. Biomaterials 2003; 24: 4551-7.
139. Weng KC, Noble CO, Papahadjopoulos-Sternberg B, et al. Targeted tumor cell internalization and imaging of multifunctional quantum dot-conjugated immunoliposomes in vitro and in vivo. Nano Lett 2008; 8: 2851-7.
140. Kumar R, Roy I, Ohulchanskyy TY, et al. Covalently dye-linked, surface-controlled, and bioconjugated organically modified silica nanoparticles as targeted probes for optical imaging. ACS Nano 2008; 2: 449-56.

141. Lee KJ, Nallathamby PD, Browning LM, Osgood CJ, Xu XH. In vivo imaging of transport and biocompatibility of single silver nanoparticles in early development of zebrafish embryos. ACS Nano 2007; 1: 133-43.
142. Skrabalak SE, Au L, Lu X, Li X, Xia Y. Gold nanocages for cancer detection and treatment. Nanomed 2007; 2: 657-68.
143. Yamada S, Fujita S, Uchimura E, Miyake M, Miyake J. Reverse transfection using gold nanoparticles. Methods Mol Biol 2009; 544: 609-16.
144. Hainfeld JF, Slatkin DN, Smilowitz HM. The use of gold nanoparticles to enhance radiotherapy in mice. Phys Med Biol 2004; 49: N309-15.
145. Yang DP, Cui DX. Advances and prospects of gold nanorods. Chem Asian J 2008; 3: 2010-22.
146. Medintz IL, Uyeda HT, Goldman ER, Mattoussi H. Quantum dot bioconjugates for imaging, labelling and sensing. Nat Mater 2005; 4: 435-46.
147. Rzigalinski BA, Strobl JS. Cadmium-containing nanoparticles: Perspectives on pharmacology and toxicology of quantum dots. Toxicol Appl Pharmacol 2009.
148. Li CZ, Male KB, Hrapovic S, Luong JHT. Fluorescence properties of gold nanorods and their application for DNA biosensing. Chemical Communications 2005: 3924-6.
149. Kuhn S, Hakanson U, Rogobete L, Sandoghdar V. Enhancement of single-molecule fluorescence using a gold nanoparticle as an optical nanoantenna. Physical Review Letters 2006; 97: -.
150. Nikoobakht B, El-Sayed MA. Surface-enhanced Raman scattering studies on aggregated gold nanorods. Journal of Physical Chemistry A 2003; 107: 3372-8.
151. Nie S, Emory SR. Probing Single Molecules and Single Nanoparticles by Surface-Enhanced Raman Scattering. Science 1997; 275: 1102-6.
152. Eghtedari M, Liopo AV, Copland JA, Oraevsky AA, Motamedi M. Engineering of hetero-functional gold nanorods for the in vivo molecular targeting of breast cancer cells. Nano Lett 2009; 9: 287-91.
153. Guo R, Li R, Li X, Zhang L, Jiang X, Liu B. Dual-functional alginic acid hybrid nanospheres for cell imaging and drug delivery. Small 2009; 5: 709-17.
154. Wu G, Mikhailovsky A, Khant HA, Fu C, Chiu W, Zasadzinski JA. Remotely triggered liposome release by near-infrared light absorption via hollow gold nanoshells. J Am Chem Soc 2008; 130: 8175-7.
155. Pissuwan D, Valenzuela SM, Cortie MB. Therapeutic possibilities of plasmonically heated gold nanoparticles. Trends Biotechnol 2006; 24: 62-7.
156. Mukherjee P, Bhattacharya R, Wang P, et al. Antiangiogenic properties of gold nanoparticles. Clin Cancer Res 2005; 11: 3530-4.
157. Chen BA, Dai YY, Wang XM, et al. Synergistic effect of the combination of nanoparticulate Fe3O4 and Au with daunomycin on K562/A02 cells. Int J Nanomedicine 2008; 3: 343-50.
158. Hainfeld JF, Slatkin DN, Focella TM, Smilowitz HM. Gold nanoparticles: a new X-ray contrast agent. Br J Radiol 2006; 79: 248-53.